Development of a data-driven ageing model for Li-ion batteries: a nonparametric approach to learn from real operation data

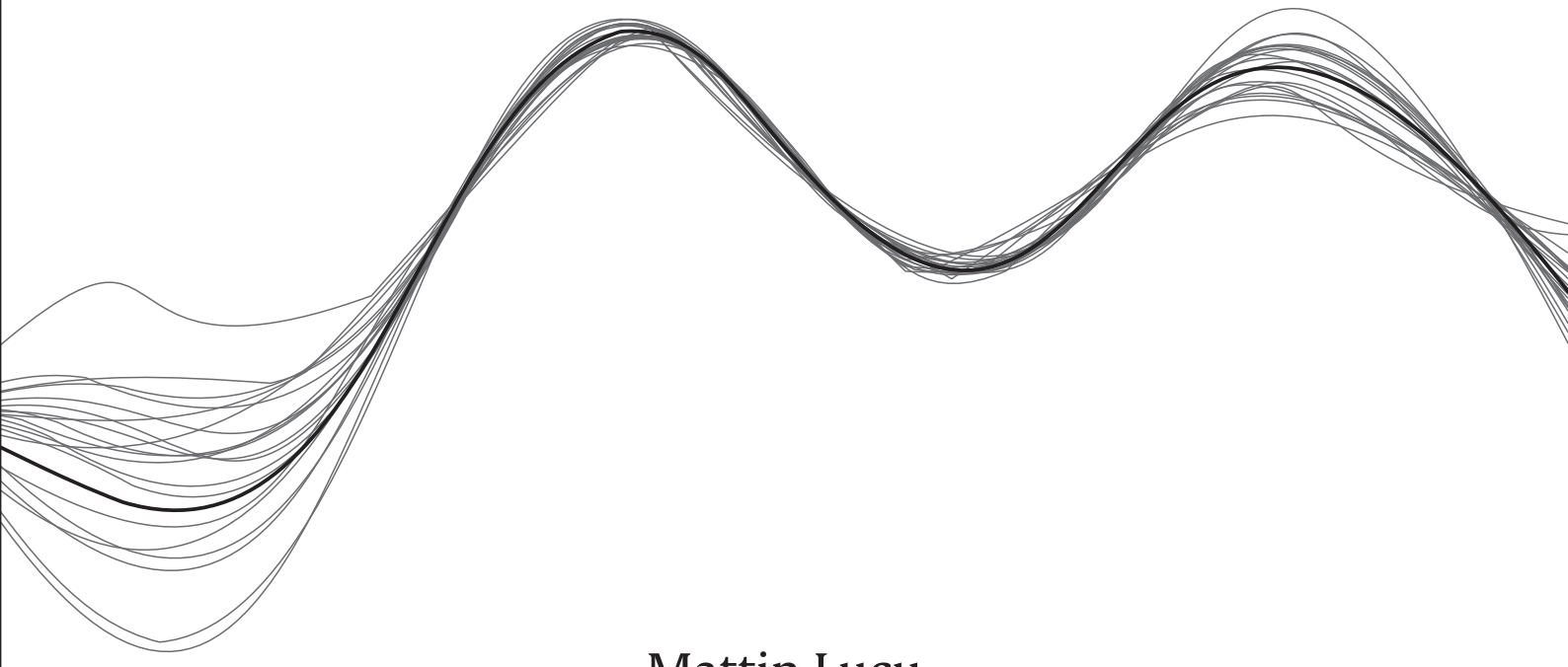

Mattin Lucu

2020

A thesis submitted for the degree of

Doctor of Philosophy

eman ta zabal zazu

Universidad del País Vasco

Euskal Herriko Unibertsitatea

Development of a data-driven ageing model for Lithium-ion batteries: a nonparametric approach to learn from real operation data

A thesis submitted for the degree of
Doctor of Philosophy

Author
Mattin Lucu Oyhagaray

Thesis supervisors
Egoitz Martinez Laserna
Haritza Camblong Ruiz

Kontrol Ingeniaritza, Automatizazioa eta Robotika Doktoregoa

Doctoral Program in Control Engineering, Automation and Robotics

Sistemen Ingeniaritza eta Automatika Saila

Automatic Control & Systems Engineering

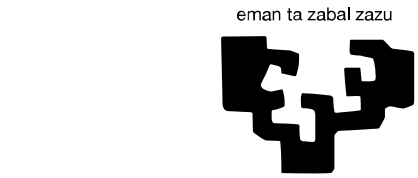

Universidad del País Vasco

Euskal Herriko Unibertsitatea

This thesis was funded by and carried out at

Authors would like to thank the FP7 European project Batteries 2020 consortium (grant agreement No. 608936) for the valuable battery ageing data provided during the project.

Eskerrak

Acknowledgement

Lehen-lehenik eskerrak eman nahi nizkizuke Igor Villarreal, duela urte batzuk trenera igotzeko eman zenidan aukeragatik, orain badakidalako niretzat momentu erabakikorra izan zela hori.

Tesia duela mende t'erdi hasi nuela iruditzen zaidan arren, bihotzez eskerrak zuri ere Eli, abentura hau nirekin hasteagatik, mundu horretaz deus ez nekien garaian oinarri guztiak eskura emateagatik eta galduta nengoen hilabete luzeetan norabideak jartzen laguntzeagatik. Gracias también a ti, Frank, por compartir conmigo estos momentos de pelea intentando entender algo de baterías.

Egoitz eta Gandi, bakoitzak 1000 orrialdeko eskerrak merezi dituzuen arren, paragrafo bakarrera mugatzen saiatuko naiz. Beti eskertua izango naiz bueltaka igerian egon naizen putzutik arrantzatzeagatik, efizienteki eta paraleloan lan egiten erakusten saiatzeagatik, gauetan eta asteburuetan nire idazki guztiak zuzentzen pasatako ordu luzeengatik, nire autoestimaren rollercoaster-a kudeatzen laguntzen saiatzeagatik, eta dakizkizuen beste mila gauzengatik. Milesker berezi bat Egoitz tesia utzi nahi nuen garaian aurrera segitzen laguntzeagatik (zu etzara gogoratuko baina ni bai). Espero dut noizbait eman didazuen laguntza guztia itzultzeko aukera izatea.

Milesker zuri ere Haritza, zure gako magikoekin gradutik doktoretzara borta guztiak idekitzeagatik, zientziaz deus ez zakien gazte horri konfiantza egiteagatik, eta

ikerketan fundamentala den kanpoko/gaineko begirada emaiteko beti prest egoiteagatik ene tesi guzian zehar. Garai batean erran zinautan hori, “lan egin behar da anitz eta ongi”, aplikatzen entseatu niz azken urteetan, espero dut noizbait nunbait ondorioak agertzea.

Bestalde, bereziki eskerrak eman nahi nizkizueke doktoretzan zehar nire inguruan egon zareten Ikerlaneko ikerlari bakoitzari eta guztieri, Galarretako giro bikaina bultzatzeagatik eta etxean bezala sentiarazteagatik, egunerokoan gure lana aurrera eramaten laguntzeagatik eta gure galdera arraro guztiei erantzuten saiatzeagatik, ez da beti ariketa errexa. Eskerrak doktoretzaren abentura hori nirekin partekatu duzuen David, Amaia, Jonan eta Iñigori, eta baita hiri ere Markel behar nuenean emandako laguntza guztiagatik! Zorte on doktoregai belaunaldi berriari, Markel, Josu, Nerea, Eneko eta Olatz! Gu lagundu gintuzten bezala zuek laguntzen ahal bazaituztet, oso pozik egingo dut beti!

I also would want to acknowledge all the people I met at WMG, first Carlos who allowed me access to this great team, I seize this opportunity to extend my warmest thanks for everything. I would want to express all my gratitude to you, James, for all the effort and time dedicated explaining me many fundamental concepts on research with your impressive pedagogical skills, and for guiding and correcting me in my research publishing processes. Dhammika, I will always be grateful for teaching me so many things, always taking the time to answer every single question despite your extremely busy agenda, and also for one big lesson I will probably never forget.

Kailong, my friend, for all these hours including nights and weekends trying to build the best models ever, learning machine learning on our own… It has been a great experience to work with you during this time. Maybe someday we will do research together again.

I would also want to thank you Chuanxin and Kai, for all the lunches we shared at Pitstop cafe, and Lili for all these talks and walks along the river. Many thanks Quirin for always trying to support me during my research and stay, and Shahjalal for inspiring me so much. Thanks to you also Shanki for sharing with me your deep philosophy and for all the pints we drunk together. Finally, I would want to acknowledge the whole WMG team, I will remember each one of you and each conversation as a wonderful memory of my stay in England.

Milesker berezi bat hiru urte horietan izan dituztan pisukide guzier eta laguner, eta orokorki ene biziaren parte izan zirezten guzier. Barkamenak ere galdegin nahi nauzkizueke tesiko urteetan zuekin pasa ez dutan denbora guziagatik! Bihartik aintzina desberdina izaitea espero dut! Goraintzi berezi bat Dani eta Etxahuni azken hilabeteetan luzaturiko gomita guziengatik, bi paragraforen artean eta biera baten denboran tesia burutik kentzen laguntzeagatik.

Finitzen joaiteko, milesker anitz gure burasoer, sortu ginenetik eman daukuzuen guziarengatik, hastapenetik gure bizia errex eginik, haurtzaro eta gaztaro kulturalki aberats bat opariturik, eta sustut tesi hunen finitzeko beharrezkoak izan diren lanaren baloreak eta burugogortasuna transmititurik.

Eta azken-azkenik, milesker aintzinetik zier, bizitzea espero dutan ondoko 50 urteetan ene inguruan izanen zizten guztier.

Milesker!

Mattin

Laburpena

Litio-ioizko baterien teknologia metatze-sistema lehenetsia bilakatu da aplikazio industrial desberdinentzat. Izan ere, ezaugarri interesgarriak erakusten ditu beste metatze teknologiei konparatuz, hala nola dentsitate energetiko handia, energia eta potentzia espezifiko handia, efizientzia energetiko handia eta heldutasun teknologiko erlatiboki aitzinatua. Hala ere, teknologia horren arazo nagusi bat baterien kostu iniziala da. Horretaz gain, Li-ioizko bateriek beren hasierako gaitasunak galtzen dituzte denboraren poderioz, baita erabilpen baldintzen arabera ere. Horrek Li-ioizko baterietan oinarrituriko sistemen errentagarritasuna kolokan ezartzen du.

Arazo hauei aurre egiteko, komunitate zientifikoa eta industria norabide desberdinak lantzen ari dira. Hauen artean, aipa genitzake metatze-sistemen dimentsionamenduaren optimizazioa, baterien bigarren bizitzan oinarrituriko negozio estrategien inplementazioa, eta baterien erabilpen estrategia optimizatuen garapena. Soluzio horien inplementaziorako, behar-beharrezkoa da Li-ioizko baterien degradazio eredu zehatzak garatzea: hain zuzen ere, eredu hauek baterien degradazioa aurreikusteko gai dira, bateriak sufrituriko erabilpen baldintzen arabera.

Degradazio eredu konbentzionalen garapenerako, eta batez ere hauen zehaztasuna segurtatzeko operazio baldintza errealisten testuinguruan, zailtasun nagusi bat laborategian egin beharreko test kantitatea da. Test hauek gauzatze denbora luzeak eta baliabide ekonomiko inportanteak inplikatzen dituzte, degradazio ereduen garapen kostua iganez. Arazo horren aitzinean, tesi honetan proposatzen den soluzioa datu-korronte jarraiki batetik etengabe ikasteko gaitasuna duten degradazio ereduen garatzea da. Planteamendu horri jarraikiz (ikus azpiko irudia), degradazio

eredu inizial bat garatu liteke, laborategiko test kopuru murriztu batean oinarrituz. Gerora, bateria-sistema aplikazioan hedatu ondotik, bertan Datu Eskuratze Sistemaren (DAS, ingelesetik *Data Acquisition System*) bidez lorturiko datuek degradazio eredu inizialaren eguneratzea ahalbidera lezakete. Horrela, degradazio eredua etengabe hobetuko litzateke, iragarpenen zehaztasuna hobetuz, ereduaren erabilpen-leihoa zabalduz eta informazio baliagarria hornituz mantentze prediktiborako, energiaren kudeaketa estrategia adaptagarrietarako edo negozio estrategien berdefinitzeko.

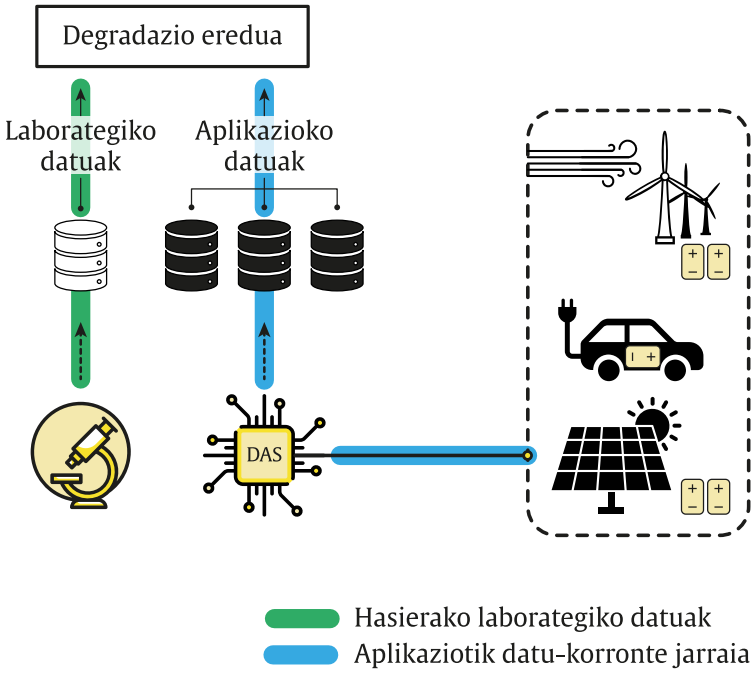

Proposaturiko degradazio ereduen planteamendua: laborategiko test kopuru murriztu batean oinarrituz, degradazio eredu inizial bat garatzen da. Gerora, bateria-sistema aplikazio desberdinetan zabaldu ondotik, bertatik DAS bidez lorturiko datuek degradazio eredu inizialaren eguneratzea ahalbidetzen dute. Modu horretan, garatutako degradazio ereduek datu-korronte jarrai batetik etengabe ikasteko gaitasuna dute.

Artearen egoeraren azterketa sakon baten ondotik, Prozesu Gaussiarren (GP, ingelesetik *Gaussian Process*) markoa identifikatu da tesiaren helburuen betetzeko ereduztatze metodo egokienen artean. Kobariantza funtzio konposizionalak proposatu dira GP ereduen garapenerako, zeinak Li-ioizko baterien degradazioaren iragarpenerako egokituak diren. Degradazio eredu holistiko bat garatu da, bi eredu independentez osatua: lehen ereduak Li-ioizko baterien "calendar" bidezko degradazioa deskribatzen du (hots, bateria geldialdi egoeran delarik ematen den degradazioa), eta bigarrenak baterien "ziklatze" bidezko degradazioa aurreikusten du (hots, bateria elektrikoki kitzikatua delarik ematen den degradazioa). Bi ereduak erabilpen baldintza estatiko, dinamiko eta errealistikoen tarte zabal batean egiaztatu dira. Horretarako laborategiko datu-base zabal bat erabili da zeinak hiru urte baino gehiagoz degradaturiko zelden datuak barneratzen dituen. Metodologia bat diseinatu da, degradazio ereduek progresiboki ikuskaturiko datuetatik etengabe ikasteko duten gaitasuna egiaztatzeko.

Tesian zehar eraman diren ikerketa lanek ondoko ondorioak azaleratu dituzte:

i) Beren izaera ez-parametrikoari esker, GP markoan oinarrituriko degradazio ereduek gaitasuna dute progresiboki ikuskaturiko erabilpen baldintzetatik ikasteko: Li-ioizko baterien erabilpen-lehio osoan zehar, degradazio ereduaren zehaztasuna hobetzen doa eta iragarpenen ziurgabetasun tarteak murrizten doaz, ereduaren fidagarritasuna hazten denaren lekuko.

ii) Testuinguru horretan, nukleo isotropikoak egokiak dira estres-faktore desberdinei dagozkien sarrerak ereduztatzeko, bateriaren erabilpena eraikitzaileek gomendaturiko erabilpen tarteetan mugatzen deno.

iii) Baterien degradazioan eragin gehien duten estres-faktoreak identifikatu daitezke, Garrantzi Determinazio Automatikoa (ARD, ingelesetik *Automatic Relevance Determination*) inplementatzen duten nukleoetan oinarrituriko sentsibilitate analisiaren bidez. Informazio hau erabilgarria izan daiteke besteak beste baterien biziraupenaren maximizazioa helburu duten energia kudeaketa estrategiak definitzeko.

iv) Desberdintasun bat bada bateriaren erabilpen baldintza estatikoen eta dinamikoen ondorioz ematen diren kapazitate galeren artean. Baliteke desberdintasun hori bateriaren deskarga sakontasunak erabilpen baldintza dinamikoetan izan lezakeen eragin murriztuaren ondorio izatea. Konstatazio horrek proposaturiko ereduen interesa areagotzen du, zeinak hedatu ondotik eboluzionatzeko gai diren, aplikazio errealean ikuskaturiko erabilpen profil dinamikoetatik ikasiz.

Tesi honetan proposaturiko ereduztatze metodoa bat dator azken urteetan arlo desberdinetan gertatzen ari den digitalizazioaren joerarekin. Industria interes handia erakusten ari da datu bilketarako telemetria teknologia berrien inplementazioan. Horren ondorioz, espero da epe motz batean aplikazio errealetatik erauzitako baterien erabilpen datuak eskuragarri izatea kantitate handian. Testuinguru horretan, aplikazioko erabilpen datuetatik ikasteko gai diren degradazio ereduen garapena soluzio interesgarria da, besteak beste i) laborategiko eta aplikazio errealeko erabilpen profilen desberdintasunetik eratorritako iragarpen akatsak zuzentzeko gai direlako, eta ii) laborategiko test kantitatea, eta beraz degradazio

ereduen garapen kostua murriztea ahalbidetzen dutelako. Ondorioz, tesi honetan aurkezturiko emaitzak interes teknologikoa ez ezik, interes komertziala ere badute, eta proposaturiko soluzioak bereziki lerrokatuak dira industriak ondoko urteetan biziko duen bilakaerarekin.

Abstract

Lithium-ion (Li-ion) battery technology has gained a significant market share as the principal energy storage solution for many industrial applications, mainly due to its relatively high technological maturity, high energy efficiency and high specific energy and power. However, Li-ion batteries are still relatively expensive compared to other storage technologies, and their performance is known to decline over time and use, which threatens their competitiveness against more affordable solutions. In order to overcome such barriers and ensure the profitability of Li-ion based systems, the global research focusses on different paths. Some of them are the implementation of optimised sizing of the storage systems, second-life business strategies and the design of effective operation strategies, which allow the reduction of the total cost of ownership and make profitable the implementation of large-scale Li-ion energy storage systems. The latter points are strongly conditioned by the development of accurate Li-ion battery ageing models, able to relate the operating conditions of a battery system to their subsequent degradation.

A significant challenge for the development of conventional Li-ion battery ageing models is the amount of laboratory tests required to verify the accuracy of the model under realistic operating conditions. In order to reduce the number of laboratory tests and at the same time ensure the validity of the model under realistic operating profiles, the solution proposed in this thesis is the development of ageing models capable to continuously learn from streaming data. Following this approach, reduced laboratory tests could be used to develop a preliminary ageing model. Further, once the battery pack has been implemented and deployed, in-field data extracted by the data acquisition system could allow updating the preliminary ageing model. In this

way, the ageing model would be continuously upgraded, improving prediction accuracy, extending the operating window of the model itself and providing useful information for predictive maintenance, adaptive energy management strategies or business case redefinition.

After an in-depth study of the state of the art, the Gaussian Process (GP) modelling framework was selected as the most suitable method to meet with the objective of the thesis. Compositional covariance functions were proposed in order to develop GP models tailored to the Li-ion battery ageing prediction application. A holistic ageing model was developed, composed of two separated models corresponding respectively to the cell degradation through calendar and cycle ageing. Both models were validated under a broad range of static, dynamic, and realistic operating conditions, using an extensive laboratory experimental dataset involving Li-ion cells tested during more than three years. A methodology was designed to validate the ability of the models to learn continuously from the data progressively observed.

The research works carried out in this thesis bring the main following findings:

i) Due to their nonparametric character, GP-based ageing models are capable to learn from progressively observed operating conditions: throughout the whole operating range of the Li-ion battery, the prediction accuracy of the model improves, and the confidence boundaries of the predictions are reduced, indicating an increased reliability of the models' predictions.

ii) In this context, isotropic kernel components are suitable to host the features corresponding to the different stress-factors, in so far as the battery operates within the limited range of the recommended operating conditions.

iii) The sensitivity analysis based on the automatic relevance determination kernels allows to identify which stress-factors have highest influence on battery ageing, providing insightful inputs for the development of energy management strategies oriented to extend the lifetime of battery systems.

iv) There is a discrepancy between the capacity loss induced by static and dynamic profiles of the stress-factors, which could be related to the lower influence of the depth of discharge in dynamic operation. This highlight the increased interest of ageing models capable to evolve after the deployment and learn from the dynamic profiles observed in real applications.

The modelling approach proposed in this thesis comes aligned with the digitalisation trends observed in the recent years in different areas. In fact, there is significant interest from industry in the introduction of new data collection telemetry technology. This implies the forthcoming availability of a significant amount of real-world battery operation data. In this context, the development of ageing models able to learn from in-field battery operation data is an interesting solution to mitigate the need for exhaustive laboratory testing and reduce the development cost of ageing models. The findings presented in this work are therefore not only of technological but also of economic interest, and the proposed solution is particularly adapted to the industry trends upcoming.

KEYWORDS: Li-ion battery, State of Health, Remaining Useful Life, Machine Learning, Data-driven model, Gaussian Process Regression.

Dissemination activities

JOURNAL PUBLICATIONS

- **M. Lucu**, E. Martinez-Laserna, I. Gandiaga, H. Camblong. A critical review on self-adaptive Li-ion battery ageing models. Journal of Power Sources, Volume 401, 15 October 2018, Pages 85-101. doi: 10.1016/j.jpowsour.2018.08.064.
- **M. Lucu**, E. Martinez-Laserna, I. Gandiaga, K. Liu, H. Camblong, D. W. Widanage, J. Marco. Data-driven nonparametric Li-ion battery ageing model aiming at learning from real operation data – Part A: storage operation. Journal of Energy Storage, Volume 30, August 2020. doi: 10.1016/j.est.2020.101409.
- **M. Lucu**, E. Martinez-Laserna, I. Gandiaga, K. Liu, H. Camblong, D. W. Widanage, J. Marco. Data-driven nonparametric Li-ion battery ageing model aiming at learning from real operation data – Part B: cycling operation. Journal of Energy Storage, Volume 30, August 2020. doi: 10.1016/j.est.2020.101410.
- K. Liu, Y. Li, X. Hu, **M. Lucu**, D. W. Widanage. Gaussian Process Regression with Automatic Relevance Determination Kernel for calendar aging prediction of Lithium-ion batteries. IEEE Transactions on Industrial Informatics, Volume 16, No. 6, June 2020. doi: 10.1109/TII.2019.2941747.
- K. Liu, T. R. Ashwin, X. Hu, **M. Lucu**, W. D. Widanage. An evaluation study of different modelling techniques for calendar ageing prediction of Lithium-ion batteries. Renewable & Sustainable Energy Reviews, Volume 131, October 2020. doi: 10.1016/j.rser.2020.110017.

CONFERENCE ARTICLES

- **M. Lucu**, M. Azkue, H. Camblong, E. Martinez-Laserna. Data-driven nonparametric Li-ion battery ageing model aiming at learning from real operation data: holistic validation with EV driving profiles. IEEE Energy Conversion Congress and Exposition (ECCE), October 2020, Detroit, Michigan, USA.
- **M. Lucu**, J. A. López-Ibarra, E. Martinez-Laserna, I. Gandiaga, H. Camblong. Development of a self-adaptive cycle ageing model for Li-ion batteries using Machine Learning methods. 32nd Electric Vehicle Symposium (EVS32), May 2019, Lyon, France.
- **M. Lucu**, J. A. López-Ibarra, E. Martinez-Laserna, I. Gandiaga, H. Camblong. Lithium-ion battery ageing models using Machine Learning methods: a nonparametric approach to learn from real-world operation data. Power our Future ’19, The 4th

International Forum on Progress and Trends in Battery and Capacitor Technologies, July 2019, Vitoria-Gasteiz, Basque Country.

- **M. Lucu**, E. Martinez-Laserna, I. Gandiaga, H. Camblong. Comparative study of self-adaptive Li-ion battery ageing models. Advanced Battery Power, April 2018, Münster, Germany.

- J. A. López-Ibarra, **M. Lucu**, N. Goitia-Zabaleta, H. Gaztañaga, V. I. Herrera, H. Camblong. Battery Aging Conscious Intelligent Energy Management Strategy for Hybrid Electric Buses. 2019 Fourteenth International Conference on Ecological Vehicles and Renewable Energies (EVER). May 2019, Monte-Carlo, Monaco.

- E. Martinez-Laserna, I.Gandiaga, E. Sarasketa-Zabala, **M. Lucu**, I. Villarreal. Analysis of Li-ion LFP/C Second Life Battery Ageing Performance, Power Our Future 2017, 2-5 July. 2017, Vitoria-Gasteiz, Basque Country.

Table of Contents

List of Tables

List of Figures

Abbreviations

AE	**A**bsolute **E**rror
Ah	**A**mpere-**h**our
ANN	**A**rtificial **N**eural **N**etwork
AR	**A**uto**R**egressive OR **A**uto**R**egression
ARMA	**A**uto**R**egressive **M**oving **A**verage
ARIMA	**A**uto**R**egressive **I**ntegrated **M**oving **A**verage
BMS	**B**attery **M**anagement **S**ystem
BOL	**B**eginning **o**f **L**ife
CC	**C**onstant **C**urrent
CHA	**C**harge OR **C**harging
CS	**C**alibration **S**core
CV	**C**onstant **V**oltage
DAS	**D**ata **A**cquisition **S**ystem
DOD	**D**epth of Discharge
EIS	**E**lectrochemical **I**mpedance **S**pectroscopy
EV	**E**lectric **V**ehicle
EOL	**E**nd **o**f **L**ife
FEC	**F**ull **E**quivalent **C**ycle
GP	**G**aussian **P**rocess
GPR	**G**aussian **P**rocess **R**egression
HEV	**H**ybrid **E**lectric **V**ehicle
HI	**H**ealth **I**ndicator
MA	**M**oving **A**verage
MSE	**M**ean **S**quare **E**rror
MAE	**M**ean **A**bsolute **E**rror
MGP	**M**ulti-scale **G**aussian **P**rocess
MGPR	**M**ulti-scale **G**aussian **P**rocess **R**egression
MidSOC	**M**iddle-**S**tate-**o**f-**C**harge
NMC	**N**ickel **M**anganese **C**obalt
OCV	**O**pen **C**ircuit **V**oltage
pdf	**P**robability **d**ensity **f**unction
RUL	**R**emaining **U**seful **L**ife
RVM	**R**elevance **V**ector Machine
RV	**R**elevance **V**ector
RMSE	**R**oot **M**ean **S**quare **E**rror
SEI	**S**olid **E**lectrolyte **I**nterface

SMO	**S**equential **M**inimal **O**ptimisation
SOC	**S**tate **o**f **C**harge
SOH	**S**tate **o**f **H**ealth
SV	**S**upport **V**ector
SVM	**S**upport **V**ector **M**achine
SVR	**S**upport **V**ector **R**egression

Symbols & Notation

Matrices are capitalised and vectors are in bold type. A subscript asterisk, such as X_*, indicates reference to a *test set* quantity. A superscript number, such as $\mathbf{x}_1$, indicate the index of the corresponding vector.

Symbol	Meaning	Refers to
$\sim$	Distributed accorded to; example $x \sim \mathcal{N}(\mu, \sigma^2)$.	-
$\|x\|$	Absolute value of x.	-
$\|K\|$	Determinant of matrix K.	-
$\|\|\mathbf{w}\|\|$	Euclidean norm of vector w.	-
$\langle w, x \rangle$	Dot product of vectors w and x.	-
$\mathbf{y}^T$	The transpose of vector **y**.	-
α	Autocorrelation coefficient.	ARIMA
	or α'. Dual variable or Lagrange multiplier.	SVR
β	Weight applied to the residuals	ARIMA
C	Constant parameter to control the trade-off between the flatness objective and the tolerated error deviation.	SVR
Charging C-rate	The value of the charging C-rate stress-factor, corresponding to the cycled Ah-throughput.	-
$\text{cov}(\mathbf{f}_*)$	Gaussian process posterior covariance.	-
$CS_{2\sigma-\Delta Q}$	Calibration score relative to a $\pm 2\sigma$ interval, calculated for ΔQ predictions.	-
$CS_{2\sigma-Q}$	Calibration score relative to a $\pm 2\sigma$ interval, calculated for Q predictions.	-
δ	Dirac function.	Particle filters
Δt	The storage time for which the calendar ageing is predicted.	-
ΔQ	Capacity loss corresponding to a Δt storage time or a ΔAh-throughput cycled.	-
ΔAh-throughput	The number of Ah-throughput for which the ageing is predicted.	-
Discharging C-rate	The value of the discharging C-rate stress-factor, corresponding to the cycled ΔAh-throughput.	-
DOD	The value of the DOD stress-factor, corresponding to the cycled ΔAh-throughput.	-
$\mathbb{E}$	Expectation.	-
ε	Residual.	-

ξ_i, ξ_i'	Slack variables.	SVR
ϵ	Insensitivity parameter.	SVR
$f(\mathbf{x})$	Model of function to be found.	-
	Transition model.	Particle filters
	or **f.** Gaussian process (or vector of) latent function values, $\mathbf{f} = (f(\mathbf{x}_1), \ldots, f(\mathbf{x}_n))^T$.	GP
$\mathbf{f}_*$	Gaussian process (posterior) prediction (random variable).	GP
$\bar{\mathbf{f}}_*$	Gaussian process posterior mean.	GP
$\mathcal{F}$	Feature space.	-
$\mathcal{GP}$	Gaussian Process: $f \sim \mathcal{GP}(m(\mathbf{x}),\ \kappa(\mathbf{x}, \mathbf{x}'))$, the function f is distributed as a Gaussian process with mean $m(\mathbf{x})$ and covariance function $\kappa(\mathbf{x}, \mathbf{x}')$.	GP
$h(\mathbf{x})$	Measurement model.	Particle filters
I	The identity matrix	-
$\kappa(\mathbf{x}, \mathbf{x}')$	Covariance (or kernel) function evaluated at $\mathbf{x}$ and $\mathbf{x}'$.	SVR, RVM, GP
K or $K(X, X)$	$n \times n$ covariance (or Gram) matrix.	GP
K_*	$n \times n_*$ matrix $K(X, X_*)$, the covariance between training and test cases.	GP
L	Loss function.	SVR
$m(\mathbf{x})$	The mean function of a Gaussian Process.	GP
$MAE_{\Delta Q}$	Mean Absolute Error, calculated for ΔQ predictions.	-
MAE_Q	Mean Absolute Error, calculated for Q predictions.	-
Middle-SOC	The value of the Middle-SOC stress-factor, corresponding to the cycled ΔAh-throughput.	-
η, η'	Dual variable or Lagrange multiplier.	SVR
$\mathcal{N}(\mu, \Sigma)$	Gaussian (Normal) distribution with mean vector μ and covariance matrix Σ.	-
$\mathcal{O}(\cdot)$	Big O notation	-
$\phi(\mathbf{x})$	Basis function which maps a D-dimensional input vector x into a N-dimensional feature space.	SVR, RVM
Q	Capacity.	-
Q_{max}	Maximum value of the capacity curve.	-
$RMSE_{\Delta Q}$	Root Mean Square Error, calculated for ΔQ predictions.	-
$RMSE_Q$	Root Mean Square Error, calculated for Q predictions.	-
SOC	The value of the SOC stress-factor, corresponding to the storage time Δt.	-
σ	Standard deviation.	-
σ^2	Variance.	-

σ_n^2	Noise variance.	GP
σ_f^2	Variance of the (noise free) signal.	GP
$\boldsymbol{\theta}$	Vector of hyperparameters (parameters of the covariance functions).	GP
$\theta_{\Delta t}$	Hyperparameter related to the Δt input.	GP
θ_{SOC}	Hyperparameter related to the SOC input.	GP
θ_T	Hyperparameter related to the T input.	GP
T^{-1}	The reciprocal of the temperature corresponding to the storage time Δt or to the cycled ΔAh-throughput.	-
$\mathbf{u}$	Vector of the noise terms, in the measurement model.	Particle filters
$\mathbf{v}$	Vector of the noise terms, in the transition model.	Particle filters
$\mathbf{w}$	Vector of parameters or weights.	SVR, RVM
	Weight of the particles.	Particle filters
$\mathbf{x}$	Input vector, $\mathbf{x} = (\mathbf{x}_1, \ldots \mathbf{x}_N)$.	-
	Vector of state variables, $\mathbf{x} = (\mathbf{x}_1, \ldots \mathbf{x}_N)$	Particle filters
$\mathcal{X}$	Input space.	-
$\mathbf{y}$	Target or output vector.	-
	Vector of measurement variables.	Particle filters
$\hat{y}$	Predicted output.	-
$y\|x$ and $p(y\|x)$	Conditional random variable y given x and its probability (density)	-

Glossary of Terms

Ageing OR **Degradation**
: Battery permanent loss of performance capabilities due to both a repeated cyclic use and the course of time. Also referred as degradation.

Ageing knee
: The point in the ageing history of a Li-ion battery in which a sudden and significant acceleration is experienced in the capacity fade and/or the DC resistance increase evolution. From an electrochemical standpoint, such acceleration is normally due to a change in the dominant ageing mechanism.

Ampere-hour-throughput [Ah]
: The cumulative sum of the amount of Ampere-hours charged or discharged in absolute terms.

Anode
: The electrode in an electrochemical cell where the oxidation takes place. It gives up electrons to the external circuit during discharge (negative electrode) and the situation reverses during charge (positive electrode).

Anode overhang
: The anode overhang is defined by the geometrical anode area, which is not opposed by a cathode. The anode is oversized in nearly all lithium-ion cells containing a graphite anode.

Autoregressive model
: Refers to a model which forecasts the variable of interest based on the past values of such variable. The term *auto*regression indicates that it is a regression of the variable against itself.

Batch learning
: Refers to a learning paradigm in which the whole training dataset is used at once to train the model.

Battery
: A device that converts chemical energy into electrical energy and vice versa. Batteries typically consist of several cells interconnected in modules, branches or racks to form a whole battery pack:

Cell
The basic electrochemical unit providing a source of electrical energy by direct conversion of chemical energy. The cell consists of an assembly of electrodes, separators, electrolyte, container and terminals.

Battery Module
One or more electrochemical cells electrically connected in series/parallel to provide the required operating voltage and current levels.

Battery pack
An assembly of battery modules, either connected in series or in parallel. Typically includes higher level interfaces for battery control, monitoring, communications and thermal management.

Battery Management System (BMS)
Electronic circuit board that manages a rechargeable battery, by sensing and monitoring its state, calculating secondary data, communicating or reporting that data, protecting the battery, controlling its environment, and/or balancing it.

Beginning of Life (BOL)
The point in time at which battery use begins.

Big-O complexity
The Big O notation provides the asymptotic upper bound for the growth rate of runtime or memory of an algorithm or program.

Calendar operation
Refers to an operation in which the cell is not electrically cycled.

Calendar ageing
The degradation of a Li-ion cell due to the ageing mechanisms happening during a purely calendar operation, i.e. when the cell is not electrically cycled.

Capacity [Ah]
The quantity of Ampere-hours that can be withdrawn from a fully charged cell or battery under specified conditions of discharge.

Actual, Current OR **Remaining Capacity [Ah]**
The total capacity that will be obtained from a cell or battery at defined discharge rates and other specified discharge or operating conditions. The capacity that can be discharged until discharge cut-off voltage from a completely charged cell.

Capacity Fade OR **Irreversible capacity loss [Ah]**
Gradual loss of capacity of a secondary battery due to ageing processes.

Reversible capacity recovery [Ah]
Reversible increase of capacity of a secondary battery. This could sometimes be observed in the initial phase of the capacity curve, or as a local phenomenon after an idle pause in cycling. According to the literature, the reversible capacity recovery could be induced by a slow, compensating flow of active lithium between the passive and the active part of the anode, where the passive part represents the geometric excess of the anode with respect to the cathode.

Nominal capacity [Ah]
Capacity of the cell or battery, expressed in Ampere-hours, measured at nominal conditions defined by the manufacturer (datasheet).

Cathode
The electrode in an electrochemical cell where the reduction takes place. It receives electrons from the external circuit during discharge (positive electrode) and the situation reverses during charge (negative electrode).

Characterisation tests
A characterisation test consists on a determined sequence of tests to periodically check the performance of the battery under test.

Charge
The conversion of electrical energy, provided in the form of a current from an external source, into chemical energy within a cell or battery.

Confidence interval OR **confidence boundary**
A confidence interval gives an estimated range of values which is likely to include an unknown population parameter, the estimated range being calculated from a given set of sample data. In this thesis the confidence intervals correspond to a 2σ confidence level.

Constant Current (CC)
A method of charging/discharging the battery using a constant current.

Constant Voltage (CV)
A method of charging the battery by applying a fixed voltage and allowing variations in the current.

Covariance
Measure of how much two random variables vary together. Formally, suppose X and Y are random variables with means μ_X and μ_Y. The covariance of X and Y is defined as

$$cov(X,Y) = E((X - \mu_X)(Y - \mu_Y))$$

Covariance function OR **kernel function** OR **kernel**

In this thesis, the terms "covariance function", "kernel function" or "kernel" are used equivalently.

The covariance function $\kappa(\mathbf{x}, \mathbf{x}')$ of a real process $f(\mathbf{x})$ is formally defined as follows:

$$\kappa(\mathbf{x}, \mathbf{x}') = \mathbb{E}\big[\big(f(\mathbf{x}) - m(\mathbf{x})\big)\big(f(\mathbf{x}') - m(\mathbf{x}')\big)\big]$$

where $\mathbf{x}$ and $\mathbf{x}'$ are two different input vectors and $m(\mathbf{x})$ is the mean function of the process.

C-rate [h^{-1}]

The discharge or charge current (in Amperes) expressed as a multiple of the rated device capacity (in Ampere-hours). For example, for a device having a capacity of one Ampere-hour under this reference condition, 5A charging/discharging would be $5A$ / $1Ah$ rate or 5C [h^{-1}].

Cycle

The discharge and subsequent or preceding charge of a secondary battery such that it is restored to its original State of Charge (SOC) condition.

Cycle ageing

The degradation of a Li-ion cell due to the ageing mechanisms happening during a purely cycling operation, i.e. when the cell is electrically cycled.

Cycle life

The number of cycles under specified conditions that a secondary battery is capable of withstanding before it fails to meet specified criteria of performance.

Cycling operation

Refers to an operation in which the cell is electrically cycled.

Data-driven OR **Empirical model**

Refers to a model only supported by experimental data, in opposition to physics-based models in which the physical laws and mechanisms are explicitly modelled.

DC Internal Resistance [Ω]

The opposition or resistance to the flow of an electric current within a cell or battery; the sum of the ionic and electronic resistances of the cell components.

Depth of Discharge (DOD) [%]

In this thesis DOD refers to the SOC window during each charge or discharge phase. That is, the DOD represents the absolute difference between the starting and ending SOC for each charge or discharge applied to the battery:

$$DOD[\%] = |SOC(k) - SOC(1)|$$

being $SOC(1)$ and $SOC(k)$ the State of Charge at the beginning and the end of the charge or discharge step, respectively.

Discharge

The conversion of the chemical energy of a cell or battery into electrical energy and withdrawal of the electrical energy into a load.

Dynamic operating profile

Refers to a cycling or calendar operating profile applied to a cell or battery, in which the values of the different stress-factors were periodically modified.

Efficiency

The ratio of the output of a battery to the input required to restore the initial SOC, under specified conditions.

Coulombic efficiency (η_{Ah})

The ratio of the number of charges that enter the battery during charging compared to the number that can be extracted from the battery during discharging.

Energy efficiency (η_{Wh})

The amount of energy that can be taken from the battery compared to the amount of energy that was charged into the battery beforehand.

Electric Vehicle (EV)

A vehicle which uses one or more electric motors for propulsion.

Hybrid Electric Vehicle (HEV)

A vehicle that combines a conventional Internal Combustion Engine (ICE) system with one or more electric motors for its propulsion. The vehicle is equipped with an ESS which can only be charged from the ICE onboard or via regenerative braking.

Electrode

The area at which electrochemical processes take place.

Electrolyte

The medium which provides the ion transport mechanism (charge transfer) between the positive and negative electrodes of a cell.

End of Life (EOL)
A condition reached when the device under test is no longer capable of meeting the applicable goals.

Energy density (volumetric) [Wh.L^{-1}]
The amount of energy that can be stored in a given volume of a substance or system.

Experimental error
Refers to the noise embedded in the data during the experimental data collection, mainly composed of the environmental and procedural error components.

Environmental error
Refers to errors that are systematic to multiple experiments and can be controlled to a limited degree within known bounds. Environmental errors include ambient temperature and humidity conditions, equipment accuracy and resolution, manufacturing tolerances on battery samples and equipment used.

Procedural error
Refers to errors introduced as a result of performing the experiment. These types of error occur during the experimental process itself and are known to be more variable. Procedural errors include the variation of the researcher in charge of the experiment, set-up variation, sample variation, repeatability.

Full Equivalent Cycles (FEC)
The number of complete (100% DOD) cycles corresponding to a certain Ah-throughput (charged and discharged Ah). FEC serve as a reference to compare battery degradation with the same Ah-throughput when the cycling is performed at different DODs inferior to 100% DOD. As an example, for a 20Ah battery, 1 FEC corresponds to a throughput of 40Ah.

Gaussian noise
Noise model which follows an independent, identically distributed Gaussian distribution with zero mean and variance σ_n^2.

Hyperparameter
Free parameter of the covariance function. We refer to the parameters of the covariance function as hyperparameters to emphasize that they are parameters of a nonparametric model.

Impedance [Ω]
The opposition or resistance of a cell or battery to an alternating current of a particular frequency.

Incremental learning
Refers to **Online learning** strategies that work with limited memory resources.

In-field data
Data collected from battery systems already deployed and under usage in an application.

Input data
Examples or observations of the input vector variable of the model.

Isotropic
If the covariance function is a function only of $|x - x'|$ then it is called isotropic.

Kernel
See **Covariance function**

Laboratory data
Data collected from specific experiments carried out in laboratory environment, typically involving climatic chambers and controllable current sources for controlling battery operating conditions.

Likelihood
Refers to the probability density of the observations given the latent variable.

$$\mathbf{y}|\mathbf{f} \sim \mathcal{N}(\mathbf{f}, \sigma_n^2 I)$$

where $\mathbf{y}$ is the vector of observations, $\mathbf{f}$ is the vector of latent function values as $\mathbf{f} = (f(\mathbf{x}_1, \ldots, \mathbf{x}_n))^T$, σ_n^2 is the noise variance, and I is the identity matrix. Under the Gaussian Process framework, the likelihood is Gaussian.

Marginal likelihood
Refers to the marginalisation of the likelihood over the function values $\mathbf{f}$, i.e. the integral of the likelihood times the prior.

$$p(\mathbf{y}|X) = \int p(\mathbf{y}|\mathbf{f}, X)\, p(\mathbf{f}|X) d\mathbf{f}$$

Mean function
The mean function $m(\mathbf{x})$ of a real process $f(\mathbf{x})$ is formally defined as follows:

$$m(\mathbf{x}) = \mathbb{E}[f(\mathbf{x})]$$

where $\mathbf{x}$ is an input vector.

Middle-SOC [%]
Refers to the average SOC value of a cycle performed at a certain DOD. For instance, a cycle performed between 50% and 80% SOC values could be referred to as a cycle at 30% DOD and 65% Middle-SOC levels.

Nominal Voltage [V]
The characteristic operating voltage or rated typical voltage of the battery given by the manufacturer, typically corresponding to the 50% SOC OCV.

Nonparametric model
Refers to a model in which the number of parameters is not fixed and is allowed to grow with the number of training data samples.

Online learning
Refers to a learning paradigm where the learning process takes place whenever new example(s) emerge and adjusts what has been learned according to the new example(s).

Open Circuit Voltage (OCV)
The difference in voltage between the terminals of a cell under no-load condition (when the circuit is open). It is near to the equilibrium potential. This thesis work refers OCV to the cell voltage after 3 hours rest (under no-load conditions).

Parallel
Term used to describe the interconnection of cells or batteries in which all of the like terminals are connected together. Parallel connections multiply the capacity of the resultant battery by the number of cells connected.

Parametric model
Refers to a model that has a finite number of parameters, independent of the size of the training dataset.

Posterior probability distribution OR **posterior**
Refers to the probability distribution over functions specified by the GP after the observation of the data.

Prior probability distribution OR **prior**
Refers to the probability distribution over functions specified by the GP before the observation of the data. Under the GP framework, the prior is gaussian $\mathbf{f}\,|X \sim \mathcal{N}(0, K)$.

Random process OR **Stochastic process**
A random process is defined as a collection of random variables defined on a common probability space. Whereas a probability distribution describes random variables which are scalars or vectors (for multivariate distributions), a stochastic process governs the properties of functions.

Realistic operating profile
Refers to a cycling, calendar or mixed operating profile applied to a cell, similar to the profiles which could be observed in a real application in terms of current, voltage and temperature time series.

Regression
The problem of learning input-output mappings from empirical data (the training dataset), for continuous outputs.

Remaining Useful Life (RUL)
Refers to the operating time or cycles the battery can perform until reaching the defined **End-of-Life** (EOL) threshold.

Second life
Post-automotive use of batteries that are not valid any longer for electromobility applications. Once retired from the automotive service, second life batteries are thought to be reused on less demanding applications (typically stationary applications).

Semi-supervised learning
Semi-supervised learning is halfway between **supervised** and **unsupervised learning**. In addition to unlabelled data, the algorithm is provided with some supervision information – but not necessarily for all examples. Often, this information standard setting will be the targets associated with some of the examples. In this case, the dataset can be divided into two parts: the samples for which labels are provided, and the samples the labels of which are not known.

Separator
An ion permeable, electrically nonconductive, spacer or material which prevents electronic contact between electrodes of opposite polarity in the same cell.

Series
The interconnection of cells or batteries in such a manner that the positive terminal of the first is connected to the negative terminal of the second, and so on. Series connections increase the voltage of the resultant battery according to the number of cells connected.

Side reactions
Refers to the reactions inside a Li-ion cell that occur in addition to the main lithium ion intercalation reaction. The effects of battery side reactions are often detrimental and lead to the degradation of the cell. Sometimes referred in the thesis as ageing mechanisms.

Sparsity

Refers to a property of some algorithms. Such an algorithm yields a sparse result when, among all the coefficients that describe the model, only a small number are non-zero. Analogously, a sparse matrix is a matrix in which most of the elements are zero.

Specific energy [Wh.kg^{-1}]

The amount of energy that can be stored in a given mass of a substance or system. Also referred in the literature as gravimetric energy density.

Static operating profile

Refers to a cycling or calendar operating profile applied to a cell, in which the values of the different stress-factors were maintained constant during the whole duration of the operation.

State of Charge (SOC) [%]

The ratio between the amount of lithium ions remaining in the negative electrode and the total amount of active lithium ions in the cell system, i.e. the sum of lithium ions in the negative and positive electrode. The SOC would be given by cell OCV characteristics ($SOC = f(OCV)$). In practical applications, SOC is used to represent the amount of available capacity in a battery. Thus, SOC is described as follows:

$$SOC[\%] = (Q_{res}/Q) \cdot 100$$

where Q is the cell actual capacity and Q_{res} is calculated as:

$$Q_{res} = Q - Ah_{discharged}$$

State of Health (SOH) [%]

It informs of battery ageing and represents the fraction of performance deterioration remaining. In a Li-ion battery, SOH is commonly determined by the capacity and/or DC internal resistance as follows:

$$SOH(Q) = 100\% - \Delta Q[\%] \qquad \text{or} \qquad SOH(IR) = 100\% - \Delta IR[\%]$$

ΔQ or ΔIR: ratio between capacity or internal resistance of the battery in use and capacity or internal resistance measured at the BOL. In this thesis, the term SOH refers to $SOH(Q)$.

Stationary Application

Application in which the batteries are designed for use in a fixed location.

Stress-factor

Refers to the operating factors of a cell or battery which have an influence on its ageing rate. In a calendar usage, the main stress-factors are identified as the storage

temperature and SOC. In a cycling usage, the main stress-factors are identified to be the cycling temperature, the DOD, the middle-SOC, the charging C-rate and the discharging C-rate.

Sudden capacity drop
Refers to the acceleration of the capacity curve of a Li-ion cell, after the occurrence of the knee point (see **Ageing knee**).

Supervised learning
The problem of learning input-output mappings from empirical data (the training dataset), in opposition to the unsupervised learning paradigm, in which the goal is to find interesting structures only in the input data. In the supervised learning paradigm, the output component of the data is called *label* or *target*.

Target data OR **output data**
Examples or observations of the output variable of the model.

Training data
Refers to the data used during the training process of the model.

Voltage [V]
The theoretical voltage of a cell is a function of the electrode materials, i.e. it is an intrinsic property of active materials. It is also dependent on temperature and concentration, as expressed by Nernst equation. OCV is a close approximation of the theoretical voltage.

bidegurutzean
beha direner

« The power of population is so superior to the power in the earth to produce subsistence for man, that premature death must in some shape or other visit the human race. »

Thomas Robert Malthus

1798 – An Essay on the Principle of Population.

« Sunita Narain – […] *The fact is that we need to put the issue of lifestyle and consumption at the centre of climate negotiations.*

Leonardo Dicaprio – *It's a very difficult argument to present to the Americans that we need to change our lifestyle, and I would also argue that it's probably not going to happen. So, we are dependent, if we want to solve the climate crisis, on the fact that hopefully renewables like solar and wind will become cheaper and cheaper and cheaper the more money we funnel into them, the more we invest into them and ultimately it will solve that problem.*

Sunita Narain – *Who will invest, Leo? Let's be real about this…* »

2016 – Before the Flood.

Population, resources & lifestyle

Climate change is claimed to be one of the great challenges of the 21st century. Overpopulation, overconsumption and carbon-based economy are widely recognised to be at the origin of the problem [1]. Several solutions could be explored to break the circle, namely i) the establishment of human reproduction limitation policies [2], ii) the formulation of lifestyle regulation or consumption constraint policies [3,4], iii) active investigation towards the colonisation of further planets in the universe [5] or iv) the implementation of alternatives to carbon-based economy [6,7].

The first two policies seem difficult to be socially accepted, especially in European and North American societies [8,9]. The third proposal could only be seriously considered as a very long-term solution [10]. Therefore, the principal short-term solution to face the climate change seems to be to overturn the carbon-based economy. According to recent greenhouse gas emissions data [11], this implies a thorough transformation of the energy production and transport sectors, oriented to the wide adoption of renewable energy production technologies, as well as the electrification of transport solutions. The major obstacle to the extensive penetration of renewable energy sources such as wind and photovoltaic is their intermittent character, which could be addressed using energy storage

Renewables & electric transportation

Need for energy storage

[12,13]. Energy storage is also one of the most challenging components in the development of electric vehicles (EV) [14]. Therefore, both applications are strongly related to the development of high-performance and low-cost energy storage solutions.

Li-ion batteries

Lithium-ion (Li-ion) battery technology has gained a significant market share as the principal energy storage solution for many industrial applications, mainly due to its relatively high technological maturity, high energy efficiency and high specific energy and power [15,16]. However, Li-ion batteries are still relatively expensive compared to other storage technologies, and their performance is known to decline over time and use, which threatens their competitiveness against more affordable solutions [16,17]. In order to overcome such barriers, the global research in Li-ion batteries focusses on different paths. On the one hand, the next generation battery technology is wanted to be developed working on improved or new materials, in order to increase the specific energy and energy density [18], minimise side reactions [19], improve safety [20] and reduce material costs [21]. On the other hand, optimised sizing of the storage systems [22], second-life business strategies [23] and the design of effective operation strategies for the currently commercialised Li-ion battery technologies allow the reduction of the total cost of ownership, making profitable the implementation of large-scale Li-ion energy storage systems [24]. The latter points are strongly conditioned by the development of accurate battery ageing models. In fact, accurate ageing predictions could help to: i) define optimal system sizing oriented to lifetime maximisation, ii) guarantee the technical feasibility of second-life applications and iii) minimise the operation cost of the system, e.g. identifying too heavy battery operating conditions and avoiding the need for system replacement [25].

Ageing models

Calendar and cycle ageing

The ageing mechanisms occurring inside Li-ion cells take place when the cell is electrically cycled (referred as 'cycle ageing'), but also simply over time, when the cell is in storage operation (referred as 'calendar ageing'). Different forms of ageing models have been widely proposed in the literature, with varying levels of complexity, accuracy and representativeness of the internal physics and chemical processes in the battery [26]. Physics-based models are known to provide a good mathematical representation of the internal variables of the battery, such as the thickness and conductivity of the Solid Electrolyte Interface (SEI) [27,28]. However, the development of electrochemical models supposes an extensive parametrisation phase typically requiring cell disassembly [26]. Models based on in-field measurable variables are argued to be more suitable for implementation in real-world applications [29]. Empirical models rely on experimental ageing tests while semi-empirical ageing models add a physicochemical support to

Physics-based, semi-empirical, and empirical ageing models

the mathematical empirical data fitting phase [30,31]. Developing such ageing models generally consists of capturing the relations between battery's Health Indicators (HI, e.g. capacity or internal resistance [32]), and stress-factors; the most widely used factors cited in the literature include operating time, temperature, State of Charge (SOC), Ampere-hour-throughput (Ah-throughput), C-rate and Depth of Discharge (DOD) [29].

Relating HIs & stress-factors

The overall operation of Li-ion batteries could be represented as the combination of different profiles over time of the above-mentioned stress-factors. These operating profiles could be roughly classified in three main categories, namely static, dynamic and realistic operating profiles, illustrated in Figure 1.

Static, dynamic & realistic operating profiles

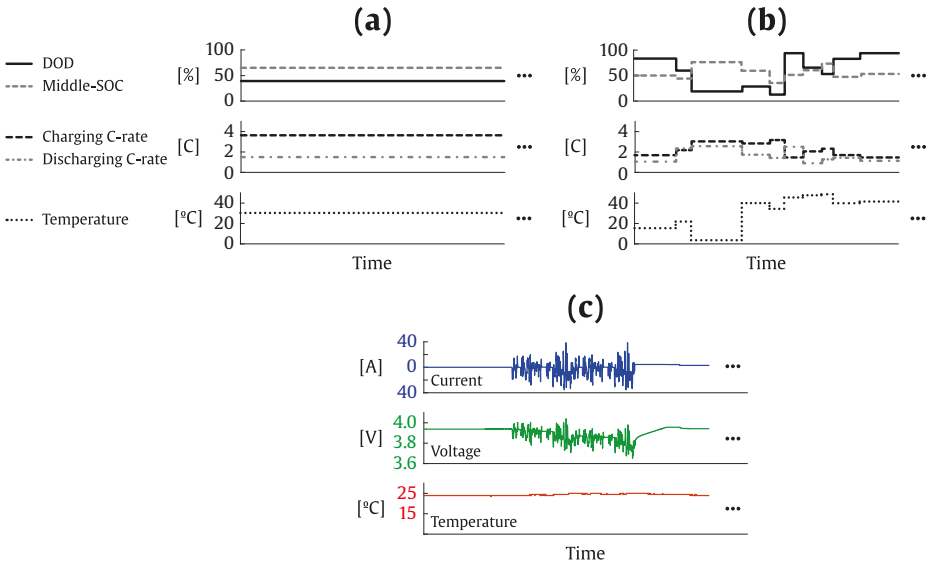

Figure 1. Illustrative example of (a) static operating factors of Li-ion batteries, in terms of different stress-factors, (b) dynamic operating factors of Li-ion batteries, in terms of different stress-factors, and (c) realistic profiles of the in-field measurable time series.

A significant challenge for the development of conventional ageing models is the amount of laboratory tests required to verify the accuracy of the model under realistic operating conditions. Conventional models are typically parametrised using laboratory tests carried out at constant ageing conditions [33,34], similar to those represented in Figure 1. (a). Furthermore, extensive validation procedures involving constant ageing conditions, slowly varying dynamic conditions and realistic ageing profiles, respectively illustrated in

Laboratory tests

Uncertainty on laboratory-based models' accuracy

Figure 1. (a), (b) and (c), are recommended to surround accurate lifetime predictions in a context of real-world operation [29]. However, even such a time and cost-intensive validation procedure cannot ensure accurate predictions for a large diversity of dynamic or realistic profiles, particularly when taking into account the reported path dependence within many battery ageing factors [35]. Summarising, this high amount of laboratory tests necessary to a proper development and validation, considerably increases the development cost of ageing models. However, trying to reduce the laboratory testing labours arise an uncertainty on the validity of the resulting model to perform predictions under realistic operating profiles.

Trade-off: model development cost vs accuracy

Learn from in-field data?

In order to reduce the number of laboratory tests and at the same time ensure the validity of the model under realistic profiles, the solution proposed in this thesis is the development of ageing models capable to continuously learn from streaming data. Following this approach, reduced laboratory tests could be used to develop a preliminary ageing model. Further, once the battery pack has been implemented and deployed, in-field data extracted by the Data Acquisition System (DAS) could allow updating the preliminary ageing model. In this way, the ageing model would be continuously upgraded, improving prediction accuracy, extending the operating window of the model itself and providing useful information for predictive maintenance, adaptive energy management strategies or business case redefinition. This approach is illustrated in Figure 2.

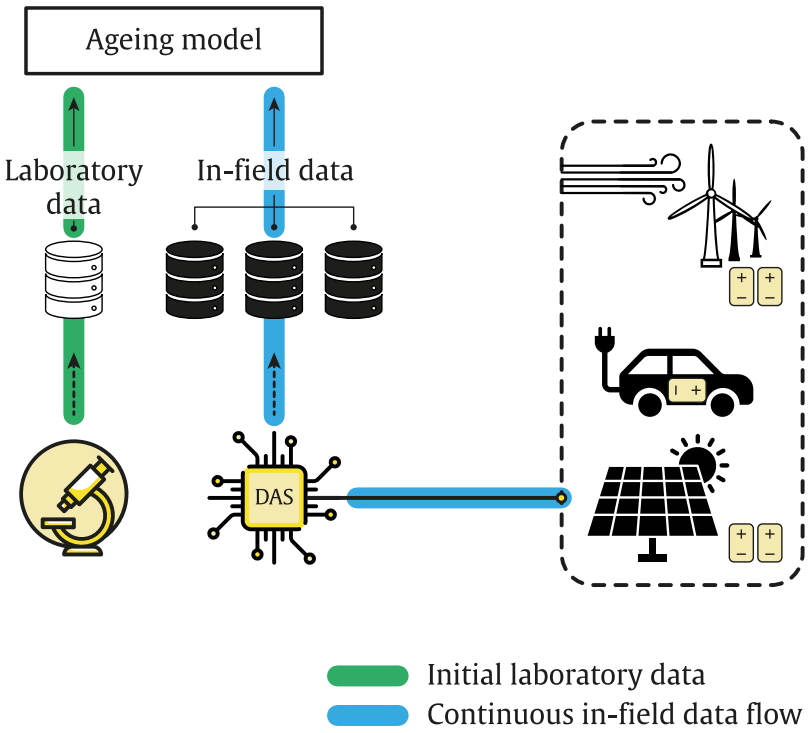

Figure 2. Ageing model training approach proposed in this thesis.

The proposed solution comes aligned with the digitalisation trends observed in the recent years in different areas [36–39]. In fact, there is significant interest from industry in the introduction of new data collection telemetry technology. This implies the forthcoming availability of a significant amount of real-world battery operation data. In this context, the development of ageing models able to learn from in-field battery operation data is an interesting solution to mitigate the need for exhaustive laboratory testing, reduce the development cost of ageing models and at the same time ensure the validity of the model for prediction under real operating conditions.

Digitalisation

In this context, the main objective formulated for this thesis is the following:

The development of an ageing model for Li-ion batteries, capable of learning continuously from the operation data collected from the battery systems deployed in real applications.

This main objective encompasses several secondary goals:

- **The ageing model must be able to perform accurate predictions for a wide range of applications.** This implies that the model must be prepared to predict the ageing of battery systems submitted to

different use-cases, involving purely calendar usages, continuously cycling usages, as well as mixed usages in which both forms of operation take place sequentially.

- **The minimum number of laboratory experiments required for the development of a relatively accurate initial ageing model is desired to be quantified.** Such initial ageing model could be used for the different tasks necessary prior the battery system deployment, e.g. system sizing, definition of initial energy management strategies, etc.

The abovementioned objectives suggest several initial directions for the ageing model to be developed. Firstly, the implication of a progressively increasing training dataset orients into data-driven modelling approaches, fed with in-field measurable variables. This initial orientation leads to the formulation of a basic hypothesis:

Hypotheses

In-field measurable variables

H0: the relations between the operation and the underlying ageing of Li-ion batteries could be described based only on in-field measurable variables.

Furthermore, the ageing models typically presented in the literature are designed and validated to predict the ageing at i) purely calendar operation, ii) purely cycling operation, or iii) very specific operating profiles corresponding to a precise application. However, the development of an overall predictive framework adapted to a wide range of applications and use-cases is a challenging task. A possible direction to achieve this objective could be the development of two separated ageing models, respectively designed for pure calendar and cycle operations, which would be combined to perform predictions under mixed operating profiles. Accordingly, the following hypothesis is formulated:

Separate calendar and cycling

H1: The development of separated calendar and cycle ageing models could be a valid approach to predict accurately the overall degradation of Li-ion batteries.

As previously mentioned, the ageing tests carried out in laboratory and used to parametrise initial ageing models, mainly involve constant operating conditions for each tested cell throughout the whole duration of the test, as illustrated in **Figure 1**. (a). Conversantly, the operation in real application is barely constant over time, and many applications imply highly varying current profiles, see **Figure 1**. (c). This leads to the subsequent hypothesis, related to the applicability of initial ageing models exclusively trained with laboratory data:

H2: Ageing models trained with static ageing laboratory tests may be able to perform accurate predictions at dynamic and realistic operating profiles different from those observed in the laboratory.

About training with static profiles

Furthermore, in order to predict the ageing corresponding to highly varying operating profiles expressed in terms of in-field measurable variables, such variables profiles must be converted into input vectors compatible to the models trained at constant conditions. This compatibility is also necessary to update the developed models with the data collected in-field. In other words, the training data collected from laboratory and the training data collected in-field should share an identical structure. Accordingly, further hypotheses must be defined:

H3: Converting the continuous operation data measurable in-field (see **Figure 1**. (c)) into equivalent dynamic profiles of the different stress-factors (see **Figure 1**. (b)), could be a valid approach to:

In-field data processing

H3.1: perform accurate predictions at real operating conditions.

H3.2: learn about the influence of new operating conditions on battery degradation and update an ageing model based on laboratory data while still improving its prediction performances[1].

As previously mentioned, one of the goals of this thesis is the mitigation of the amount of laboratory tests required to achieve accurate ageing models, and subsequently the reduction of the models' development cost. The whole thesis is then articulated around the evaluation of the following core hypothesis:

H4: The development of ageing models able to learn from in-field battery operation data could allow mitigating the needs for exhaustive laboratory testing.

Minimise laboratory tests

Finally, a last hypothesis is formulated related to the nature of the updating process of the modelling framework adopted in this thesis, which is selected after the study of the state of the art. Although such hypothesis is properly introduced in Section 1.3.3, it is reproduced here for convenience:

[1] The different metrics adopted to evaluate the prediction performances of the ageing model are further described in Chapter 3.

H5: The nonparametric frameworks are able to learn about the influence of new values of the different stress-factors on battery degradation, including new data in the training set.

Beyond the completion of the above-mentioned objectives, this thesis aims to evaluate the different hypotheses formulated. For this purpose, the dissertation document has been organised in five main chapters.

Document organisation

Chapter 1 aims to identify the most suitable data-driven modelling framework for the development of ageing models able to: i) learn continuously from the newly available data, and ii) minimise to the extent possible the laboratory tests required for the development of the initial ageing model. For this purpose, a systematic and critical review of the state of the art is presented, which reviews, classifies and compares the different methods proposed in the literature in this field. The main gaps of the literature are identified, and the most suitable modelling frameworks are suggested.

Chapter 2 introduces the overall methodology designed to govern the main research activities carried out in this thesis. The designed methodology aims to i) lead to the development of an ageing model complying with the objectives of the thesis, ii) to fulfil the gaps identified during the analysis of the state of the art and iii) to assess the different hypotheses formulated at the outset of the research activities.

Chapter 3 corresponds to the development of an ageing model for Li-ion batteries operating at storage conditions. The model is trained with ageing data produced in laboratory at different stress-factors values (temperature and SOC storage condition) and is validated at static and dynamic profiles of such stress-factors. The ability of the developed model to learn progressively from new data is illustrated. The minimal number of laboratory tests required for the design of an accurate initial calendar ageing model is quantified. Finally, a sensitivity analysis of the capacity loss with respect to the different stress-factors is derived from the developed model.

Chapter 4 follows analogous objectives and structure of Chapter 3, transposed to the development of an ageing model tailored to a purely cycling use-case. The model is developed based on an extensive dataset produced in laboratory considering the main stress-factors specific to the cycling operation (temperature, DOD, middle-SOC, charging and discharging currents).

Chapter 5 corresponds to the integration of both calendar and cycle ageing models developed respectively in Chapter 3 and Chapter 4. The complete

model is validated under realistic operating profiles for two different applications, namely EV driving scenarios and power smoothing renewable energy integration application. Data processing algorithms are designed to i) convert in-field measurable current, voltage and temperature time series into input vectors compatible to the ageing models developed in Chapter 3 and Chapter 4, and ii) decompose the overall ageing periodically observed in-field into its calendar- and cycle-induced ageing components. The ability of the developed models to learn progressively from the data provided by cells operating under realistic profiles is evaluated.

Finally, Chapter 6 draws the main conclusions from the different activities carried out in the thesis. The contributions of the thesis are enumerated, and the limitations of developed models are stated, highlighting the identified further works and uncertainty areas in the study. The formulated hypotheses are evaluated, and future research paths are proposed for the development of next generation ageing models for Li-ion batteries.

Chapter 1.

State of the Art

This chapter aims at reviewing, classifying, and comparing the different methods proposed in the literature for the development of ageing models capable of continuously learning from streaming data

This chapter is structured as follows, Section 1.1 classifies the different updating methods proposed in the literature for Li-ion battery ageing models, and defines specific criteria to assess and compare the accuracy and computational cost of the different models. Section 1.2 describes and evaluates in detail these different methods proposed in the literature. Finally, in Section 1.3 the different methods are compared based on the defined criteria, the main gaps of the literature are identified and a specific modelling framework is selected to carry out the different research activities of the thesis.

1.1. Identification of model updating methods and definition of assessment criteria

In this section, the different methods used in the literature to periodically update Li-ion battery ageing models are identified, and specific criteria are defined to allow the assessment of such methods.

1.1.1. Characteristics of model updating methods

Amid the different methods presented in the literature, different characteristics influence the ability of a model to update itself.

Parametric vs nonparametric

Firstly, an intrinsic feature of the model is its parametric or nonparametric character. A model is called parametric when the number of unknown parameters is fixed and independent of the size of the dataset. Oppositely, the structure of nonparametric models is not fixed and is allowed to grow with the number of input data. In other words, its complexity is not specified, it is left to be determined from the available data [40].

Periodical re-training

Moreover, two main approaches were identified in the literature to update an ageing model whenever new data is available. The first approach is based on a periodical re-training of the full model developed beforehand. Using experimental training data, a regression technique is applied to relate different variables and build a first ageing model. During the in-field operation of the battery, operating conditions and ageing data are periodically recorded by the DAS, and this new data is combined with the experimental training data, creating a more complete database. The model is then re-trained using the previously selected regression technique, giving rise to an updated ageing model.

Online learning

Batch training

Incremental training

In a situation in which the DAS periodically provides new battery ageing data, the ageing model is still getting trained after the first predictions were performed. There is no clear difference between the training and prediction phases, and this is usually referred as online learning scenario in the Machine Learning discipline [41]. Different training methods were used in the literature to face such situation, namely batch training and incremental training. The batch training method consists on completing the previously available dataset with new data and re-training the model from scratch considering the whole available data. Oppositely, incremental training methods do not consider the whole available dataset to update the model, resulting in computationally fewer intensive algorithms. Different incremental training strategies were proposed for Li-ion battery ageing prediction applications [42,43], further described in sections 1.2.2.2 and 1.2.3.2.

Filtering

The second approach consists in updating the parameters of a parametric model, using filtering techniques. A parametric model is firstly trained on the basis of the experimental data. Once the battery is working on the target application, a Bayesian filter is employed to update model's parameters, using the new measurements continuously provided by the DAS. Table 1 classifies the different research studies identified in the literature, according to the selected updating approach and involved model.

Table 1. Self-adaptive Li-ion ageing models proposed in the literature, according to the selected model and updating approach.

Re-training	Autoregressive Integrated Moving Average (ARIMA)	[44–46]
	Support Vector Regression (SVR)	[42,47–49]
	Gaussian Process Regression (GPR)	[50–53]
	Relevance Vector Machine (RVM)	[43,54–61]
	Artificial Neural Network (ANN)	[62–69]
Filtering	Parametric model	[70–96]

A classification

Figure 3 proposes a classification of the different methods proposed in the literature to proceed to a periodical update of Li-ion battery ageing models.

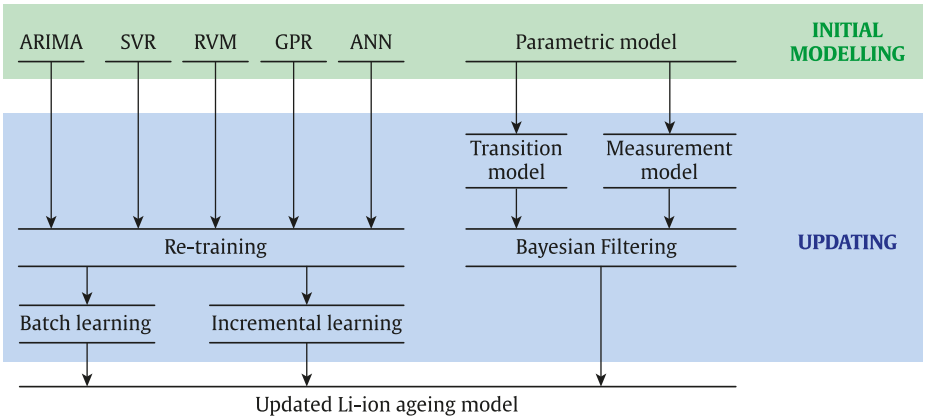

Figure 3. A classification for Li-ion battery ageing models updating methods proposed in the literature.

1.1.2. Definition of assessment criteria for methods' comparison

In order to compare the different model updating methods, specific assessment criteria were defined, and gathered into two main groups.

1.1.2.1. Accuracy

The ability of a model to perform accurate predictions was evaluated according to the following features:

Nonlinearities

A1: Ability to deal with nonlinearities. Relations between some battery stress-factors and HIs are strongly nonlinear [32,33,97]. Furthermore, a Li-ion battery does not necessarily degrade similarly in the Beginning of Life (BOL) and when approaching the End of Life (EOL), even if operating conditions remain the same [98]. Consequently, the initial ageing model, as well as the updating method should ideally be able to consider those nonlinear behaviours.

Uncertainty

A2: Expression of uncertainty. The predictions of the developed model could have a variable reliability. This reliability level should ideally be expressed in the prediction, e.g. in form of a probabilistic quantification of the corresponding uncertainty. Some sources of the prediction uncertainty could be i) the scarcity of training data and ii) the uncertainty on the input and output values' estimation in the training dataset.

The first source is highly relevant, taking into account the objectives stated in the introduction. In fact, considering that the number of Li-ion ageing tests carried out in laboratory is desired to be minimised, the training data available for the development of the initial model is reduced. The influence of some stress-factors' operation range on ageing could be under- or non-represented in the initial training dataset, increasing this way the uncertainty of the model predictions at such operation windows.

The second source of uncertainty could be related to the limited accuracy of the data measurement equipment (e.g. current, voltage and temperature sensing), which induces noise in the training dataset. Furthermore, some of the stress-factors affecting on the ageing of Li-ion batteries, as well as the periodically extracted SOH target training data, are not directly measurable. They need to be estimated through dedicated algorithms with uneven level of accuracy, inducing additional uncertainty in the data.

Therefore, the Li-ion battery ageing prediction models should ideally be probabilistic to express the uncertainty level of the performed predictions [99].

A3: Sensitivity to irrelevant data. In order to perform accurate predictions, a robust behaviour is necessary in front of noisy measurements, outliers and irrelevant data. This is partially related to the bias-variance dilemma and regularisation methods: a suitable model must be able to describe the main trend of the data, without fitting the noise embedded in data.

1.1.2.2. Computational cost

The computational cost is evaluated in terms of computation time and required memory. Since the computational cost of an algorithm is rarely specified in the literature, different criteria were determined to assess the computation requirements of the models published to date.

C1: Indicative computation time. The computation time varies depending on the programming efficiency of the algorithm itself, but also on the hardware in which it is implemented. Consequently, it is difficult to compare the computation time of the different algorithms described in the literature, since they were implemented by different authors and on different platforms. However, indicative information of the computation time was reported, when available.

Big-O complexity

C2: Big-O complexity. The big-O notation provides an order of the growth of the computational complexity in function of the input data size. Taking into account that i) in the context of online learning, the size of the model training vector increases gradually, and ii) the developed ageing models may be implemented in hardware systems with limited memory and computation power (e.g. Battery Management System), it is essential to have an idea about the big-O complexity of each model, both for time and memory requirements, respectively reported as criteria C2.1 and C2.2 (see **Table 2**). The models reviewed in this chapter have a theoretical big-O time complexity, specified in related handbooks or journal publications, and defined in this work as criterion C2.1.1. Furthermore, researchers regularly propose optimised algorithms, reducing the big-O complexity of the original algorithm. The reduced time complexity of any improved algorithm was reported as criterion C2.1.2. No information was provided in the literature with respect to any improvement in the memory complexity, and hence only the theoretical complexity was reported.

C3: Sparsity. This criterion assesses the algorithm's ability to reduce the size of the training dataset, i.e. to work with sparse matrices. Such criterion is crucial for algorithms with an elevated big-O complexity, for which a small increment of the size of the dataset could lead to unacceptable computation times on the real application. Moreover, some of the described models have an inherent ability to reduce the amount of training data.

Table 2 summarises the different criteria defined in this section for model assessment.

Table 2. Summary table of the different criteria for model assessment.

Accuracy	**A1**			Ability to deal with nonlinearities
	A2			Expression of uncertainty
	A3			Sensitivity to irrelevant data
Computational cost	**C1**			Indicative computation time
	C2	**C2.1**	**C2.1.1**	Big-O time complexity (theoretical algorithm)
			C2.1.2	Big-O time complexity (improved algorithm)
		C2.2		Big-O memory complexity (theoretical algorithm)
	C3			Sparsity

1.2. Li-ion battery ageing model updating methods: description and assessment

This section reviews the Li-ion battery ageing models updating methods proposed in the literature. Each subsection corresponds to a specific model, including ARIMA, SVR, RVM, GPR, ANN and particle filtering, and provides: i) a short theoretical explanation, ii) a literature review for Li-ion ageing modelling application, and iii) the assessment of the model based on the criteria defined in Section 1.1.2.

1.2.1. Autoregressive Integrated Moving Average

1.2.1.1. Theoretical basis

Autocorrelation

Moving average

ARIMA models rely on the combination of two main concepts: the autocorrelation and the moving average. The autocorrelation coefficient α measures the linear relation between an observation at sample N and the observations at previous samples $(N-1, N-2, \dots, N-p)$ [100]. In the context of time series forecasting, this concept can be used to perform a linear regression, building thereby an Autoregressive (AR) model of the time series. A Moving Average (MA) is conceptually a linear regression of one or more prior error values of the time series [101]. AR and MA models can be expressed through equations (1) and (2), respectively:

$$\mathbf{y}_{N+1} = \sum_{i=0}^{p-1} \boldsymbol{\alpha}_i \mathbf{y}_{N-i} + \boldsymbol{\varepsilon}_{N+1} \quad (1)$$

$$\mathbf{y}_{N+1} = \sum_{i=0}^{q-1} \boldsymbol{\beta}_i \boldsymbol{\varepsilon}_{N-i} \quad (2)$$

where $\mathbf{y}_N$ is the N^{th} target value; $\boldsymbol{\alpha}_i$ is the autocorrelation coefficient at lag i; $\boldsymbol{\varepsilon}_N$ is the residual corresponding to the N^{th} target value; $\boldsymbol{\beta}_i$ is the weight applied to the residual at lag i; parameters p and q respectively represent the order of AR and MA models, i.e. the number of prior data taken into account for the regression.

The sum of both equations results in an ARMA model. The main idea is that the AR model captures the linear trend of the time series, and the MA model represents the uncertainty through previous errors regression. As ARMA model estimation could be skewed by a seasonal or cyclical component of time series, a previous differencing stage of the dataset is sometimes used, completing the ARIMA framework.

1.2.1.2. Application to Li-ion battery ageing modelling

Several ARIMA models were presented in the literature for Li-ion battery ageing prognosis. Long et al. [44] built an AR model for capacity prediction. At each prediction step, an optimization algorithm was used in order to determine the optimal order of the AR model. Figure 4. (a) shows the obtained prediction curve. It can be observed that the AR model was not able to fit the nonlinear trend of the measured capacity fade.

Optimal order AR

Liu et al. attempted to solve this problem applying to the AR model an empirical two parameter nonlinear degradation factor correlated with the number of cycles performed by the cell [45]. Figure 4. (b) displays the results obtained with their approach at different ageing stages. Reversible capacity recoveries are punctually observable in the experimental dataset, typically due to electrochemical cell relaxation after a pause or idle period [61,102]. Such reversible capacity recoveries were linked in the literature to the anode overhang (geometrically oversized anode compared to the cathode) and to the homogeneity of lithium distribution [103]. Performing predictions from those capacity peak points may provide erroneous results, as it can be observed in the pink line (Prediction by ARIMA) in Figure 4. (c).

Reversible capacity recoveries

Zhou et al. tried to avoid such difficulties employing a time series decomposition method on the battery ageing dataset, obtaining thereby different components of the initial dataset [46]. Then, an ARIMA model was built independently for each dataset component. After combining the several ARIMA models a complete capacity prediction model was generated, leading to improved prediction results, as displayed by the red line (Prediction by EMD-ARIMA) in Figure 4. (c).

Time series decomposition

In the several literature publications previously mentioned [44–46], the predictions of the ARIMA models were performed considering a limited number of previous capacity data points, corresponding to the order of the model. The validity of such approach is questionable for Li-ion battery ageing prediction since the capacity loss caused by any cycle performed under any given condition is not necessarily the same for new and aged cells [98]. Hence, the predicted linear trend may not be representative for long-term predictions. Furthermore, the dataset used for training and validation of the ARIMA models corresponded to a single cell aged under constant operating conditions, and models were not validated at different operating conditions.

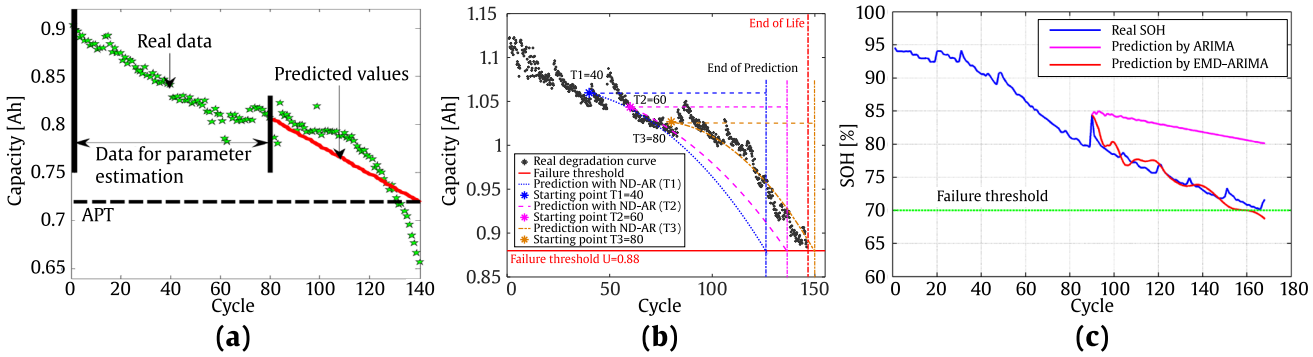

Figure 4. Li-ion battery ageing predictions obtained through (a) optimal order AR model [44]**, (b) nonlinear factor AR model** [45]**, and (c) ARIMA model combined with time series decomposition method** [46]**. In subfigure (a), APT signifies Acceptable Performance Threshold.**

1.2.1.3. Assessment through defined criteria

Parametric

The ARIMA framework proposes a parametric autoregressive method to solve an online learning situation. The training vector size is limited by the order of the model. While the model order remains constant, learning each new data sample is accompanied by the removing of the older one. Long et al. performed the optimal order calculation at each re-training step [44], but the size of the input vector did not change significantly. Fast deletion of the old data makes the ARIMA model very reactive but unstable.

Nonlinearities

ARIMA models are not able to describe nonlinear relations (A1). Although some works proposed empirical nonlinear versions relating the battery capacity and the cycle number [45], it would be complicated to employ such methods to develop predictive models including different stress-factors.

Uncertainty

Besides, ARIMA models do not output probabilistic predictions (A2), which would be the ideal solution to manage uncertainty, as specified in Section 1.1.2.1. However, the MA component performs a regression of previous residuals, which could be considered as an indirect way to take uncertainty into account.

Sensitivity

ARIMA is highly sensitive to outliers and irrelevant data (A3). In fact, only previous p data is used for training, without any mechanism to assess data relevance, and this could skew the prediction (e.g. as in Figure 4. (c), where ARIMA is computed during a reversible capacity recovery stretch).

Computational cost

The computational complexity of a low-order ARIMA model is relatively low. As long as the model order does not vary, the size of the training vector does not increase. Then the model keeps more or less a constant computational time, and the big-O complexity cannot be conceived (C2). In this sense, such model benefits from a considerable advantage compared to other more complex regression techniques, in which growing training vectors or matrices are typically used. Finally, ARIMA could be regarded as a very sparse method (C3), as it considers only a few data samples of the dataset. Nevertheless, the relevance of last p data is questionable for long term predictions.

1.2.2. Support Vector Regression

1.2.2.1. Theoretical basis

The theoretical explanations given below are mainly based on Smola and Schölkopf's work [104]. Considering the input training vector $\mathbf{x} = (\mathbf{x}_1, \dots, \mathbf{x}_N)$ and the target training vector $\mathbf{y} = (\mathbf{y}_1, \dots, \mathbf{y}_N)$ in the input space $\mathcal{X}$, the main idea of an SVR is to find a function $f(\mathbf{x})$, which meets two requirements: i)

to be as flat as possible and ii) to obtain an error of $f(\mathbf{x})$ smaller than a properly defined constant ϵ[2], for all training data.

Flatness and error restriction

Considering equation (3) as a general definition of a linear regression, where $\langle \mathbf{w}, \mathbf{x} \rangle$ denotes the dot product of vectors $\mathbf{w}$ and $\mathbf{x}$ in the input space $\mathcal{X}$, it is possible to formally write the flatness and error restriction objectives using the standard form of optimisation problems, as defined by equations (4) and (5), where $\mathbf{w}$ is the vector of parameters and $\boldsymbol{\varepsilon}$ denotes the bias or residual.

$$f(\mathbf{x}) = \langle \mathbf{w}, \mathbf{x} \rangle + \varepsilon \tag{3}$$

$$\text{minimise} \quad \frac{1}{2}\|\mathbf{w}\|^2 \tag{4}$$

$$\text{subject to} \quad \begin{cases} \mathbf{y}_i - \langle \mathbf{w}, \mathbf{x}_i \rangle - \varepsilon \leq \epsilon \\ \langle \mathbf{w}, \mathbf{x}_i \rangle + \varepsilon - \mathbf{y}_i \leq \epsilon \end{cases} \tag{5}$$

The flatness can be traduced as a $\mathbf{w}$ minimisation task, and it can be evaluated using the Euclidean norm, i.e. $\|\mathbf{w}\|^2$. The error restriction is represented through the ϵ-sensitive loss function, defined as:

ϵ-sensitive loss function

$$L\big(\mathbf{y}, f(\mathbf{x})\big) = \begin{cases} |\mathbf{y} - f(\mathbf{x})| - \epsilon, & \text{if } |\mathbf{y} - f(\mathbf{x})| > \epsilon \\ 0, & \text{if } |\mathbf{y} - f(\mathbf{x})| \leq \epsilon \end{cases} \tag{6}$$

As both loss functions are convex, SVR can be resumed as a convex optimisation problem. Therefore, a single minimum exists and SVR is not affected by the problem of local minima. As shown in equation (6), the ϵ-sensitive loss function only considers errors larger than ϵ, and each data sample fulfilling this requirement is called Support Vector (SV).

Support Vectors

Equation (5) assumes that a function f which approximates all pairs $(\mathbf{x}_i, \mathbf{y}_i)$ with ϵ precision exists, i.e. that the convex optimisation problem is feasible. When that is not the case, some errors could be allowed, and the so-called slack variables $\boldsymbol{\xi}_i$ and $\boldsymbol{\xi}_i'$ are introduced to provide increased flexibility, obtaining the formulation stated by Vapnik in [105] and described in equations (7) and (8). A constant $C > 0$ is introduced in order to control the trade-off between the flatness of $f(\mathbf{x})$ and the tolerated error deviations (trade-off between bias and variance).

Slack variables

[2] More information about the selection of ϵ in [104].

$$\text{minimise} \quad \frac{1}{2}\|\mathbf{w}\|^2 + C\sum_{i=1}^{N}(\boldsymbol{\xi}_i + \boldsymbol{\xi}_i') \tag{7}$$

$$\text{subject to} \quad \begin{cases} \mathbf{y}_i - \langle \mathbf{w}, \mathbf{x}_i \rangle - \varepsilon \leq \epsilon + \boldsymbol{\xi}_i \\ \langle \mathbf{w}, \mathbf{x}_i \rangle + \varepsilon - \mathbf{y}_i \leq \epsilon + \boldsymbol{\xi}_i' \\ \boldsymbol{\xi}_i, \boldsymbol{\xi}_i' \geq 0 \end{cases} \tag{8}$$

The duality principle specifies that any optimisation problem may be split into the primal problem (minimisation task) and the dual problem (error restriction). A dual formulation can be obtained constructing the Lagrangian loss function (equation (9)).

Lagrangian loss function

$$L := A + B - D - E - F \qquad \text{where} \qquad \begin{aligned} A &= {}^1\!/_2\,\|\mathbf{w}\|^2 \\ B &= C\sum_{i=1}^{N}\left(\boldsymbol{\xi}_i + \boldsymbol{\xi}_i'\right) \\ D &= \sum_{i=1}^{N}\boldsymbol{\alpha}_i(\epsilon + \boldsymbol{\xi}_i - \mathbf{y}_i + \langle \mathbf{w}, \mathbf{x}_i \rangle + \varepsilon) \\ E &= \sum_{i=1}^{N}\boldsymbol{\alpha}_i'(\epsilon + \boldsymbol{\xi}_i' + \mathbf{y}_i - \langle \mathbf{w}, \mathbf{x}_i \rangle - \varepsilon) \\ F &= \sum_{i=1}^{N}\left(\boldsymbol{\eta}_i\boldsymbol{\xi}_i + \boldsymbol{\eta}_i'\boldsymbol{\xi}_i'\right) \end{aligned} \tag{9}$$

The term A corresponds to the flatness objective; the term B reflects the cost of slack variables. Both terms resume the primal problem, and then $(\mathbf{w}, \varepsilon, \boldsymbol{\xi}_i, \boldsymbol{\xi}_i')$ are called primal variables. Terms D, E and F represent the constraints of the optimisation problem, and $(\boldsymbol{\alpha}_i, \boldsymbol{\alpha}_i', \boldsymbol{\eta}_i, \boldsymbol{\eta}_i') \geq 0$ are the dual variables or Lagrange multipliers.

Due to the convexity of the Lagrangian loss function, optimal values of the primal variables $(\mathbf{w}, \varepsilon, \boldsymbol{\xi}_i, \boldsymbol{\xi}_i')$ could be obtained solving the partial derivatives of the loss function with respect to such variables. The vanished partial derivative of L with respect to $\mathbf{w}$ leads to the equation (10), and therefore $f(\mathbf{x})$ can be re-written as in the equation (11).

$$\mathbf{w} = \sum_{i=1}^{N} (\boldsymbol{\alpha}_i - \boldsymbol{\alpha}_i') \mathbf{x}_i \tag{10}$$

$$f(\mathbf{x}) = \sum_{i=1}^{N} (\boldsymbol{\alpha}_i - \boldsymbol{\alpha}_i') \langle \mathbf{x}_i, \mathbf{x} \rangle + \varepsilon \tag{11}$$

Thanks to the Lagrangian dual formulation, parameter $\mathbf{w}$ is expressed as a linear combination of the training data $\mathbf{x}_i$, and the complete algorithm can therefore be described in terms of dot product of the input data.

If the data does not follow a linear trend, a preliminary stage of data preprocessing could be applied in order to capture nonlinear trends. The main idea is to bring the input vector $\mathbf{x}$, defined in the low-dimensional input space $\mathcal{X}$, to some high-dimensional feature-space $\mathcal{F}$, via a basis function ϕ (also called mapping function). The dot product of two mapped input vectors in the feature space is defined as kernel function (12).

$$\kappa(\mathbf{x}, \mathbf{x}') = \langle \phi(\mathbf{x}), \phi(\mathbf{x}') \rangle \tag{12}$$

Kernel trick

A nonlinear regression task in the input space $\mathcal{X}$ becomes linear in the feature space $\mathcal{F}$, and this is typically called the kernel trick. Thereby, the nonlinear function $f(\mathbf{x})$ can be expressed as:

$$f(\mathbf{x}) = \sum_{i=1}^{N} (\boldsymbol{\alpha}_i - \boldsymbol{\alpha}_i') \kappa(\mathbf{x}_i, \mathbf{x}) + \varepsilon \tag{13}$$

In practice, no information is required with respect to the feature space or the basis function ϕ. Choosing the adequate kernel function, the insensitivity parameter ϵ and the trade-off parameter C would be sufficient to build the algorithm.

1.2.2.2. Application to Li-ion battery ageing modelling

In the literature, different Li-ion lifetime estimation methods were proposed based on SVR modelling. Nuhic et al. introduced an SVR based model, trained with experimental data obtained in different operating conditions (temperature, SOC, DOD and C-rate) [47]. Six high power Li-ion cells, three new cells and three aged, were stressed according to real driving profiles recorded in different hybrid vehicles. The available dataset was split into a training set, composed by 2/3 of the available data, and a validation set, composed by 1/3 of the data. Battery SOC, temperature and current data were preprocessed through dwell-time counting and rainflow counting methods to train the developed ageing model. The dwell-time counting provided information about the occurrence frequency of a certain

Dwell-time and rainflow counting

combination of the values of two different stress-factors. In this case, the occurrence of some temperature and current values combination, and some SOC and temperature values combination were counted during the battery cycling. Rainflow counting quantified the number of cycles occurred at different DODs. The input training vector was composed of the results obtained from the dwell-time and rainflow counting, and the target training vector stored the corresponding measured capacity data. Thereby, a linear kernel SVR was used to build the relation between the capacity and the number of events counted by dwell-time and rainflow counters.

Linear kernel

Figure 5 shows the capacity prediction results obtained for two cells. To perform a prediction, the operating conditions of the last training load profile were used as model input. The model initially tended to overestimate the capacity fade, as it can be observed in Figure 5 (1st prognosis instant, indicated by the leftmost dashed bar). According to the publication, this was mainly due to the less intense conditions of the second ageing phase marked between the two dashed bars [13]. The second ageing prediction took such milder operating conditions into account, providing a less pessimistic prediction. In order to assess the ability of the model to generalise its predictions, validation data included new load profiles and temperatures from those observed in the training process. The accuracy of the prediction was not significantly affected. In this work, model training was focussed on EV real driving profiles, and its implementability in different applications is questionable.

In [48], Patil et al. proposed a different strategy for the Remaining Useful Life (RUL) estimation. Assuming that for onboard scenarios an accurate RUL estimation is only required when the battery is close to the EOL, a two-stage strategy was adopted. First, the quartile of the cell lifetime was determined by a Support Vector Machine (SVM[3]) classifier. Secondly, if the cell was working in the last quartile of its life, an SVR model estimated the RUL more accurately. The strategy was applied considering the ageing data of 19 cells from the NASA repository [106], which were aged at different temperatures, DODs and C-rates. Among eight different features extracted from the battery voltage, current and temperature curves, two of them involving voltage values were selected as input data, and the lifetime quartile of the cell was defined as target data. Then, the SVM was trained using a Gaussian kernel.

SVM classifier

SVR for RUL prediction

Voltage-based inputs

[3] In this chapter, the term SVM refers to the classification algorithm analogous to the SVR.

The SVR lifetime model used the same 2 features in the input training vector, but the target training data was changed for direct RUL values.

Different types of kernels were assessed, and the Multi-Layer Perceptron kernel showed the most accurate results. The cycles of the 19 datasets were randomly split, using 70% of the data for training and 30% for validation. In the validation set, the classification accuracy was 81.17%, and a 0.357% Root Mean Square Error (RMSE) value was obtained on the RUL estimation. This methodology was patented by Samsung Electronics Co., Ltd. [49]. In this work, the model outputs RUL values, defining the EOL as a 20 or 30% capacity fade threshold, depending on the dataset. This criterion is typically used for EV application [107] but could be debatable for other applications where the capacity requirements were not so restrictive as in electromobility. Simply providing a certain capacity prediction value could be adequate for a wider applicability.

Incremental training

Zhou et al. applied an incremental training method (described in Ref. [108]) to a Li-ion battery ageing model for online SVR training [42]. When a new capacity data point $\mathbf{x}_c$ arrives, the algorithm tries to find the corresponding optimal coefficient $\mathbf{w}_c = (\boldsymbol{\alpha}_c - \boldsymbol{\alpha}'_c)$, which would be integrated into equation (13). For this purpose, the basic idea was to change $\mathbf{w}_c$ in a finite number of discrete steps until it meets Karush-Kuhn-Tucker conditions[4]. The relation between each w_c increment and the corresponding update of the optimal parameters related to the older data was previously established.

Decremental algorithm

Furthermore, the method integrated a decremental algorithm, analogous to the incremental one, to allow the unlearning or removal of the old data. The method was experimented with a single cell cycled under constant operating conditions [106], and the Mean Absolute Error (MAE) obtained was 0.026 Ah for a 50 cycles-ahead prediction. Nevertheless, the model did not take into account any battery stress-factors and was not validated for different operating conditions.

[4] Necessary conditions for a solution to be optimal.

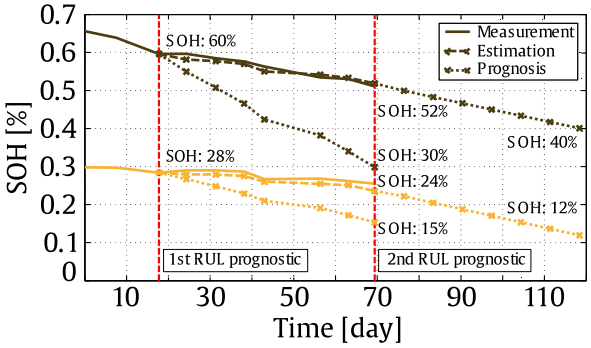

Figure 5. Li-ion battery ageing predictions obtained through counting methods and SVR, for two different cells [47].

1.2.2.3. Assessment through defined criteria

Nonparametric

The SVR algorithm proposes a nonparametric regression method, which could be updated through model re-training. Both batch [47–49] and incremental [42] training methods were applied to Li-ion battery lifetime estimation in the literature. The incremental and decremental algorithms described in [42,108] allowed integrating rapidly each newly available data sample, and progressively unlearn samples that did not contribute to the SVR solution. Thereby, a good trade-off could be ensured between the stability and reactivity of the model. Furthermore, such approach improved drastically the computational complexity of the SVR training, as it will be reviewed in the C2 criterion.

Batch & incremental learning

Nonlinearities

SVR models are able to capture nonlinear relations by preprocessing input data through the kernel use (A1). Kernel selection is a critical task in SVR modelling [42], but there is not any universally accepted method in the literature in order to choose the most suitable kernel. The predictions of SVR models are not probabilistic (A2), and the RVM algorithm, discussed in Section 1.2.3, provides a probabilistic framework in which SVR main concepts are recovered. The use of a ϵ-insensitive loss function makes the algorithm less sensitive to small deviations, as deviations smaller than ϵ are not taken into account (A3). A correct selection of the parameter ϵ should allow capturing the main trend of the curve, reducing model sensitivity when facing small local data fluctuations. Nevertheless, it is noteworthy that important deviations such as outliers would likely become SVs, then participating in the optimisation of the model.

Uncertainty

Sensitivity

The big advantage of properly optimised SVR is its ability to condense thousands of training points to a manageable number of SVs [47]. In fact, the use of the ϵ-insensitive loss function makes SVR a very sparse solution (C3). As indicative information, Patil et al. reported the computational cost of the

Computational cost

proposed methodology implemented on a desktop MATLAB system (Intel i3 3.2 GHz dual-core processor, 4.0 GB RAM, 32-bit Microsoft Windows 7): the computation time for RUL estimation of the battery (including feature computation, classification and regression) was c.a. 1.26 ms, for 196 cycles (C1). Solving a quadratic programming task (as the Lagrangian problem during SVR training step) supposes in general O(n^3) growing in computation time (C2.1.1) and O(n^2) in memory (C2.2) [40]. However, since Platt proposed a Sequential Minimal Optimisation (SMO) algorithm to solve quadratic programming [109], SVR training is usually faster. An efficient implementation of SMO lead to an empirical training time that scales between O(n) and O($n^{2.3}$) [40]. Furthermore, using the incremental training of the SVR algorithm, Ma et al. improved the computational complexity to the order of O(log(n)) (C2.1.2) [108].

1.2.3. Relevance Vector Machine

1.2.3.1. Theoretical basis

Probabilistic & sparse

The RVM emerged in 2001 in order to improve some aspects of the SVM algorithm [99]. Indeed, two main advantages over the SVR are: i) the probabilistic character of the estimation, and ii) the higher degree of sparsity observed in practice. The basic idea is that the training data points that are not significantly contributing to describing the overall trend defined by the remaining data points should be removed, resulting in a sparse model [110].

Relevant Vectors

Survival data are called Relevance Vectors (RVs), and the number of RVs is usually more reduced than the number of SVs in SVR models. RVM explanations below are based on [43,99].

The relationship among inputs $\mathbf{x} = (\mathbf{x}_1, \dots, \mathbf{x}_N)$ and targets $\mathbf{y} = (\mathbf{y}_1, \dots, \mathbf{y}_N)$ is described by a model $f(\mathbf{x})$ and error ε. As specified in equation (14), the model $f(\mathbf{x}_i)$ is a linear combination of basis functions $\boldsymbol{\phi}_j(\mathbf{x}_i)$, defined as $\boldsymbol{\phi}_j(\mathbf{x}_i) \equiv \kappa(\mathbf{x}_i, \mathbf{x}_j)$ (the concepts of basis function ϕ and kernel κ were introduced in Section 1.2.2.1).

$$f(\mathbf{x}_i) = \sum_{j=1}^{N+1} \boldsymbol{\phi}_j(\mathbf{x}_i)\mathbf{w}_j = \boldsymbol{\phi}(\mathbf{x}_i)\mathbf{w} \qquad (14)$$

being $\mathbf{w} = [\mathbf{w}_1, \dots, \mathbf{w}_{N+1}]^T$ the column of weights, and $\boldsymbol{\phi}(\mathbf{x}_i) = [1, \boldsymbol{\phi}_1(\mathbf{x}_i), \dots, \boldsymbol{\phi}_N(\mathbf{x}_i)]$ the vector of basis functions relating the input data $\mathbf{x}_i$ to the set $\mathbf{x}$. Defining Φ as a $N \times (N+1)$ matrix with $\Phi = [\boldsymbol{\phi}(\mathbf{x}_1), \dots, \boldsymbol{\phi}(\mathbf{x}_N)]^T$, target values can be expressed in matrix notation, as described in equation (15).

$$\mathbf{y} = \Phi\mathbf{w} + \varepsilon \qquad (15)$$

The error ε is assumed to be a zero-mean Gaussian noise with variance σ^2. Therefore, the likelihood of the function y (equation (15)) can be expressed as

$$p(\mathbf{y}|\mathbf{w},\sigma^2) = (2\pi\sigma^2)^{-N/2}\exp\left\{\frac{-1}{2\sigma^2}\|\mathbf{y}-\Phi\mathbf{w}\|^2\right\} \quad (16)$$

Nonparametric

Due to its nonparametric nature, there are as many parameters in the model as training samples, which could lead to severe overfitting problems. To avoid such problem, additional constraints are imposed on the parameters. When the model is parameterised by the likelihood maximisation, a 'complexity' penalty term is added to the marginal likelihood to avoid overfitting. Otherwise, in a Bayesian setting, a prior probability distribution is defined upon the parameters [5]. Using such prior distribution, the likelihood (defined in equation (16)) and the Bayes' rule, the posterior distribution of the weights can be calculated. In this way, most probable weight values are iteratively estimated from the data.

Avoiding overfitting

1.2.3.2. Application to Li-ion battery ageing modelling

The most relevant and comprehensive work on ageing model updating methods proposed in the literature was a fatigue model approach presented by Nuhic et al. [43]. The model was initially trained using experimental laboratory ageing data of three pairs of high-power Li-ion cells for Hybrid Electric Vehicle (HEV) application, degraded through cyclically repeated real-world current profiles at room temperature. Input data was organised using a rainflow cycle-counting algorithm: each cycle was classified in function of the corresponding mean temperature, mean voltage, charge or discharge C-rate and DOD, building in that way a histogram reflecting the number of performed cycles at different operating conditions. Associated capacity data was used as target to train the RVM.

Rainflow counting

The authors aimed at updating such initial model with further data obtained during Battery Management Systems (BMS) testing and HEV durability testing steps. For this purpose, two different models were developed: i) a model oriented to vehicle fleet management and off-board application, updated using a batch training strategy, and ii) a model designed for onboard implementation, adopting an incremental learning strategy originally proposed for SVR in [111], and also implemented with RVM in [54,55] for Li-ion ageing prediction. The incremental adaptive procedure was the following: whenever a new data sample was available and the last prediction

Batch training for fleet management

Incremental learning for onboard implementation

[5] Further explanations on prior distributions selections are detailed in [99].

error was higher than a certain threshold, a new training set was created including previous RVs and the new data sample. Then, the RVM was subsequently re-trained. This approach allowed a reduced computation and memory cost but assumed the disadvantage that all data assessed as irrelevant were deleted, even if it could be potentially relevant in a future training.

Comparing SVR and RVM

The models were updated using other six cells at different degradation levels, which were exposed to varying real operating profiles, in terms of current, temperatures and SOC occurred during the BMS testing and HEV durability tests. Furthermore, both batch and incremental RVM models were compared with analogous SVR models. Although obtained results were similar, the RVM framework was chosen due to its probabilistic outputs.

The developed models required to know the operating conditions of future cycles as input information, in order to predict the battery degradation. As future battery operation is not known, the input data used for the off-board model prediction was obtained by randomly placing cycles in a continuous probability density extracted from the histogram of the counted cycles. Such method could not be applied to the onboard prediction model due to the limited computational capabilities, and hence the future battery load was achieved weighting the already stored input values.

Finally, both RVM models were validated on an HEV battery cycled in laboratory according to recorded real duty cycles profiles. Prediction results, displayed in Figure 6. (a), showed very spread confidence intervals, which should be narrowed for increased accuracy. Calendar ageing, which may be especially relevant considering that most vehicles remain parked the biggest part of the day [30], was not considered in this work.

Parametric model

Wang et al. introduced a method combining the RVM algorithm with an empirical three-parameter capacity degradation model, which related capacity (target data) and the number of cycles performed (input data) [56]. The model was trained with experimental battery ageing data, obtained at a single constant operating condition and provided by CALCE research group [112]. The RVM algorithm was only used in order to identify the relevant training vectors and calculate the uncertainty boundaries associated with the target training data. At each prediction step, the empirical degradation model was trained with the RVs through nonlinear least-squares regression, and capacity predictions were computed until reaching the 80% EOL threshold. The method was applied to three different cells, performing predictions at various ageing stages, and the biggest Absolute Error (AE) was 9 cycles. An analogous method was proposed in [57], using a two-term

RVM to identify relevant data

exponential empirical model and improving the kernel selection of the RVM, but similar results were obtained.

Time series decomposition

Zhang et al. assumed the reversible capacity recovery phenomenon as noisy data [58], and they decided to apply a time series decomposition method to the battery ageing dataset (NASA's data [106]). Further, they used an optimisation algorithm in order to determine the value of the Gaussian kernel parameter. The obtained RVM model predicted capacity on the basis of the amount of performed cycles input data. The same authors used a similar approach in a posterior work [59], involving a multiple kernel RVM which was the weighted sum of thirteen different kernels. Weights and parameters corresponding to every single kernel were calculated using the optimisation algorithm. The method was applied to two different cells, performing predictions at various ageing stages, and the biggest Mean Square Error (MSE) was 6.6203e-04 Ah. Results were compared with an SVR algorithm, showing more accurate predictions for the proposed RVM approach.

Voltage falloff HI

Noticing that full charge/discharge cycles were hardly realisable in in-field operation, and consequently that it was difficult to obtained capacity and resistance data, Zhou et al. proposed a novel battery HI based on the voltage falloff in the discharge voltage curve [60], – understood as the difference between the maximum battery voltage and the voltage measured after 1000s of discharge (at a certain constant rate). A Gaussian kernel RVM model was used to capture the relation between the voltage falloff target and the amount of performed cycles. The 80% of the rated capacity EOL criterion was translated to the voltage falloff HI. For a 44 steps-ahead prediction, a 0.0117 Ah RMSE of the capacity curve and an AE of 4 cycles were obtained. Yet, according to the authors, this prediction method might not be applicable to Li-ion batteries that show a flat discharging voltage curve (e.g. LiFePo4 cathode).

Sample entropy

Widodo et al. proposed a sample entropy input feature extracted by discharge voltage and time data, used to predict the capacity [61]. An SVM model was compared with a Gaussian kernel RVM. The latter showed more accurate results. The method was applied to two different cells, and the biggest RMSE was 0.54% for a 30 steps-ahead prediction.

Overall, in several literature publications tackling the implementation of RVM algorithms for battery ageing prediction [56–61], the models were trained with the capacity data obtained from a single cell, which was generally stressed under constant operating conditions. The ability of such models to perform accurate predictions is questionable for different static

operating conditions and especially in more realistic dynamic conditions. Furthermore, a first fold of the capacity curve was typically used for model training and the remaining data for prediction. This approach assumes that a battery degrades similarly in the BOL and when approaching the EOL. As reported in Section 1.2.1, this should not necessarily be the case for Li-ion batteries.

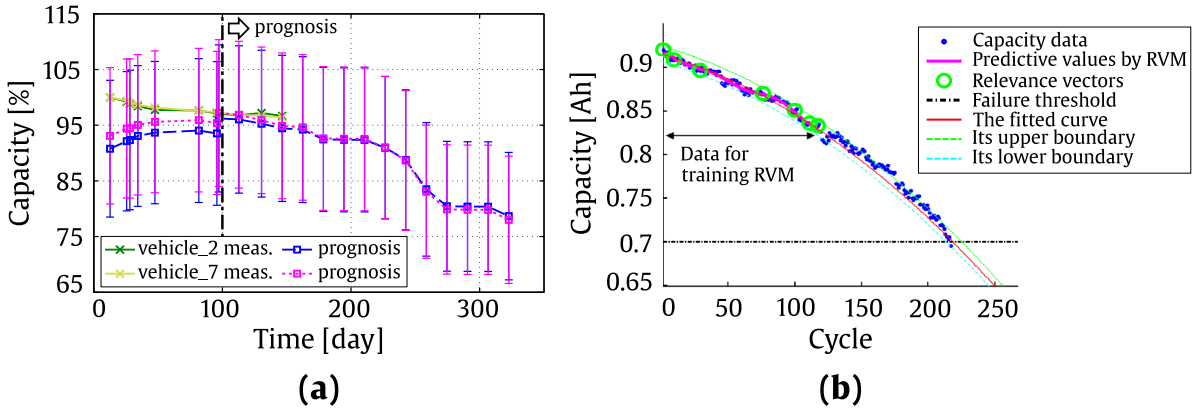

Figure 6. Li-ion battery ageing predictions obtained through (a) counting method and batch learning RVM [43]**, and (b) RVM and three-parameters empirical model combination** [56].

1.2.3.3. Assessment through defined criteria

Nonparametric

The RVM provides a nonparametric framework, which could be updated through model re-training. Both batch and incremental training methods were used to update the proposed Li-ion ageing models.

Nonlinearities

Uncertainty

Sensitivity

The RVM algorithm is able to handle nonlinear relations (A1) through the use of basis functions ϕ, and provides probabilistic predictions (A2). The RVM algorithm tends to discard irrelevant data, which reduces its sensitivity to noisy data and outliers (A3). Overfitting is avoided imposing additional constraints on the parameters. In this case, parameters are constrained by defining an explicit prior probability distribution over them [99], or by adding a complexity penalty term for marginal likelihood maximisation.

Computational cost

No information was provided in the literature about the computation time required to compute Li-ion ageing predictions with RVM. The original RVM algorithm supposes an $\mathcal{O}(n^3)$ time complexity (C2.1.1) and an $\mathcal{O}(n^2)$ memory complexity (C2.2) [99]. Although faster algorithms were further proposed [113], big-O complexity data were not specified for such improved

algorithms (C2.1.2). The basic idea of RVM is that basis functions that are not significantly contributing to explaining the data should be removed [110], and this results in practice on a very sparse framework (C3). This sparse character is observable in Figure 6. (b), where selected RVs were displayed.

1.2.4. Gaussian Process Regression

1.2.4.1. Theoretical basis

This section aims to provide a brief overview of Gaussian Process (GP) models, introducing the main concepts and the predictive equations. Detailed explanations are available in [110].

Random process

The GP is a random process, i.e. a random entity whose realisation is a function $f(\mathbf{x})$ instead of a single value. Rather than assuming a parametric form for the function to fit the data, $f(\mathbf{x})$ is assumed to be a sample of a Gaussian random process distribution. Since the GP is a nonparametric model, even when observations have been added, the model is always able to fit the new upcoming data.

Nonparametric

Mean and covariance functions

A GP is fully determined by its mean and covariance functions. Defining the mean function $m(\mathbf{x})$ and the covariance function $\kappa(\mathbf{x}, \mathbf{x}')$ of a real process $f(\mathbf{x})$ as:

$$m(\mathbf{x}) = \mathbb{E}[f(\mathbf{x})] \tag{17}$$

$$\kappa(\mathbf{x}, \mathbf{x}') = \mathbb{E}\big[\big(f(\mathbf{x}) - m(\mathbf{x})\big)\big(f(\mathbf{x}') - m(\mathbf{x}')\big)\big]$$

the GP can be expressed as

$$f(\mathbf{x}) \sim \mathcal{GP}(m(\mathbf{x}), \kappa(\mathbf{x}, \mathbf{x}')) \tag{18}$$

where $\mathbf{x}$ and $\mathbf{x}'$ are two different input vectors.

Similarity

Both mean and covariance functions encode the prior assumptions about the function to be learnt. They also express the expected behaviour of the model when the prediction inputs diverge from the inputs observed during training. The covariance function, also called the kernel, underpins the information about how relevant one target observation y of the training dataset is to predict the output y^*, on the basis of the similarity between their respective input values $\mathbf{x}$ and $\mathbf{x}^*$.

The mean and covariance functions depend on some hyperparameters $\boldsymbol{\theta}$, which must be learnt from the training dataset. From a GP point of view, the mean and covariance function selection and learning the corresponding

hyperparameters are the main tasks which must be carried out during the training phase. Hyperparameters are typically estimated by the maximisation of the marginal likelihood logarithm, using the gradient of the marginal likelihood with respect to such hyperparameters [110]. The marginal likelihood is defined as the integral of the likelihood times the prior.

Under the GP framework, the prior is gaussian $\mathbf{f}|X \sim \mathcal{N}(0, K)$, and the likelihood is a factorised gaussian $\mathbf{y}|\mathbf{f} \sim \mathcal{N}(\mathbf{f}, \sigma_n^2 I)$, where $\mathbf{f}$ is the vector of latent function values as $\mathbf{f} = (f(\mathbf{x}_1, \ldots, \mathbf{x}_n))^T$; X is the matrix of the training input values; $\mathcal{N}$ is the gaussian (normal) distribution; K is the covariance matrix for the (noise free) $\mathbf{f}$ values; $\mathbf{y}$ is the vector of the training target values; σ_n^2 is the noise variance and I is the identity matrix.

The obtained log marginal likelihood is expressed in equation (19)

$$\log\, p(\mathbf{y}|X) = -\frac{1}{2}\mathbf{y}^T(K + \sigma_n^2 I)^{-1}\mathbf{y} - \frac{1}{2}\log|K + \sigma_n^2 I| - \frac{n}{2}\log 2\pi \quad (19)$$

The GP predictive equations are expressed in equations (20), (21) and (22).

Predictive equations

$$\mathbf{f}_*|X, \mathbf{y}, X_* \sim \mathcal{N}(\bar{\mathbf{f}}_*, \text{cov}(\mathbf{f}_*)) \quad (20)$$

with

$$\bar{\mathbf{f}}_* = \mathbf{m}(X_*) + K(X_*, X)[K(X, X) + \sigma_n^2 I]^{-1}(\mathbf{y} - \mathbf{m}(X)) \quad (21)$$

$$\text{cov}(\mathbf{f}_*) = K(X_*, X_*) - K(X_*, X)[K(X, X) + \sigma_n^2 I]^{-1}K(X, X_*) \quad (22)$$

where $\mathbf{f}_*$, $\bar{\mathbf{f}}_*$, and $\text{cov}(\mathbf{f}_*)$ are the GP posterior prediction, its corresponding mean and its covariance, respectively; X_* is the matrix of test inputs; $\mathbf{m}(X)$ and $\mathbf{m}(X_*)$ are the vectors of mean functions for the training and test inputs respectively; $K(X, X)$, $K(X_*, X_*)$, and $K(X, X_*)$ are the covariance matrices between training inputs, the test inputs, and training and test inputs, respectively. The mathematical development and conceptual relations between the different kernel machines (SVR, RVM and GPR) are more widely described in [110].

1.2.4.2. Application to Li-ion battery ageing modelling

Reversible capacity recovery

In [50] and [52], the authors attempted to capture the decreasing trend of the Li-ion battery degradation curve, taking into account the fluctuations generated by the reversible capacity recovery phenomenon. For this purpose, two different strategies were adopted, both tested using the NASA's

battery ageing data. Liu et al. built and compared GPR models with different combinations of the kernel and mean functions, using the amount of performed cycles as input data and the capacity data as a target [50]. The kernel function was decomposed in two parts: the functional kernel which described the unknown system model, and the noise part kernel. The functional kernel was defined as the sum of a squared exponential and a periodical kernel, being the latter specifically tailored to fit sudden capacity recoveries. Moreover, the functional kernel was combined with i) a linear mean function and ii) a quadratic mean function. Hyperparameters were trained by log-likelihood maximisation. Although both models obtained similar accuracy, the linear mean GPR showed narrower confidence bounds. In this work, the prediction of reversible capacity recoveries was approached using the periodical kernel. Such modelling approach is questionable, because as reported in Section 1.2.1, those capacity recuperations are typically explained by battery rest or relaxation periods, and have not to be necessarily periodicals [103]. This remark is also valid for the method presented in [51], in which a similar approach was adopted.

Squared-exponential and periodical kernels

Linear and quadratic mean functions

He et al. proposed to combine a time series decomposition method with a GPR model, in order to develop a Multi-scale Gaussian Process Regression (MGPR) [52]. The time series decomposition method was used to separate the dataset into different components: the global degradation trend was reflected in low-frequency components, and the sudden capacity recovery points were collected in high-frequency components. A GPR model was developed for each data component, with linear mean function and two different kernels: i) a squared-exponential kernel, and ii) a periodic kernel. GP models of several data components were then combined to finally obtain the complete MGP model of the Li-ion battery degradation dataset. Additionally, a Spectral-Mixture kernel GPR model was built using the original dataset (prior to the time series decomposition). In order to determine the best approach, RMSE values were compared also including the results obtained in [50]: best results were achieved with the squared-exponential MGPR model, obtaining as largest error ca. 2.11% RMSE for a 68 cycles ahead prediction.

Time series decomposition

Linear mean function

Comparing kernels

Richardson et al. proposed a wide study aiming at predicting the lifetime of Li-ion batteries by using GPR, also considering the amount of performed cycles as input data and capacity data as target [53]. They first looked into the kernel optimisation issue: based on the squared-exponential, periodic and Matérn kernels, ten compound kernels were constructed, and their respective accuracy was compared using the ageing data of three cells from the NASA repository. Hyperparameters were optimised minimising the negative log marginal likelihood, and most accurate results were obtained

Compound kernels

Semi-parametric

Multi-output GP

through a Matérn based compound kernel. Furthermore, different combinations of a GPR and an empirical exponential model produced three parametric, semi-parametric and nonparametric models. These models were assessed extracting ageing data from [82], originally derived from the data repository of the CALCE research group [112]. The semi-parametric model was the most accurate. Finally, the authors considered the possibility of correlation among the degradation trends experienced by different cells, employing the multi-outputs GP framework to three Li-ion battery ageing datasets. Results showed that considering the data from multiple cells in a multi-output framework could significantly improve the prediction accuracy (ca. 0.02 Ah RMSE for 40% of training data), but also the computational cost due to the larger data vectors to be handled.

As pointed out in previous sections the lack of more extensive validation results hinders assessing the true accuracy of the presented models [50–53], especially under dynamic operating conditions. Furthermore, models were trained with a certain fold of the dataset to predict further capacity data: this approach assumes that a battery degrades similarly in the BOL and when approaching the EOL. As reported in Section 1.2.1, this is not necessarily the case for Li-ion batteries.

1.2.4.3. Assessment through defined criteria

Nonparametric

The GP framework allows developing nonparametric models which could be updated through online re-training. In [50–53], only the batch training method was implemented.

Nonlinearities

Uncertainty

Sensitivity

GP models are able to capture nonlinearities (A1), and hence the prediction accuracy is not affected by nonlinear relations in data. Furthermore, predictions are probabilistic (A2), so uncertainties can be dealt. The noise component within the data could be quantified and modelled through a dedicated hyperparameter in the covariance function (namely the noise variance σ_n^2), making the model's performances relatively insensitive to noisy training data (A3).

Computational cost

Training the GPR algorithm usually need the inversion of the covariance matrix, and this task corresponds to a $\mathcal{O}(n^3)$ computational time complexity (C2.1.1), being $\mathcal{O}(n^2)$ the memory complexity (C2.2) [40]. Furthermore, the mean and kernel prediction computations are respectively $\mathcal{O}(n)$ and $\mathcal{O}(n^2)$ for time complexity [114]. In order to reduce the computational cost, various sparse methods were developed [110], which are based on the utilisation of a subset of size $m < n$ of the training examples (C3). In these way, time and memory complexities can be reduced to $\mathcal{O}(m^3) + \mathcal{O}(m^2)$ (initialisation + prediction), and $\mathcal{O}(m^2)$, respectively. Furthermore, improved GPR algorithms

could provide more efficient results [114,115]. Ranganathan et al. proposed an online sparse solution to reach $\mathcal{O}(n)$ time complexity (C2.1.2) [114].

1.2.5. Artificial Neural Network

1.2.5.1. Theoretical basis

ANNs encompass a wide family of learning machines, which consist of interconnected neurons distributed in inputs, outputs and hidden layers. Each neuron is fed by the linear combination of its corresponding inputs, transformed by an activation function, and the resulting signal is propagated to the following layers. The main characteristics of an ANN can be explained in two parts: i) the architecture, related to the topology used to house the interconnected neurons, and ii) functional properties, which refer to the learning algorithms used to determine the weights of interconnections [116]. This way, input $\mathbf{x} = (\mathbf{x}_1, \dots, \mathbf{x}_N)$ and target $\mathbf{y} = (\mathbf{y}_1, \dots, \mathbf{y}_M)$ training vectors are used to estimate the weight vector w of the ANN.

Architecture and functional properties

Static ANN architectures (typically feedforward networks) do not include any feedback connections. Dynamic architectures, by contrast, incorporate feedbacks from output values (adaptive ANN architectures) or interconnections between hidden nodes (recursive ANN architectures). The architecture is also defined by the number of hidden layers, neurons for each layer, inputs and outputs.

Static and dynamic networks

Among the many different learning algorithms, the most popular is the back-propagation algorithm, which consists on calculating the error contribution of each neuron and optimising its corresponding weight by applying a gradient descent optimisation, in order to minimise the overall loss function. Besides, different activation functions can be used to determine the state of a neuron (e.g. sigmoid, radial basis, linear, etc.).

Back-propagation

Activation functions

1.2.5.2. Application to Li-ion battery ageing modelling

Liu et al. developed an adaptive recursive ANN, which considers inputs, output feedback and the feedback from the previous states for prediction [63]. The temperature was used as network input and the sum $R_E + R_{CT}$ was chosen as output, being R_E the electrolyte resistance and R_{CT} the charge transfer resistance in a lumped-parameter battery model [75]. Assuming that the battery capacity was inversely proportional to $R_E + R_{CT}$, the capacity of each cell was deduced. Further, battery RUL was estimated, defining EOL through 70% capacity fade criterion. The learning algorithm of the ANN was recursively applied in order to update the weights of the model. Results were compared with a classical Recursive NN, a Recursive Neuro-Fuzzy, GPR, RVM and particle filter-based models, developed in previous works. The

developed ARNN model showed most accurate results. However, no information was provided about the implementation of the other models.

Rufus et al. proposed a complex procedure using fuzzified C-rate, DOD and temperature data to obtain multimodal distributions of batteries' RUL, combining various ANNs [65]. The probabilistic character of the output was achieved using a Confidence Prediction ANN.

Wu et al. developed an in-field BMS implementable prediction model, although they did not reach to train the model online. The model predicted the RUL from the voltage curves of the charging process [62]. The ageing data of two cells was used for training and validation. The importance sampling (IS) method allowed selecting a limited number of data samples from the charging voltage curve, which were employed as input. EOL was defined according to the 80% capacity threshold criterion. The ANN model was a feedforward network involving 11 inputs, one hidden layer and one output, with a hyperbolic tangent sigmoid activation function. The model was trained through back-propagation, and the results were compared for a different number of hidden neurons. The forty-neuron architecture was selected as a trade-off solution of accuracy and computational cost, achieving a maximum AE of 29.4218 cycles for a lifespan of 2000 cycles.

Autoregressive approach

Other authors adopted a pure autoregressive approach of the capacity data to develop different ANN models. Rezvani et al. proposed an adaptive ANN [66], Huang et al. compared a feedforward back-propagation ANN with an SVR model [67], and Razavi-Far et al. presented comparative studies of different types of ANNs for various learning algorithms [68,69]. Pure autoregressive approaches assumed that the future capacity loss could be accurately predicted solely based on the previous capacity data. Particularly in the case of Li-ion batteries, the suitability of this assumption should be analysed with care, mainly because of i) the well-known influence of the operating conditions on ageing, and ii) the path dependence of Li-ion batteries [117], which would become especially relevant under dynamic operating conditions.

1.2.5.3. Assessment through defined criteria

Parametric

Assuming that the topology does not change over time, ANN could be considered as a parametric framework able to perform regression in an online learning paradigm [116].

Nonlinearities

Uncertainty

In theory, ANNs are able to approximate any continuous function [118]. The activation functions permit to capture nonlinearities between input and outputs (A1). Inherently, ANNs cannot quantify uncertainty (A2). However, a probabilistic character could be integrated into the ANN framework, e.g.

using Bayesian priors over the weights [119] or confidence prediction ANNs [65]. In general, models which handle many parameters are prone to fit the data very closely, leading to overfitting problems. Regarding ANNs, the amount of weights increases according to the number of inputs, hidden layers and neurons per layers, therefore, big networks could have more problems with outliers and noise (A3). Regularisation methods may also be used to avoid overfitting problems [120].

Computational cost

Although many works mention the high computational cost of the ANN model, it is difficult to find quantitative indications of time or memory cost for ANN training and prediction. In [121], authors quantified the time complexity of a multilayer perceptron trained through the standard gradient descent algorithm as $\mathcal{O}(nDHC)$, being n the number of training samples, D the input dimension, H the number of hidden units and C the number of outputs (C2.1.1). Assuming that the ANN's architecture remains constant over time, D, H and C are constant, and then the complexity growth would be reduced to $\mathcal{O}(n)$. ANNs have not any inherent sparse mechanism (C3), but sparse ANN training methods were proposed in [122].

1.2.6. Particle filtering method

1.2.6.1. Theoretical basis

Bayesian filters provide a framework to track the states of a time-dependent system, based on the measurements of a related variable, in a situation in which they cannot be directly measured and compulsorily have to be estimated. Two models are required: i) a model describing the evolution of the state over time (the state transition model), and ii) a model relating the measurement to the state (the measurement model) [123]. From a Bayesian probabilistic perspective, such models are expressed as probability density functions (pdf), see equations (23)-(24).

State transition model

Measurement model

$$\mathbf{x}_k = f_k(\mathbf{x}_{k-1}, \mathbf{v}_{k-1}) \quad \leftrightarrow \quad p(\mathbf{x}_k|\mathbf{x}_{k-1}) \tag{23}$$

$$\mathbf{y}_k = h_k(\mathbf{x}_k, \mathbf{u}_k) \quad \leftrightarrow \quad p(\mathbf{y}_k|\mathbf{x}_k) \tag{24}$$

Prediction stage

where $\mathbf{x}$ is the vector of states; $\mathbf{y}$ is the vector of measurement variables; $\mathbf{u}$ and $\mathbf{v}$ are the noise terms. In the prediction stage, it is assumed that the prior state probability density function $p(\mathbf{x}_{k-1}|\mathbf{y}_{1:k-1})$ is known, and the actual state can be estimated via the Chapman-Kolmogorov equation (equation (25)):

$$p(\mathbf{x}_k|\mathbf{y}_{1:k-1}) = \int p(\mathbf{x}_k|\mathbf{x}_{k-1})\, p(\mathbf{x}_{k-1}|\mathbf{y}_{1:k-1}) d\mathbf{x}_{k-1} \quad (25)$$

Updating stage

In the update stage, a new measurement $\mathbf{y}_k$ becomes available at sample k, and the prior state estimate can be updated using the Bayes' rule (equation (26)):

Bayes' rule

$$p(\mathbf{x}_k|\mathbf{y}_{1:k}) = \frac{p(\mathbf{y}_k|\mathbf{x}_k)p(\mathbf{x}_k|\mathbf{y}_{1:k-1})}{p(\mathbf{y}_k|\mathbf{y}_{1:k-1})} \quad (26)$$

where $p(\mathbf{x}_k|\mathbf{y}_{1:k-1})$ and $p(\mathbf{x}_k|\mathbf{y}_{1:k})$ are respectively the prior and posterior states estimate; $p(\mathbf{y}_k|\mathbf{x}_k)$ is the likelihood function defined by the measurement model. The normalising constant is computed as follows:

$$p(\mathbf{y}_k|\mathbf{y}_{1:k-1}) = \int p(\mathbf{y}_k|\mathbf{x}_k)p(\mathbf{x}_k|\mathbf{y}_{1:k-1}) d\mathbf{x}_k \quad (27)$$

Prediction and update stages are recursively computed whenever a new measurement data sample is available. There are different tools in the Bayesian filters family, including Kalman filters and particle filters [124]. In the Li-ion ageing prediction literature, the use of particle filters is much more widespread than the use of Kalman filters. Moreover, some comparative studies showed more accurate results with particle filtering [91]. Therefore, this section scopes particularly on particle filters.

Particle filters

The particle filter is based on Monte Carlo sampling method to approximate the posterior states density function. The key idea is to represent the required posterior pdf by a set of random samples called particles, which represent discrete state hypotheses, with their respective associated weight. The estimate is then computed based on these samples and weights [123]. Let $\{\mathbf{x}_{0:k}^i, \mathbf{w}_k^i\}_{i=1}^{N_s}$ denote the N_s amount of particles and weights couples, being the weights normalised such that $\sum_i \mathbf{w}_k^i = 1$. The posterior distribution at state k is approximated as:

$$p(\mathbf{x}_k|\mathbf{y}_{1:k}) \approx \sum_{i=1}^{N_s} \mathbf{w}_k^i \delta(\mathbf{x}_{0:k} - \mathbf{x}_{0:k}^i) \quad (28)$$

where δ denotes the Dirac function. The weights are typically chosen using the principle of importance sampling [123,124].

Using the particle filter framework, the prediction of Li-ion battery ageing could be handled from different points of view, depending on which state variable is tracked, which variable is measured, and which transition and

measurement equations are defined. Next section provides an overview of main works presented in the literature.

1.2.6.2. Application to Li-ion battery ageing modelling

A very common trend in the literature in order to update Li-ion battery ageing models is to build an empirical parametric ageing model and update its parameters with a particle filter every time a new data is available. For this purpose, different models relating battery capacity $\mathbf{C}_k$ and cycle number k were proposed. Table 3 lists several models found in the literature, specifying corresponding references. In these works, parametric models were used as the measurement equation of the particle filter, and model parameters were defined as system states. The state transition equation was specified as

Parametric models

$$\begin{bmatrix}\boldsymbol{\alpha}_{1,k}\\ \cdots \\ \boldsymbol{\alpha}_{n,k}\end{bmatrix} = \begin{bmatrix}\boldsymbol{\alpha}_{1,k-1}\\ \cdots \\ \boldsymbol{\alpha}_{n,k-1}\end{bmatrix} + \begin{bmatrix}\mathbf{v}_1\\ \cdots \\ \mathbf{v}_n\end{bmatrix}, \qquad \begin{matrix}\mathbf{v}_1 \sim \mathcal{N}(0,\sigma_1^2)\\ \cdots \\ \mathbf{v}_n \sim \mathcal{N}(0,\sigma_n^2)\end{matrix} \tag{29}$$

State transition equation

where $\boldsymbol{\alpha}_{n,k}$ depicted the n^{th} parameter of the empirical model; $\mathcal{N}(0,\sigma_n^2)$ was a Gaussian noise with zero mean and standard deviation σ_n. Figure 7. (a) displays the results obtained in [72], showing up the capacity prediction particles propagated over time, and the corresponding RUL probability distribution.

Table 3. Empirical models used in the literature for Li-ion capacity prediction.

	Model	Model equation	Reference
(1)	Quadratic Polynomial	$\boldsymbol{C}_k = \boldsymbol{\alpha}_1 k^2 + \boldsymbol{\alpha}_2 k + \boldsymbol{\alpha}_3$	[70]
(2)	One-term Exponential	$\boldsymbol{C}_k = \boldsymbol{\alpha}_1 e^{\boldsymbol{\alpha}_2 k}$	[71]
(3)	Two-term Exponential	$\boldsymbol{C}_k = \boldsymbol{\alpha}_1 e^{\boldsymbol{\alpha}_2 k} + \boldsymbol{\alpha}_3 e^{\boldsymbol{\alpha}_4 k}$	[70,82,90–96]
(4)	Ensemble model 1	$\boldsymbol{C}_k = \boldsymbol{\alpha}_1 e^{\boldsymbol{\alpha}_2 k} + \boldsymbol{\alpha}_3 k + \boldsymbol{\alpha}_4$	[70]
(5)	Ensemble model 2	$\boldsymbol{C}_k = \boldsymbol{\alpha}_1 e^{\boldsymbol{\alpha}_2 k} + \boldsymbol{\alpha}_3 k^2 + \boldsymbol{\alpha}_4$	[70]
(6)	Ensemble model 3	$\boldsymbol{C}_k = \boldsymbol{\alpha}_1 e^{\boldsymbol{\alpha}_2 k} + \boldsymbol{\alpha}_3 k^2 + \boldsymbol{\alpha}_4 k + \boldsymbol{\alpha}_5$	[70]
(7)	Two-term logarithmic	$\boldsymbol{C}_k = \boldsymbol{\alpha}_1 + \boldsymbol{\alpha}_2 \ln(k+m) + \boldsymbol{\alpha}_3 \ln(1-\boldsymbol{\alpha}_4)$	[72]

Goebel et al. proposed to update an exponential empirical model of the resistance growth using a particle filter [73]. The study was based on a first-order Li-ion battery electrical model, whose parameters were fitted through Electrochemical Impedance Spectroscopy (EIS) curves. Due to their negligible changes, the double layer capacity and the Warburg resistance parameters were neglected. In this way, the values of the electrolyte resistance R_E and the charge-transfer resistance R_{CT} were deduced for different ageing stages, and a RVM model was built involving time input vector and resistance target values, in order to reject irrelevant data. Then,

First-order battery model

RVM to discard irrelevant data

State & measurement variables

an empirical exponential impedance growth model was fitted on the RVM curve. This exponential model was regularly updated by a particle filter, in which both R_E and R_{CT} values and impedance growth model parameters were defined as state variables. The measurement variables were R_E and R_{CT}, and the measurement equation contained the resistance state vector and a zero-mean Gaussian noise component. Assuming a strong linear relation among the capacity fade and $R_E + R_{CT}$ growth, the EOL was set according to the 70% capacity fade criterion. Figure 7. (b) shows the RUL pdfs predicted at different ageing stages. The second RUL prediction provided more accurate results and narrower pdf compared to the first prediction, which indicates how the accuracy of the model improves as the considered dataset becomes larger.

Comparison with other methods

The same method was compared in [74] with two different models, based on Extended Kalman Filter and ARIMA, respectively. The particle filter method showed the best suited probabilistic RUL estimations. The method was completed in [75,76] improving the particle filter and combined with an SVR algorithm for re-sampling in [77]. All these works were based on EIS measurements and then required dedicated equipment and measurement conditions, hardly available on in-field operating conditions.

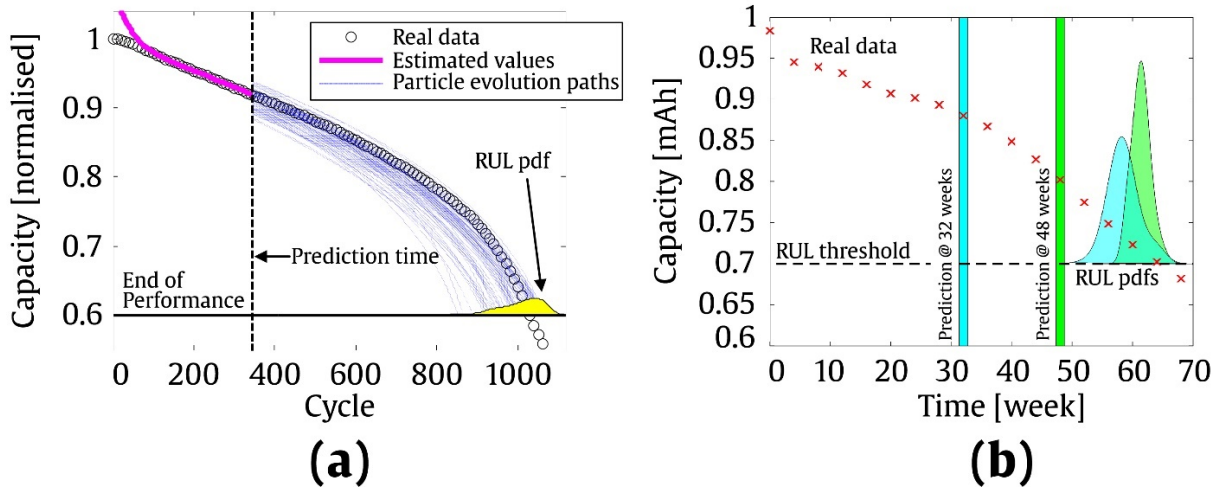

Figure 7. Capacity fade curve predictions and RUL pdfs obtained in (a) [72] **and (b)** [73].

Saha et al. [78] proposed a capacity fade empirical model based on the Coulombic efficiency. The reversible capacity recovery phenomenon was

also involved, by a time-dependent two-term exponential model component depending on the resting time. The model was implemented as transition function into the particle filter. The state vector included both capacity values and model parameters, and the measurement variable was capacity. An identical approach was used in [79], with similar results.

Combining particle filters

Su et al. introduced a different approach based on the combination of three particle filters [88]. Three empirical parametric models, namely the quadratic polynomial, the two-term exponential and the Verhulst model (previously used in [89]), were formulated in difference equations. Then, each of them was inserted in a respective particle filter as state transition equation, being the measurement equation the sum of the actual state's value and a zero-mean Gaussian noise. Finally, the three EOL probability densities were combined in order to obtain the overall probability density estimation, reaching this way smaller prediction errors and a narrower prediction pdf.

Stress-factors

Previously mentioned works used the particle filter framework in order to update parametric models, which related capacity or internal resistance targets to either time or cycles inputs. The suitability of such empirical parametric models, which do not consider the effect of stress-factors, would be debatable for Li-ion battery ageing modelling. Nevertheless, a particle filter approach would still be valid to be implemented considering a semi-empirical battery ageing model as the measurement equation, which should certainly provide more reliable prediction results.

Combined approach

Beyond the utilisation of parametric empirical models, some works proposed to combine the particle filtering framework with other modelling tools. Main works based on such combinations are summarised in **Table 4**, specifying for each case the involved modelling tools, the state and measurement variables, and how the transition and measurement equations were obtained.

Table 4. Other methods based on the combination of different ageing models and particle filter framework

Combination	State variable x	State Transition equation	Measurement variable y	Measurement equation	References
ARIMA Parametrical empirical model Particle filter	Capacity	Empirical exponential	Capacity	Nonlinear degradation factor + ARIMA	[80,81,83][6]
SVR Particle filter	Capacity	Multi-order equation, built by SVR	Capacity	$\mathbf{y}_k = \mathbf{x}_k + \text{noise}$	[84]
SVR Parametrical empirical model Particle Filter Similarity-based	Internal Resistance	Empirical exponential	Capacity	SVR	[85] [7]
Mixture of GPRs Parametrical empirical model Particle Filter	Measurement equation's parameters	Mixture of GPRs	Capacity	Empirical	[86]
Parametrical empirical model Particle Filter ANN	Internal Resistance and Transition equation's parameters	Empirical exponential	Internal Resistance	$\mathbf{y}_k = \mathbf{x}_k + \text{noise}$	[87][8]

[6] In [83], particle filter was replaced by an Extended Kalman Filter.

[7] Similarity-based approach was used to predict future capacity measurement.

[8] $\mathbf{x}_k$ only involve of the internal resistance states. ANN was used to predict future capacity measurement.

1.2.6.3. Assessment through defined criteria

Uncertainty

Nonlinearities

Sensitivity

The Particle Filter framework allows tracking a non-Gaussian probability density function for the state variable (A2), based on the measurements of a related variable. Such filter is able to handle nonlinear transition and measurement models (A1), which are previously specified. The basic formulation of the particle filter could be sensitive to noisy data samples, and as mentioned in [124], outliers may cause the divergence of the filter or produce inaccurate performances (A3). Many works proposed improved algorithms to reduce the sensitivity to outliers [125]. Moreover, the accuracy of a particle filter depends on the transition and measurement models and the number of particles, amongst others [124].

Computational cost

As indicative information, Walker et al. reported the computational cost of the proposed methodology implemented in Matlab (desktop information: 3.4 GHz processor, 16.0 GB RAM, 64-bit operating system): the computation time for 100 particles was approximately 3.62 ms (C1) [91]. One of the advantages of particle filter is that the complexity is independent of the state dimension and increases in function of the number of particles N_p. Corresponding time complexity is $\mathcal{O}(N_p)$ (C2.1.1) [124].

1.3. Discussion & Conclusions of the chapter

This section aims at comparing the different models proposed in the literature, on the basis of the criteria defined in Section 1.1, in order to find the most suitable framework to develop periodically updated ageing models. Furthermore, some considerations are discussed concerning some advisable ways to develop the selected models, for the particular application case of Li-ion battery ageing prediction.

1.3.1. Critical comparison of the different models

Table 5 collects the different characteristics of the studied models, easing the comparison of their main characteristics.

Nonparametric vs parametric

For the particular application case of Li-ion battery ageing prediction, the intrinsic structure of the selected model is relevant. Parametric models can only vary the value of their parameters, being their functional form constant. In an online learning situation, this could limit the ability of the model to fit future ageing data. ARIMA models could certainly experience such problems. Methods involving particle filters to update parametric ageing models could also be exposed to such limitation, and hence the ability to perform accurate predictions strongly depends on the reliability of the initial model. In order to obtain accurate initial models, it would be then necessary to carry out a minimal number of laboratory ageing tests. Therefore, adopting parametric

modelling approaches could not be the most suitable solution, considering that one of the objectives of this thesis is the minimisation of the initial number of laboratory ageing tests (see introduction). Assuming a constant architecture over time, ANN models also have a fixed number of weights and they can also be considered as parametric models. However, ANNs are theoretically able to approximate any continuous function within some desired accuracy range, as long as the network size is accordingly defined. SVR, GPR and RVM are nonparametric models, and in such case each data point has its associated parameter, giving to the model increased flexibility to update itself to the new data logged during in-field operation.

Periodical re-training vs filtering

Two main approaches were identified in the literature to develop periodically updated Li-ion ageing models: i) periodical model re-training and ii) model updating through particle filtering. In cases in which a reliable parametric ageing model is already available from previous works, the use of filtering techniques might be an advisable solution to update it, from a parameter correction perspective. Oppositely, in a situation in which the model would need to be developed from the beginning, opting for a nonparametric probabilistic model might be a more appropriate choice, from a laboratory tests minimisation perspective. As already mentioned, such an approach would allow an enhanced flexibility to adapt the model when facing new data points, while still limiting the battery testing labours required to train the model.

Nonlinearities

The ability to model nonlinear relations is crucial when modelling Li-ion battery ageing since the relation between some battery stress-factors and HIs is strongly nonlinear. SVR, GPR, RVM and ANN frameworks allow performing nonlinear regressions. Particle filters accept nonlinear models for both transition and measurement equations. As for ARIMA, it can only provide a linear autoregression, and hence it may not be suitable for Li-ion battery ageing prediction.

Uncertainty

The capability to manage uncertainty is also one of the key features analysed in this review. As explained in Section 1.1.2.1, predictions should ideally be probabilistic, in order to express the reliability of the predictions provided by the model [99]. RVM, GPR and the particle filter methods provide probabilistic frameworks. Confidence bounds typically spread over time for a longer prediction horizon, showing that as the number of prediction steps increases, the future uncertainty increases as well [65]. Thus, early predictions usually produce wide EOL pdf estimations. However, such estimations are expected to narrow over time as the battery approaches its true EOL value.

Sensitivity

Another criterion mentioned in Section 1.1.2 is the sensitivity of the models to noisy data or outliers. As reported in Section 1.2.1.3, ARIMA showed difficulties to appropriately handle data fluctuations. The basic formulation of the particle filter could also be quite sensitive, and outliers may cause the divergence of the filter or produce an inaccurate performance [124]. Many works proposed improved forms of filter algorithms to reduce the sensitivity to outliers [125]. Big ANNs could tend to overfit data and regularisation methods should be used to avoid overfitting problems [120]. Because of the use of the ϵ-sensitive loss function, the SVR algorithm is insensitive to small noisy fluctuations in the data. However, outliers would likely become SVs and then influence the predictions of the ageing model. RVM and GPR would present more suitable behaviour when facing small data fluctuation and outliers. Indeed, RVM possesses inherent mechanisms to discard irrelevant data from the training process. In the GPR framework, the noise component within the data could be quantified and modelled through a dedicated hyperparameter in the covariance function, making the model's performances relatively insensitive to noisy training data.

Computational cost

Finally, the computational complexity of the described models deserves a deeper discussion. In fact, observing the main trends and evolution perspective in the domain of energy storage solutions, two different approaches could be contemplated for the deployment of ageing models in real applications, considering the implementation of the models i) within the local hardware of each battery system, or ii) in an external data server (cloud server), connected to a fleet of battery systems. An illustrative figure as well as some thoughts and considerations on the implications arising from each deployment approach are provided in Chapter 6. The computational complexity of the described models is particularly critical from the perspective of the model implementation in local battery system hardware.

Computation times

Computation times indicated in the literature are reported in **Table 5**. Such information is of very limited use, as it strongly depends on the hardware employed for such computation, and the efficiency of the code itself. Moreover, local hardware of battery systems (e.g. BMS) typically have a reduced computational power compared to personal computers, yet the literature does not provide any information regarding the execution of each proposed algorithm in any certain local processor. In this context, the computation time in personal computers is a suitable information insofar it allows gauging the possibility of implementing any algorithm in a local processor. The computation times indicated in the literature were of the order of milliseconds in personal computers. Hence it could be possible to contemplate the implementation of such algorithms in a hardware system of more reduced computation power. Furthermore, in an online learning

situation, the amount of input data is expected to increase, and the computation time strongly depends on the big-O complexity of the implemented algorithm. Therefore, most of the literature publications to date lack of in-field experimental validation results, and a deeper analysis would still be necessary to evaluate on what extent each of the proposed algorithms may actually be implementable on a real local hardware.

About required computational power

The required computational power for the local processor can be approximated considering: i) the number of available data points expected to perform the predictions, ii) the maximum time available to compute such prediction and iii) the big-O complexity of the algorithm. The former two factors strongly depend on the particular application in which the batteries are deployed. Hence, to what extent any of the reviewed algorithms could actually be implementable depends both on the nature of the application itself and on the power of the local processor.

Sparsity

In cases in which computational challenges are faced, sparsity may become a crucial feature to enable a reduction of the amount of input data. The ϵ-sensitive loss function makes SVR a sparse algorithm. RVM algorithms even have an increased sparsity compared to SVR algorithms [99]. Due to this sparse character, RVM training and prediction is usually faster than non-sparse GPR models [110]. GPR models are not inherently sparse, but different methods can be used to reduce the number of training data [110]. Finally, filtering approaches and ANNs have not any inherent mechanism to achieve sparsity. However, this would not represent a critical issue due to their parametrical character, leading to a relatively limited relation among their computation complexity and the amount of training data.

Table 5. Comparison of different models used in the literature based on the defined criteria.[9]

				ARIMA	SVR	GPR	RVM	ANN	Particle Filter
Parametric/nonparametric model				Parametric[10]	Nonparametric	Nonparametric	Nonparametric	Parametric[11]	Parametric[12]
Model updating approach				Re-training	Re-training	Re-training	Re-training	Re-training	Parameters filtering
Accuracy (A)	**Ability to deal with nonlinearities (A1)**			No	Yes	Yes	Yes	Yes	Yes[13]
	Uncertainty management (A2)			Not probabilistic	Not probabilistic	Probabilistic[14]	Probabilistic[15]	Not probabilistic[16]	Probabilistic[17]
	Sensitivity to irrelevant data (A3)			High sensitivity.	Insensitive to small deviations, sensitive to outliers.	Ability to model noisy data.	Ability to discard irrelevant data.	Potential overfitting problems.	Outliers could lead to divergence.
Computational cost (C)	**Indicative computation time (C1)**			NA	1.26 ms[18]	NA	NA	NA	3.62 ms[19]
	big-O complexity (C2)	**big-O time complexity (C2.1)**	**Theoretical algorithm (C2.1.1)**	-[20]	$O(n^3)$	$O(n^3)$	$O(n^3)$	$O(nDHC)$[21]	$O(N_p)$
			Improved algorithm (C2.1.2)	-	$O(\log(n))$	$O(n)$	$\leq O(n^3)$[22]		
		big-O memory complexity (C2.2)		-	$O(n^2)$	$O(n^2)$	$O(n^2)$	Variable[23]	Variable[24]
	Sparsity (C3)			Very sparse[25]	Sparse	Not inherently	Very sparse	Not inherently	Not inherently

[9] Every model could be trained in either batch or incremental training methods, and hence, this aspect does not figure in the table.
[10] Assuming a constant order ARIMA.
[11] Assuming that the topology of the ANN does not change over time.
[12] This column refers to updating the parameters of a parametric ageing model.
[13] Depending on the selected model. Particle filters allow using nonlinear transition and measurement models.
[14] Gaussian shape pdf.
[15] Gaussian shape pdf.
[16] Could become probabilistic (see section 1.2.5.3).
[17] Non-Gaussian shape pdf.
[18] Including features computation, classification and regression stages.
[19] For 100 particles.
[20] Assuming constant order ARIMA models, big-$\mathcal{O}$ complexity cannot be defined.
[21] or $O(n)$, assuming that the topology of the ANN does not change over time.
[22] Faster RVM algorithms were proposed in [83]. Not precise big-O complexity data was specified for such improved algorithms.
[23] Depending on the number of training samples, the input dimension, the number of hidden units and the number of outputs.
[24] Depending on the number of particles.
[25] However, selected data are not necessarily the most relevant (see section 1.2.1.3).

1.3.2. Considerations for future developments of data-driven ageing models for Li-ion batteries

The implementation of Machine Learning techniques to Li-ion battery ageing prediction is still at an early stage of maturity, and hence several improvement niches were identified.

About EOL criterion

Firstly, the applicability of models that directly output a RUL estimation (e.g. [48,62]) might be debatable beyond EV applications. In fact, the EOL definition corresponding to the 80% remaining capacity threshold was first defined by USABC for EV batteries back in 1996 [107], and it may not be widely suitable for other applications where the range would not be so critical. Models providing a capacity or internal resistance prediction value would probably allow a wider applicability. Therefore, a more suitable practice could be to develop capacity prediction models and further apply the certain EOL criteria representative of each specific application.

Stress-factors

Furthermore, the applicability of empirical models, which do not consider any stress-factors, also demands an in-depth analysis. Indeed, most of the methods proposed in the literature related the dependency of a certain HI with respect to the amount of performed cycles, fitting the model on ageing data obtained under constant operating conditions. Such models were neither validated at different constant operating conditions, nor at dynamic operating conditions. Li-ion battery ageing phenomena strongly depend on the operating conditions, and therefore, to perform reliable predictions, the applicability of those models should be restrained to batteries operating at similar conditions to those corresponding to the training data. If different applications or a wider operation range needs to be covered, a wider training set would be required, and more extensive validation tests would certainly be advisable.

Validation

Moreover, and as highlighted in the introduction, the accuracy of ageing models developed only with laboratory data is questionable for real-world ageing predictions, due to the intrinsic discrepancies between the operating conditions in laboratory and in real applications. In such a context, ageing models continuously updated with in-field data have an increased interest: the main patterns relating the battery operation and subsequent ageing could be approximated using laboratory experimental ageing data, and then corrected, re-calibrated or completed with in-field data to fit capture better the implications of being operating at real application profiles. In any case, the use of realistic application profiles during the offline validation phase may help to improve the performance of the initial ageing model once implemented onboard.

In the same way, preliminary offline training is advisable for Li-ion battery ageing model development. Actually, as already mentioned, a Li-ion battery does not necessarily degrade similarly in the BOL and when approaching the EOL [98]. Some cells show a sudden capacity drop, explained by a change of the dominant degradation mode [97]. There is a widespread trend in the literature, in which a single dataset (from a single cell) is used both for training and validation. Such an approach is undeniably cost- and time-efficient, as the laboratory testing stage is minimised. Nevertheless, it may not be appropriate considering that the model would be fit according to a local degradation trend of the battery (at BOL), which may significantly differ from the ageing trend experienced at more advanced stages of degradation. In most publications in the literature which used a single ageing dataset for training and prediction, early long-term predictions were usually incorrect. For probabilistic models, the EOL true value was often recorded out of the initially predicted confidence bounds (e.g. [70,92]). This could be explained by the absence of preliminary offline training. For the same reason, pure autoregressive approaches may not be advisable for the specific case of Li-ion battery ageing modelling. Moreover, such a modelling approach completely neglect the implication of the different stress-factors values on the subsequent ageing and could only be contemplated within the context of identical operation throughout the whole battery lifetime.

An adequate training procedure, already introduced e.g. in the field of conventional semi-empirical ageing modelling (i.e. not oriented to periodical updates) but under-implemented in the literature reviewed in this section, would be the four-steps development of the initial ageing model [29], involving i) a training phase including static ageing tests at different levels of the different stress-factors, ii) a first validation step at static operating profiles but unobserved during the training phase, iii) a second validation step at dynamic operating profiles of the stress-factors, and iv) a third validation step at realistic operating profiles of in-field measurable variables.

Minimising laboratory tests

However, such benchmark modelling procedure would often be limited in practice by the economic resources available for model development, which are directly related to the number of laboratory tests to be performed. The degrees of freedom to constrain the amount of laboratory tests could mainly be i) the number of stress-factors of which the influence is desired to be modelled, ii) the operation range of the stress-factors for which the ageing is desired to be modelled, and iii) the degree of validation of the initial model desired before deployment (e.g. skipping the second validation step). Minimising laboratory tests while maintaining a relatively wide operation range of the predictive model is one of the objectives highlighted in the

introduction, and its importance is reinforced by the study of the state of the art.

Reversible capacity recovery

The approach adopted to deal with battery reversible capacity recovery phenomena may also be critical in some cases. Some authors considered such recoveries as a periodical phenomenon and proposed to model it using periodical kernels [50,51]. Such modelling approach is not advisable for Li-ion batteries since such recoveries find a physical explanation on battery rest or relaxation periods [61,102,103], which do not necessarily follow a periodical behaviour for most applications. Others authors adopted time series decomposition methods to separate the overall degradation trend (low frequencies) from the reversible capacity recoveries (higher frequencies) [46,52,58,59]. Such approach would also require a deeper analysis as the authors typically tried to model the obtained high-frequency time series on the basis of the amount of performed cycles, yet a direct correlation between reversible capacity recoveries and the amount of performed cycles may not be evident. Finally, some authors [78,79] employed an empirical exponential model (relating the rest time to the actual capacity recovery), which appears to be the more appropriate solution to model reversible capacity recovery considering the physical nature of such phenomenon, yet such an approach would require experimental support and further validation from the battery ageing perspective. Overall, the long-term trend of capacity decrease seems not to be influenced by sudden capacity recoveries (e.g. in Figure 4. (b) and (c)). Therefore, not modelling those recoveries might be considered as a valid alternative to long term predictions, neglecting the corresponding data points before training.

Availability of training data

The development of ageing models often involves capacity values as training data. In the literature, such capacity values were considered as known and accurate. Although this could be the case in the context of laboratory testing, in which specific testing procedure ensure a relatively accurate estimation of the capacity, it may not be so evident for the training data collected in-field. In fact, SOH estimation in real operation requires dedicated algorithms [126], and the estimation error would induce uncertainty in the training data, propagated throughout the predictions of the ageing models. More considerations on this topic are available in Chapter 6.

1.3.3. Selection of the modelling framework and main gaps identified in the literature

In this chapter, the different methods proposed in the literature to periodically update Li-ion ageing models were reviewed, classified and compared according to several criteria to assess their accuracy and computational costs implications.

The comparative study suggests that GP and RVM could be the most suitable frameworks to design Li-ion ageing models periodically updated by upcoming in-field operation data. This is mainly justified by the following two key features they share:

- The nonparametric character: the size of these models increases along with the amount of training data. In the context of this research and according to the objectives defined in the introduction, this suggests an increased capability of these models to integrate new information from the data collected in-field after system deployment. This capability further suggests that the data scarcity raised from the minimisation of laboratory testing could be effectively compensated. Nevertheless, it is noteworthy that the minimisation of laboratory tests would still be detrimental for the accuracy of the initial model, not yet completed with in-field data and required for e.g. system sizing purposes. However, the issue of the uncertainty on initial model's reliability is minimised by the second key feature of GP and RVM.
- The probabilistic character: as mentioned in Section 1.1.2 of this chapter, one advantage of probabilistic models is their ability to quantify noise in the data. Furthermore, some of them could also identify and quantify knowledge scarcity within the training data and propagate the corresponding uncertainty throughout ageing predictions. This characteristic is of paramount importance, as it allows giving an idea about the reliability of the model's predictions.

The main drawback of GP and RVM frameworks is the computational complexity, as highlighted in Section 1.3.1. Nevertheless, a large quantity of algorithmic improvements was proposed to overturn such challenge. Furthermore, this issue would not necessarily be critical considering the recent trends in industry consisting on the implementation of cloud computing system.

Finally, and as the main conclusion of this chapter, the GP modelling framework was selected for the development of the overall Li-ion battery

Gaussian Processes

ageing predictive tool and to carry out the different research works of this thesis. The GP was favoured over the RVM because i) of the more active worldwide research activities aiming to improve the computational complexity of the GP, compared to RVM, ii) the higher level of controllability on the decision to discard or not the training data, which could be automatically removed from RVM algorithm.

Main gaps

In a nutshell, the use and development of Li-ion battery ageing models capable to learn continuously from in-field operation data is still in an early maturity stage, and hence, the applicability and usefulness of these models may be insufficient for their industrial acceptation. The most critical gaps identified in the literature are summarised as follows:

i) Most of the models proposed in the literature do not consider the different stress-factors, completely neglecting their influence on the ageing rate of the Li-ion batteries. This strongly limits the reliability of models' predictions in the context of real applications.

ii) The validation procedures implemented were insufficient or inexistent. As highlighted in Section 1.3.2, the developed models should ideally be validated through a three-step procedure, involving i) a static validation stage, in which the performances of the models are validated under constant operating conditions unobserved during the training process, ii) a dynamic validation stage, in which the performances of the model are validated under a periodically varying operation of the cells, and iii) a last validation stage, in which the performances of the model are validated under realistic operating profiles of in-field measurable variables.

iii) Most of the ageing models proposed in the literature refers to the degradation of the Li-ion batteries when the cell is electrically cycled. However, some applications are characterised by a dominant storage operation of the battery system (e.g. Uninterruptible Power Supplies, EV applications, etc.), and the development of pure calendar ageing models is also necessary.

iv) Due to the very early maturity stage of the proposed ageing models, a general picture describing the nature of the model updating process is missing in the literature. For this reason, it is difficult to perceive which kind of information could or could not be learnt posteriori, and then which information shall be incorporated within or could be saved from the initial model.

This hinders the optimised definition of the laboratory ageing test matrix, from the perspective of the test minimisation. Furthermore, it is difficult to quantify the room for improvement left to the model from the continuous learning of the in-field data.

The latter point suggests the formulation of an additional hypothesis related to the nature of the updating process of the selected GP modelling framework.

Growing the training dataset

H5: The nonparametric frameworks are able to learn about the influence of new values of the different stress-factors on battery degradation, including new data in the training set.

The verification of such hypothesis would suggest that the number of laboratory tests could be reduced by limiting the stress-factors' range or number of stress levels covered by the laboratory testing matrix.

Chapter 2.

Methodology

In the previous chapter, a critical review of the state of the art was provided, in order to identify the most suitable modelling frameworks for the development of an ageing model for Li-ion batteries, capable of learning continuously from the operation data collected from the battery systems deployed in real applications. The GP framework was identified as the most suitable candidate and selected for the further steps of this thesis. Furthermore, the main gaps of the literature were identified.

In this chapter, the overall methodology designed to govern the main research activities carried out in this thesis is described in detail.

The designed methodology aims to i) lead to the development of an ageing model complying with the main objectives of the thesis, ii) fulfil the main gaps identified during the analysis of the state of the art and iii) assess the different hypotheses formulated at the outset of the research activities, in the introductory part.

2.1. Methodology overview

As explained in the introduction, the main objective of this thesis is the development of ageing models able to learn about the influence of the battery operating conditions on the degradation, directly by observing the battery operation data collected in real application.

Following the proposed approach, illustrated in Figure 2 of the introduction, reduced laboratory tests could be used to develop a preliminary ageing model. Further, once the battery pack has been implemented and deployed, in-field data extracted by the DAS could allow updating the preliminary ageing model. In this way, the ageing model would be continuously upgraded, improving its prediction accuracy, extending the operating window of the model itself and providing useful information for predictive maintenance, adaptive energy management strategies or business case redefinition.

In Chapter 1, an extensive study of the state of the art was presented, allowing to identify some of the key features desired for an ageing model suitable for this context. First, the developed model should be able to consider the influence of the different stress-factors on ageing. These stress-factors have been identified in the literature as: i) the time elapsed in storage, ii) the cycled Ah-throughput, iii) the operating temperature, iv) the DOD, v) the middle-State-of-Charge (middle-SOC, or MidSOC) and vi) the charging and discharging C-rate. The combinations of such stress-factors define the hardness of the operation of a battery with respect to the ageing, and they should therefore be included in the development of the model.

Stress-factors to define operation

Furthermore, the validation of the developed model should be enough to ensure a correct generalisation ability of the model for predictions at realistic battery operation. This implies a validation procedure involving static, dynamic and realistic operating profiles [29].

Validation

Finally, as the battery operation in real application could involve successive stages of calendar and cycling operation, the developed model should be able to handle independently such different operating conditions.

Calendar and cycling

The in-depth analysis of the state of the art also allowed identifying the main modelling frameworks used in the literature to address similar objectives. The GP and the RVM models were identified as promising candidates. In fact, beyond their ability to perform probabilistic, relatively robust and computationally acceptable predictions, these models enjoy the very interesting feature of being nonparametric: in other words, the complexity

Probabilistic & nonparametric

of these models depends on the volume of training data. Within the context of Li-ion battery ageing prediction, this implies:

- A progressive spread of the operating window for the model. Each time a new data sample related to previously unobserved operating conditions is included within the training set, additional knowledge is obtained about the influence of stress-factors on ageing. The resulting models should provide an increasingly comprehensive picture of the ageing of Li-ion batteries.
- A higher level of specialisation of the model. The preliminary ageing model developed from the laboratory ageing data could be upgraded by including new training data extracted from the in-field operation. In-field data encodes the intrinsic operating profiles of each application, as well as the corresponding battery ageing. This implies the possibility to move from a generic ageing model to a specialised model tailored to the specific applications.

Gaussian Process

The GP was favoured over the RVM because i) of the more active worldwide research activities aiming to improve the computational complexity of the GP, compared to RVM, ii) the higher level of controllability on the decision to discard or not the training data, which could be automatically removed from RVM algorithm. Furthermore, the RVM model was shown to be a special case of the GP framework, involving a distinctive covariance function [110]. For the sake of a higher flexibility during the development of the ageing model, the general framework of GP was then selected.

Methodology

An overall methodology was designed to govern the main research activities carried out in this thesis. The designed methodology aimed to i) lead to the development of an ageing model complying with the main objectives of the thesis, ii) fulfil the main gaps identified during the analysis of the state of the art and iii) assess the different hypotheses formulated at the outset of the research activities, in the introductory part.

The designed methodology, illustrated in Figure 8, is composed of four main stages:

Stage 1: Data gathering.

Stage 2: Data preprocessing.

Stage 3: Ageing models' development and validation at static and dynamic operating conditions.

Stage 4: Validation of the ageing models at realistic operating profile.

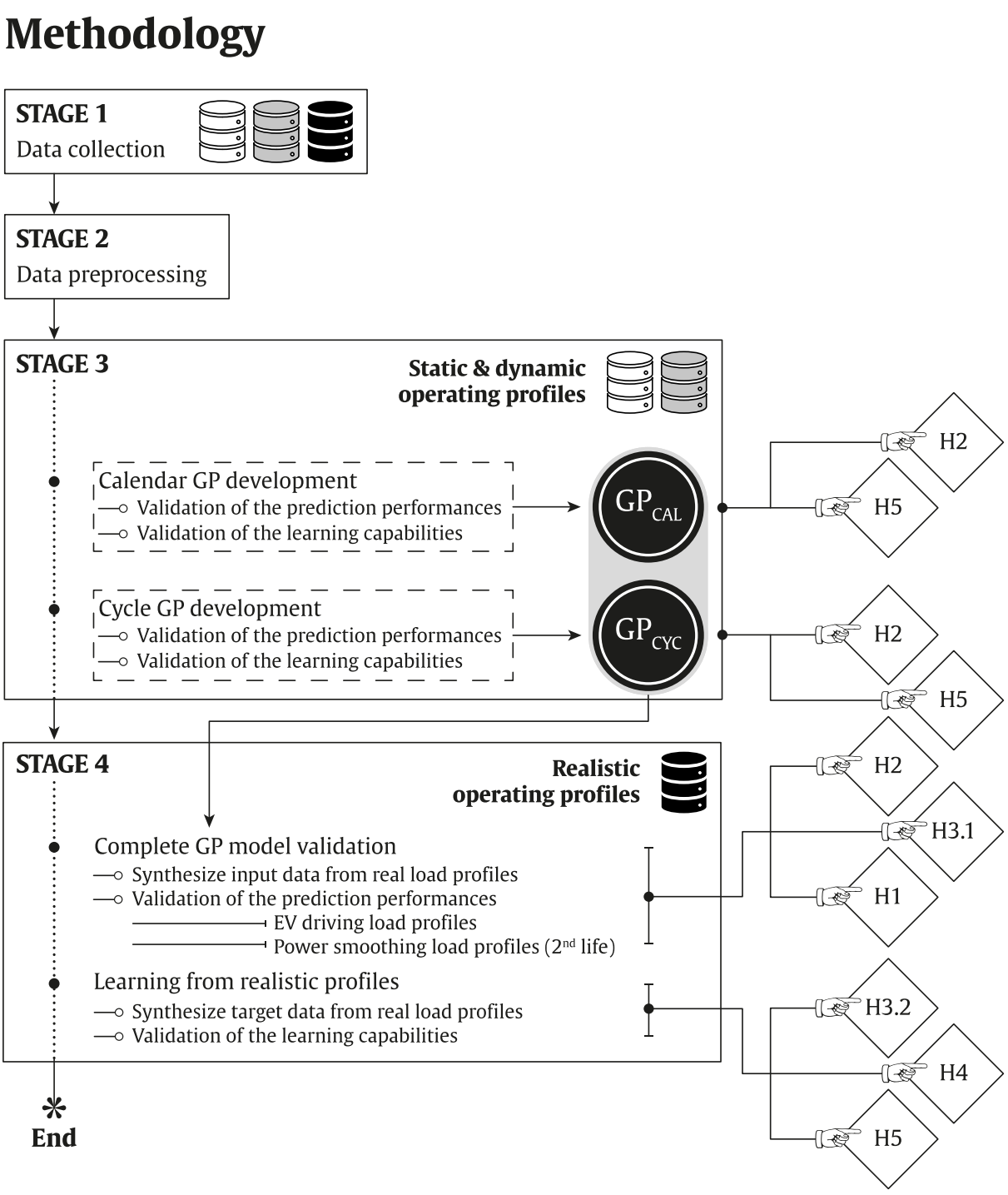

Figure 8. Overall methodology designed to govern the main research activities carried out in the context of the thesis. For each stage of the methodology, the principal tasks are specified, as well as the hypotheses evaluated from each task.

2.2. Stage 1: data collection

Within the context of the development of data-driven ageing models, the data gathering represents a critical part strongly related to the quality of the resulting model. Within the proposed approach, the ageing models are trained using the data collected from two different sources, namely i) laboratory environments and ii) real-world application environments.

Laboratory data

The collected data could present very different features depending on its provenance. On the one hand, laboratory facilities provide temperature-controlled chambers and controllable power sources to govern current and voltage signals. This ensures a relatively accurate estimation of the operating conditions applied to the cells tested in laboratory, resulting in the relative accuracy of the input values within the training dataset. Furthermore, a suitable scheduling of the experimental ageing tests involves periodical characterisation tests which aims to track the evolution of the HIs of the cells. Such characterisation tests are generally carried out with a defined periodicity and they involve high-quality measurement equipment. Furthermore, the participation of the storage and cycle operation on the evolution of the HIs could be decomposed, designing experimental ageing test matrices which separate calendar ageing tests from accelerated cycling ageing tests. Therefore, the laboratory environment allows generating relatively accurate target values for the training dataset.

In-field data

On the other hand, the operation data of battery packs implemented and deployed in real applications could be collected from a DAS. In such context, the operation data is expressed in terms of temperature, current and voltage time series. Depending on the DAS design and data gathering constraints, the quality of the data collected from the real application could be disparate. In fact, the accuracy of the current, voltage and temperature sensors, as well as the data registration frequency significantly influence the usability of the collected operation data. Moreover, the possibility to perform periodical characterisation cycles strongly depends on the application. State of Health (SOH) estimation algorithms, presenting uneven levels of accuracy, could then be necessary to track the evolution of the HIs. The quality of both input and target values of the training dataset collected from real application could then be uncertain. Table 6 summarises the characteristics of the data collected from laboratory and real application environment.

Table 6. Characteristics of the training data arising from laboratory environment and real application.

	Input training data	Target training data
Laboratory environment	- Accurate sensing - Relatively high registration frequency - Controlled operation	- Scheduled characterisation tests - Decomposed participation of storage and cycling
Real application	- Variable measurement accuracy - Variable data sampling	- SOH estimators - Indistinguishable contribution of storage and cycle operation

2.3. Stage 2: data preprocessing

Within the context of data-driven modelling, the raw data obtained from the data gathering stage must be analysed before starting any modelling task. For instance, this could consist on removing samples that may embed potential errors and possibly separate the components which are desired to be modelled from those which deserve to be discarded.

Ageing phases

The curves describing the evolution of the HIs typically reveal several ageing phases, corresponding to the occurrence of different ageing mechanisms, as illustrated in Figure 9. (a). Depending on the objectives of the developed ageing models, the modelling stage could then focus on the data corresponding to one or the other mechanisms. The combination of several analysis methods, e.g. post-mortem analysis, EIS, Incremental Capacity – Differential Voltage analysis, Energy-Dispersive X-ray Spectroscopy, etc. could help to explain the full cell degradation, allowing the identification of the main ageing mechanisms involved behind each phase of the degradation curves. Typically, the applied data preprocessing method strongly depends on the characteristics of the dataset under study. In this thesis, the dataset used to perform the different research activities was collected within the context of the FP7 European project titled Batteries2020 (grant agreement No. 608936), in the laboratories of the different partners of the project consortium. The identification of the different ageing phases, the assumptions of the corresponding ageing mechanisms and the underlying adopted data preprocessing method are detailed in Chapter 3 and Chapter 4.

Environmental & procedural errors

Furthermore, the data collected from the laboratory ageing tests embeds some experimental error part, mainly composed of i) the environmental error component and ii) procedural error component [127]. Environmental errors are systematic to multiple experiments and can be controlled to a limited degree within known bounds. Environmental errors include ambient

temperature and humidity conditions, equipment accuracy and resolution, manufacturing tolerances on battery samples and equipment used. Oppositely, procedural errors are the errors introduced as a result of performing the experiment. These types of error occur during the experimental process itself and are known to be more variable. Procedural errors include the variation of the researcher in charge of the experiment, set-up variation, sample variation, repeatability [127].

The environmental error component is intrinsic to the data and could difficultly be identified in the battery degradation curve. This is not a drastic limitation as the GP models could handle such error component, typically fitting an additive Gaussian noise [110]. However, the data samples involving high procedural errors could sometimes be identified in the ageing curve, as illustrated in Figure 9. (b). In such cases, corrective measures should then be applied to the data in order to preserve the performances of the data-driven models. In this research work, the data samples showing clear implication of experimental errors component were discarded from the modelling dataset.

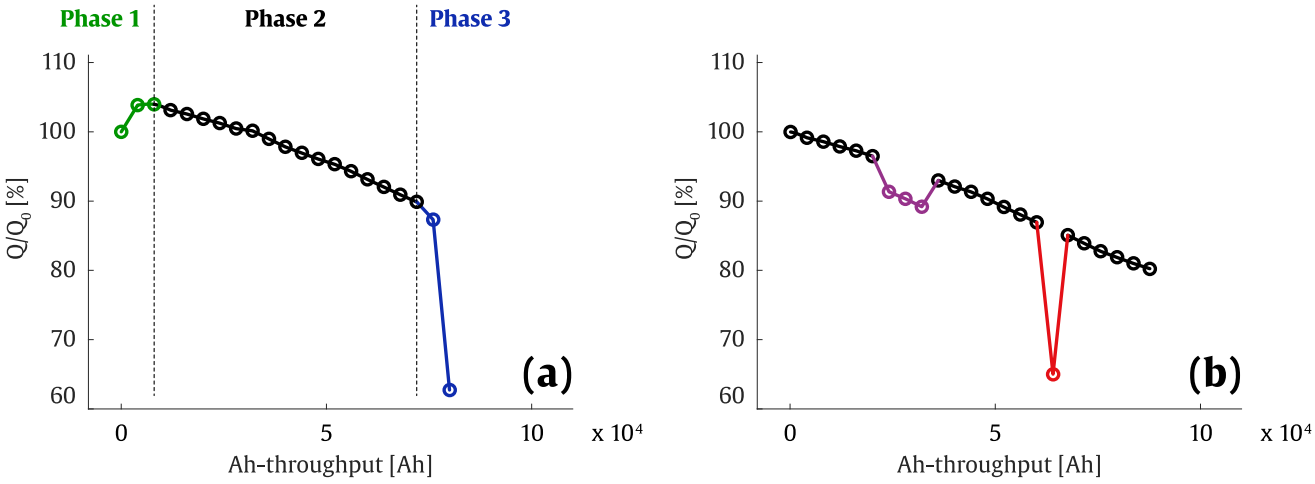

Figure 9. Illustration of different situation which could be possibly faced in the data preprocessing stage. (a) Different ageing phases sometimes observable in the capacity curves of Li-ion batteries, and (b) Experimental errors sometimes clearly observable in the ageing curves. The shift of the purple circles could e.g. be provoked by the temporary exchange of the testing device and the red circle by an accidental stopping of the characterisation test.

2.4. Stage 3: ageing model development & validation at static and dynamic operating conditions

The data collected in Stage 1 and preprocessed in Stage 2 is used in Stage 3 for the development of the ageing models. As already advanced in the introduction part, in order to achieve an overall ageing predictive framework adapted to a wide range of applications and use-cases, the overall degradation of Li-ion batteries is proposed to be modelled separating the calendar and cycling operations. The Stage 3 of the methodology, summarised in Figure 10, is then applied successively to the developed calendar and cycle ageing models. This is an important stage of the designed methodology, as it results on several substantial outcomes.

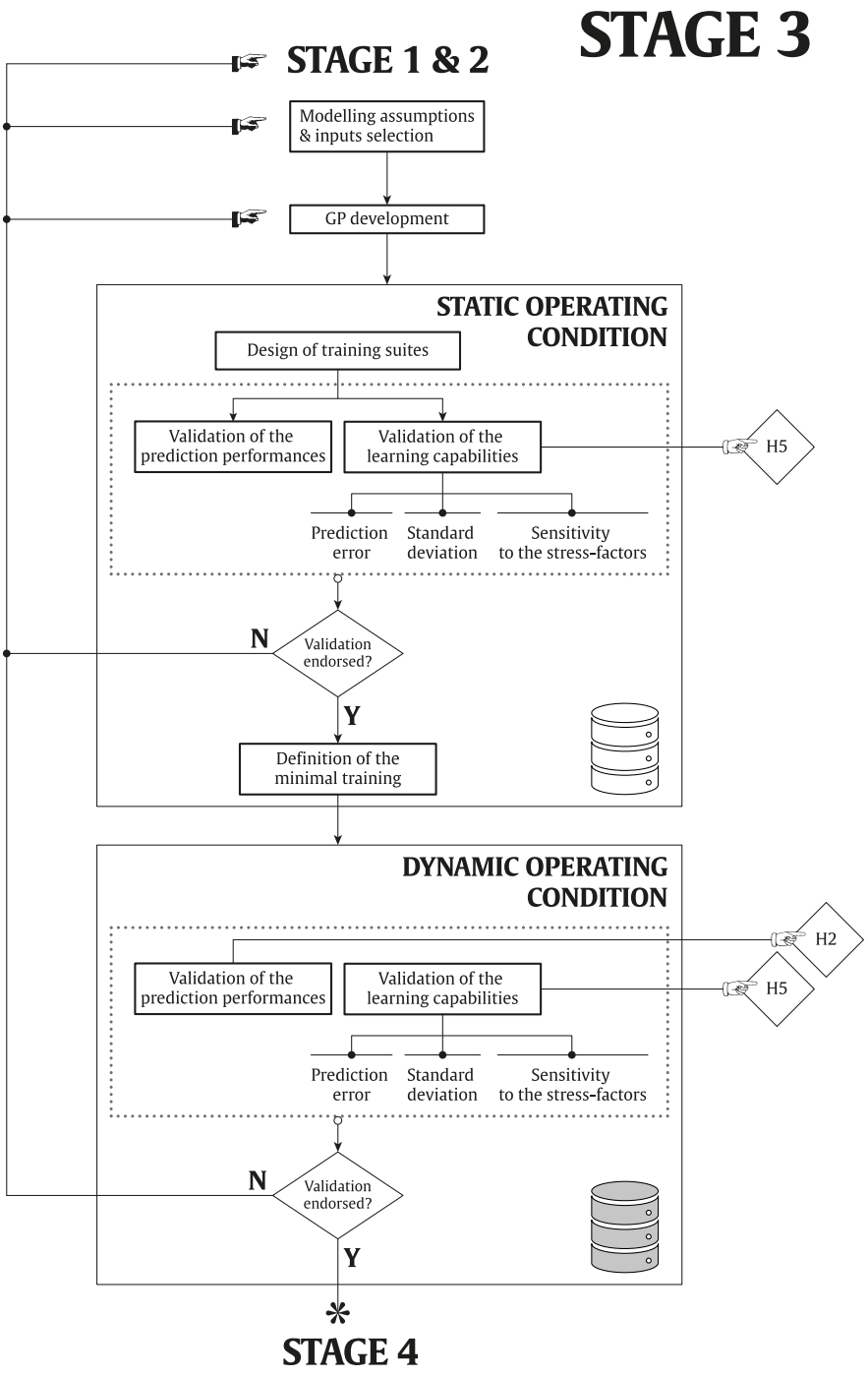

Figure 10. Detailed procedure of the Stage 3 of the methodology, applied separately to the development of the calendar and cycle ageing models.

Assumptions

The first step consists on the formulation of the main assumptions which support the development of the model, as well as on the selection of the different inputs and output variables. Within the GP framework, the assumptions formulated prior observing the data are encoded in the development of the mean and covariance functions. Both mean and covariance functions completely define the developed GP model. As explained in Chapter 1, for the development of a suitable Li-ion ageing model, the selected input variables should at least include the stress-factors values corresponding to the battery operation.

Mean and covariance

Another important and related point is the operating period covered by each data sample. Many research studies in the literature dispose of one HI data for each cycle, and then the operating period covered by each training data sample is defined as one cycle. Although such method could be pertinent for laboratory experimental data, its applicability is disputable within the context of real operating data. In fact, the availability of one HI data per cycle could be hardly conceivable in real application. Furthermore, as the ageing of Li-ion battery is a relatively slow process, the difference of the HI values obtained from one cycle to another would be reduced and highly conditioned by the measurement or estimation error components. A more appropriate method adopted in this thesis is to extend the operating period covered by each ageing data sample to higher durations (e.g. one ageing data per month, encoding the ageing corresponding to several cycles or analogously storage days). Such method also implies the reduction of the amount of training data of the developed ageing models, minimising this way the computational cost of model training.

Learning capability

One of the main goals of this research work is to ensure that, each time new data is observed about the operation of Li-ion batteries, the developed model is effectively able to infer about the relations between the operating conditions and the underlying degradation. This objective, which also corresponds to the evaluation of the hypothesis H5, is partially assessed in this stage. In fact, the ability to the developed models to learn from static and dynamic operating conditions is analysed in this stage. Such analysis is extended to the realistic operating profiles in stage 4.

Training suites

In order to simulate a situation in which the training dataset is growing along with the number of involved information, the following method is proposed: from the ageing data obtained at static operating conditions, a suite of several training cases is constructed, defining a training case as a training dataset involving a specific number of training data. The suite of the training cases is designed in such a manner that i) an increasing number of training data is involved from a training case to the following one, and ii) each

training case presents an additional value of some stress-factors, yet unobserved in the previous training case. The developed model is then successively trained with the dataset corresponding to the different training cases, following the designed training suite. The design of the training cases suites contemplated in this methodology is illustrated in Table 7.

Table 7. Illustration of the design of training suites. From the training case #1 to the training case #n, the number of training data is increasing. Furthermore, each training case introduces an additional combination of the different stress-factors yet unobserved in the previous stress-factors.

	Training case #1	Training case #2	…	Training case #n
Number of training data	78	359		6597
Involved operating conditions	Condition 1	Condition 1 Condition 2		Condition 1 Condition 2 … Condition n

The method of the training suites represents a useful approach for the validation of i) the prediction performances of the developed model and ii) the learning capabilities of the developed model.

The performances of the model are proposed to be evaluated in terms of: Accuracy

- **Accuracy of the mean prediction:** the error of the mean prediction of the developed GP model with respect to the data. The metrics adopted to evaluate the prediction error are formally defined in Section 3.4.1, Chapter 3.
- **Accuracy of the predicted confidence intervals:** as the GP models provide probabilistic predictions, the accuracy of the predicted confidence intervals should also be evaluated. The metric used to evaluate the accuracy of the confidence intervals is the calibration score (CS), defined as the percentage of data samples that are within a predicted confidence interval. Within a $\pm 2\sigma$ interval, corresponding to a 95.4% probability for a Gaussian distribution, the CS should be approximately 95.4% if the uncertainty predictions are accurate. Higher or lower scores indicate under- or over-confidence, respectively [128]. The CS is formally introduced in Section 3.4.1, Chapter 3.

Prediction errors

Furthermore, for each training case in the defined training suite, the performances of the model are assessed separately for:

- **The training cells:** the mean value of the accuracy metrics obtained for all the cells involved in the training case is calculated. Such result is informative about the ability of the model to fit the training data.
- **The validation cells:** the mean value of the prediction errors obtained for all the cells not involved in the training case is calculated. Such result is relevant to evaluate the generalisation ability of the model.
- **All the cells:** the mean value of the prediction errors obtained for all the cells. Such result is informative about the global accuracy of the model.

The learning capabilities of the developed model could be evaluated by analysing the evolution of the model's performances throughout the defined training suite. The prediction errors corresponding to the validation cells, as well as the overall error are expected to reduce, indicating that the generalisation ability as well as the global accuracy of the developed ageing models are improving. As the GP is a nonparametric framework, the complexity of the model follows the number of training data, and therefore the prediction errors corresponding to the training cells are expected to hold a roughly constant value.

Confidence intervals

The evolution of the confidence boundaries is proposed to be analysed from two different perspectives. First, the standard deviation of the models' predictions is governed by the equation (22), Chapter 1, implying that it is expected to reduce if the training dataset contains data samples with input values similar to those for which a prediction is desired to be performed. Therefore, the incorporation of different combinations of the stress-factors throughout the different cases of the training suite should be accompanied by the reduction of the predicted confidence intervals in similar input values.

Furthermore, as the number of training data increases throughout the different cases of the training suite, the evolution of the confidence intervals corresponding to the operating conditions already explored should be accompanied by the convergence of the CS metric values to 95.4%.

Sensitivity analysis

Moreover, the proposed methodology includes an additional indicator of the performances of the GP model, which is the sensitivity analysis of the model's output with respect to the different defined inputs. In fact, under particular circumstances, the observation of the optimised hyperparameters of the designed covariance function could allow interpreting how the GP

model understand the data: the relevance of each input variable for the accurate prediction of the output – from the point of view of the developed model – could be presumed. The perceptions of the model could then be compared with the general knowledge on battery degradation reported in the literature and deduce if the developed model correctly understands the relationship between the operating conditions and the ageing of Li-ion batteries. The evolution of such understanding throughout the different cases of the training suite testifies about the learning abilities of the developed model. At this point, it is important to highlight that although such sensitivity analysis could clarify how the GP model perceives the data, it is more a general indicator than a formal criterion for the evaluation of the model's performances.

Minimal number of laboratory tests

One of the objectives of the thesis listed in the introduction was the determination of the minimal number of ageing tests required from laboratory experiments to obtain an ageing model able to achieve accurate ageing predictions for a broad range of battery operation. As a method to achieve this goal, a specific training case corresponding to such minimal number of ageing tests is pursued among the different cases of the designed training suite, defining as selection criteria: i) the achievement of a prediction error less than a determined threshold in terms of training, validation and overall error, ii) the meeting of the inflexion point since which the performances curves of the model throughout the training suite do not improve anymore.

Dynamic operating conditions

The operating conditions of Li-ion batteries are barely constant in real applications. This implies that the ageing models developed in the basis of ageing tests realised at constant operating conditions must be validated at dynamic operating conditions. Furthermore, as this study focusses on the development of ageing models oriented to learn from ageing data collected from real-world operation, the analysis of the possibility to infer about the correlations between the dynamic operating profiles and the underlying ageing is necessary. After the model validation at static operating conditions, an additional validation step is designed to validate the performances and the learning capabilities of the model at dynamic operating conditions. The GP model obtained from the training case corresponding to the minimal number of laboratory ageing test is defined as baseline model and adopted to perform predictions at dynamic operating profiles. Again, the performances and the learning capability of the model are evaluated in terms of prediction errors, accuracy of the confidence interval and sensitivity analysis.

The hypotheses formulated as H2 and H5 (reported below for convenience), which are related respectively to the prediction performances and learning capabilities of the developed ageing model, are partially evaluated in stage 3. Such evaluation is completed in the last stage of the methodology, extending such assessments to the realistic operating profiles.

> **H2:** Ageing models trained with static ageing laboratory tests may be able to perform accurate predictions at dynamic and realistic operating profiles different from those observed in the laboratory.
>
> **H5:** The nonparametric frameworks are able to learn about the influence of new values of the different stress-factors on battery degradation, including new data in the training set.

2.5. Stage 4: Validation of the complete ageing model at realistic operating profiles

In the previous stages of the methodology, calendar and cycle ageing models are developed and validated at static and dynamic operating conditions. The fourth and last stage aims to connect the developed models with the load profiles observed in the real applications, validating the prediction performances and the learning capability of the model at such profiles. The fourth stage of the methodology is illustrated in Figure 11.

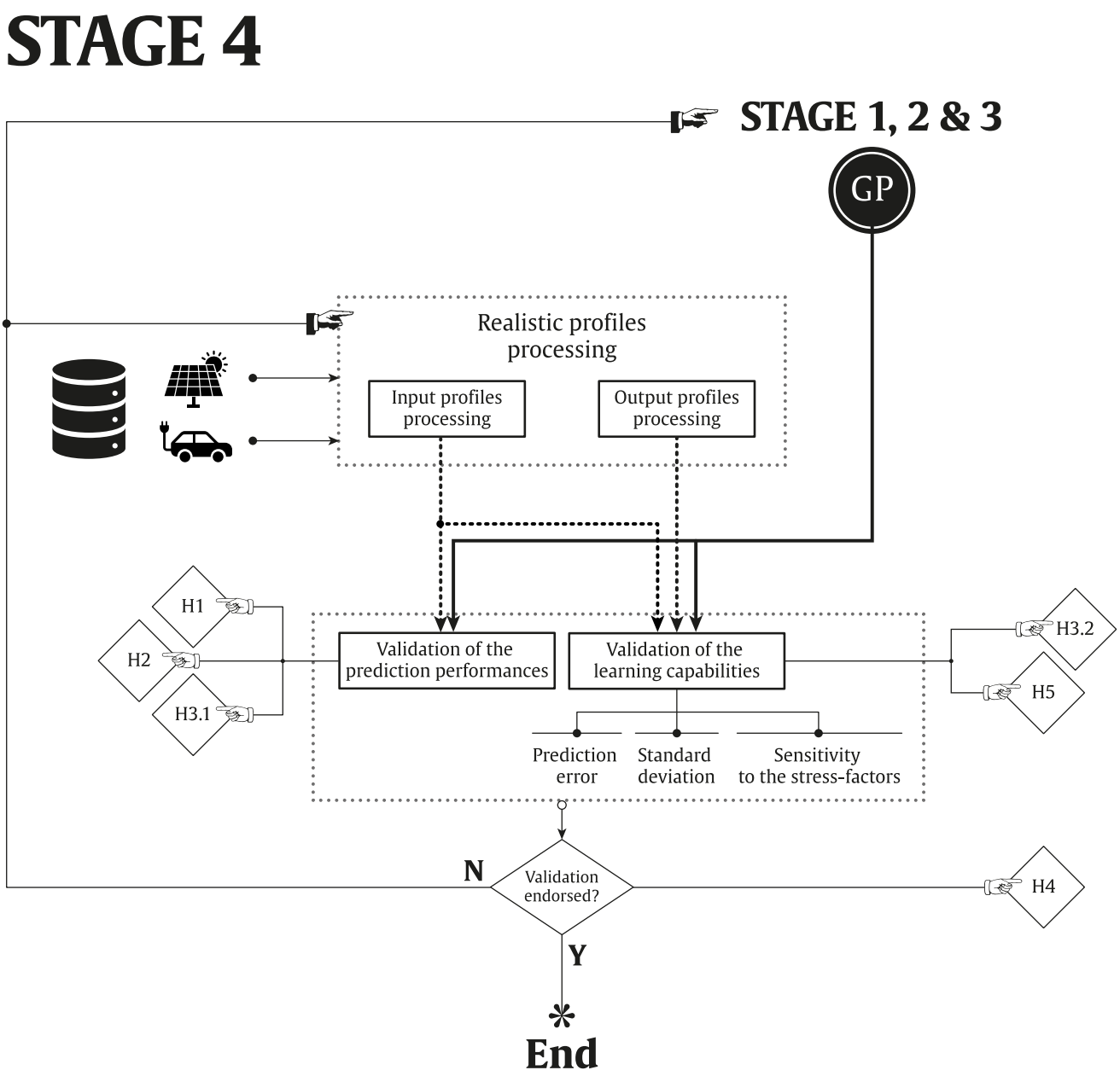

Figure 11. Detailed procedure of the Stage 4 of the methodology. The baseline GP model (including both calendar & cycle models) arising from Stage 3 corresponds to the training case related to the minimal number of required laboratory ageing tests. The input and target processing algorithms are detailed in Chapter 5.

The connection between the models developed in the previous stages and the real operation profiles presents several challenges. In fact, the operation profiles extracted from the DAS implemented in the deployed battery packs are typically expressed in terms of current, voltage and temperature time series, with uneven level of measurement accuracy and data registration frequency. However, as already explained in Chapter 1, the input of the developed models should at least involve the different stress-factors influencing on the battery ageing, and therefore the current, voltage and temperature time series must be converted into equivalent profiles of stress-factors before to be applied to the models.

Furthermore, the battery operation at real application could potentially involve successive storage and cycling operations phases. One objective of the research work is then to guarantee that the developed ageing models would be able deal with both operations, and the adopted approach contemplates the development of two separated calendar and cycle ageing models working in tandem. The time series processing algorithm should then execute two main tasks, namely i) the synthesis of stress-factors profiles equivalent to the recorded current, voltage and temperature time series with respect to the battery ageing, and ii) the decoupling of the real load operation into its equivalent calendar and cycling operation components. These objectives are summarised in Figure 12, and the designed input processing algorithm is detailed in Chapter 5.

Input processing algorithm

Although the input processing algorithm allows performing ageing predictions for batteries operating in real application, an additional challenge must be resolved in order to give to the developed models the capability to learn about the influence of the different stress-factors on the underlying degradation directly from real operating conditions. In fact, as the ageing models are developed under a supervised learning paradigm, the training dataset is composed of the input and target data. The target data corresponding to the processed inputs must then be extracted from the characterisation tests periodically carried out. Again, an additional algorithm is necessary to decompose the implication of the storage and cycling operation from the degradation quantified between two characterisation tests. The target processing algorithm is described in detail in Chapter 5.

Supervised learning

Once both operating conditions (input data) and underlying degradation (target data) are extracted from the real operating profiles, the training dataset could be completed. Both calendar and cycle ageing models could then be updated using the data extracted from real applications. The proposed approach is illustrated in Figure 12.

Target processing algorithm

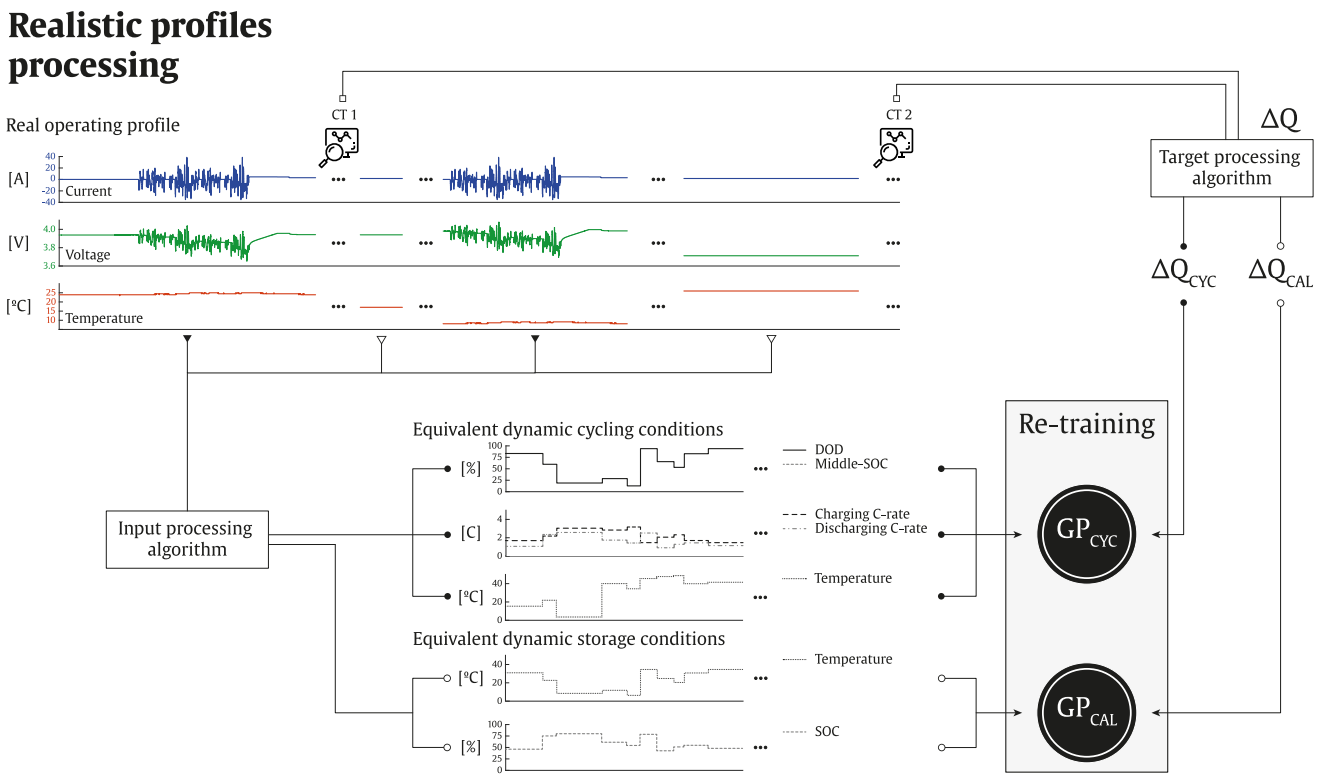

Figure 12. Illustration of the proposed approach to learn about the correlations between the operating conditions and the underlying degradation, directly from realistic profiles processing. The input and target processing algorithms are detailed in Chapter 5.

Baseline model

In the stage 4 of the proposed methodology, the calendar and cycle ageing models obtained from the training case corresponding to the minimal number of required laboratory ageing tests – determined in stage 3 – are defined as baseline models. The prediction performances, as well as the learning capability of such models are then evaluated using the real operation profiles corresponding to different applications, specified in Chapter 5. Such an evaluation is performed in terms of prediction error, accuracy of confidence intervals and sensitivity analysis, as implemented in the stage 3 of the methodology.

The implementation of this last stage of the methodology closes with the evaluation of the main objectives and the underlying hypotheses formulated in the introductory part. In fact, the validation of the prediction performances and the learning capabilities of the developed model at real operating profiles corresponds to the assessment of the hypotheses H3.1 and H3.2, respectively, reported below for convenience. It also completed the evaluation of the hypothesis H2 and H5, partially explored in the stage 3 of the proposed methodology.

H3: Converting the continuous operation data measurable in-field (see **Figure 1**. (c)) into equivalent dynamic profiles of the different stress-factors (see **Figure 1**. (b)), could be a valid approach to:

H3.1: perform accurate predictions at real operating conditions.

H3.2: learn about the influence of new operating conditions on battery degradation and update an ageing model based on laboratory data while still improving its prediction performances.

It is noteworthy that, at this stage, the ability of nonparametric frameworks to learn the influence of new ageing conditions on battery degradation is already validated for both static and dynamic operation of Li-ion batteries. Therefore, the denial of the hypothesis H5 in stage 4 would better suggest the unsuitability of the real operation time series input and target processing algorithms, rather than the incapacity of the models to learn from new operating conditions.

As the baseline models used in stage 4 are obtained from the training case corresponding to the minimal number of required laboratory tests determined in stage 3, the validation of the baseline models in stage 4 would lead to the conclusion that, "the realisation of ageing models able to learn from in-field battery operation data could allow mitigating the needs for exhaustive laboratory testing", corroborating with the hypothesis H4.

2.6. Conclusions of the chapter

In this chapter, a four-stage methodology was presented to govern the main research activities carried out in this thesis. The designed methodology aims to i) lead to the development of an ageing model complying with the main objectives of the thesis, ii) fulfil the main gaps identified during the analysis of the state of the art and iii) assess the different hypotheses formulated at the outset of the research activities, in the introductory part.

The methodology encompasses the different topics of data gathering, data preprocessing, development and validation of calendar and cycle ageing models and finally the validation of the holistic model under realistic battery operation profiles.

The following chapters are dedicated to the implementation of the designed methodology, using an extensive Li-ion battery ageing dataset.

Chapter 3.

Calendar ageing model

As previously mentioned, the approach adopted in this thesis for modelling the overall ageing of Li-ion battery is based on decomposing the ageing on two components: i) a first model corresponding to a pure calendar use-case of the battery, and ii) a second model related to a pure cycling usage of the system.

This chapter focusses on the systematic modelling and experimental verification of the cell degradation through calendar ageing, covering the implementation of the stages 1, 2 and 3 of the methodology described in Chapter 2.

This chapter is structured as follows, Section 3.1 describes the experimental ageing tests carried out in order to produce the ageing data. The raw data obtained from the experimental tests are analysed and preprocessed before the development of the model. Section 3.2 details the processing of the raw data and evaluate the relevance of the obtained data for ageing modelling. Section 3.3 presents the development of the proposed calendar ageing model under the GP framework. In Section 3.4 and 3.5, the prediction results of the developed model are presented for the cells tested at static and dynamic storage conditions, respectively. Furthermore, both sections aim to illustrate the ability of the GP model to learn from new data observation. Finally, Section 3.6 closes the study depicting the main conclusions.

3.1. Experimental calendar ageing data

Within the context of the European project titled as Batteries2020, extensive experimental works were carried out over a time span of more than three years, in order to analyse the ageing of Li-ion batteries, covering different possible operations. The capacity retention of a 20 Ah Lithium Nickel-Manganese-Cobalt (NMC 4:4:2) cathode-based pouch cell with a graphite anode was evaluated. The nominal characteristics of the cell, as well as the operating conditions recommended by the manufacturer are specified Table 8.

Table 8. Nominal characteristics of the tested cell

Electrical characteristics	
Nominal voltage [V]	3.65
Nominal capacity [Ah]	20
AC impedance (1 kHz) [mOhm]	< 3
Specific energy [Wh.kg-1]	174
Energy density [Wh.L-1]	370

Operating conditions	
End of charge voltage [V]	4.15
End of discharge voltage [V]	3.0
Recommended charge current [A]	10
Maximum discharge current (continuous) [A]	100
Operating temperature [°C]	-30/+55
Recommended charge temperature [°C]	0/+40

A testing batch of 124 cells, related to the study of the ageing in cycling operation, is described in Chapter 4, which corresponds to the development of a cycle ageing model [129]. In this chapter, the experimental works associated with the study of the calendar operation will be presented.

Temperature and SOC

From the ageing point of view, the operation of a Li-ion battery in storage is conditioned by the level of different stress-factors, mainly identified in the literature as the storage temperature and SOC [29]. A total of 32 cells were tested in temperature-controlled climatic chambers, at different combinations of such stress-factors. Periodical characterisation tests were carried out at 25°C in order to evaluate the progressive capacity retention of the cells. The determination of the capacity started 30 minutes after its surface temperature reached 25°C degrees, ensuring that the cells has stabilised at the target temperature. The test started with a constant current – constant voltage (CC-CV) charge: the CC charge was done at 6.667 A (C/3) until reaching 4.15 V, and the following CV charge was stopped when achieving current values below 1 A (C/20). After a period of 30 minutes, the

Capacity test

cell was discharged using a CC discharge current at 6.667 A (C/3) until the terminal voltage measured 3 V, followed by a pause period of 30 minutes. The procedure was repeated three times. The capacity value obtained in the last repetition was considered as the cell capacity.

Depending on the variability of the stress-factors' profiles in the whole duration of the tests, two types of ageing experiments were distinguished, namely i) the ageing tests at static operating conditions and ii) the ageing tests at dynamic operating conditions.

3.1.1. Experimental calendar ageing tests at static operating conditions

In the ageing tests performed at static conditions, the value of the stress-factors remained constant throughout the whole duration of the tests. A total of 30 cells were tested at 10 different storage conditions, specified in Table 9. These tests were performed in the laboratories of ISEA-RWTH Aachen university, which was a partner of the Batteries2020 European project consortium. The cells were characterised approximately every 28 days. In order to ensure the repeatability of the results, 3 cells were allocated to each testing condition. The capacity curves resulting from the experimental ageing tests at static conditions are observable in Figure A. 1. (a-c), Appendix A. The variability of the capacity curves obtained for each tested storage conditions is indicated in Table A. 1, Appendix A. As already reported in the literature [130], a clear effect of temperature and SOC levels is observable, in that higher temperature and SOC levels are known to induce faster capacity loss.

Table 9. Calendar ageing tests matrix, for the tests at static ageing conditions. For each testing conditions, the number of tested cells is indicated.

Temperature [°C]	SOC [%]					
	100	80	65	50	35	20
25		3		3		
35	3	3	3	3	3	3
45		3		3		

Test matrix

3.1.2. Experimental calendar ageing tests at dynamic operating conditions

As the battery stress conditions in real-world applications are not constant over time, the developed ageing models should be able to perform accurate

Dynamic operating conditions

predictions at dynamic operating profiles. The ability of the GP model to learn from dynamic profiles should also be analysed. Therefore, 2 additional cells were tested in the laboratories of Ikerlan Technology Research Centre, under variable ageing conditions, namely the temperature and SOC level were modified between each periodic characterisation experiment. The cells were characterised approximately every 28 days. The obtained capacity curves and the corresponding dynamic operating profiles are depicted in Figure A. 1. (d-e), Appendix A. It is noteworthy that the lower capacity measurement observable in Figure A. 1. (d), between days 1200 – 1300 were induced by environmental testing errors, due to temperature control issues in the climatic chambers.

3.2. Calendar ageing data preprocessing

Four phases

In the context of data-driven modelling, an important step is to analyse and preprocess the raw data before any modelling task, in order to address data inconsistency and noise issues and achieve effective models [131]. The capacity curves obtained from the experimental ageing tests described in Section 3.1 could be decomposed into four distinct phases, as illustrated in Figure 13.

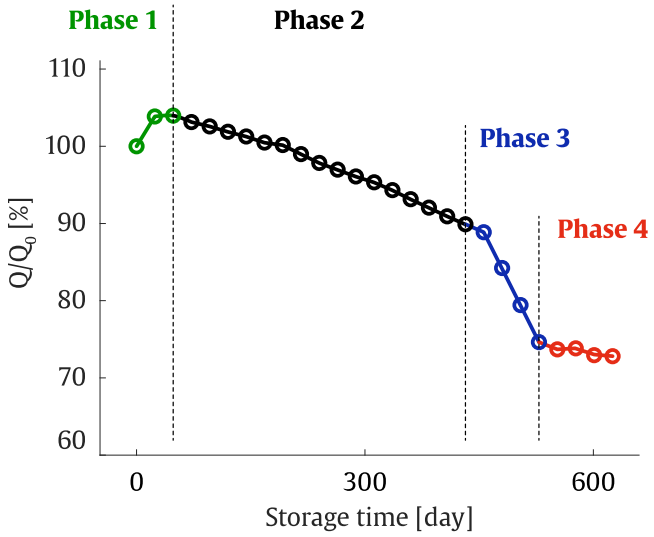

Figure 13. The four different phases of the capacity retention curve of the cells. The first phase is an increase of the capacity, the second is a progressive degradation, the third phase is a sudden capacity drop and the fourth phase is a slowdown of the capacity loss. Modified from [132].

Phase 1

The first phase corresponds to an initial capacity rise appearing at the BOL. This is clearly observable in cells exposed to relatively light ageing conditions (e.g. low temperature and SOC levels, Figure A. 1, Appendix A) and matches with the calendar experimental data already published in the literature [102,133]. According to the literature, the capacity recovery could be induced by a slow, compensating flow of active lithium between the passive and the active part of the anode, where the passive part represents the geometric excess of the anode with respect to the cathode [103,133,134]. However, no clear relationship was found between the initial capacity recovery and any ageing mechanism. Therefore, it was assumed that the initial capacity recovery phenomenon is not provoked by an ageing mechanism itself and does not have any influence on the subsequent ageing trend of the cells. This assumption should be verified in further work (see Chapter 6). Accordingly, the data corresponding to Phase 1 was discarded for the development of the ageing model. During the data preprocessing stage, the maximal capacity point of each cell was designated as the BOL point and assigned to the 'zero storage days' state.

Phase 2

After the initial capacity increase, a progressive rate-constant decrease of the cell capacity is observable, identified in Figure 13 as Phase 2. This phase is the main phase corresponding to the regular degradation of Li-ion batteries, mainly linked to the growth of the SEI, in calendar operation [135].

Phase 3

After a rate-constant decline of capacity, some cells showed a clear acceleration of the ageing rate (Phase 3), especially those stored at high temperature and SOC levels (e.g. black curves, Figure A. 1. (b), and green and blue curves, Figure A. 1. (c), Appendix A). Similar behaviour has been reported in the literature for calendar ageing [32,130,136]. One of the cells stored at 35°C and 100% SOC (black curves, Figure A. 1. (b), Appendix A) was reserved to carry out post-mortem analysis, and revealed lithium plating at one electrode edge, even after a short storage time of 240 days [132]. The early appearance of lithium deposition for this cell suggests a most advanced propagation of lithium plating for the cells aged at similar and more significant ageing conditions. Therefore, the sudden capacity drop was linked to the occurrence of lithium deposition. The turning point of the sudden capacity drop, often referred to as "knee point" [23], was diagnosed as the state in which lithium deposition starts to become irreversible [137]. Lithium plating mechanism usually takes place in cycling conditions, and its occurrence in calendar ageing is not widely reported in the literature. According to [132], the plating phenomena in these cells could have been provoked by overcharging during the periodical characterisation tests, or uneven charge distribution within the float storage.

Phase 4

In some cases, a fourth phase describing a slowdown of the capacity loss was also observable (black curves since ca. 500 days in Figure A. 1. (b), and a green curve since ca. 300 days in Figure A. 1. (c), Appendix A). The references to similar observations are scarce in the literature. Petzl et al. introduced the theory of self-weakening phenomenon of the lithium plating mechanism, explaining the decrease of the ageing rate by a counter-effect of the lithium deposition [138]. Their hypothesis was that pore clogging induced by the lithium plating leads to a loss of the active material and obstructs the full charge of the cell, making electrochemically impossible for the graphite anode to reach low voltages close to the metallic lithium's voltage. This leads to a continuous reduction of the lithium plating after the turning point of the sudden capacity reduction, until the whole disappearing of the lithium plating mechanism.

In order to develop ageing models able to predict the capacity fade corresponding to Phase 3 and 4, a deep research work would be necessary to extract and validate consistent features which could explain such occurrences, as suggested in [139]. However, this requires of large amount of data, and resulted impossible with the available dataset. For this reason, modelling the Phase 3 and 4 remained out of the scope of this research work, and the corresponding data was discarded from the modelling dataset.

Focus on Phase 2

Therefore, in the context of this study, the modelling work focussed on capturing the relations between the storage conditions and the capacity loss of the cells, during the progressive degradation corresponding to the second phase in Figure 13.

Besides, some unexpected trends were identified within the experimental data, for instance, a clear capacity recovery for the cells #26 and #28 at day 480 (respectively green and blue curves, Figure A. 1. (c), Appendix A). Such deviations are related to procedural errors during the capacity tests (e.g. exchange of the testing device, etc.). These noisy data samples could affect the performances of the model and were therefore removed from the modelling dataset.

On average, 64.64% of the initial experimental data corresponding to static ageing conditions was preserved after the preprocessing stage. The percentage of the remaining data for each cell is indicated in Table 10. Overall, all the ageing conditions of the initial experimental ageing matrix were still represented in the processed dataset. However, a large part of the cells exposed to light ageing conditions were discarded, mainly due to neglecting of the initial capacity recovery phenomenon. One of the cells stored at 35°C and 35% SOC depicted increasing capacity values until the end

of the tests and was therefore completely removed from the modelling dataset. Regarding to the cells submitted to dynamic ageing profiles, 75.56% and 52.17% of the ageing data was maintained for the cells # 31 and #32 respectively. Figure 14 illustrates the resultant ageing data obtained after the processing stage.

Table 10. Remaining data percentage ranges for each storage condition, after the data preprocessing.

Temperature [°C]	SOC [%]					
	100	80	65	50	35	20
25		94.4 – 100%		14.3 – 64.7%		
35	66.6 – 87.5	95.2%	85.7 – 90.5%	70.0 – 90.0%	10.0 – 50.0%	10.0% – 15.0%
45		30.0 – 75.0%		52.9 – 88.2%		

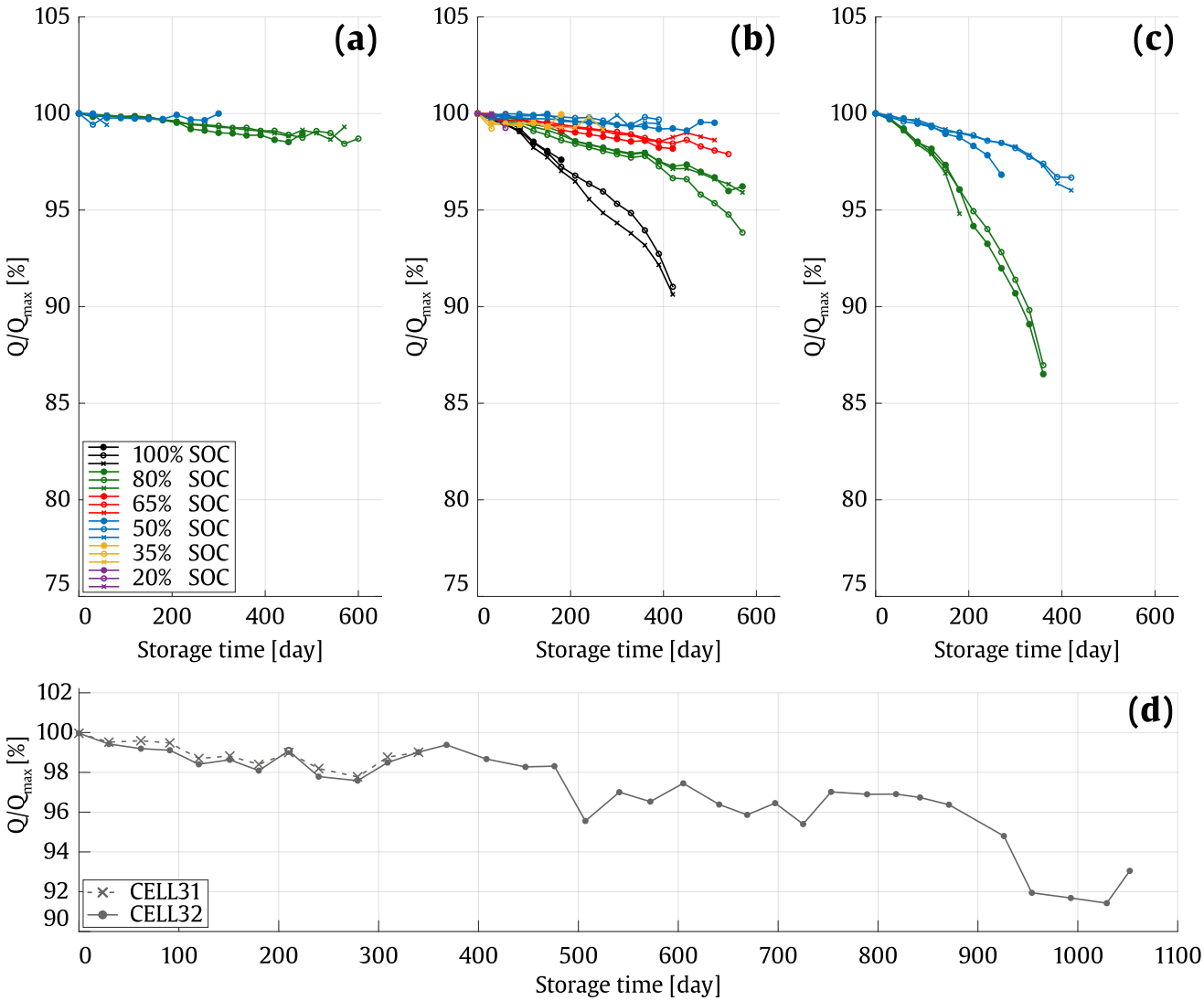

Figure 14. Normalised (with maximum value Q_{max}) capacity, obtained after the preprocessing phase of static ageing tests at (a) 25°C, (b) 35°C and (c) 45°C. (d) Normalised capacity obtained after the preprocessing phase of the dynamic ageing tests for the cells #31 and #32.

3.3. Development of the calendar ageing model

3.3.1. Assumptions and input selection

For an accurate prediction of Li-ion battery ageing at several static and dynamic operating conditions, it is necessary to consider the effect of the different stress-factors and their influence on the ageing mechanisms.

In the literature, a significant percentage of the ageing models based on Machine Learning methods do not consider the influence of such stress-factors [140]. Apart from the authors' recent work [141], only two publications were found to this effect [128,142]. Both proposed to classify and count "load patterns" depending on the stress-factors' values, defining a subset of stress-factor ranges for which the ageing is assumed to be equivalent. Then, the counted "loads" at different conditions are applied to the model. However, the definition of such "equivalency ranges" independently of the data inference could be a difficult and uncertain task, and could significantly vary from some commercial battery reference to another. The selection of too broad ranges supposes a low resolution in the input space and could lead to a poor accuracy of the model. The selection of too narrow ranges induces an increased number of inputs, increasing the computational cost and the uncertainty associated to each range.

Stress-factors as input

The GP framework allows quantifying the similarities of the input space with respect to the output through data inference, depending on the kernel properties. Therefore, a better solution could be to introduce the stress-factors' values directly as an input, as already highlighted in a previous publication [141]. As a result, the "equivalency" or "similarity ranges" of each stress-factor are directly inferred from data and updated each time new data is available.

Within the context of calendar ageing, in addition to the time-dependence, the main stress-factors involved are assumed to be the cell temperature and the SOC [130]. Therefore, the model we proposed in this section considered three inputs:

- Δt: the storage time for which the ageing is predicted.
- T^{-1}: the reciprocal of the temperature corresponding to this storage time (for alignment to the Arrhenius law).
- SOC: the SOC level corresponding to this storage time.

Output

The output of the model was the capacity loss ΔQ corresponding to a Δt storage time at T and SOC storage conditions.

3.3.2. Kernel construction

As explained in Section 1.2.4.1, the kernel $\kappa(\mathbf{x}, \mathbf{x}')$ specifies how similar or correlated the outputs y and y' are expected to be for two inputs $\mathbf{x}$ and $\mathbf{x}'$, respectively. The selection of the structural form of the kernel is the most important challenge in nonparametric regression [110]. However, it remains a largely subjective process based on trial and error and designer experience, as there is not any broadly accepted method to perform this task [143]. For all the GP ageing models presented in the literature, the selection of the kernel was based on trial and error methods. In this way, the kernel function presenting the lowest error with respect to a specific dataset was considered as the most suitable. Following this method, the suitability of the selected kernel in the general context of Li-ion battery ageing prediction could hardly be guaranteed, due to its high correlation to the used dataset. In order to develop GP models tailored to Li-ion battery ageing application, a stronger justification of the kernel selection is desirable.

Compositional kernels

Zero-mean function

As noted in Section 3.3.1, the model must be able to handle different input dimensions. Consequently, compositional kernels' framework is a suitable solution to construct a main kernel composed of interpretable components, each one related to a specific input dimension [143]. In order to focus on the behaviour of the composed kernels, a zero-mean function was defined in this work. This is not a significant limitation, since the mean of the posterior process is not confined to be zero [110].

3.3.3. Selecting individual kernel components

As explained in Section 1.2.4.1, the GP framework is a nonparametric model, and therefore the learning problem is the problem of finding the suitable properties of the function (isotropy, anisotropy, smoothness, etc.), rather than a particular functional form [110].

Isotropic kernels

The range of the SOC input dimension is intrinsically limited between 0 – 100%. This is defined to be a local modelling problem. In the context of the development of ageing models oriented to learn from the data observed after their deployment in real application, the definition of the similarity using the Euclidean distance seems suitable, as it could allow the model to cover the whole SOC range after the observation of a few data points. Therefore, the kernel components corresponding to the SOC input space could be represented by isotropic kernels. Furthermore, the operation window corresponding to the temperature input is limited by the recommendations of the manufacturer (i.e. storage temperatures between -30°C and 55°C), specified in Table 8. Accordingly, isotropic kernel could also be assigned to

such input dimensions. Furthermore, different kind of isotropic kernels could be selected for these inputs, depending on the smoothness assumption for the process. The Ornstein-Uhlenbeck kernel, detailed in [110], was deemed too rough to describe the influence of the stress-factors on ageing. Besides, although the squared-exponential kernel is the most widely used isotropic kernel, its strong smoothness assumption was claimed to be unrealistic for modelling many physical processes (e.g. implication of charging C-rate deviations on underlying capacity loss) and the Matérn kernel class was recommended instead [110]. Therefore, a 5/2 Matérn kernels were selected to host independently the input dimensions corresponding to each stress-factor.

Matérn

The kernel component related to the Δt input dimension requires several Δt values to be involved in the training data, in order to optimise the associated hyperparameters. In order to limit the training computation time, only three different values of Δt were processed in the training data (which are 30, 60 and 90 days). Table 11 illustrates the structure of the training data. In this context, the use of an isotropic kernel requires a large amount of different values of Δt for long-term prediction, implying a large quantity of training data and increased computation times. Therefore, this kernel component should be anisotropic. In the second phase of the Li-ion cells ageing described in Figure 13, the capacity loss seems to be linear with respect to Δt. Therefore, a linear kernel component was selected for this input dimension.

Linear kernel

Table 11. Example of the training data structure

		Input vector **x**			Target y
		Δt [days]	T^{-1} [K^{-1}]	SOC [%]	ΔQ [%]
CELL02	data vector 1	30	0.0034	80	-0.041
	data vector 2	60			-0.136
	data vector 3	90			-0.181
	data vector 4	30			-0.095
	data vector 5	60			-0.140
…	…	…	…	…	…
CELL09	data vector 1	30	0.0032	100	-0.310
	data vector 2	60			-0.572
	data vector 3	90			-0.949
	data vector 4	30			-0.261
	data vector 5	60			-0.638
…	…	…	…	…	…

Although the data vectors ‘CELL002 – data vector 1’ and ‘CELL002 – data vector 4’ in Table 11 have the same inputs values, the target is different because both correspond to a the capacity loss from a different starting point,

in the capacity curve of the CELL002. The data vectors with identical input values and different outputs are useful for the determination of the noise hyperparameter of the GP models (see Equation (30)).

3.3.4. Composing the whole kernel

In the GP framework, the kernel function is also a covariance function and therefore must be positive semidefinite [110]. Moreover, positive semidefinite compositional kernels are closed under the addition and multiplication of basic kernels. The effect of these operations is well explained in [143], for example: "A sum of kernels can be understood as a [logical] OR operation. Two points are considered similar if either kernel has a high value. Similarly, multiplying kernels is a [logical] AND operation, since two points are considered similar only if both kernels have high values".

Additive kernels assume the added stochastic processes to be independent. However, the inputs T and SOC interact in the kinetics reactions inside the electrode [28], hence additive kernel composition should be avoided. In order to account for the interactions between the different input dimensions, the tensor product is suggested within [110,143] and is used in the composed kernel (equation (30)).

Tensor product

$$\kappa(\mathbf{x},\mathbf{x}') = {\sigma_f}^2 \cdot \left[\begin{array}{c} \left(1+\sqrt{5}\cdot\frac{|\mathbf{x}_1-\mathbf{x}'_1|}{\theta_T}+\frac{5}{3}\cdot\frac{|\mathbf{x}_1-\mathbf{x}'_1|^2}{{\theta_T}^2}\right)\cdot\exp\left(-\sqrt{5}\cdot\frac{|\mathbf{x}_1-\mathbf{x}'_1|}{\theta_T}\right) \\ \cdot\left(1+\sqrt{5}\cdot\frac{|\mathbf{x}_2-\mathbf{x}'_2|}{\theta_{SOC}}+\frac{5}{3}\cdot\frac{|\mathbf{x}_2-\mathbf{x}'_2|^2}{{\theta_{SOC}}^2}\right)\cdot\exp\left(-\sqrt{5}\cdot\frac{|\mathbf{x}_2-\mathbf{x}'_2|}{\theta_{SOC}}\right) \\ \cdot\left(\mathbf{x}_3\cdot\mathbf{x}'_3+{\theta_{\Delta t}}^2\right) \end{array} \right] + {\sigma_n}^2\cdot I \qquad (30)$$

where $\mathbf{x}$ and $\mathbf{x}'$ are different input vectors structured as $\mathbf{x}=(\mathbf{x}_1,\mathbf{x}_2,\mathbf{x}_3)$, with $\mathbf{x}_1 = T^{-1}$, $\mathbf{x}_2 = SOC$, $\mathbf{x}_3 = \Delta t$;

Hyperparameters

θ_T, θ_{SOC}, and $\theta_{\Delta t}$ are the hyperparameters related to the T, SOC and Δt inputs respectively. The additional hyperparameters ${\sigma_f}^2$ and ${\sigma_n}^2$ are respectively the signal variance, which plays the role of scaling the outputs in the dimension of the capacity loss ΔQ, and the noise variance, which models an additive Gaussian noise from the data.

3.4. Learning from static operating conditions

This section aims to illustrate the ability of the developed GP model to improve its prediction performances while observing an increasing number of battery calendar operation data. Indeed, as new observations of storage conditions are presented to the model, the training dataset of the model involves a more comprehensive view of the influence of the different combinations of stress-factors on the capacity loss. Therefore, for each prediction, the covariance function is able to find more similar examples in the training dataset, in term of storage conditions. The prediction performances of the model improve throughout the whole operation window of the Li-ion cells.

Completing the training dataset

In this section, the improvement of the model performances was evaluated in terms of:

- **Accuracy of the prediction:** as the training dataset increases, a reduction of the prediction errors is expected over the whole operation window. The metrics used to evaluate the prediction error are detailed in Section 3.4.1.

Accuracy

- **Confidence in the prediction:** as the training dataset increases, the model disposes of more information about the ageing throughout the whole operation window. In accordance with the covariance equation (22), the confidence intervals of the predictions are expected to reduce, signifying that the model is more confident about its predictions. The metric used to evaluate the accuracy of the confidence intervals is detailed in Section 3.4.1.

Confidence

3.4.1. Evaluation metrics

Six different metrics were used to assess the prediction performances of the two ageing models. The first one was the root-mean-square error (RMSE) of the output of the model, which was the capacity loss ΔQ, defined according to equation (31).

$$RMSE_{\Delta Q}(\hat{\boldsymbol{y}}_i, \boldsymbol{y}_i) = \sqrt{\frac{1}{N_T}\sum_{i=1}^{N_T}(\hat{\boldsymbol{y}}_i - \boldsymbol{y}_i)^2} \qquad (31)$$

where $\hat{\boldsymbol{y}}_i$ is the predicted output, $\boldsymbol{y}_i$ is the measured output and N_T is the number of points to be evaluated. The second metric was defined as the RMSE of the predicted capacity curve:

$$RMSE_Q(\hat{\boldsymbol{Q}}_i, \boldsymbol{Q}_i) = \sqrt{\frac{1}{N_T}\sum_{i=1}^{N_T}(\hat{\boldsymbol{Q}}_i - \boldsymbol{Q}_i)^2} \tag{32}$$

where $\hat{\boldsymbol{Q}}_i$ is the predicted capacity calculated by accumulation of the output and $\boldsymbol{Q}_i$ is the measured capacity. This second metric is useful in order to evaluate the accumulative error of the model.

The RMSE is useful to assess the prediction performances of a model, with an emphasis on the high deviations which are strongly penalised. In order to evaluate the ability of the model to capture the main trends of the data, the analysis was completed with the implementation of the Mean Absolute Error (MAE), defined in equation (33) and (34) in terms of model output and capacity curve, respectively.

$$MAE_{\Delta Q}(\hat{\boldsymbol{y}}_i, \boldsymbol{y}_i) = \frac{1}{N_T}\sum_{i=1}^{N_T}|\hat{\boldsymbol{y}}_i - \boldsymbol{y}_i| \tag{33}$$

$$MAE_Q(\hat{\boldsymbol{Q}}_i, \boldsymbol{Q}_i) = \frac{1}{N_T}\sum_{i=1}^{N_T}|\hat{\boldsymbol{Q}}_i - \boldsymbol{Q}_i| \tag{34}$$

Acceptable prediction error

In the context of this study, the main objective of the model was to capture the main trends of Li-ion battery ageing in different operating conditions, rather than achieving a perfect fit of each data point. Therefore, a 2% MAE_Q threshold was defined as acceptable prediction error.

The final metric was the Calibration Score (CS), which aimed at quantifying the accuracy of the uncertainty estimates. It is defined as the percentage of measured results in the test dataset that are within a predicted credible interval. Within a $\pm 2\sigma$ interval, corresponding to a 95.4% probability for a Gaussian distribution, the CS is given by equations (35) and (36).

$$CS_{2\sigma-\Delta Q} = \frac{1}{N_T}\sum_{i=1}^{N_T}[|\hat{\boldsymbol{y}}_i - \boldsymbol{y}_i| < 2\sigma] \cdot 100 \tag{35}$$

$$CS_{2\sigma-Q} = \frac{1}{N_T}\sum_{i=1}^{N_T}\left[\left|\widehat{\boldsymbol{Q}}_i - \boldsymbol{Q}_i\right| < 2\sigma\right] \cdot 100 \qquad (36)$$

Therefore, $CS_{2\sigma}$ should be approximately 95.4% if the uncertainty predictions are accurate. Higher or lower scores indicate under- or over-confidence, respectively [128].

Target calibration score

3.4.2. Training case studies to illustrate the learning of new operating conditions

In order to illustrate how the GP model could learn from new observations and improve prediction performances, 7 distinct training cases were defined, each one involving a different number of training data from the ageing dataset presented in Section 3.1. From the training case 1 to the training case 7, the number of training data increased: the data corresponding to new storage conditions was included progressively, revealing one by one the influence of the different levels of the different stress-factors.

Training suite

Accordingly, the distinct temperature values were introduced from case 1 to case 2, followed by the different SOC levels from case 3 to case 7. The training case 1 involved the single 80% SOC condition at the temperature extrema of the static test matrix (25°C and 45°C). The temperature range was completed in case 2 with the additional value of 35°C. Since the training case 3, different SOC storage values were introduced, starting by the 50% SOC value at the three temperatures. The SOC range was then progressively completed alternating the incorporation of highest and lowest values, i.e. 100%, 20%, 65% and 35% SOC respectively in training cases 4, 5, 6, and 7. The characteristics of each training case are summarised in **Table 12** specifying the different storage conditions involved during the training process, as well as the corresponding ratio of the amount of training data with respect to the whole available data.

Table 12. Summary of the different case studies, specifying the different cells involved and the related storage conditions, as well as the ratio of the amount of training data with respect to the whole available data.

		Learning Temperature	Learning SOC	# Training data / # Total data [%]
CASE 1	T	25 45		24.86
	SOC	80		
CASE 2	T	25 45 35		42.40
	SOC	80		
CASE 3	T	25 45 35	25, 35, 45	70.13
	SOC	80	50	
CASE 4	T	25 45 35	25, 35, 45 35	79.70
	SOC	80	50 100	
CASE 5	T	25 45 35	25, 35, 45 35	80.44
	SOC	80	50 100 20	
CASE 6	T	25 45 35	25, 35, 45 35	95.43
	SOC	80	50 100 20 65	
CASE 7	T	25 45 35	25, 35, 45 35	100
	SOC	80	50 100 20 65 35	

3.4.3. Prediction results

3.4.3.1. Accuracy improvement

The black curves in Figure 15 indicate the prediction accuracy of the GP model proposed in Section 3.3, trained with the different training cases defined in Section 3.4.2, in term of $MAE_{\Delta Q}$ and MAE_Q. The corresponding RMSE values are indicated in Table A. 2, Appendix A. For each training case, the error calculation was performed separately for:

Fitting

- The training cells: the mean value of the prediction errors obtained for all the cells involved in the training case was calculated (Figure 15. (a)). Such errors are informative about the ability of the model to fit the training data.

Generalisation

- The validation cells: the mean value of the prediction errors obtained for all the cells not involved in the training case was calculated (Figure 15. (b)). Such error is relevant to evaluate the generalisation ability of the model.

- All the cells: the mean value of the prediction errors obtained for all the cells (Figure 15. (c)). Such error is informative about the global accuracy of the model.

As expected, the predictions errors of the training cells in Figure 15. (a) fulfil the 2% MAE_Q threshold for all the training cases. Regarding the validation cells, the threshold of the 2% MAE_Q is reached for the training case 2 (see

Figure 15. (b)). For the training case 3, the model achieved 0.64% MAE_Q accuracy and the performances of the model seem not to improve significantly since such training case.

Learning the influence of

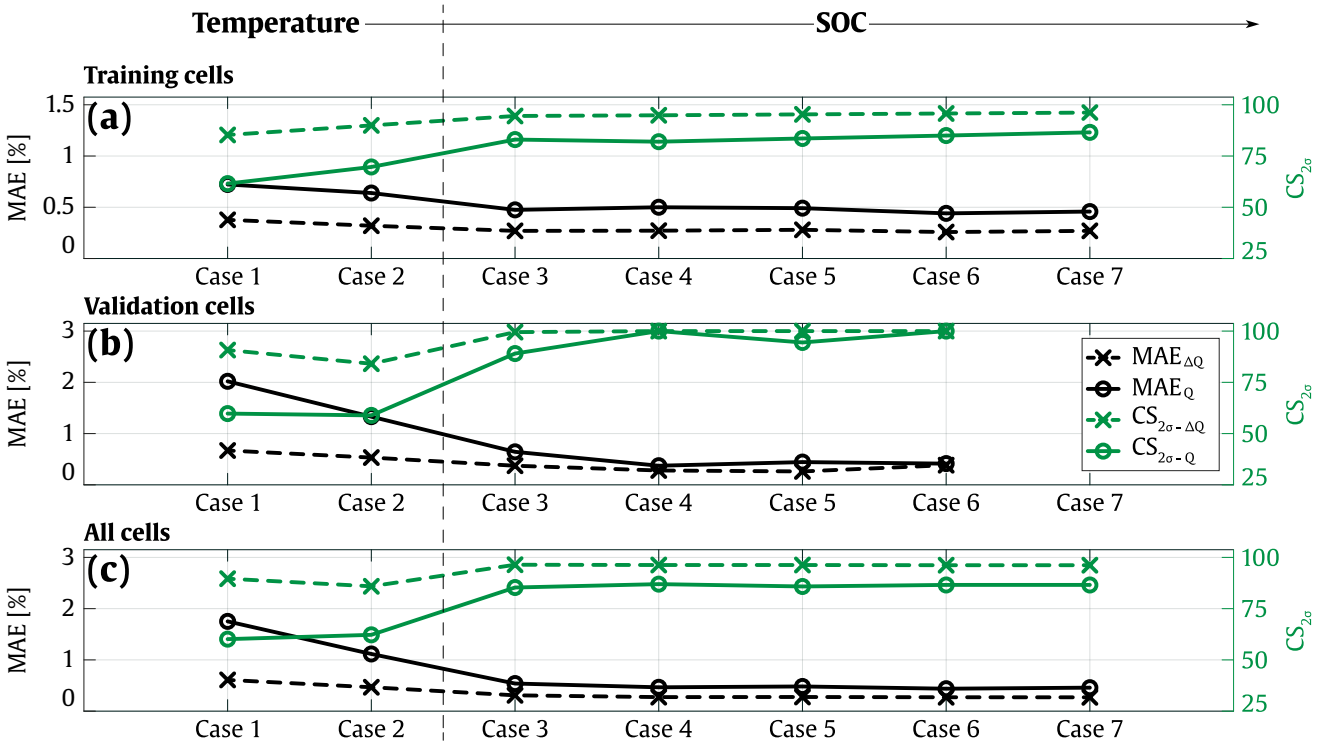

Figure 15. Prediction results corresponding to each training case, in term of MAE_Q and $CS_{2\sigma}$, distinguishing the errors of (a) all the training cells, (b) all the validation cells and (c) all the cells.

Figure 16. (a-d) illustrates the capacity predictions of the GP model resulting from the training case 3, for different storage conditions involved in the training data. The average $MAE_{\Delta Q}$ and MAE_Q errors of the model corresponding to the training case 3 were 0.27% and 0.47%, respectively, for the training cells. The average $CS_{2\sigma-\Delta Q}$ and $CS_{2\sigma-Q}$ were respectively 94.54% and 83.03%.

Results in training conditions

Figure 16. (e-h) aims to underpin the improvement of the generalisation performances of the GP, while increasing the number of training values in

Showing model improvement

the input space of the SOC. To this end, the capacity predictions were represented for the cells stored at 35°C and 65% SOC, using GP models obtained from different training cases. The model obtained from the training case 1 did not have any information neither about the degradation at 35°C nor about the effect of SOC on the capacity loss, as the training data involved the single input of 80% SOC. At this stage, the prediction at lower SOC levels were over-estimated (see Figure 16. (e)). The mean error obtained at 35°C and 65% SOC storage condition was 3.15% MAE_Q. In the training case 2, the incorporation of the 35°C storage temperature in the training data improved significantly the prediction, reaching a 1.12% MAE_Q, Figure 16. (f). In the training case 3, the model started to learn the effect of the SOC by incorporating a 50% SOC condition in the training data. The mean error of the prediction improved drastically (0.34% MAE_Q), as the model could infer from two different SOC values and gain a numerical intuition about the effect of the SOC on capacity loss (see Figure 16. (g)). For comparison, the results obtained with a fully trained GP (training case 7) were also plotted in Figure 16. (h): there was not significant improvement in term of error reduction. However, the confidence intervals were slightly reduced, indicating a higher confidence of the model to perform predictions in at 65% SOC, since such operating condition was represented in the training data (more details in Section 3.4.3.2). At this point, it is noteworthy that the model corresponding to the training case 7 is only used in this study for a sake of comparison with the previous cases. In fact, such a model would be unreliable for deployment, as it involves all the available data for training and then its performances would not be further validated under static conditions.

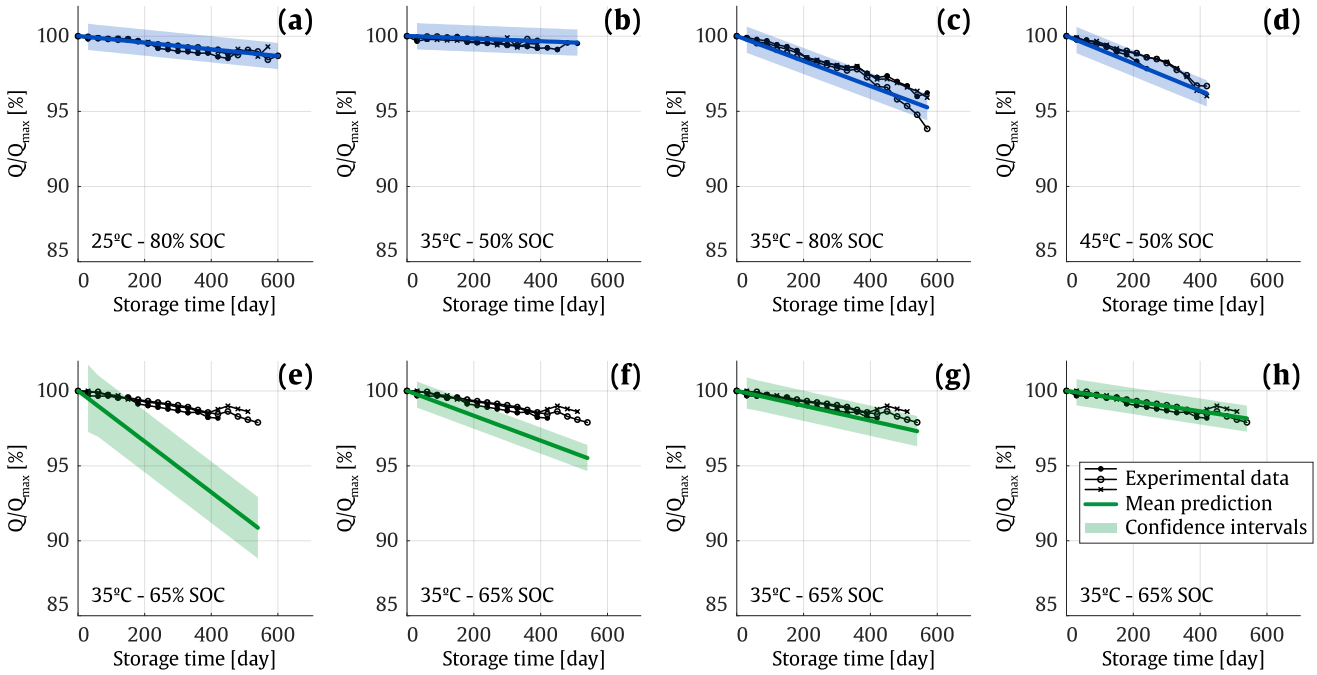

Figure 16. Capacity predictions with the GP model trained at training case 3, for the training cells stored at (a) 25°C and 80% SOC, (b) 35°C and 50% SOC, (c) 35°C and 80% SOC, (d) 45°C and 50% SOC. Capacity predictions for the cells stored at 35°C and 65% SOC, with the GP models trained at (e) training case 1, (f) training case 2, (g) training case 3 and (h) training case 7.

3.4.3.2. Increase of confidence

As stated by the variance equation (22), the confidence intervals of a prediction reduce if the training dataset involves data samples similar to the predicted input values. Informally, this means that the model feels more confident to do predictions in case it already observed similar operating conditions in training data. Therefore, the analysis of the width of the confidence intervals – or equivalently the standard deviation value - along a large operating range of each stress-factor is informative about how confident the model feels to perform predictions throughout a broad operating window. In this sense, the evolution of the standard deviation throughout the input space testifies about the learning process of the model.

Evolution of standard deviation

Figure 17 shows the evolution of the standard deviation of the GP model predictions throughout the whole operation window of the Li-ion cell under study, for the different training cases. In Figure 17. (a), the standard deviation of the model obtained from the training case 1 indicates lowest values around 25°C and 45°C, which are the only storage temperatures experienced at this stage. The observation of the effect of a 35°C operation in the training case 2 flattened the curve around such temperature: at this stage, the

Gaining confidence

Uncertainty at unknown temperatures

obtained model felt relatively confident to perform predictions within the 20°C - 50°C temperature range. It is noteworthy that the model presented high standard deviation values at low and negative temperatures, due to the lack of information in such storage regions. Figure 17. (b), (c), (d) and (e) corresponds to the learning of the influence of the SOC, showing the evolution of the standard deviation of the GP model predictions throughout the whole SOC range and at constant 15°C, 25°C, 35°C and 45°C, respectively. As expected, the lowest standard deviation stood near 50% and 80% for training case 3, and the observation of intermediate SOC levels from the training cases 4 to 7 lead to reduced values in the whole range, unless below 20% SOC operation which still was an unknown storage condition. It is noteworthy that the lowest standard deviation values are observable at 35°C, Figure 17. (d), as the SOC input space was explored at this temperature. Besides, the standard deviation of the predictions at 15°C, Figure 17. (b), achieved highest values for the training case 7. This is due to the higher relevance associated to the temperature in such training case (see sensitivity analysis in Section 3.4.3.3), which led to a higher gradient in the evolution of the standard deviation throughout unknown temperatures, e.g. colder temperatures than those involved in the training dataset.

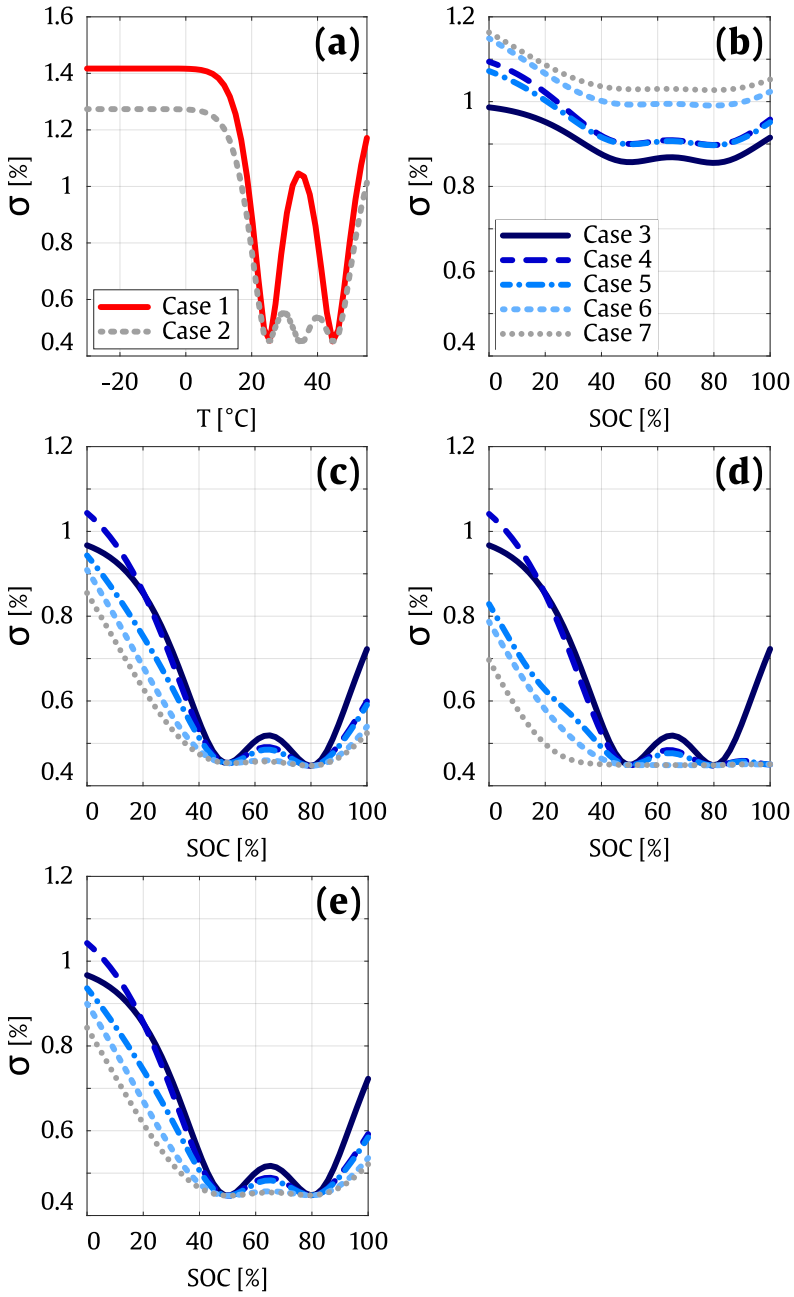

Figure 17. Evolution of the standard deviations of the GP model predictions throughout the whole operation window of the Li-ion cell under study, from training case 1 to 7. (a) Evolution throughout the temperature space, at constant 80% SOC (b) Evolution throughout the SOC space, at constant 15°C, (c) Evolution throughout the SOC space, at constant 25°C, (d) Evolution throughout the SOC space, at constant 35°C and (e) Evolution throughout the SOC space, at constant 45°C.

The reduction of the standard deviation in Figure 17 testifies about the increment of the model's confidence to perform prediction throughout a broad operating window, as input spaces are progressively explored. Furthermore, the accuracy of the confidence level of the model was evaluated using the CS metric, introduce in Section 3.4.1. As previously explained, the $CS_{2\sigma}$ values should be approximately 95.4% if the uncertainty predictions are accurate. Higher or lower scores indicate under- or over-confidence of the model, respectively [128].

Slightly over-confident

In Figure 15, the evolution of the mean value of the CSs were plotted for each training case of the GP model, in term of capacity loss and accumulated capacity. Since the training case 3, the overall $CS_{2\sigma-Q}$ values converge into approximately 86.55% (Figure 15. (c)). This traduces a slightly over-confident behaviour of the model in term of the accumulated capacity. However, regarding the CSs values corresponding to the output of the model, the overall $CS_{2\sigma-\Delta Q}$ values converge into approximately 96.19%.

3.4.3.3. Sensitivity of the capacity loss to the stress-factors

Automatic Relevance Determination

For many covariance functions, the observation of the hyperparameters allows one to interpret how the GP model understand the data. For isotropic kernels, the hyperparameters play the role of characteristic length-scale. Such covariance functions implement automatic relevance determination, since the inverse of the length-scale determines how relevant an input is: if the length-scale has a very large value, the covariance will become almost independent of that input, effectively removing it from the inference [8]. Therefore, the sensitivity of the capacity loss to the different stress-factors could be analysed by observing the inverse of their respective hyperparameters. Figure 18 displays, for each training case, the inverse of the hyperparameters corresponding to the temperature and SOC, relatively normalised to each other.

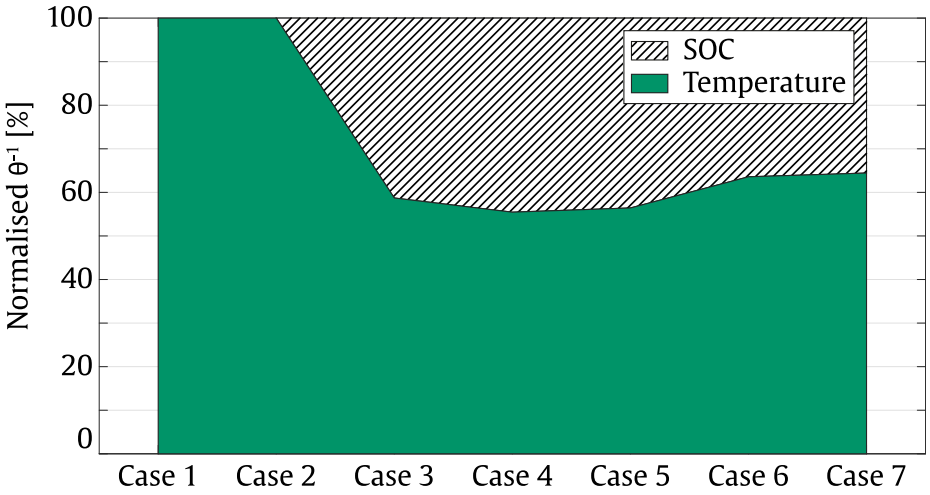

Figure 18. Evolution of the relative relevance of the different stress-factors, from the training case 1 to 7.

In the training cases 1 and 2, only the temperature involved different storage values in the training dataset, as the single value of 80% was available for the SOC input. In absence of data to guide the optimisation of the corresponding hyperparameters, a high initial hyperparameter value was imposed to the SOC input, in order to hinder its optimisation and then remove its effect from inference. In this context, the unique relevant stress-factor for the GP model was the temperature.

From the training case 3 to 7, different SOC levels were progressively included in the training dataset, and the corresponding hyperparameter was 'released' for optimisation. In Figure 18, it could be observed that the relative relevance of the SOC input with respect to the capacity loss increased for the training case 3; however, the temperature variations was still considered slightly more impactful on the capacity loss than SOC variations. The training case 4 included the data corresponding to 100% SOC storage condition, which present a relatively high acceleration of the capacity loss: this increased the relative weight of the SOC with respect to the temperature. The following cases 5, 6 and 7 included the data corresponding to the lower SOC levels, highlighting that the variation of SOC at its low values has a reduced effect on capacity loss (observable in Figure 14. (b)). This resulted in the mitigation of the relative relevance of the SOC input, compared to the temperature. At this point, it is important to highlight that although such comparison could clarify how the GP model understand the data, it does not imply causality.

3.5. Learning from dynamic operating conditions

Learning from dynamic operation

The operating conditions of Li-ion batteries are barely constant in real applications. This implies that the ageing models developed in the basis of ageing tests realised at constant operating conditions must be validated at dynamic operating conditions. Furthermore, as this study focusses on the development of ageing models oriented to learn from ageing data collected from real-world operation, the analysis of the possibility to infer about the correlations among the different stress-factors and the capacity loss directly from dynamic operation profile is necessary.

For this purpose, the model developed in Section 3.3 was employed to perform ageing predictions for cells #31 and #32, the operating profiles of which were presented in Figure 19. (b). In Section 3.4, the GP model reached satisfying prediction results for the training case 3 achieving an overall error of 0.53% MAE_Q, and the performances of the model did not improve significantly since such training case. In this section, such training case was therefore selected as initial state of the model, in order to evaluate the prediction performances of the model at dynamic operating conditions. The obtained predictions are presented in black line (mean prediction) and grey area (confidence intervals) in Figure 19. (a), for the cells #31 and #32.

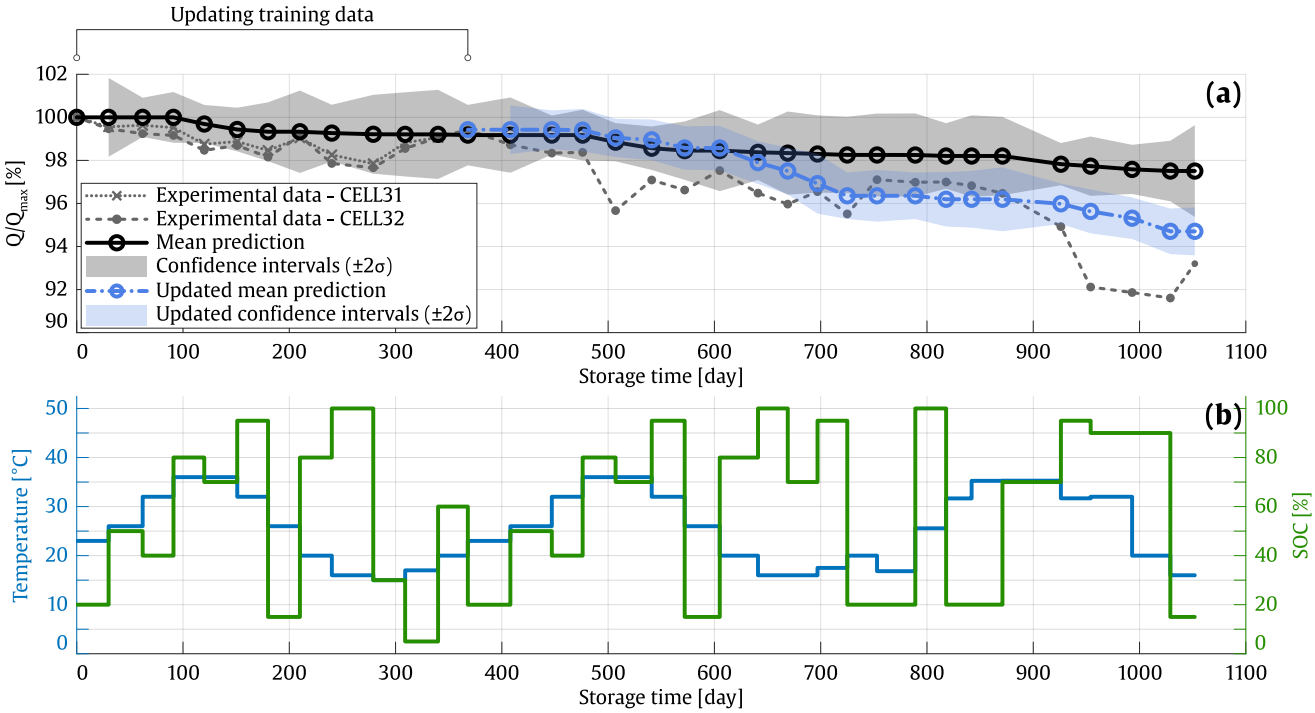

Figure 19. (a) Normalised capacity (with initial value Q_{max}) of the cells #31 and #32, after the preprocessing of the raw data obtained from the dynamic ageing tests (dotted grey lines) and the corresponding ageing predictions for the initial model (training case 3, black line and grey area) and the updated model (blue line and area). (b) Storage temperature and SOC dynamic profiles, applied during the dynamic ageing tests for the cells #31 and #32.

The errors of the predictions for the model obtained from training case 3 were 0.72% and 0.42% in terms of $MAE_{\Delta Q}$, and 1.78% and 0.62% in terms of MAE_Q, for the cells #31 and #32 respectively. At approximately 368 days in storage, the whole range of the temperature profile was experienced for the cells #31 and #32, Figure 19. (b). For the cell #32, different combinations of the temperature and SOC level were also observed, some of them reproduced on the remaining storage profiles (e.g. the combinations between ca. 0 - 368 days were reproduced between ca. 368 – 641 days). Such point was then deemed to be a suitable updating point for the model, to be able to evaluate the learning ability of the model at dynamic operating conditions. Therefore, the operating conditions as well as the corresponding capacity loss values observed between 0 – 368 days were included in the training dataset in order to obtain an updated GP model.

Updating model

The predictions performed with the updated model were represented in blue in Figure 19. (a), for cell #32. The initial model predicted larger confidence intervals at cold temperatures (between 15°C - 25°C), as the coldest

Learning effect of cold temperatures

temperature experienced in the training case 3 was 25°C. The inclusion of such values in the training set increased the confidence of the model to perform predictions in this range. This is traduced in Figure 19. (a) by reduced confidence intervals at cold temperatures, compared with the initial predictions.

Learning effect of low SOC

When updating the model with the different temperature and SOC combinations observed in the dynamic profiles, the confidence of the model for predicting throughout the whole window of the storage conditions accordingly improved. This is observable in Figure 20, which reflects the evolution of the standard deviation of the model's predictions, for the model corresponding to the training case 3 and the model updated with the data obtained from dynamic storage profiles until 368 days. Regarding the range of the storage temperatures, Figure 20. (a), it is remarkable that the model gained confidence at coldest temperatures, which is reflected by a reduction of the standard deviation in such region. This is also observable in Figure 20. (b), which indicates the standard deviations of the predictions at constant 15°C and throughout the whole SOC range: the models' predictions are clearly more confident at such temperatures, with minimal values around 35% and 100% SOC levels, which are the values at which the cell was stored when experiencing cold temperatures (Figure 19. (b), between 240 – 309 storage days). Figure 20. (c), (d) and (e) depicts the evolution of the standard deviation respectively at 25°C, 35°C and 45°C. It could be observed that the model gained confidence notably between the range of 0% - 40% SOC storage conditions.

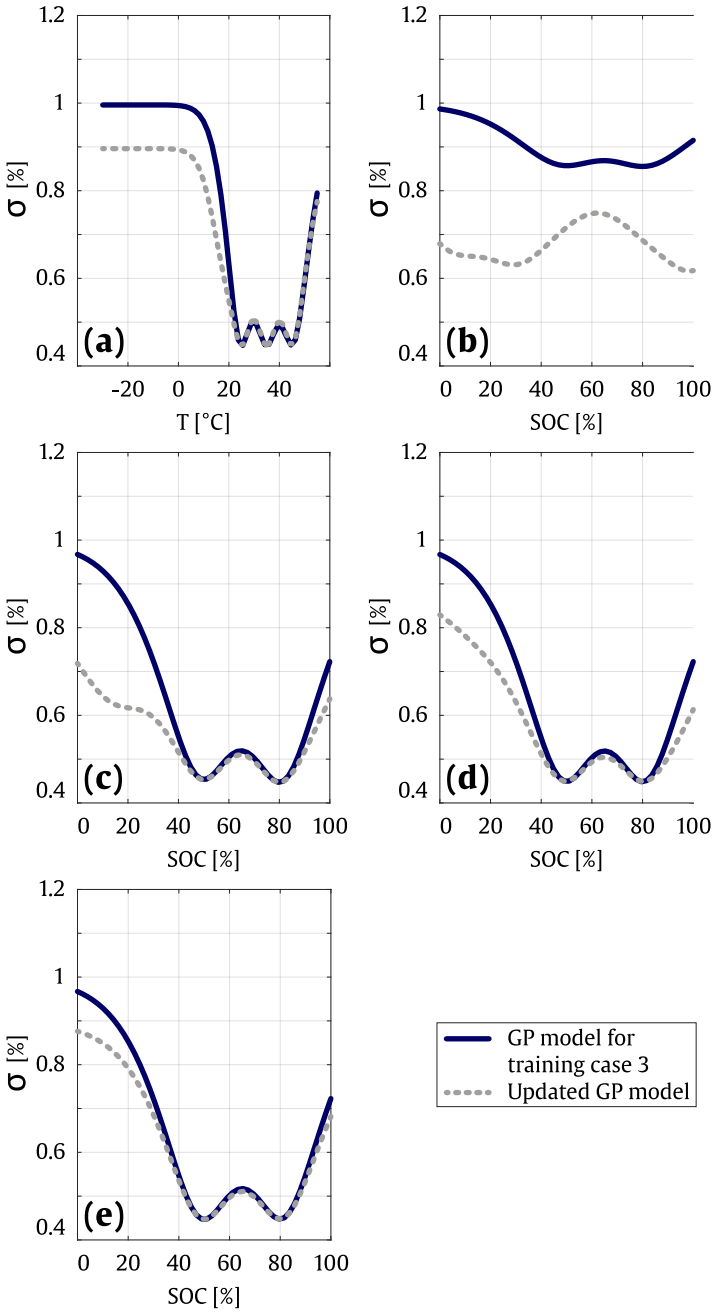

Figure 20. Evolution of the standard deviations of the GP model predictions throughout the whole operation window of the Li-ion cell under study, from the model trained at case 3 and the model updated at dynamic operating conditions. (a) Evolution throughout the temperature space, at constant 80% SOC (b) evolution throughout the SOC space, at constant 15°C, (c) evolution throughout the SOC space, at constant 25°C, (d) evolution throughout the SOC space, at constant 35°C and (e) evolution throughout the SOC space, at constant 45°C.

3.6. Conclusions of the chapter

Good fitting

In this chapter, a calendar capacity loss model was developed based on the GP framework. The model developed in Section 3.3 demonstrated suitable performances to fit the data, independently from the number of training data and involved stress-factors. This is observable in Figure 15. (a), where both $MAE_{\Delta Q}$ and MAE_{Q} curves of the training cells showed a constant level under the defined 2% threshold, from the training case 1 to 7.

Learning capability

Moreover, this chapter illustrates the ability of GP-based calendar ageing models to learn from the operating conditions progressively observed, increasing both accuracy and confidence of the model. This contribute to the verification of the hypothesis H5, which states that the nonparametric frameworks are able to learn about the influence of new values of the different stress-factors on battery degradation, including new data in the training set.

Accuracy improvement

Gaining confidence

The improvement of the model's prediction accuracy is demonstrated in Figure 15. (b) and (c), as the new temperature and SOC storage conditions are incorporated in the training dataset. Moreover, the reduction of the standard deviation in Figure 17 and Figure 20 testified about the increment of the model's confidence to perform predictions throughout a broad window of the storage conditions, as the temperature and SOC input spaces are progressively explored. However, it is noteworthy that the developed GP model turned out to be slightly over-confident, according to the CS curves represented in Figure 15. As previously explained, the $CS_{2\sigma}$ values should be approximately 95.4% if the uncertainty predictions are accurate: the obtained $CS_{2\sigma-Q}$ and $CS_{2\sigma-\Delta Q}$ values converged approximately into 86.55% and 96.19% respectively (Figure 15. (c)). The difference between the $CS_{2\sigma-Q}$ and $CS_{2\sigma-\Delta Q}$ suggests that the overconfidence of the model was induced by the error accumulation of the iterative prediction process.

Minimal number of laboratory tests

Regarding the amount of experimental ageing tests necessary from the laboratory for the development of the initial ageing model, the training case 3 seems to present an adequate trade-off between the performances and the development cost of the model, insofar as the cell is used at the operating conditions recommended by the manufacturer (Table 8). In fact, the model achieved an overall error of 0.53% MAE_{Q}, which is below the defined 2% MAE_{Q} threshold, for 30 cells operating between 25°C-45°C and 20-100% SOC storage conditions, using only 18 cells tested at 6 storage conditions for training. Furthermore, the performances of the model seem not to improve significantly since such training case (see Figure 15. (b) and (c)).

Validation at dynamic operation

In Section 3.5, the developed model was validated at dynamic operating conditions, achieving a 1.78% and 0.62% in terms of MAE_Q for cells #31 and #32 respectively. This result allows to partially verify the hypothesis H2, which states that ageing models trained with static ageing laboratory tests may be able to perform accurate predictions at dynamic operating profiles. The thorough evaluation of the hypothesis, which would also contemplate the model performances under realistic operating profiles, is completed in Chapter 5.

Isotropic kernels

Additionally, in Section 3.4.3, the suitability of isotropic kernel components to host the features corresponding to temperature and SOC storage conditions is also explored and validated, within the specific context of Li-ion ageing models able to evolve and improve their performances even after deployment in real application.

Sensitivity

Finally, the sensitivity analysis shows that the developed model tends to assign a higher influence of the temperature variations on the capacity loss, compared to the SOC.

In the following chapter, analogous objectives and methods are transposed to the development of an ageing model tailored to a purely cycling use-case of Li-ion batteries.

Chapter 4.

Cycle ageing model

As mentioned in the previous chapters, the approach adopted in this thesis for modelling the overall ageing of Li-ion battery is based on decomposing the ageing on two components: i) a first model corresponding to a pure calendar use-case of the battery, and ii) a second model related to a pure cycling usage of the system.

The previous chapter focussed on the systematic modelling and experimental verification of cell degradation through calendar ageing. Conversantly, this chapter addresses the same research challenge when the cell is electrically cycled, covering the implementation of the stages 1, 2 and 3 of the methodology described in Chapter 2.

This chapter is structured as follows, Section 4.1 describes the experimental ageing tests carried out in order to produce the ageing data. The raw data obtained from the experimental tests is analysed and preprocessed before the development of the model. Section 4.2 details the processing of the raw data and evaluates the relevance of the obtained data for ageing modelling. Section 4.3 presents the development of the proposed cycle ageing model under the GP framework. In Section 4.4 and 4.5, the prediction results of the developed model are presented for the cells tested at static and dynamic storage conditions, respectively. Furthermore, both sections aim to illustrate the ability of the GP model to learn from new data observation. Finally, Section 4.6 closes the chapter depicting the main conclusions.

4.1. Experimental cycle ageing data

Within the context of the European project titled as Batteries2020, extensive experimental works were carried out over a time span of more than three years, in order to analyse the ageing of Li-ion batteries, covering different possible operations. The capacity retention of a 20 Ah NMC cathode-based pouch cell with a graphite anode was evaluated. The nominal characteristics of the cell, the operating conditions recommended by the manufacturer, as well as the experimental results obtained from a testing batch of 32 cells related to the study of the ageing in storage operation, were described in Chapter 3. In this chapter, the experimental works associated with the study of the cycling operation will be presented.

Stress-factors in cycling

From the ageing point of view, the operation of a Li-ion battery in cycling is conditioned by the level of different stress-factors, mainly identified in the literature as the operating temperature, DOD, middle-SOC, and the charging and discharging C-rates [29]. A total of 124 cells were cycled in temperature-controlled climatic chambers, at different combinations of such stress-factors. Periodical characterisation tests were carried out at 25°C in order to evaluate the progressive capacity retention of the cells. The determination of the capacity started 30 minutes after its surface temperature reached 25°C degrees, ensuring that the cells has stabilised at the target temperature. The test started with a CC-CV charge: the CC charge was done at 6.667 A (C/3) until reaching 4.15 V, and the following CV charge was stopped when achieving current values below 1 A (C/20). After a period of 30 minutes, the cell was discharged using a CC discharge current at 6.667 A (C/3) until the terminal voltage measured 3 V, followed by a pause period of 30 minutes. The procedure was repeated three times. The capacity value obtained in the last repetition was considered as the cell capacity.

Capacity test

Depending on the variability of the stress-factors' profiles in the whole duration of the tests, two types of ageing experiments were distinguished, namely i) the ageing tests at static operating conditions and ii) the ageing tests at dynamic operating conditions.

4.1.1. Experimental cycle ageing tests at static operating conditions

In the ageing tests performed at static conditions, the value of the stress-factors remained constant throughout the whole duration of the tests. 122 cells were tested at 34 different operating conditions, specified in Table B. 1, Appendix B. Most of these tests were performed in the laboratories of the Vrije Universiteit Brussel and were completed by the laboratories of Ikerlan

Technology Research Centre, ISEA – RWTH Aachen University, Leclanché and Centro Ricerche Fiat. The cells were characterised every 4000 Ah, or equivalently 100 Full-Equivalent-Cycles (FECs). In order to ensure the repeatability of the results, at least 3 cells were allocated to each testing condition. The capacity curves resulting from the experimental ageing tests at static conditions are observable in Figure B.1, Appendix B. The variability of the capacity curves obtained for each tested cycling conditions is indicated in Table B. 2, Appendix B.

4.1.2. Experimental cycle ageing tests at dynamic operating conditions

Dynamic operating conditions

As the battery stress conditions in real-world applications are not constant over time, the developed ageing models should be able to perform accurate predictions at dynamic operating profiles. The ability of the GP model to learn from dynamic profiles should also be analysed. Therefore, 2 additional cells were tested at dynamic profiles of the different stress-factors. The value of the stress-factors was modified between each characterisation test, during the whole duration of the tests. One cell was tested at constant 80% DOD, 50% middle-SOC, C/3 rate in charge, 1C rate in discharge and a variable temperature profile following the seasonal temperatures over a year, between a range of 15°C - 36°C. Furthermore, one additional cell was submitted to the same seasonal temperature profile, but also variable DOD, middle-SOC and charging and discharging C-rates. The cells were characterised approximately every 28 days. The variating profiles of the stress-factors, as well as the corresponding capacity retention of the tested cells are depicted in Figure B.2, Appendix B.

4.2. Cycle ageing data preprocessing

In the context of data-driven modelling, it is important to analyse and preprocess the raw data before any modelling task, in order to address data inconsistency and noise issues and achieve effective models [131]. The capacity curves obtained from the experimental ageing tests described in Section 4.1 present clearly three distinct phases, as illustrated in Figure 21.

Three phases

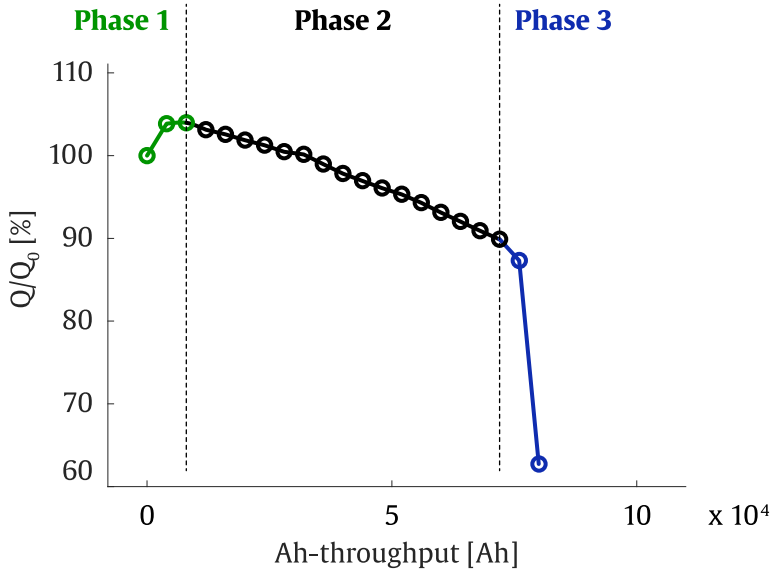

Figure 21. The three different phases of the capacity curve of the cells. The first phase is an increase of the capacity, the second is a progressive degradation and the third phase is a sudden capacity drop. Modified from [132].

Phase 1

The first phase corresponds to an initial capacity rise appearing at the BOL. As detailed in Chapter 3, this behaviour could be explained by the geometrical characteristics of the cells and it is not related to any ageing mechanism. Accordingly, the data corresponding to Phase 1 was discarded for the development of the ageing model. During the data preprocessing stage, the maximal capacity point of each cell was designated as the BOL point and assigned to the 'zero cycled Ah-throughputs' state.

Phase 2 & 3

The second phase is characterised by a progressive rate-constant decrease of the cell capacity, and it is sometimes followed by a third phase describing a sudden capacity drop, as illustratively depicted in Figure 21. According to [132], in these tested cells, this third phase was provoked by the occurrence of lithium plating. For the reasons exposed in Chapter 3, the modelling of the Phase 3 remained out of the scope of the study, and the corresponding data was discarded from the modelling dataset.

Focus on Phase 2

Therefore, in the context of this study, the modelling work focussed on capturing the relations between the cycling conditions and the capacity loss of the cells, during the progressive degradation corresponding to the second phase in Figure 21.

Besides, some unexpected trends were identified within the experimental data, for instance, abnormally reduced capacity measurements around 25000 Ah in the cells #21-23 (green curves in Figure B.1. (a), Appendix B). Such deviations are related to procedural errors during the capacity tests (e.g. exchange of the testing device, etc.). These noisy data samples could affect the performances of the model and were therefore removed from the modelling dataset. Furthermore, the cell #56 showed a clearly defective behaviour (isolated red curve in Figure B.1. (f), Appendix B) and was also discarded from the dataset.

On average, 76.5% of the raw experimental data corresponding to the static ageing conditions was preserved after the preprocessing stage. The percentage of the remaining data for each cell is indicated in **Table 13**. Overall, all the ageing conditions of the initial experimental ageing matrix were still represented in the processed dataset. It is noteworthy that most of the discarded data corresponds to cells cycled at low DOD values, due to the decision to neglect the initial capacity rise points. Regarding to the cells submitted to dynamical ageing profiles, 90% and 95.45% of the ageing data was maintained for the cells #124 and #125 respectively. **Figure 22** and **Figure 23** illustrates the resultant ageing data obtained after the preprocessing stage.

Table 13. Remaining data percentage ranges for each cycling condition, after the data preprocessing.

Temperature [°C]		25					35				45
C-Rate [C] (charge - discharge)		C/3-1C	1C-1C	C/3-C/3	C/3-1C	C/3-2C	C/2-1C	1C-1C	2C-1C	2C-2C	C/3-1C
DoD [%]	MidSOC [%]										
100	50	89.6%			85.7 – 92.8%						83.3 – 91.6%
80	50	70 – 95%	88.5 – 94.1%	66.6 – 83.3%	62.5 – 100%	77.2 – 81.8%	100%	66.6 – 88.8%	50 – 66.6%	62.6 – 72.7%	80 – 92.8%
65	50	50 – 87.5%			88.8 – 100%						80 – 100%
50	65				88.2 – 100%						
	50	82.7 – 72.4%			88.2 – 100%						73.3 – 80%
	35				76.4 – 77.7%						
35	50	50%			77.7 – 88.8%						80%
20	80				83.3 – 94.4%						
	65				33.3 – 44.4%						
	50	47 – 73.3%			55.5 – 61.1%						63.6 – 78.5%
	35				11.1– 44.4%						
	20				38.8 – 50%						
10	80				94.4%						
	65				33.3%						
	20				22.2 – 66.6%						

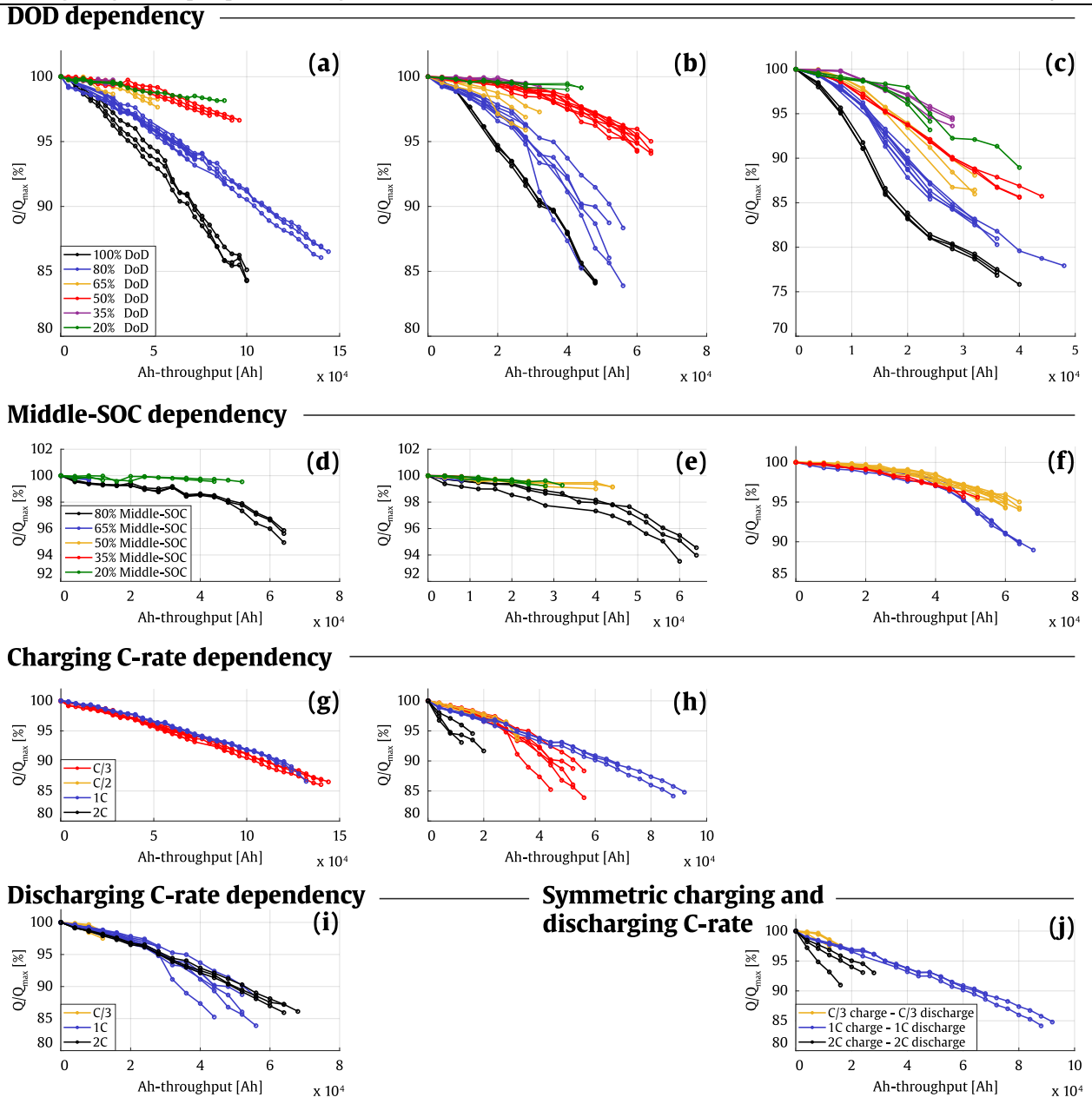

Figure 22. Normalised capacity (with maximum value Q_{max}), after the preprocessing of the raw data obtained from the static ageing tests at (a) 25°C, 50% middle-SOC, C/3 – 1C, and several DOD values, (b) 35°C, 50% middle-SOC, C/3 – 1C, and several DOD values, (c) 45°C, 50% middle-SOC, C/3 – 1C, and several DOD values, (d) 35°C, 10% DOD, C/3 – 1C, and several middle-SOC values, (e) 35°C, 20% DOD, C/3 – 1C, and several middle-SOC values, (f) 35°C, 50% DOD, C/3 – 1C, and several middle-SOC values, (g) 25°C, 80% DOD, 50% middle-SOC, 1C discharging rate, and several charging rate values, (h) 35°C, 80% DOD, 50% middle-SOC, 1C discharging rate, and several charging rate values, (i) 35°C, 80% DOD, 50% middle-SOC, C/3 charging rate, and several discharging rate values, and (j) 35°C, 80% DOD, 50% middle-SOC and several symmetric charging and discharging rate values.

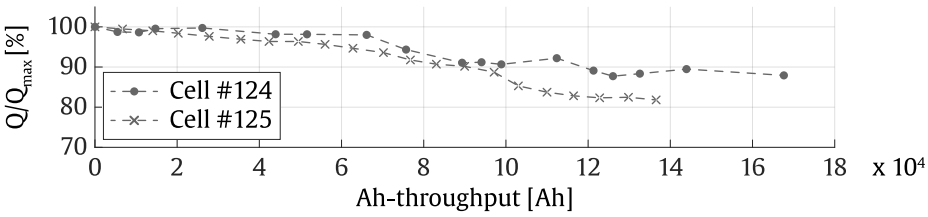

Figure 23. Normalised capacity (with initial value Q_{max}), after the preprocessing of the raw data obtained from the dynamic ageing tests, for the cell #124 and #125.

Effect of temperature

The analysis of the capacity curves in **Figure 22** allows understanding the relations between the values of the different stress-factors and the underlying ageing of the cells. Comparing the curves corresponding to identical DOD operations in **Figure 22**. (a), (b) and (c), it is noteworthy that the increased cycling temperature in (c) accelerated the capacity loss of the cells. This observation is in accordance with the literature [144,145]. In fact, the growth of the SEI layer is a chemical reaction and then obeys to the Arrhenius law: the SEI formation rate increases exponentially with temperature.

Effect of DOD

By studying them independently, the **Figure 22**. (a), (b) and (c) also illustrate the DOD dependency of the capacity loss. Higher values of the DOD increased the capacity loss. As explained in [146], at relatively low current rates of battery operation the SEI cracking and reforming is the main mechanism inducing capacity loss. Such capacity loss was shown to be dependent to the state of lithiation swing (which could be approximated by the DOD) of the electrode, during lithiation [146]. Similar experimental results were reported in [32,147,148].

Effect of middle-SOC

Regarding the effect of the middle-SOC stress-factor, the cycling at higher lithiation ranges of the anode is expected to lead to accelerated ageing, due to i) the effect of the calendar ageing, in which higher SOC values induce faster degradation [130,132], ii) the increased mechanical stress accumulated in the anode at higher lithiation states, conducting to accentuated SEI cracking and reforming [149] and iii) the crossing of the transitions between voltage plateaus of the negative electrode, which provokes changes in the lattice parameters of the material and leads to material expansion and contraction, increasing again the mechanical stress [32]. The latter element suggests a U-shape dependency of the capacity loss

to the middle-SOC, with an optimum around 50% SOC and stronger degradations at higher and lower cycle ranges [32]. A similar behaviour is observable in **Figure 22**. (f), in which the cells cycled at 35% and 65% middle-SOC aged slightly faster than the cells operating at 50% middle-SOC. As for the 10% and 20% DOD operation, **Figure 22**. (d) and (e) reflect an increased capacity loss at 80% middle-SOC operation, compared with lower middle-SOC levels.

Effect of C-rate

Furthermore, the effect of high charging and discharging C-rate values on capacity loss was also demonstrated in the literature. High C-rates lead to additional stress in the electrodes, due to i) a non-homogeneous intercalation of lithium on graphite which create Li-concentration gradients and ii) more important volume expansions and compressions [149]. This increase the probability of particle fracture, conducting to a loss of active material. In the negative electrode, the particle cracking reveals fresh anode surface, which react with electrolyte reforming SEI and augmenting capacity loss [149,150]. Furthermore, the charging at high C-rate could generate the lithium plating reaction, because of the heterogeneous lithium repartition in the material which could locally induce voltages close to the 0V vs. Li/Li^+ [137]. The study of the C-rate effect in the experimental works was limited to a C/3 – 2C range, in order to obtain enough resolution. These are relatively low levels compared to the actual EV market requirement (~6C in charge [151]). The obtained results showed relatively high variability, and not clear influence of the C-rate was remarkable below 1C for both charging and discharging C-rates (see **Figure 22**. (g-j)). However, an increased degradation rate was observed at 2C charging (discharging at 1C in **Figure 22**. (h) and at 2C in **Figure 22**. (j)).

Limitations of the dataset

Summarising, the experimental works carried out with 122 cells allowed obtaining an extensive dataset which describes effectively the influence of temperature, DOD, and middle-SOC for a relatively broad operating window of Li-ion cells, which overlaps the typical operating conditions in many real applications. It is noteworthy that high C-rate levels, as well as negative temperatures are not represented in the data, which could limit the applicability of the developed model in such operating conditions (see limitations in Chapter 6). Furthermore, the additional tests realised at dynamic operating conditions allow validating the performances of the model under time-varying stress-factors profiles, which are closer to real-world operation.

4.3. Development of the cycle ageing model

4.3.1. Assumptions and input selection

As stated in Section 4.2, this research study focusses on the modelling of the progressive capacity loss corresponding to the second phase represented in Figure 21. The development of the model was based on the following assumptions:

SEI growth

The predominant ageing mechanism involved in such phase is the formation of the SEI layer on the anode surface, which could be moderated, accelerated or expanded by the cycling conditions, characterised by the values of the different stress-factors mentioned in Sections 3.2 and 4.2.

Interactions of the stress-factors

The capacity loss is strongly dependent on the interactions between the different stress-factors, as described in Section 4.2.

Inputs

As explained in Chapter 3, corresponding to the calendar ageing model, the influence of the stress-factors should be considered introducing the corresponding values directly as an input. Therefore, the model proposed in this section considered six inputs:

- ΔAh-throughput: the number of Ah-throughput for which the ageing is predicted.
- T^{-1}: the reciprocal of the temperature corresponding to the cycled Ah-throughput (for alignment to the Arrhenius law).
- DOD: the DOD level corresponding to the cycled Ah-throughput.
- Middle-SOC: the average SOC corresponding to the cycled Ah-throughput.
- Charging C-rate: the charging C-rate corresponding to the cycled Ah-throughput.
- Discharging C-rate: the discharging C-rate corresponding to the cycled Ah-throughput.

Output

The output of the model was the capacity loss ΔQ corresponding to the ΔAh-throughput cycled at T^{-1}, DOD, Middle-SOC, Charging C-rate and Discharging C-rate conditions.

4.3.2. Kernel construction

Compositional kernels

As justified in Chapter 3, the framework of compositional kernels is a suitable solution to develop covariance functions tailored to Li-ion battery ageing application: a main kernel could be constructed composed of interpretable components, each one related to a specific input dimension [143]. In order to focus on the behaviour of the composed kernels, a zero-mean function was defined in this work. This is not a significant limitation, since the mean of the posterior process is not confined to be zero [110].

Zero-mean function

4.3.2.1. Selecting individual kernel components

As explained in Section 1.2.4.1, the GP framework is a nonparametric model, and therefore the learning problem is the problem of finding the suitable properties of the function (isotropy, anisotropy, smoothness, etc.), rather than a particular functional form [110].

The range of the DOD and Middle-SOC input dimensions is intrinsically limited between 0 – 100%. Furthermore, the operation window corresponding to the Temperature, Charging C-rate and Discharging C-rate inputs is also limited by the recommendations of the manufacturer (e.g. cycling and storage temperatures between -30°C and 55°C), specified in Chapter 3. This is defined to be a local modelling problem and therefore the kernel components corresponding to the stress-factors' input spaces could be represented by isotropic kernels, as justified in Chapter 3. Among the different isotropic kernels, the 5/2 Matérn kernels imply a suitable smoothness assumption to represent the physical processes inside the battery (as suggested in Chapter 3), and were then selected to host independently the input dimensions corresponding to each stress-factor.

Isotropic kernels

Matérn

The kernel component related to the $\Delta Ah - throughput$ input dimension requires several $\Delta Ah - throughput$ values to be involved in the training data, in order to optimise the associated hyperparameters. In order to limit the training computation time, only three different values of $\Delta Ah - throughput$ were processed in the training data (which are 4000, 8000 and 12000 ΔAh). **Table 14** illustrates the structure of the training data. In this context, the use of an isotropic kernel requires a large amount of different values of $\Delta Ah - throughput$ for long-term prediction, implying a large quantity of training data and increased computation times. Therefore, this kernel component should be anisotropic. In the second phase of the Li-ion cells ageing described in Figure 21, the capacity loss seems to be linear with respect to $\Delta Ah - throughput$. Therefore, a linear kernel component was selected for this input dimension.

Linear kernel

Table 14. Example of the training data structure, relating the input data to the corresponding target.

		Input vector x						Target **y**
		$\Delta Ah - throughput$ [Ah]	T^{-1} [K^{-1}]	DOD [%]	Middle-SOC [%]	Charging C-rate [C]	Discharging C-rate [C]	ΔQ [%]
CELL002	Data vector 1	4000	0.0034	100	50	C/3	1C	-0.163
	Data vector 2	8000						-0.743
	Data vector 3	12000						-1.101
	Data vector 4	4000						-0.579
	Data vector 5	8000						-0.937
...	...	...	...	...	...	...	...	...
CELL055	Data vector 1	4000	0.0032	50	35	C/3	1C	-0.135
	Data vector 2	8000						-0.142
	Data vector 3	12000						-0.451
	Data vector 4	4000						-0.007
	Data vector 5	8000						-0.316
	...	...	...	...	...			...

Although the data vectors 'CELL002 – data vector 1' and 'CELL002 – data vector 4' in **Table 14** have the same inputs values, the target is different because both correspond to the capacity loss from a different starting point, in the capacity curve of the CELL002. The data vectors with identical input values and different outputs are useful for the determination of the noise hyperparameter of the GP models (see Equation (37)).

4.3.2.2. Composing the whole kernel

In the GP framework, the kernel function is also a covariance function and therefore must be positive semidefinite [110]. Moreover, positive semidefinite compositional kernels are closed under the addition and multiplication of basic kernels. Additive kernels assume the added stochastic processes to be independent [143]. However, as specified in Section 3.3.1, the different inputs were assumed to have a strong interaction on their influence on the capacity loss, and hence an additive kernel composition should be avoided. In order to account for the interactions between the different input dimensions, the tensor product is suggested within [110,143] and is used in the composed kernel (equation (37)).

Tensor product

$$\kappa(\mathbf{x},\mathbf{x}') = {\sigma_f}^2 \cdot \left[\prod_{n=1}^{5} \left(1 + \sqrt{5} \cdot \frac{|\mathbf{x}_n - \mathbf{x}'_n|}{\boldsymbol{\theta}_n} + \frac{5}{3} \cdot \frac{|\mathbf{x}_n - \mathbf{x}'_n|^2}{{\boldsymbol{\theta}_n}^2} \right) \cdot \exp\left(-\sqrt{5} \cdot \frac{|\mathbf{x}_n - \mathbf{x}'_n|}{\boldsymbol{\theta}_n} \right) \right] + {\sigma_n}^2 \cdot I \quad (37)$$
$$\cdot \left(\mathbf{x}_6 \cdot \mathbf{x}'_6 + {\boldsymbol{\theta}_6}^2 \right)$$

where $\mathbf{x}$ and $\mathbf{x}'$ are different input vectors structured as $\mathbf{x} = (\mathbf{x}_1, \mathbf{x}_2, \mathbf{x}_3, \mathbf{x}_4, \mathbf{x}_5, \mathbf{x}_6)$, with $\mathbf{x}_1 = T^{-1}$, $\mathbf{x}_2 = DOD$, $\mathbf{x}_3 = Middle\text{-}SOC$; $\mathbf{x}_4 = Charging\ C\text{-}rate$; $\mathbf{x}_5 = Discharging\ C\text{-}rate$ and $\mathbf{x}_6 = \Delta Ah\text{-}throughput$.

Hyperparameters

$\boldsymbol{\theta}_1, \boldsymbol{\theta}_2, \boldsymbol{\theta}_3, \boldsymbol{\theta}_4, \boldsymbol{\theta}_5$ and $\boldsymbol{\theta}_6$ are the hyperparameters related to the corresponding input spaces. The additional hyperparameters ${\sigma_f}^2$ and ${\sigma_n}^2$ are respectively the signal variance, which plays the role of scaling the outputs in the dimension of the capacity loss ΔQ, and the noise variance, which models an additive Gaussian noise from the data.

4.4. Learning from static operating conditions

This section aims to illustrate the ability of the developed GP model to improve its prediction performances while observing an increasing number of cycling data. Indeed, as new observations of cycling conditions are presented to the model, the training dataset of the model involves a more comprehensive view of the influence of the different combinations of stress-factors on the capacity loss. Therefore, for each prediction, the covariance function is able to find more similar examples in the stored training dataset, in term of cycling conditions. The prediction performances of the model improve throughout the whole operation window of the Li-ion cells.

In this section, the improvement of the model performances was evaluated in terms of:

- Accuracy of the prediction: as the training dataset increases, a reduction of the prediction errors is expected over the whole operation window. The metrics used to evaluate the prediction error were detailed in Section 3.4.1.

  Accuracy

- Confidence in the prediction: as the training dataset increases, the model disposes of more information about the ageing throughout the whole operation window. In accordance with the covariance equation (22), the confidence intervals of the predictions are expected to reduce, signifying that the model is more confident

  Confidence

about its predictions. The metric used to evaluate the accuracy of the confidence intervals was detailed in Section 3.4.1.

4.4.1. Training case studies to illustrate the learning of new operating conditions

Training suite

Following the method introduced in Chapter 3, 16 training cases were defined in order to illustrate how the GP model could learn from new observations and improve prediction performances. Each training case involved a different number of training data from the ageing dataset presented in Section 4.2. From the training case 1 to the training case 16, the number of training data increased: the data corresponding to new cycling conditions was included progressively, revealing one by one the influence of the different levels of the different stress-factors.

The distinct temperature values were introduced from case 1 to case 2, followed by the DOD levels from case 3 to case 7, the middle-SOC levels from case 8 to case 11, the charging C-rate levels from case 12 to case 14 and finally the discharging C-rate levels from case 15 to case 16. The introduction of each stress-factors level was guided by the following process: the highest level was introduced first, followed by the lowest level, and then the range was completed adjoining one by one the levels equidistant to the already known values, alternating the highest and lowest values. Illustrating the process in the DOD range: i) 100% DOD, the highest value, was already included in cases 1 and 2, then ii) the lowest value i.e. 20% DOD was included in case 3, iii) the equidistant would be 60% DOD, then the closest available values 65% and 50% DOD were included in case 4 and case 5 respectively, and iv) the highest (%80 DOD) and lowest (35% DOD) remaining levels were respectively added in cases 6 and 7. Notice that the 10% DOD level was included later, because the 50% middle-SOC level was not available at such DOD. **Table 15** indicates the characteristics of each training case. The different cells and the related cycling conditions involved during the training process are specified, as well as the corresponding ratio of the amount of training data with respect to the whole available data.

Table 15. Summary of the different case studies, specifying the different cells involved and the related cycling conditions, as well as the ratio of the amount of training data with respect to the whole available data.

		Learning Temperature	Learning DOD	Learning MidSOC	Learning charging C-rate	Learning discharging C-rate	# Training data / # Total data [%]
CASE 1	T	25 45					7.56
	DOD	100					
	MidSOC	50					
	C-rate CHA	C/3					
	C-rate DCH	1C					
CASE 2	T	25 45 35					10.08
	DOD	100					
	MidSOC	50					
	C-rate CHA	C/3					
	C-rate DCH	1C					
CASE 3	T	25 45 35	25, 35, 45				15.70
	DOD	100	20				
	MidSOC	50	50				
	C-rate CHA	C/3	C/3				
	C-rate DCH	1C	1C				
CASE 4	T	25 45 35	25, 35, 45				21.13
	DOD	100	20 65				
	MidSOC	50	50				
	C-rate CHA	C/3	C/3				
	C-rate DCH	1C	1C				
CASE 5	T	25 45 35	25, 35, 45				37.22
	DOD	100	20 65 50				
	MidSOC	50	50				
	C-rate CHA	C/3	C/3				
	C-rate DCH	1C	1C				
CASE 6	T	25 45 35	25, 35, 45				59.97
	DOD	100	20 65 50 80				
	MidSOC	50	50				
	C-rate CHA	C/3	C/3				
	C-rate DCH	1C	1C				
CASE 7	T	25 45 35	25, 35, 45				64.25
	DOD	100	20 65 50 80 35				
	MidSOC	50	50				
	C-rate CHA	C/3	C/3				
	C-rate DCH	1C	1C				
CASE 8	T	25 45 35	25, 35, 45	35			71.05
	DOD	100	20 65 50 80 35	10, 20			
	MidSOC	50	50	80			
	C-rate CHA	C/3	C/3	C/3			
	C-rate DCH	1C	1C	1C			
CASE 9	T	25 45 35	25, 35, 45	35			74.03
	DOD	100	20 65 50 80 35	10, 20 10, 20			
	MidSOC	50	50	80 20			
	C-rate CHA	C/3	C/3	C/3			
	C-rate DCH	1C	1C	1C			
CASE 10	T	25 45 35	25, 35, 45	35			78.00
	DOD	100	20 65 50 80 35	10, 20 10, 20 10, 20, 50			
	MidSOC	50	50	80 20 65			
	C-rate CHA	C/3	C/3	C/3			
	C-rate DCH	1C	1C	1C			
CASE 11	T	25 45 35	25, 35, 45	35			80.11
	DOD	100	20 65 50 80 35	10, 20 10, 20 10, 20, 50 20, 50			
	MidSOC	50	50	80 20 65 35			
	C-rate CHA	C/3	C/3	C/3			
	C-rate DCH	1C	1C	1C			

Table 15 (continued). Summary of the different case studies, specifying the different cells involved and the related cycling conditions, as well as the ratio of the amount of training data with respect to the whole available data.

			Learning Temperature	Learning DOD	Learning MidSOC	Learning charging C-rate	Learning discharging C-rate	# Training data / # Total data [%]
CASE 12	T		25 45 35	25, 35, 45	35	35		80.88
	DOD		100	20 65 50 80 35	10, 20 10, 20 10, 20, 50 20, 50	80		
	MidSOC		50	50	80 20 65 35	50		
	C-rate	CHA	C/3	C/3	C/3	2C		
		DCH	1C	1C	1C	1C		
CASE 13	T		25 45 35	25, 35, 45	35	35 25, 35		92.41
	DOD		100	20 65 50 80 35	10, 20 10, 20 10, 20, 50 20, 50	80		
	MidSOC		50	50	80 20 65 35	50		
	C-rate	CHA	C/3	C/3	C/3	2C 1C		
		DCH	1C	1C	1C	1C 1C		
CASE 14	T		25 45 35	25, 35, 45	35	35 25, 35 35		94.09
	DOD		100	20 65 50 80 35	10, 20 10, 20 10, 20, 50 20, 50	80		
	MidSOC		50	50	80 20 65 35	50		
	C-rate	CHA	C/3	C/3	C/3	2C 1C C/2		
		DCH	1C	1C	1C	1C		
CASE 15	T		25 45 35	25, 35, 45	35	35 25, 35 35	35	98.83
	DOD		100	20 65 50 80 35	10, 20 10, 20 10, 20, 50 20, 50	80	80	
	MidSOC		50	50	80 20 65 35	50	50	
	C-rate	CHA	C/3	C/3	C/3	2C 1C C/2	C/3 2C	
		DCH	1C	1C	1C	1C	2C 2C	
CASE 16	T		25 45 35	25, 35, 45	35	35 25, 35 35	35	100.00
	DOD		100	20 65 50 80 35	10, 20 10, 20 10, 20, 50 20, 50	80	80	
	MidSOC		50	50	80 20 65 35	50	50	
	C-rate	CHA	C/3	C/3	C/3	2C 1C C/2	C/3 2C C/3	
		DCH	1C	1C	1C	1C	2C 2C C/3	

4.4.2. Prediction results

4.4.2.1. Accuracy improvement

The black curves in Figure 24 indicate the prediction accuracy of the GP model proposed in Section 4.3, trained with the different training cases defined in Section 4.4.1, in term of $MAE_{\Delta Q}$ and MAE_Q. The corresponding RMSE values are indicated in Table B. 3, Appendix B. For each training case, the error calculation was performed separately for:

- The training cells: the mean value of the prediction errors obtained for all the cells involved in the training case was calculated (Figure 24. (a)). Such errors are informative about the ability of the model to fit the training data. — Fitting
- The validation cells: the mean value of the prediction errors obtained for all the cells not involved in the training case was calculated (Figure 24. (b)). Such error is relevant to evaluate the generalisation ability of the model. — Generalisation
- Some targeted validation cells: the mean value of the prediction errors obtained for the validation cells which operated at unobserved levels of the partially explored stress-factors (Figure 24. (c)). For instance, the influence of the DOD is learned from the training case 3 to 7; in the training case 4, the training data included the data corresponding to the 20%, 65% and 100% DOD operation. Then the prediction error corresponding to the training case 4 plotted in Figure 24. (c) was calculated only for the validation cells corresponding to the 50%, 80% and 35% DOD cycling conditions, neglecting the errors corresponding to the cells cycled at different values of the further stress-factors. Such error is relevant to evaluate the generalisation ability of the model, to the extent of the partially explored input spaces. — Generalisation in the space of each input
- All the cells: the mean value of the prediction errors obtained for all the cells (Figure 24. (d)). Such error is informative about the global accuracy of the model.

As expected, the predictions errors of the training cells in Figure 24. (a) fulfil the 2% MAE_Q threshold for all the training cases. Regarding the validation cells, the threshold of the 2% MAE_Q is reached for the training case 4 (see Figure 24. (b)), and the performances of the model seem not to improve significantly since such training case.

Learning the effect of DOD

Figure 24. (c) describes the evolution of the generalisation ability of the model throughout the whole range of each stress-factor. Focussing on the part related to the learning of the influence of the DOD, the first points correspond to the mean value of the MAE errors obtained with the GP model trained with training case 2 and performing predictions for all the cells tested at the cycling conditions corresponding to the learning of the DOD in **Table 15**. At this training stage, the model only observed the influence of cycling at 100% DOD, and then all the predictions at lower DOD values were overestimated, resulting in a high error of 4.89% MAE_Q. In the training case 3, the model started to learn the effect of the DOD by incorporating a 20% DOD condition in the training data. The mean error of the targeted validation cells improved drastically, as the model could infer from two different DOD values and gain a numerical intuition about the effect of the DOD on capacity loss. In the training case 4, the model possessed capacity loss values corresponding to 20%, 65% and 100% DODs in the training dataset. The mean error of the predictions corresponding to the cells at the remaining DOD values drop below the 2% MAE_Q threshold, indicating a good generalisation of the model throughout the whole available range of DOD operation. Finally, the inclusion of new DOD values to the training dataset in the training cases 5 and 6 did not seem to significantly improve the generalisation ability of the model throughout the DOD operation range. Notice that for the training case 7, all the DOD values available from the dataset were involved in training, and therefore, there was no validation cells yet to evaluate the evolution of the generalisation ability of the model, and then the error cannot be calculated.

Regarding the evolution of the errors from training cases 7 to 10, which is related to the learning of the influence of the middle-SOC, the results were unaltered by the inclusion of new middle-SOC values in the training dataset (Figure 24. (c)). This is explainable by the relatively reduced influence on the capacity loss assigned by the model to the middle-SOC stress-factor (more details in Section 4.4.2.3). Furthermore, concerning the learning of the charging C-rate, an increase of the error is observable from training case 11 to 12, before the final reduction in case 13. This is due to the initial inclusion of the 2C charging condition in training case 12, which presents a faster capacity loss compared to the remaining levels of charging C-rate (see **Figure 22**. (h)). At this stage, the model tends to overestimate the ageing at intermediate charging C-rate values. This is corrected in the training case 13 by the incorporation of the 1C charging data.

Learning the influence of

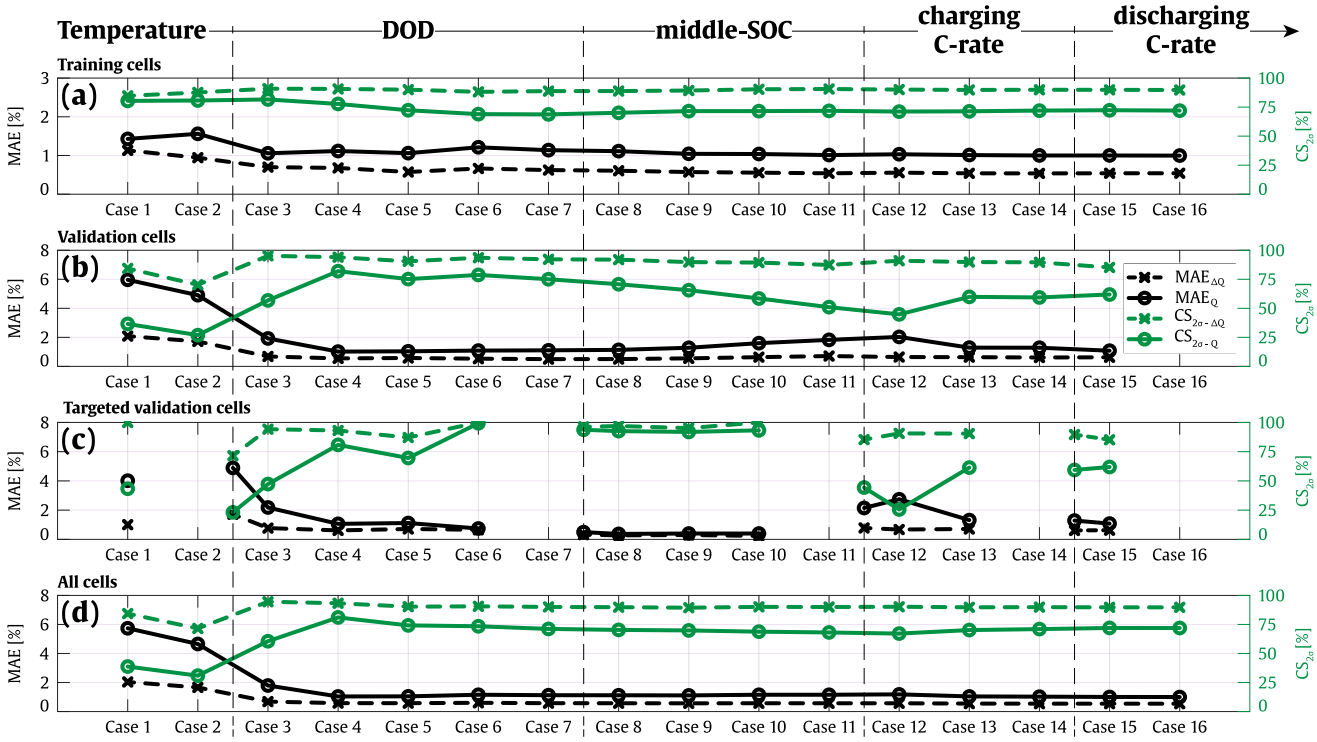

Figure 24. Prediction results corresponding to each training case, in term of MAE_Q and $CS_{2\sigma}$, distinguishing the errors of (a) all the training cells, (b) all the validation cells, (c) targeted validation cells and (d) all the cells.

Figure 25. (a-e) illustrate the capacity loss predictions of the GP model resulting from the training case 4, for different cycling conditions involved in the training data. The average $MAE_{\Delta Q}$ and MAE_Q errors of the model corresponding to the training case 4 were 0.68% and 1.12%, respectively, for the training cells. The average $CS_{2\sigma-\Delta Q}$ and $CS_{2\sigma-Q}$ were respectively 90.65% and 77.75%. Furthermore, **Figure 25**. (f-j) depict the capacity loss predictions of the GP model resulting from the training case 4, for different validation cycling conditions, which were not involved in the training data. The average $MAE_{\Delta Q}$ and MAE_Q errors of the model corresponding to the training case 4 were 0.55% and 1.02%, respectively, for the validation cells. The average $CS_{2\sigma-\Delta Q}$ and $CS_{2\sigma-Q}$ were respectively 94.02% and 82.01%. **Figure 25**. (k-o) aims to underpin the improvement of the generalisation performances of the GP, while increasing the number of training values in the input space of the DOD. To this end, the capacity loss predictions were represented for the cells #004 to #011 (which operated at 25°C, 80% DOD, 50% middle-SOC and C/3 –

Results in training conditions

Results in validation conditions

1C charging and discharging C-rates), using GP models obtained from different training cases.

Showing model improvement

As previously explained, the models obtained from the training cases 1 and 2 did not have any information about the effect of the DOD on the capacity loss, as the training data involved the single input of 100% DOD. At this stage, the prediction at lower DOD levels were over-estimated (see **Figure 25**. (k) and (l)). The mean error in such condition was 3.91% and 3.88% MAE_Q, respectively. In the training cases 3 and 4, the integration of the 20% and 65% DOD operating conditions in the training dataset allowed improving the predictions at 80% DOD, reaching 2.34% and 0.42% MAE_Q values, respectively (see **Figure 25**. (m) and (n)). For comparison, the results obtained with a fully trained GP (training case 7) were also plotted in **Figure 25**. (o): there was not significant improvement in term of error reduction. However, the confidence intervals were slightly reduced, indicating a higher confidence of the model to perform predictions in at 80% DOD, since such operating condition was represented in the training data (more details in Section 4.4.2.2). At this point, it is noteworthy that the model corresponding to the training case 7 is only used in this study for a sake of comparison with the previous cases. In fact, such a model would be unreliable for deployment, as all the available DOD levels were observed in training and then the generalisation ability of the model could not be validated in the space of DOD.

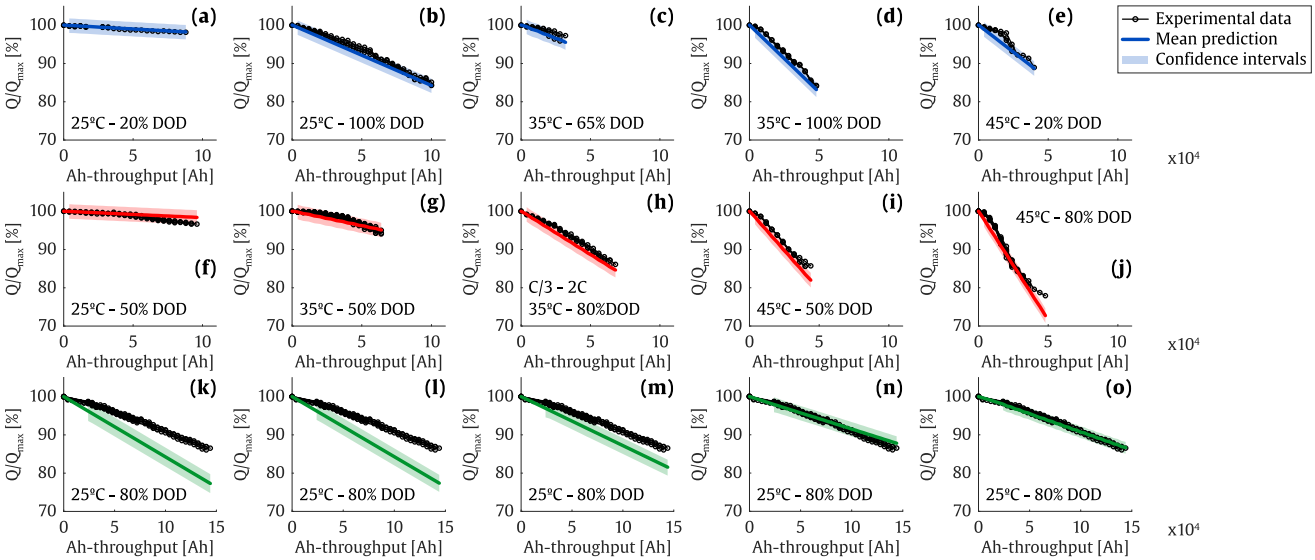

Figure 25. (a-e) Capacity predictions with the GP model trained at training case 4, for the training cells cycled at the Temperature and DOD levels indicated in each graph. (f-j) Capacity predictions with the GP model trained at training case 4, for the validation cells cycled at the Temperature and DOD levels indicated in each graph. (k-o) Capacity predictions for the cells cycled at 25°C and 80% DOD, with the GP models trained at (k) training case 1, (l) training case 2, (m) training case 3, (n) training case 4 and (o) training case 7. Unless otherwise specified, the cells involved in (a-o) were cycled at 50% Middle-SOC, C/3 charging C-rate and 1C discharging C-rate.

4.4.2.2. Increase of confidence

According to the variance equation (22), the confidence intervals of a prediction reduce if the training dataset involves data samples similar to the predicted input values. Informally, this means that the model feels more confident to do predictions in case it already observed similar operating conditions in training data. Therefore, the analysis of the width of the confidence intervals – or equivalently the standard deviation value - along a large operating range of each stress-factor is informative about how confident the model feels to perform predictions throughout a broad operating window. In this sense, the evolution of the standard deviation throughout the input space testifies about the learning process of the model.

Evolution of the standard deviation

In Figure 26, the evolution of the standard deviation of the GP model predictions is depicted throughout the whole operation window of the Li-ion cell under study, for the different training cases. For the model obtained from the training case 1, the standard deviation indicates lowest values around 25°C and 45°C, Figure 26. (a), which are the only temperatures experienced at this stage. The observation of the effect of a 35°C operation in the training case 2 flattened the curve around the such temperature: at this stage, the obtained model felt relatively confident to perform predictions within the 20°C - 50°C temperature range. Notice that the model presented high standard deviation values at low and negative temperatures, due to the lack of information in such cycling regions. Figure 26. (b) corresponds to the learning of the influence of the DOD. As expected, the lowest standard deviation stood near 20% and 100% for training case 3, and the observation of intermediate DOD levels from the training cases 4 to 7 lead to reduced values in the whole range, unless below 20% DOD operation which still was an unknown cycling condition. Identical interpretation could be done from Figure 26. (c), (d) and (e) regarding the evolution of the standard deviation in the operation ranges of the middle-SOC, charging and discharging C-rate, respectively.

Learning the effect of temperature

Learning the effect of DOD

Learning the effect of other stress-factors

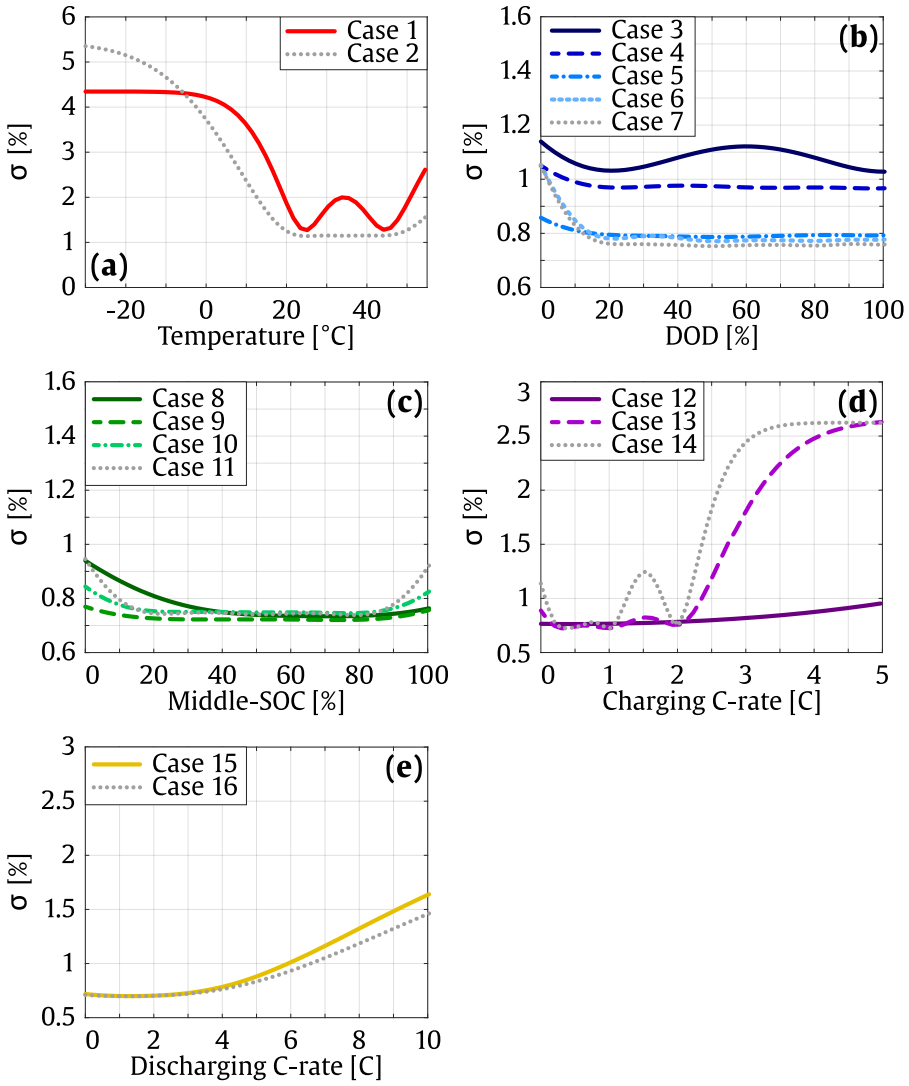

Figure 26. Evolution of the standard deviations of the GP model predictions throughout the whole operation window of the Li-ion cell under study, from training case 1 to 16. (a) Evolution throughout the temperature space, at constant 80% DOD, 50% middle-SOC and C/3 – 1C charging and discharging C-rate (b) Evolution throughout the DOD space, at constant 35°C, 50% middle-SOC and C/3 – 1C charging and discharging C-rate (c) Evolution throughout the middle-SOC space, at constant 35°C, 20% DOD and C/3 – 1C charging and discharging C-rate (d) Evolution throughout the space of the charging C-rate, at constant 35°C, 80% DOD, 50% middle-SOC and 1C discharging C-rate and (e) Evolution throughout the space of the discharging C-rate, at constant 35°C, 80% DOD, 50% middle-SOC and C/3 charging C-rate.

The reduction of the standard deviation in Figure 26 testifies about the increment of the model's confidence to perform prediction throughout a broad operating window, as input spaces are progressively explored. Moreover, the accuracy of the confidence level of the model was evaluated using the CS metric, introduced in Section 3.4.1. As previously explained, the $CS_{2\sigma}$ values should be approximately 95.4% if the uncertainty predictions are accurate. Higher or lower scores indicate under- or over-confidence of the model, respectively [128].

Slightly over-confident

In Figure 24, the evolution of the mean value of the CSs are plotted for each training case of the GP model, in term of capacity loss and accumulated capacity. Since the training case 4, the overall $CS_{2\sigma-Q}$ values converge into approximately 75% (Figure 24. (d)). This traduces a slightly over-confident behaviour of the model in term of the accumulated capacity. However, regarding the CSs values corresponding to the output the model, the overall $CS_{2\sigma-\Delta Q}$ values converge into approximately 90%.

4.4.2.3. Sensitivity of the capacity loss to the stress-factors

Isotropic covariance functions implement automatic relevance determination, since the inverse of the length-scale determines how relevant an input is: if the length-scale has a very large value, the covariance will become almost independent of that input, effectively removing it from the inference [8]. Therefore, the sensitivity of the capacity loss to the different stress-factors could be analysed by observing the inverse of their respective hyperparameters. Figure 27 displays, for each training case, the inverse of the hyperparameters corresponding to each input dimension, relatively normalised to each other.

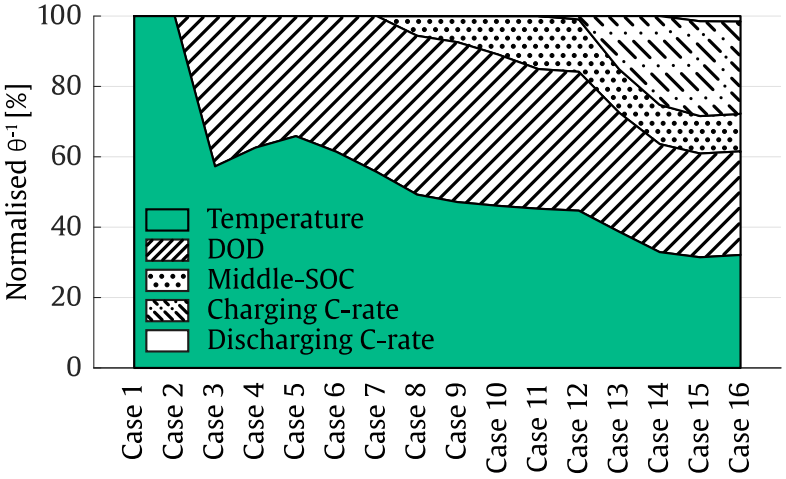

Figure 27. Evolution of the relative relevance of the different stress-factors, from the training case 1 to 16.

Relative relevance of the stress-factors

Figure 27 illustrates the relative relevance of the different stress-factors, for the GP model corresponding to training case 1 to 16. In the training cases 1 and 2, only the temperature involved different operating values in the training dataset, as a single value was available for the remaining stress-factors. In absence of data to guide the optimisation of the corresponding hyperparameters, a high initial hyperparameter value was imposed to those stress-factors, in order to hinder their optimisation and then remove their effect from inference. In this context, the unique relevant stress-factor for the GP model was the temperature.

From the training case 3 to 7, different DOD levels were progressively included in the training dataset, and the corresponding hyperparameter was 'released' for optimisation. In Figure 27, it could be observed that the relative relevance of the DOD input with respect to the capacity loss increased; however, the temperature variations was still considered slightly more impactful on the capacity loss than DOD variations. From the training case 8 to 11, the evolution of the importance assigned to the middle-SOC is observable, which was still limited compared to the temperature and DOD. In training case 12, a reduced impact of the charging rate was inferred, considering the difference in capacity losses between C/3 and 2C training data. However, the observation of the 1C and C/2 charging rates in training cases 13 and 14, which both lead to similar capacity loss as C/3 charging rate, suggested that all such difference stood between 1C and 2C: from this new perspective, small changes of charging C-rate induces relatively high changes in capacity loss, traducing a high covariance between these two variables. Then the GP assigned high relevance to the charging C-rate input

in the training case 14. Finally, a reduced dependence of the capacity loss on the discharging C-rate was captured from the training cases 15 and 16, which is in accordance with the observations done in Section 4.2.

In this way, the fully trained GP classified the relevance of the different stress-factors with respect to the capacity loss prediction in this order: 1/ temperature, 2/ DOD, 3/ charging C-rate, 4/ middle-SOC and 5/ discharging C-rate. At this point, it is important to highlight that although such comparison could clarify how the GP model understand the data, it does not imply causality.

4.5. Learning from dynamic operating conditions

Learning from dynamic operation

Baseline model

As the operating conditions of Li-ion batteries are barely constant in real applications, the ageing models developed in the basis of ageing tests realised at constant operating conditions must be validated at dynamic operating conditions. Furthermore, as this study focusses on the development of ageing models oriented to learn from ageing data collected from real-world operation, the analysis of the possibility to infer about the correlations among the different stress-factors and the capacity loss directly from dynamic operation profile is necessary. To this end, the model developed in Section 4.3 was employed to perform ageing predictions for cells #124 and #125, whose operating profiles were presented in Figure 28. (b, c) and (e, f), respectively. For the training case 4 (see Section 4.4), the GP model reached satisfying prediction results, achieving errors below the defined 2% MAE_Q threshold. In this section, such training case was therefore selected as initial state of the model, in order to evaluate the prediction performances of the model at dynamic operating conditions. The obtained predictions are presented in black line (mean prediction) and grey area (confidence intervals) in Figure 28. (a) and (d), for the cells #124 and 125 respectively.

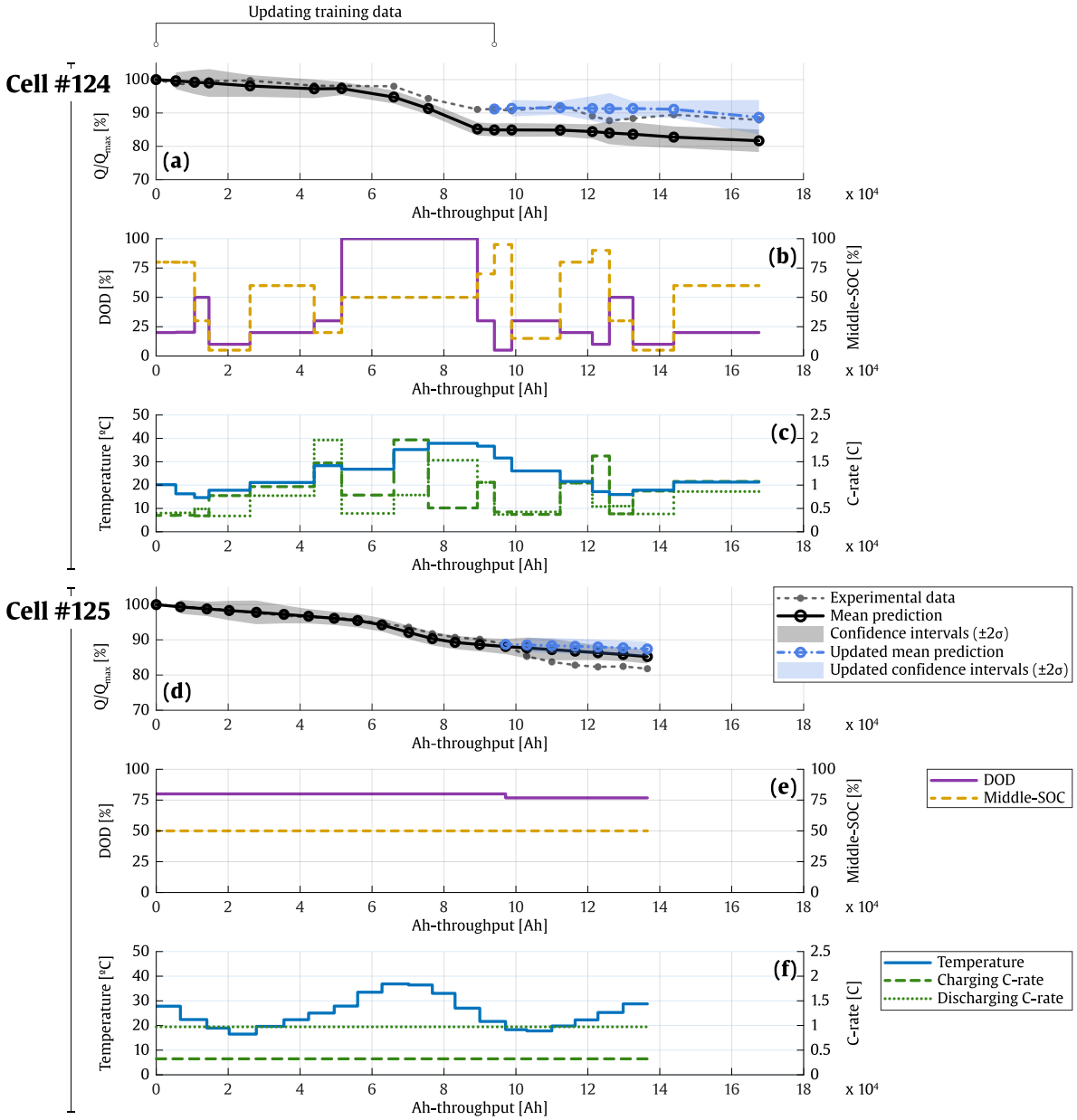

Figure 28. (a) Normalised capacity (with maximum value Q_{max}) data and the corresponding ageing predictions for the initial model (training case 4, black line and grey area) and the updated model (blue line and area), for the cell #124. (b) DOD and middle-SOC profiles and (c) temperature and charging and discharging C-rate profiles applied to the cell #124. (d) Normalised capacity (with maximum value Q_{max}) data and the corresponding ageing predictions for the initial model (training case 4, black line and grey area) and the updated model (blue line and area), for the cell #125. (e) DOD and middle-SOC profiles and (f) temperature and charging and discharging C-rate profiles applied to the cell #125.

Updating model

The model obtained from training case 4 achieved 1.13% and 0.46% errors in terms of $MAE_{\Delta Q}$, and 3.76% and 1.46% in terms of MAE_{Q}, for the cells #124 and #125 respectively. At approximately 90000 Ah-throughput of cycling, the whole range of the temperature profile was experienced for the cells #124 and #125. For the cell #124, different combinations of the remaining stress-factors were also observed, some of them reproduced on the remaining cycling profiles (e.g. the combinations between ca. 11000-43000 Ah-throughput, were reproduced between ca. 126000-167000 Ah-throughput). Such point was then deemed to be a suitable updating point for the model, to be able to evaluate the learning ability of the model at dynamic operating conditions. Therefore, the operating conditions as well as the corresponding capacity loss values observed between 0 – 90000 Ah-throughput were included in the training dataset in order to obtain an updated GP model.

Learning the effect of cold temperatures

In Figure 28. (a) and (d), the blue curves represent the predictions performed with the updated model, for the cells #124 and #125 respectively. For the cell #125, only the temperature profile was varying, the remaining stress-factors being constant. The initial model predicted larger confidence intervals at cold temperatures (between 15°C - 25°C), as the coldest temperature experienced in the training case 4 was 25°C. The observation of such values increased the confidence of the model to perform predictions in this range. This is traduced in Figure 28. (d) by reduced confidence intervals at cold temperatures, compared with the initial predictions[26].

The cell #124 was cycled at dynamic temperatures, DOD, middle-SOC and charging and discharging C-rates profiles (see Figure 28. (b) and (c)). In Figure 28. (a), it could be observed that while the confidence intervals were reduced at some point (e.g. around 132000 Ah-throughput), they became larger at some other points (e.g. around 167000 Ah-throughput). In fact, in the training case 4 only different temperature and DOD values were observed, and the remaining stress-factors were then neglected from inference by imposing high initial hyperparameters (as explained in Section 4.4.2.3). When updating the model with the different stress-factors combinations observed in the dynamic profiles, all the stress-factors were

[26] It is noteworthy that the updated model's prediction is worse than the original prediction in Figure 28. (d). This is due to the starting point of the updated prediction, which is located just before the critical point (around 100.000 Ah) inducing the shift of the predictions with respect to the data. In fact, one of the reasons to select this updating point was to reveal that the updated predictions also depend on the initial value of the updating point.

involved in the learning process, and the confidence of the model for predicting throughout the whole operating window was modified. This is observable in Figure 29, which reflects the evolution of the standard deviation of the model's predictions, for the model corresponding to the training case 4 and the model updated with the data obtained from dynamic operating profile until 90000 Ah-throughput. Regarding the range of the cycling temperatures, Figure 29. (a), it is remarkable that the model gained confidence around approximately 15°C - 25°C, which is reflected by a reduction of the standard deviation in such region. Furthermore, a strong influence of the charging C-rate was detected from the dynamic profiles, leading to a large variability on the standard deviation even for small charging C-rate variations, Figure 29. (d). This explains why the confidence intervals became larger in some prediction point in Figure 28. (a): around 167000 Ah-throughput, for instance, the updated model predicted larger confidence intervals, because the ~1C charging C-rate value was identified as an 'uncertain' region for prediction due to i) the lack of training data in such charging rates region and ii) to the high influence of this stress-factor on the capacity loss, which was inferred from the previously observed ageing at dynamic operating profile.

Detection of strong influence of the charging C-rate

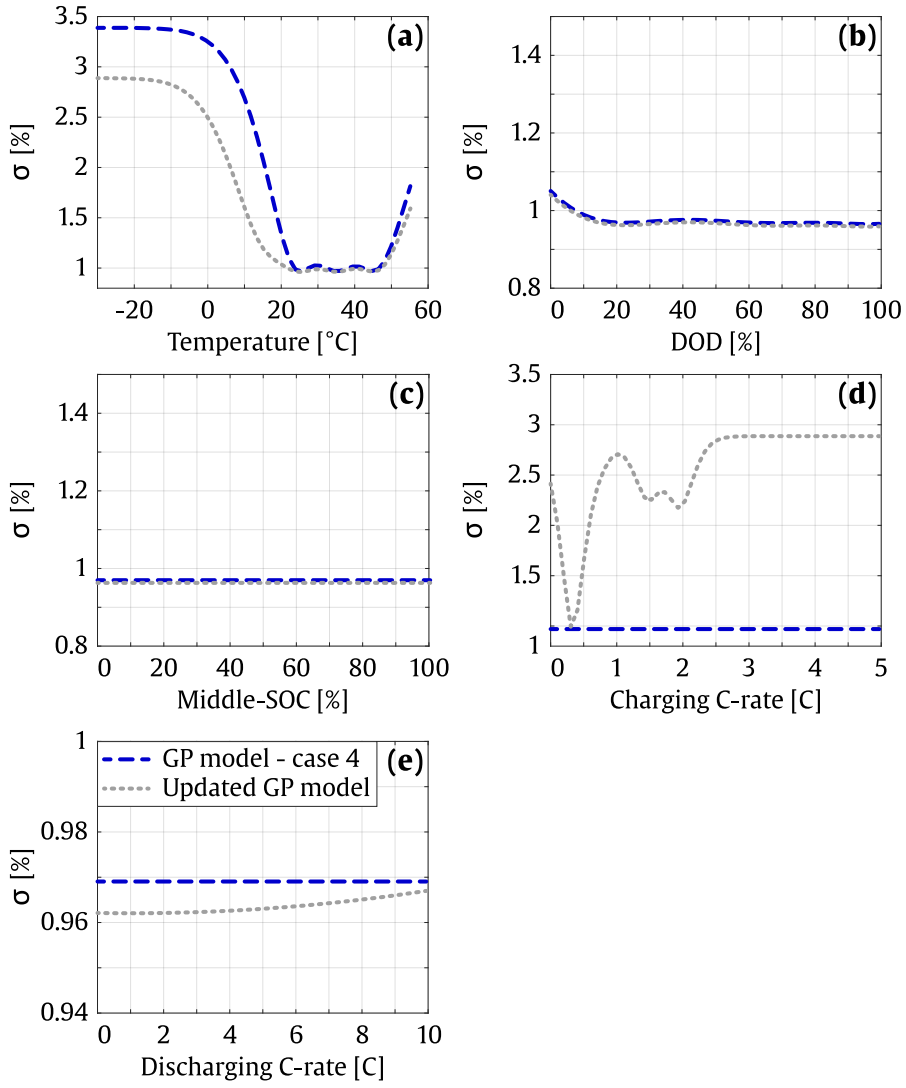

Figure 29. Evolution of the standard deviations of the GP model predictions throughout the whole operation window of the Li-ion cell under study, from the model trained at case 4 to the model updated at dynamic operating conditions. (a) Evolution throughout the temperature space, at constant 80% DOD, 50% middle-SOC and C/3 – 1C charging and discharging C-rate (b) Evolution throughout the DOD space, at constant 35°C, 50% middle-SOC and C/3 – 1C charging and discharging C-rate (c) Evolution throughout the middle-SOC space, at constant 35°C, 20% DOD and C/3 – 1C charging and discharging C-rate (d) Evolution throughout the space of the charging C-rate, at constant 35°C, 80% DOD, 50% middle-SOC and 1C discharging C-rate and (e) Evolution throughout the space of the discharging C-rate, at constant 35°C, 80% DOD, 50% middle-SOC and C/3 charging C-rate.

4.6. Conclusions of the chapter

In this chapter, a cycling capacity loss model is developed based on the GP framework. The model developed in Section 4.3 demonstrated suitable performances to fit the data, independently from the number of training data and involved stress-factors. This is observable in Figure 24. (a), where both $MAE_{\Delta Q}$ and MAE_{Q} curves of the training cells showed a constant level under the defined 2% threshold, from the training case 1 to 16.

Good fitting

Moreover, this chapter illustrates the ability of GP-based cycle ageing models to learn from the operating conditions progressively observed, increasing both accuracy and confidence of the model. This way, the verification of the hypothesis H5 is extended to the cycle ageing use-case. This hypothesis, already verified in Chapter 3 for calendar ageing, states that the nonparametric frameworks are able to learn about the influence of new values of the different stress-factors on battery degradation, including new data in the training set.

Learning capability

The improvement of model's prediction accuracy is demonstrated in Figure 24. (b), (c) and (d), as the new cycling conditions are incorporated in the training dataset. The analysis of the uncertainty boundaries corroborates the findings observed in Chapter 3: the reduction of the standard deviation in Figure 26 and Figure 29 testified about the increment of the model's confidence to perform prediction throughout a broad operating window, as input spaces are progressively explored. Again, the developed GP model turned out to be slightly over-confident, according to the CSs curves represented in Figure 24. As previously explained, the $CS_{2\sigma}$ values should be approximately 95.4% if the uncertainty predictions are accurate: the obtained $CS_{2\sigma-Q}$ and $CS_{2\sigma-\Delta Q}$ values converged approximately into 75% and 90% respectively (Figure 24. (d)). As already observed in Chapter 3, the difference between the $CS_{2\sigma-Q}$ and $CS_{2\sigma-\Delta Q}$ suggests that the overconfidence of the model was induced by the error accumulation of the iterative prediction process.

Accuracy improvement

Gaining confidence

Regarding the minimum amount of experimental ageing tests necessary from the laboratory for the development of the initial ageing model was determined: the training case 4 seems to present an adequate trade-off between the performances and the development cost of the model, insofar as the cell is used at the operating conditions recommended by the manufacturer (specified in Chapter 3). In fact, the model achieved 1.04% MAE_Q average prediction errors for 122 cells operating between 25°C-45°C, 20%-100% DOD, 20%-80% middle-SOC, C/3-2C charging C-rates and C/3-2C discharging C-rates, using only 26 cells tested at 9 cycling conditions for

Minimal number of laboratory tests

training. Furthermore, the performances of the model seem not to improve significantly since such training case (see Figure 24. (b) and (d)).

Overestimation at dynamic conditions

In Section 4.5, the developed model was validated at dynamic operating conditions, achieving 3.76% and 1.46% in terms of MAE_Q, for the cells #124 and #125 respectively. In Figure 28. (a), the initial model overestimated the degradation trend, mainly due to a large cycling step at 100% DOD around 80000 Ah-throughput. In fact, the cells tested at 100% DOD in static cycling conditions observed increased capacity losses, compared to the cell tested at the same DOD but within a dynamic ageing test. A similar behaviour was already reported in [34], in which it was suggested that the dynamic character of the DOD stress-factor's profile may induce reduced ageing rates compared to static DOD profiles. This result allows to partially deny the hypothesis H2, which states that ageing models trained with static ageing laboratory tests may be able to perform accurate predictions at dynamic operating profiles.

…because of dynamic DOD profile?

Isotropic kernels

Additionally, the research works carried out in this chapter with cycle ageing data corroborates the findings observed with calendar ageing data in the previous chapter: isotropic kernel components are suitable to host the features corresponding to the different stress-factors, in so far as the battery operates within the limited range of the recommended operating conditions.

Sensitivity

Finally, the sensitivity analysis shows that, for this dataset, the developed model tends to classify the influence of the stress-factors' variation on capacity loss in this order: 1/ temperature, 2/ DOD, 3/ charging C-rate, 4/ middle-SOC and 5/ discharging C-rate. Nevertheless, it is noteworthy that, manipulating the equation (37), which corresponds to the developed covariance function, some terms involving the products among the different stress-factors' hyperparameters appear. Such terms could be interpreted as the covariance components corresponding to the interactions between the different stress-factors. The sensitivity analysis of the capacity loss to the stress-factors could be extended by involving such covariance components, in order to have a feedback about which combinations of stress-factors levels are most critical according to the GP model.

The following chapter is dedicated to the integration of the calendar and cycle ageing models, developed respectively in Chapter 3 and Chapter 4. The holistic ageing model is applied to predict the ageing of Li-ion batteries cycled under realistic operating profiles.

Chapter 5.

Validation of the holistic ageing model under realistic operating profiles

Chapter 3 and Chapter 4 were dedicated to the development of pure calendar and cycle ageing models, respectively. In this chapter, the Stage 4 of the methodology described in Chapter 2 is implemented. Both calendar and cycle models are combined in order to obtain a holistic view of Li-ion battery ageing. The holistic model is validated under realistic operation profiles corresponding to two different applications, in which both calendar and cycle use-cases are sequentially experienced: i) a full EV driving application and ii) a power smoothing application for renewable energy integration. The ability of the models to learn from realistic battery operation profiles is also evaluated.

This section is structured as follows, Section 5.1 describes the experimental ageing tests carried out in order to produce the ageing data corresponding to the operation in the two different applications. Moreover, the data collected from deployed battery systems is typically expressed in terms of current, voltage and temperature time series. Section 5.2 describes the processing algorithm used to convert such time series into a profile of the different stress-factors, suitable for prediction and training of the GP models developed in Chapter 3 and Chapter 4. Sections 5.3 and 5.4 are dedicated to the application of the holistic ageing model to the EV driving and to the power smoothing applications, respectively. Finally, Section 5.5 summarises the main conclusions of the chapter.

5.1. Data gathering

Missing in-field data

The digitalisation of the industry is still in an early stage of maturity, and although some companies already showed interest on collecting and analysing the operation data extracted from deployed battery packs, the availability of significantly degraded battery data is yet scarce. Therefore, the real-world operation data considered in the context of this research was not directly taken from in-field battery operation, but rather replicated in the laboratory environment, again as part of the project Batteries2020. The operating profiles of two different applications were reproduced in laboratory, namely i) full EV driving application and ii) power smoothing for renewable energy integration application (herein referred as 'power smoothing application'). The operating profiles corresponding to such applications are particularly interesting, as they provide a considerably different participation of the storage and cycling operation. The synthesised EV load profiles imply a substantial participation of the storage operation, whereas the power smoothing load profiles involve a quasi-exclusive cycling operation. Throughout the whole duration of the tests, periodical characterisation tests were carried out to observe the degradation induced by such operating profiles.

Two applications

5.1.1. Synthesis of EV real driving load profiles

EV driving profiles

In order to validate the predictive and learning capabilities of the developed ageing models under realistic operating conditions, several EV driving profiles were synthesized. The profiles synthesis was based on the Worldwide harmonised Light vehicle Test Cycle (WLTC), because it appropriately matched the conditions found in the normal operation of an EV, according to measured real-life driving data [152,153].

Two different EV driving profiles were defined. The first profile (herein referred as 'Driver 1') was representative of an urban driver, while the second profile (herein referred as 'Driver 2') combined the driving conditions corresponding to an urban and suburban traffic area.

On the basis of the WLTC speed profile [152], a cell-level current profile was synthesised for both driving conditions Driver 1 and 2, illustrated respectively in Figure 30. (a) and (b). The positive current values represent charging events while negative current values refer to discharging events. The sampling frequency of the synthesised time series was 1Hz.

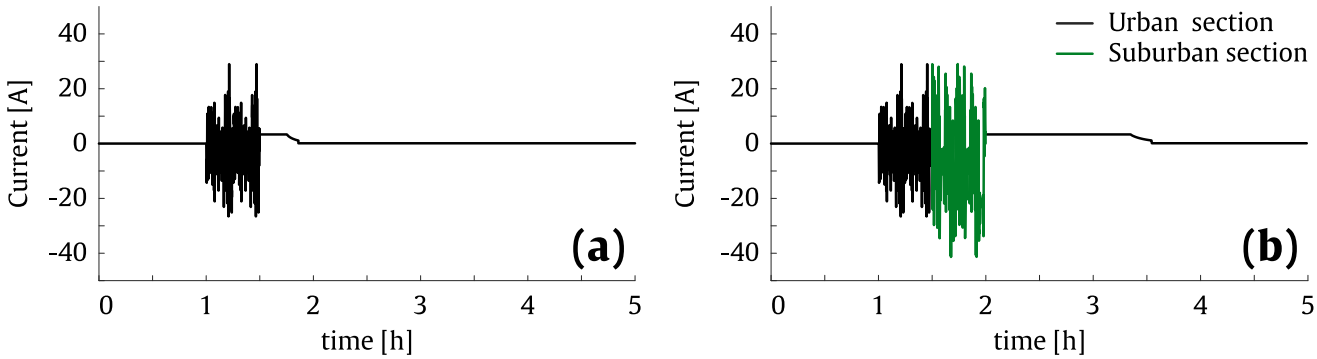

Figure 30. Cell-level current profiles synthesised on the basis of WLTC speed profiles, for (a) Driver 1 and (b) Driver 2.

The current profiles synthesised from the WLTC speed profiles were adapted to cover a real-life driving application. Starting from 90% SOC, the designed scenario was the following:

From Monday to Friday:

- 8:00 am: unplug charged car (90% SOC) from home charging station and drive to work.
- 8:30 am: get to work and plug car in for charging.
- 6:30 pm: get home and plug car into charge again.

Saturday:

- 10:00 am: drive a few kilometres for an errand.
- 12:30 am: get home and charge the car.

Sunday:

- The EV is not used.

Seasonal temperatures

Although the temperature of the cells in EVs is typically controlled by a thermal management system during the driving operation, this is not the case during the multiple idle periods of the EV. Therefore, a seasonal temperature profile corresponding to the monthly averages registered in Seville was applied to the tested cells throughout the whole duration of the tests. The temperature profile, depicted in Figure 31, reached a maximum and minimum values of 36°C and 15°C, respectively.

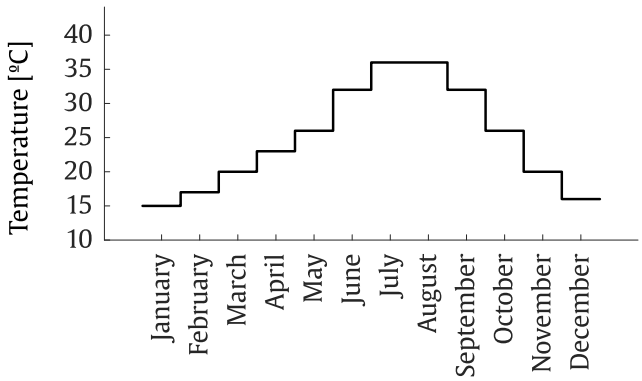

Figure 31. Monthly average seasonal temperature profile in Seville.

The evolution of the capacity of the cells submitted to the real driving profiles are depicted in Figure 32, for both synthesised profiles corresponding to Driver 1 and 2.

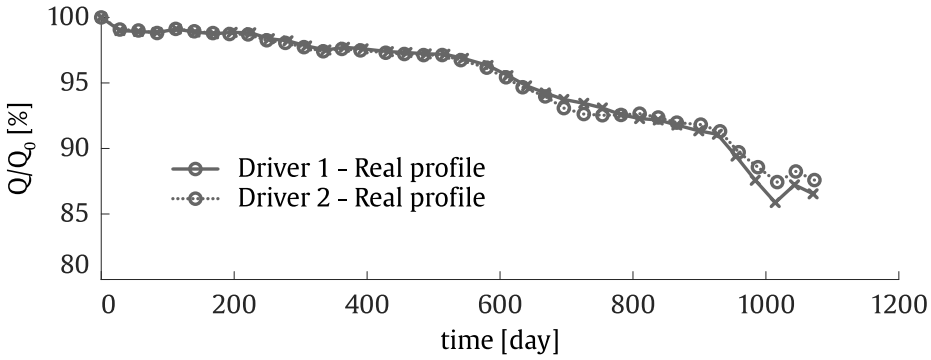

Figure 32. Evolution of the normalised capacity of the cells tested under the synthesised driving profiles.

5.1.2. Synthesis of the power smoothing load profiles

Power smoothing renewable energy application

In addition to the EV driving profiles described in Section 5.1.1, supplementary cells were submitted to power smoothing renewable energy integration application profiles. More precisely, the power profile observed by a second life energy storage system connected to a grid-scale PV plant was synthesised, within the context of the mitigation of the power variability of the plant [23,154].

First life profile

In order to simulate a 'first life' of the cells before the power smoothing application, two cells previously submitted to static and accelerated cycling conditions were selected. The cycling conditions of the selected 'first life' corresponded to a 35°C, 80% DOD, 50% Middle-SOC and C/3 and 1C charging and discharging C-rate operation. The total duration of the first life was ca. 532 days. However, it is noteworthy that as the corresponding operation was designed to accelerate the ageing, such operation could represent a larger duration of 'real life' of the cell. After the first life operation, the cells were submitted to a storage period of 120 days at 20°C and 50% SOC, representing the idle transition period of the cell after the first life operation and before the implementation in the second life operation.

Second life profile

The detailed procedure adopted for the synthesis of the second life battery operating profiles were explained in [23,154]. The resulting current profile, depicted in Figure 33, showed current pulses until 2.5C and was combined with a constant cycling temperature of 35°C. The sampling frequency of the synthesised time series was 0.0083 Hz (one sample per two minutes). The capacity curves obtained for the corresponding cells were represented in Figure 34. It is noteworthy that, in Figure 34, a capacity recovery is observable during the idle transition period between the first and second life. This is explained in the literature by the effect of the anode overhang (geometrical oversized anode) and the homogeneity of lithium distribution: during rest periods at relatively low SOC levels, the lithium ions located in the anode overhang tends to return into the active part of the anode, inducing this way a capacity recovery [103].

Capacity recovery

Anode overhang

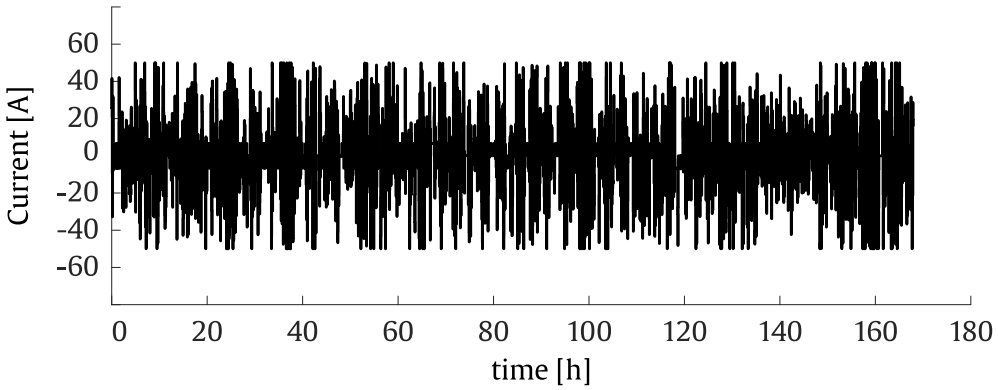

Figure 33. Cell-level current profile synthesised for the power smoothing renewable energy integration application, applied to 'second life' cells. The profile corresponding to one week is plotted.

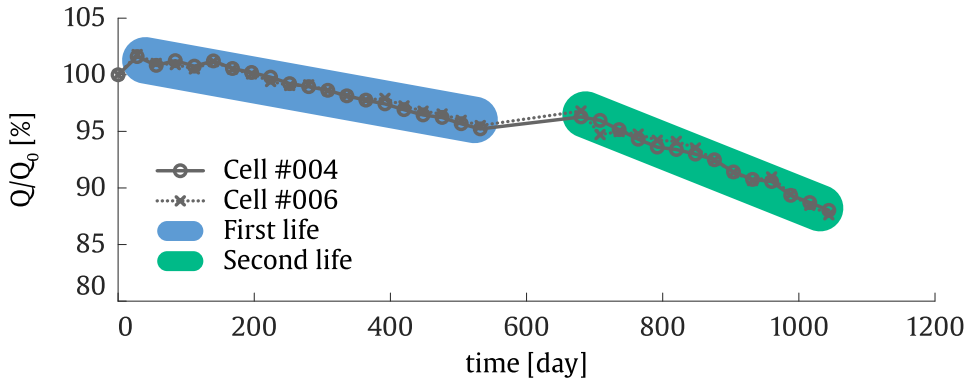

Figure 34. Evolution of the normalised capacity of the cells tested under successively i) first life cycling conditions, based on static and accelerated testing profiles, and ii) second life cycling conditions, based on synthesised power smoothing current profiles.

5.2. Realistic profiles processing

Once the battery-pack is implemented and deployed in a real application, the real operation data collected from the DAS is typically extracted in term of current, voltage and temperature time series. Nevertheless, as explained in Chapter 2, such time series must be processed prior performing any prediction, in order to extract the different stress-factors influencing the ageing of Li-ion batteries and defined as inputs of the models developed in Chapter 3 and Chapter 4.

Input processing algorithm

As the model developed in this thesis is thought to be trained under a supervised learning paradigm, the target training values corresponding to the input values must also be extracted. This could be done on the basis of i) periodical characterisation tests performed to the battery-packs in operation, or ii) SOH estimation algorithms developed to estimate the capacity of the battery-packs in operation [126].

Target processing algorithm

5.2.1. Input profiles processing algorithm

Figure 35 illustrates the different steps of the algorithm designed to convert the current, voltage and temperature time series.

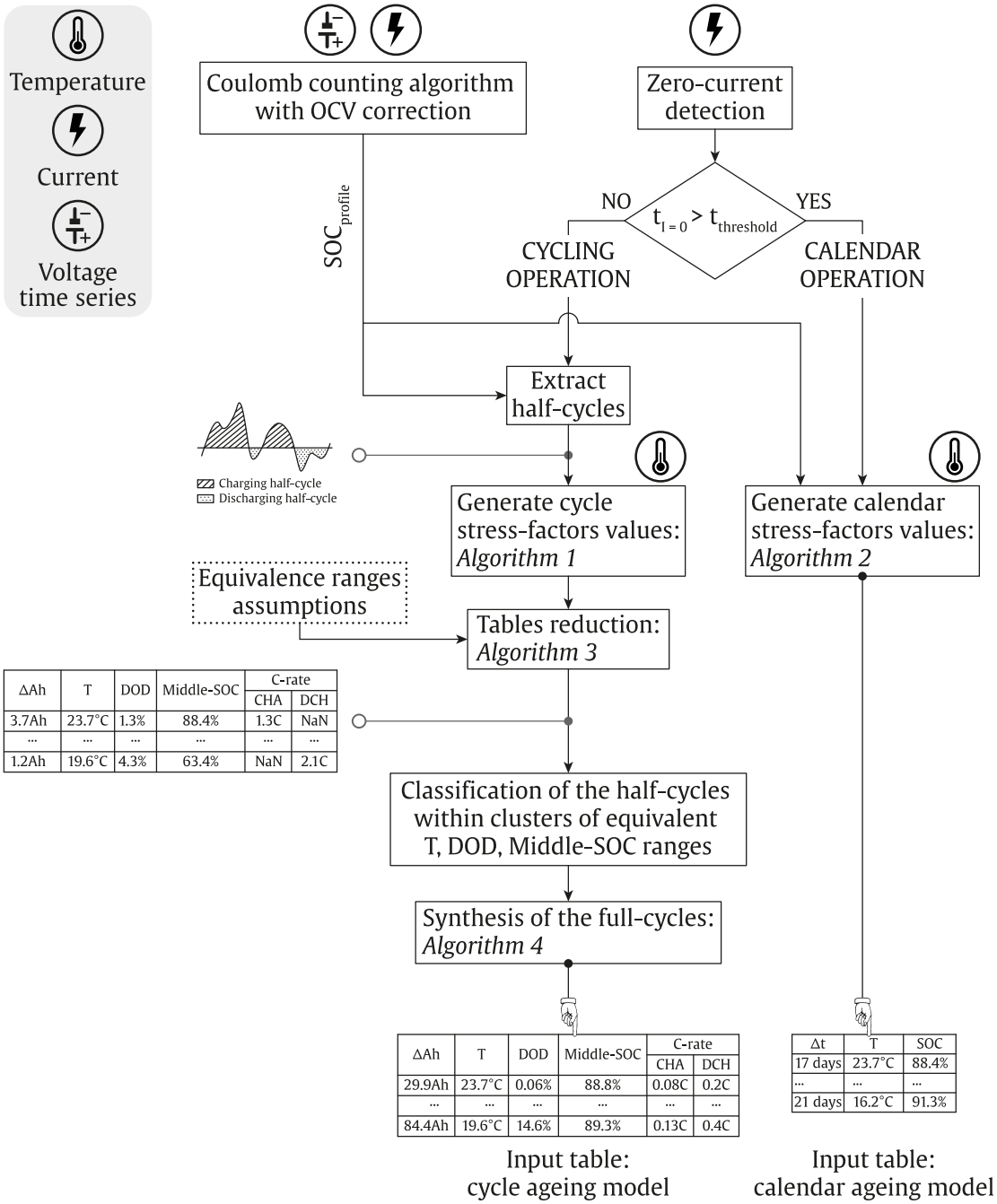

Figure 35. Input processing algorithm: temperature, current and voltage time series are converted into input tables for the calendar and cycle ageing models.

Input processing algorithm

The starting point of the input processing algorithm is the decomposition of the time series, which will derive to the calendar and cycling components of the operation of the cell. The decomposition is based on a zero-current detection step applied to the current time series recorded from the DAS: if the current applied to the cell held a zero value during a time period superior to a priorly defined time threshold $t_{threshold}$, such section of the current time series, as well as the corresponding sections of the voltage and temperature time series are assigned to the calendar operation of the cell. Conversantly, the remaining sections of the current time series, as well as the corresponding voltage and temperature sections are assigned to a cycling operation.

Further, the current, voltage and temperature time series' sections assigned to the cycling operation of the cell are processed as follows: i) based on the current and voltage time series, a coulomb counting algorithm with Open-Circuit-Voltage (OCV) calibration is applied to generate a SOC profile of the cell [155]; ii) from the current time series, positive and negative half-cycles are distinguished; iii) for each half-cycle, the corresponding stress-factors are processed in Algorithm 1, from the current, temperature and SOC time series; iv) some stress-factors ranges are defined, for which the corresponding influence on cell ageing is assumed to be equivalent; v) based on such equivalence ranges assumptions, the Ah-throughput corresponding to charging and discharging half-cycles are separately accumulated in Algorithm 3, for the half-cycles which belong within the same equivalence ranges, leading to a reduced table specifying the different stress-factors corresponding to accumulated half-cycles; vi) the accumulated charging and discharging half-cycles which belong within the same equivalent temperature, DOD and Middle-SOC ranges are classified within associated clusters; and vii) from each cluster involving charging and discharging half-cycles corresponding to identical stress-factors ranges, full-cycles are synthesised in Algorithm 4. This way, an input table is finally generated for the cycle ageing model, consistent with the required input data structure, described in Chapter 4, **Table 14**.

Calendar profile processing

In parallel, the sections of the current, temperature and SOC time series which were assigned to the calendar operation of the cell are processed in Algorithm 2, in order to generate an analogue input table for the calendar ageing model, consistent with the required input data structure described in Chapter 3, **Table 11**. The pseudo-codes of the Algorithms 1 – 4 are detailed in Appendix C.

Figure 36 illustrates representative examples of the dynamic input profiles extracted from the cycle operation component of the current, voltage and

Equivalent dynamic profiles

temperature time series, applying the input processing algorithm described in Figure 35. The obtained dynamic profiles are depicted for (a, b) the EV driving profiles, Driver 1, (c, d), the EV driving profiles, Driver 2, and (e, f) the power smoothing profiles.

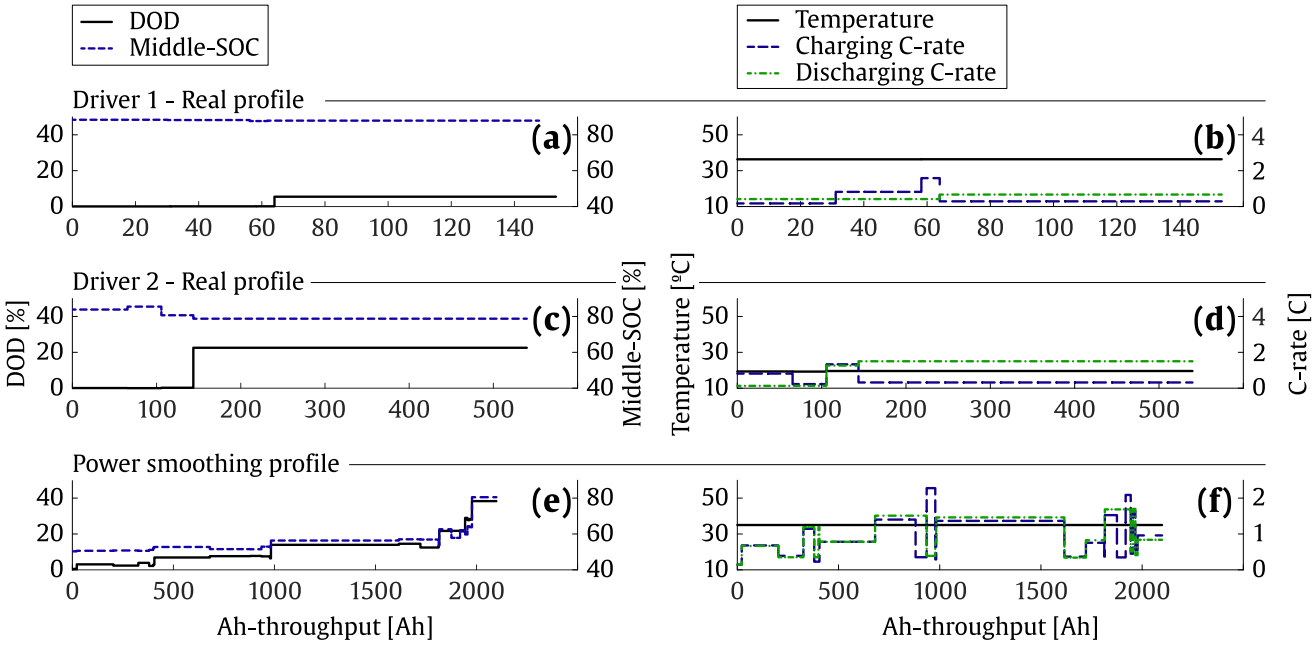

Figure 36. Dynamic profiles of the different stress-factors with respect to the Ah-throughput, extracted from temperature, current and voltage time series, applying the input processing algorithm described in Figure 35.

Table 16 summarises the operating ranges of the different stress-factors profiles, for the EV (Driver 1 and 2) and power smoothing applications.

Table 16. Equivalent operating conditions corresponding to the real EV and power smoothing profiles described in Section 5.1.1 and 5.1.2.

	EV - Driver 1	EV - Driver 2	Power smoothing
Temperature [°C]	15 - 36	15 - 36	35
DOD [%]	ca. 5.7	ca. 23	< 40
Middle-SOC [%]	ca. 88.7	ca. 79.4	50 – 80
C-rate CHA [h-1]	C/5 in charging, 0C – 1.5C in driving	C/5 in charging, 0C – 1.5C in driving	0C – 2.5C
C-rate DCH [h-1]	0C - 1.5C	0C - 2C	0C – 2C

5.2.2. Target processing algorithms

Although the input processing algorithm allows performing ageing predictions for batteries operating in real application, an additional challenge must be resolved in order to give to the developed models the capability to learn about the influence of the different stress-factors on the underlying degradation directly from real operating conditions.

Supervised learning

For the calendar and cycle ageing models developed respectively in Chapter 3 and Chapter 4, the training stage was performed under a supervised learning paradigm. In fact, the laboratory tests were designed in such a manner to observe separately the calendar and cycle ageing of the tested Li-ion cells. Furthermore, the operating conditions applied to the cells between two characterisation tests remained constant. This way, for both calendar and cycle ageing models, it was possible to associate i) one training input vector, expressing the values of the stress-factors corresponding to the static operating conditions of the cell, with ii) one training target data, corresponding to the capacity loss calculated from the capacity data obtained in the characterisation tests. The association of both input and target training components led to the complete training data of the models.

Target data issues

Nevertheless, during many real-world operating conditions, the cell is subject to both calendar and cyclic ageing taking place successively. Furthermore, the characterisation tests (or equivalently the computation of a SOH algorithm) are not necessarily carried out at every transition between storage and cycling operation of the cells. For these reasons, the direct association of input and target training data is not possible, for the data extracted from real operating conditions.

The designed input processing algorithm, described in Section 5.2.1, allows converting current, voltage and temperature time series into a dynamic profile of the different stress-factors, illustrated in Figure 36. Such dynamic profiles could be expressed as a succession of constant stress-factors, consistently with the required input data structure for the models' training. However, as depicted in Figure 37, the synthesised input component of the training data does not have any target component directly associated. The training data available to update the initial GP model is then composed of i) the data obtained from the laboratory tests, which includes both input and target components, and ii) the data obtained from real operation of the deployed battery-packs, which only includes the input component, as well as a single target capacity loss value extracted from the characterisation tests carried out in-field (or equivalently the computation of a SOH algorithm). This new learning paradigm could be assimilated to the semi-supervised

Data imputation

learning problem defined in the literature [156]. Under such learning paradigm, data imputation methods are typically applied in order to associate a target data component to the input data. As depicted in Figure 37, a target processing algorithm was developed to partition the capacity loss data into a target component vector of the training data.

The developed target processing algorithm proceeded as follows: i) the overall capacity loss data[27] was first decomposed into a calendar and cycle components, applying a decomposition factor based on the respective duration of the storage and cycling with respect to the total duration of the cell operation; ii) the calendar capacity loss component was then partitioned among each row of the input component of the calendar ageing models' training data, applying a decomposition factor based on the respective duration of each row with respect of the total duration of the storage operation; and iii) the cycle capacity loss component was partitioned among each row of the input component of the cycle ageing models' training data, applying a decomposition factor based on the ΔAh value of each row with respect of the total Ah-throughput of the cycling operation. The pseudo-code of the target processing algorithms is detailed in Appendix C.

[27] Calculated as the difference between two consecutive capacity data from characterisation tests or SOH estimations.

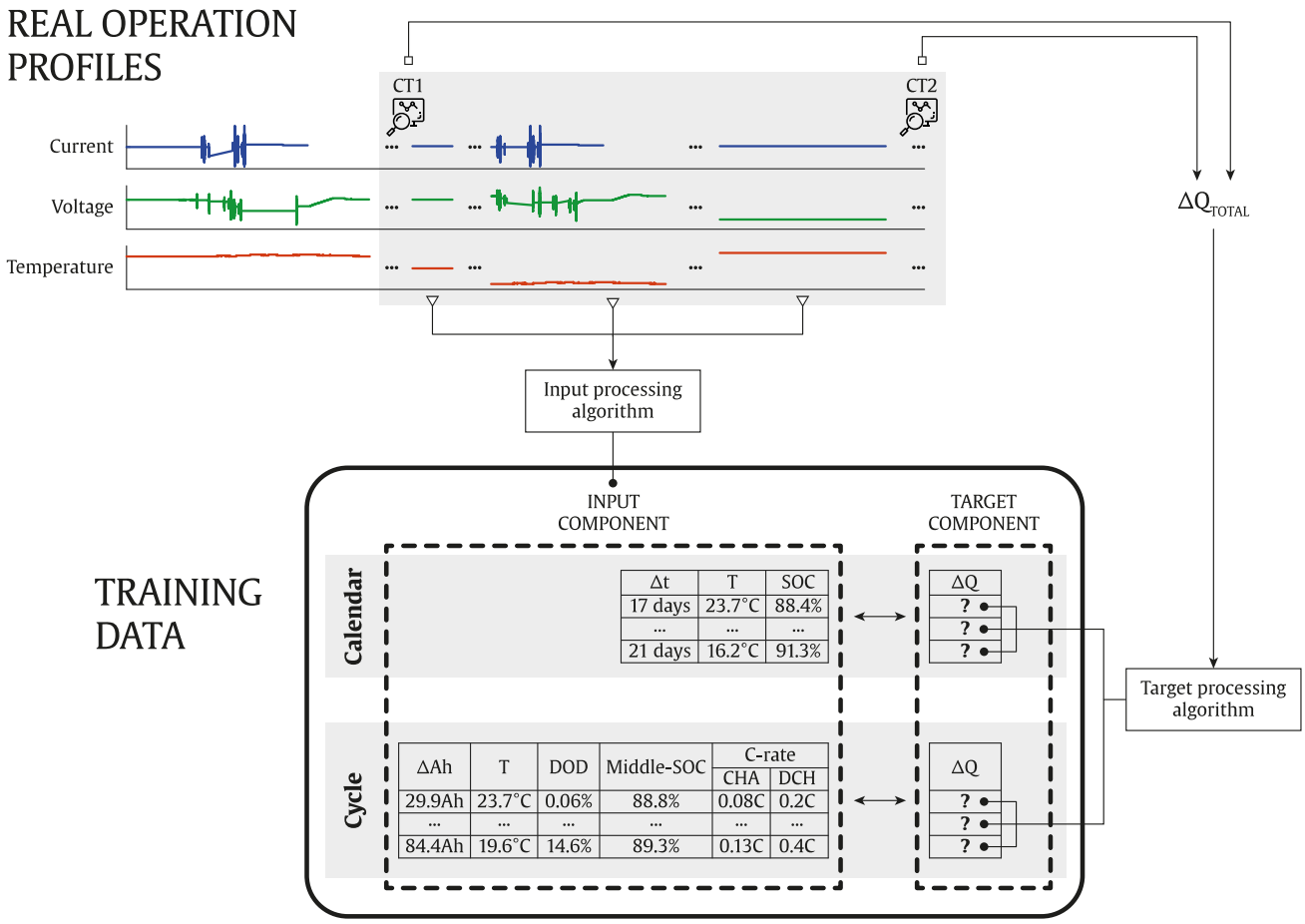

Figure 37. Proposed method for the extraction of the training data from real operation profiles, for the calendar and cycle ageing models training.

5.3. Use-case 1: EV driving profiles

Learning from EV profiles

Baseline model

The main goal of this section is to evaluate the prediction performances, as well as the learning capability of the developed ageing models, in terms of prediction error, accuracy of confidence intervals and sensitivity analysis, for an EV driving use-case of the cells. First, the capacity loss of the cells submitted to such operating profiles was predicted with a baseline model, defined to be the GP model corresponding to the minimal required training cases, determined as the training case 3 and 4 for the calendar and cycle ageing model respectively, in Chapter 3 and Chapter 4. After a real operation data gathering period, the collected current, voltage and temperature time series data, as well as the periodically estimated capacity data are processed and included within the training data of the baseline model. An updated

ageing model is obtained by retraining the covariance function of the GP model with the completed training dataset.

Completing the training dataset

The data gathered from the real operation potentially includes new combinations of the different stress-factors values, unobserved during the laboratory ageing tests. Each time the training dataset is completed with new data collected from the real operation, the resulting GP model could perform more accurate and confident predictions for a broader window of battery operating conditions.

For the cell submitted to the synthesised real EV driving profile, driver 1, described in Section 5.1.1, Figure 38. (a), (b) and (c) depict the predictions performed with the baseline model for the overall capacity loss, and the calendar and cycle capacity loss components extracted from the target processing algorithm, respectively.

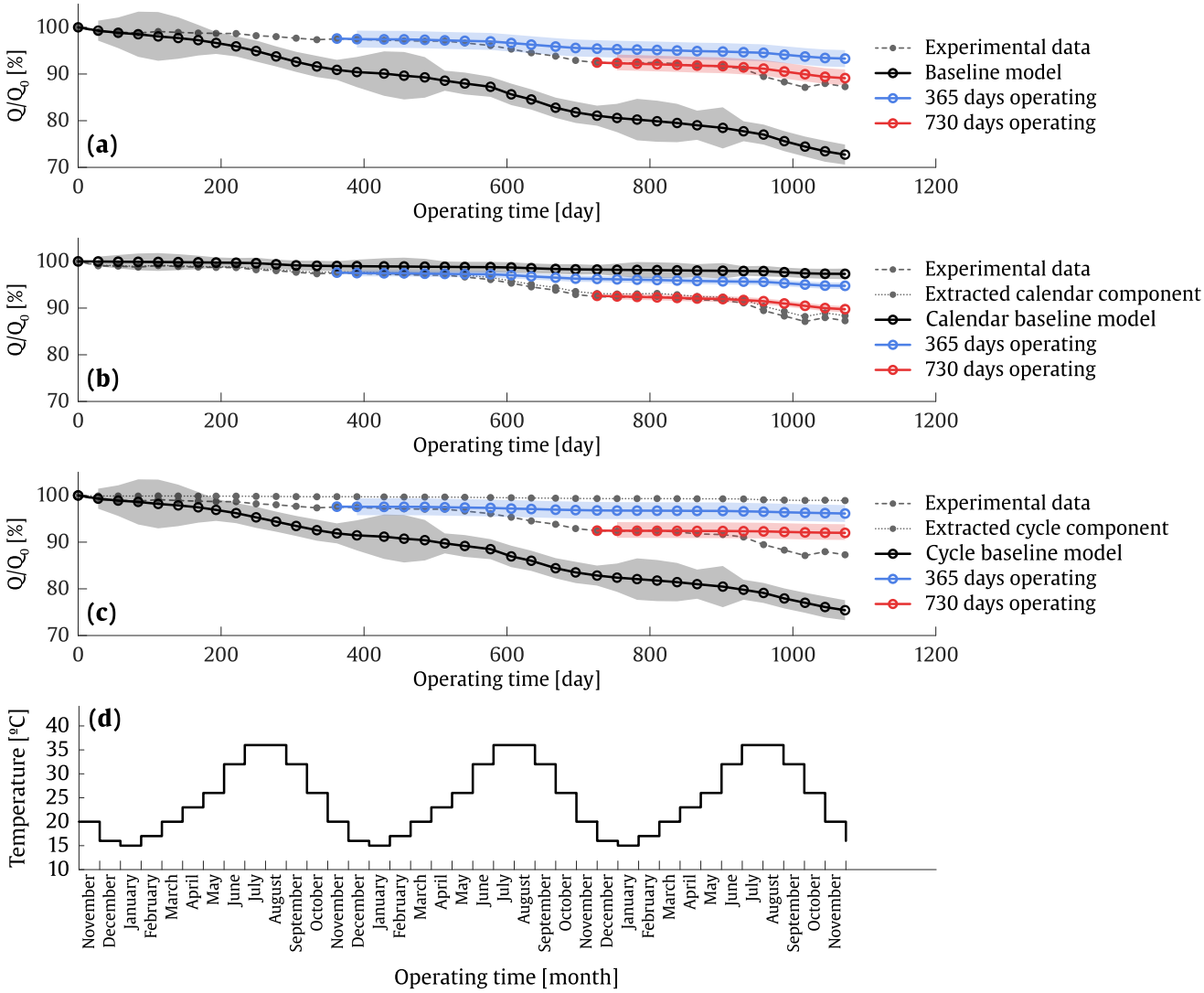

Figure 38. (a) Overall capacity experimental data for the 'Real EV profile – Driver 1', capacity loss prediction of the baseline model (black line and grey area), the model updated after 365 days operating (blue line and area) and the model updated after 730 days operating (red line and area). (b) Overall capacity experimental data, calendar capacity curve component extracted from the target processing algorithm, predictions of the calendar baseline model (black line and grey area), the model updated after 365 days operating (blue line and area) and the model updated after 730 days operating (red line and area). (c) Overall capacity experimental data, cycle capacity curve component extracted from the target processing algorithm, predictions of the cycle baseline model (black line and grey area), the model updated after 365 days operating (blue line and area) and the model updated after 730 days operating (red line and area). (d) Monthly average seasonal temperature profile in Seville.

Overestimation

As expected, it is noteworthy that the target processing algorithm assigned most of the capacity loss to the calendar operation of the cell, due to large periods in which the EV was parked and the battery was submitted to a storage operation. In Figure 38. (a), it could be observed that the overall ageing prediction of the baseline model was clearly overestimated. The visualisation of the predicted calendar and cycle ageing components respectively in Figure 38. (b) and (c) indicates that the cycle ageing model was responsible of the deviation. Such a behaviour was already observed in Chapter 4, Figure 28, and was linked in [97] to the dynamic character of the DOD stress-factor's profiles, which may induce lower ageing rates compared to the static DOD ageing profiles. Indeed, the baseline model was trained based on ageing data obtained from static DOD operation profiles (namely 20%, 65% and 100% DOD), and this could be why it overestimated the ageing under dynamic DOD conditions.

Dynamic DOD

Underestimation of calendar component

In parallel, the calendar component of the ageing prediction was underestimated. One cause of this deviation could be the limited extrapolation capabilities of the Matérn class kernels [157], coupled to the fact that the highest storage SOC level involved in the training dataset of the baseline model was 80% SOC. However, observing the evolution of the calendar ageing prediction, Figure 38. (b) and the corresponding seasonal temperature profiles, Figure 38. (d), it is noteworthy that the underestimation occurred especially during the periods corresponding to the highest temperatures in summer. The capacity loss corresponding to the summer periods increased throughout the whole duration of the tests. In fact, the first summer led to a 1.1% capacity loss in 141 days (between 221 – 362 operating days), the second summer led to a 3.57% capacity loss in 149 days (between 577 – 726 operating days), and the last summer led to a 3.88% capacity loss in 96 days (between 931 – 1017 operating days). Although not any strong evidence were found in this sense, this phenomenon could be caused by the cycle-induced calendar ageing, also reported in [158,159]. Following this theory, the cycling phases of the cell could intensify the ageing observed during the subsequent storage phases of the cell. In fact, the cycling of the cell could provoke the cracking of the SEI or of the particle itself in the negative electrode, potentially revealing fresh anode surfaces or areas of thinner SEI film, which are prone to further SEI formation [146,149,150]. These phenomena are magnified during the summer periods, in which the higher temperatures accelerate the SEI formation within such sensible areas of the negative electrode. For the calendar ageing tests carried out in laboratory and described in Chapter 3, some cycle-induced calendar ageing could also have happened due to the periodical characterisation tests performed once a month. However, such phenomenon should have a higher

Cycle-induced calendar ageing?

impact on the ageing corresponding to the EV driving profiles, due to the repeated driving cycles which punctuate the storage phases when the car is parked. This could explain why the baseline model, composed of a calendar ageing model based exclusively on laboratory calendar ageing tests data, tended to underestimate the effect of cycle-induced calendar ageing in the prediction of the real operation EV profile ageing curve.

Uncertain predictions in winter

Furthermore, the predictions of the baseline model showed a periodical spread of the confidence intervals, corresponding to the colder temperatures experienced during winter (see the applied temperature profile, Figure 31). In fact, although the model seemed to be relatively confident to perform predictions between 23°C – 36°C, the uncertainty increased when predicting the ageing below the 20°C, i.e. between November - March. This is consistent with the training data managed by the baseline model, involving ageing data only for a 25°C, 35°C and 45°C storage and cycling operation, and then reducing the reliability of the predictions below 25°C.

Fleet learning paradigm

In order to update the baseline model, the operation and the underlying ageing response of two cells were used, namely the cells corresponding to the real operation EV profiles related to "Driver 1" and "Driver 2" (see Section 5.1.1). The learning example considered in this section could then be compared to a "fleet learning" paradigm, in which the developed ageing model would be learning in parallel from different usages of the EV operation [25,160].

Updating model

Corrected predictions

After data gathering periods of one and two years, the baseline model was updated by retraining the covariance function with the completed training data. The overestimation of the cycle ageing model, linked above to the dynamic character of the DOD profiles, was corrected in the updated models' predictions. In fact, the predictions of the updated models seem to follow correctly the capacity curve corresponding to the cycle ageing component, Figure 38. (c). The underestimation of the calendar ageing in Figure 38. (b) was also rectified in the predictions of the updated models, particularly after the observation of the data corresponding to the second summer (between 577 – 726 operating days), which revealed more clearly the accelerated ageing effect assigned above to the cycle-induced calendar ageing. The predictions errors of the overall ageing models were respectively 0.46%, 0.29% and 0.26% $MAE_{\Delta Q}$ and 8.17%, 1.91% and 0.78% MAE_{Q}, respectively for the baseline model, and the models updated after 365 and 730 operation days.

In order to evaluate the quality of the training data extracted from real operation, the calendar ageing models updated after 365 and 765 operating

Looking back to static storage operating conditions

days were submitted to an additional validation test which consisted on predicting the ageing of the cells tested in laboratory at 100% SOC and 35°C storage conditions. It is noteworthy that such storage condition was not observed in training. The initial hypothesis was that, after the observation of the 90% SOC storage condition in the EV profiles, the predictions of the models at 100% SOC should indicate an improvement. Indeed, Figure 39. (a), (b) and (c) illustrate such improvement, displaying the predictions of the baseline model and the models obtained after 365 and 730 operating days, respectively.

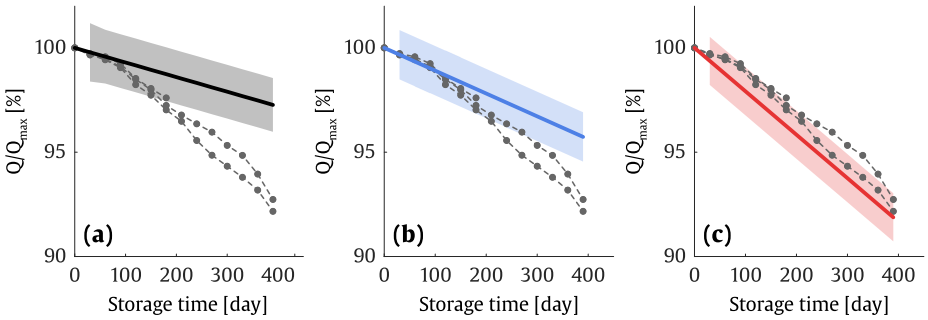

Figure 39. Experimental data obtained from the laboratory calendar ageing tests for the cells tested at 100% SOC and 35°C storage conditions, and predictions of the (a) baseline model, and the models updated after (b) 365 and (c) 730 operating days.

Accurate quantification of the uncertainty

Looking back at Figure 38, an standardisation of the confidence intervals was observable throughout the whole prediction of the updated models, mainly associated with the learning of cold temperatures' influence on both calendar and cycle ageing, which was the main source of uncertainty for the baseline model. The CS of the models were respectively 18.92%, 59.46% and 94.59% $CS_{2\sigma-Q}$, for the baseline model, and the models updated after 365 and 730 operation days. It is noteworthy that the model obtained after 2 years of EV profile observation provided a very accurate quantification of the uncertainty, very close to the 95.4% target value.

Evolution of the uncertainty throughout the input space

As explained in Chapter 3 and Chapter 4, the analysis of the width of the confidence intervals – or equivalently the standard deviation value - along a large operating range of each stress-factor is informative about how confident the model feels to perform predictions throughout a broad operating window. In this sense, the evolution of the standard deviation throughout the input space testifies about the learning process of the model. Figure 40 and Figure 41 depict respectively the evolution of the standard deviation of the calendar and cycle ageing models components, for the baseline model and the models updated after 365 and 730 operation days.

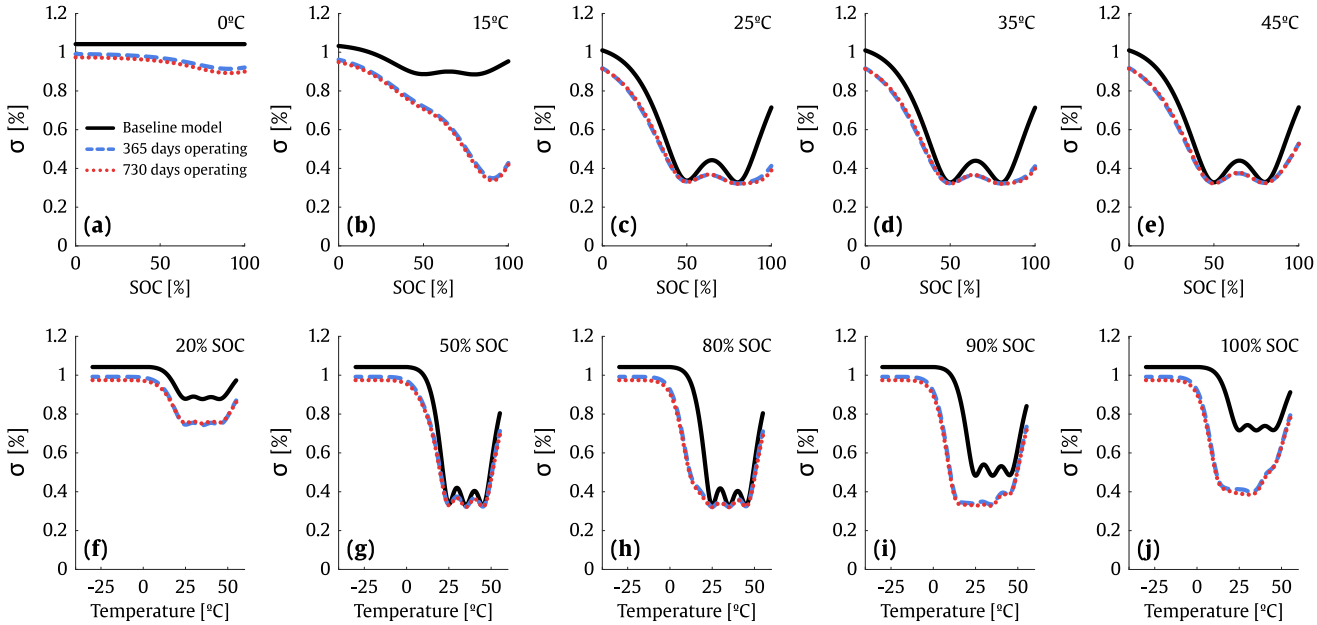

Figure 40. Evolution of the standard deviations of the GP model predictions throughout the SOC and temperature operation window of the Li-ion cell under study, for the calendar components of the baseline model and the updated models after 365 and 730 days operating. (a - e) Evolution throughout the SOC space, respectively at constant (a) 0°C, (b) 15°C, (c) 25°C, (d) 35°C and (e) 45°C. (f - j) Evolution throughout the space of the temperature, respectively at constant (f) 20% SOC, (g) 50% SOC, (h) 80% SOC, (i) 90% SOC and (j) 100% SOC.

In Figure 40, it could be observed that the baseline model indicated higher confidence levels (reduced standard deviation values) when predicting the ageing around 50% and 80% SOC storage conditions, particularly at 25°C, 35°C and 45°C (Figure 40. (c - e), (g), (h)). In fact, those were the storage conditions of the laboratory calendar ageing tests involved in the training of model. Moving away from such combinations of the storage conditions, the standard deviation bent to higher values, although traces of some "confidence peaks" were still observable in Figure 40. (b), (f), (i), and (j). Too far from the storage conditions involved in the training data, the model's predictions were completely uncertain, independently of the SOC values e.g. in Figure 40. (a).

Confidence peaks

As mentioned in Section 5.1.1, the storage part of real EV driving profiles were mainly concentrated around a 90% SOC storage condition, during the time periods when the cars were parked at work and home, for both "Driver 1" and "Driver 2" profiles. Such SOC condition was combined with a different storage temperature between 15°C - 36°C, depending on the period of the year. In Figure 40, a reduction of the standard deviation is observable around

the storage conditions corresponding to such SOC and temperatures combinations, for the models updated after 365 and 730 operation days. This is particularly pronounced in Figure 40. (b), in which a clear "confidence peak" dropped around 15°C and 90% SOC, which corresponds to the storage condition observed during the parking periods in January. Figure 40. (i), and (j) also clearly indicated a reduction of standard deviation values throughout the temperature ranges observed during the whole year, at 90% SOC and by extension also at 100% SOC.

An analogous analysis could be performed from Figure 41, for the cycle ageing components of the models.

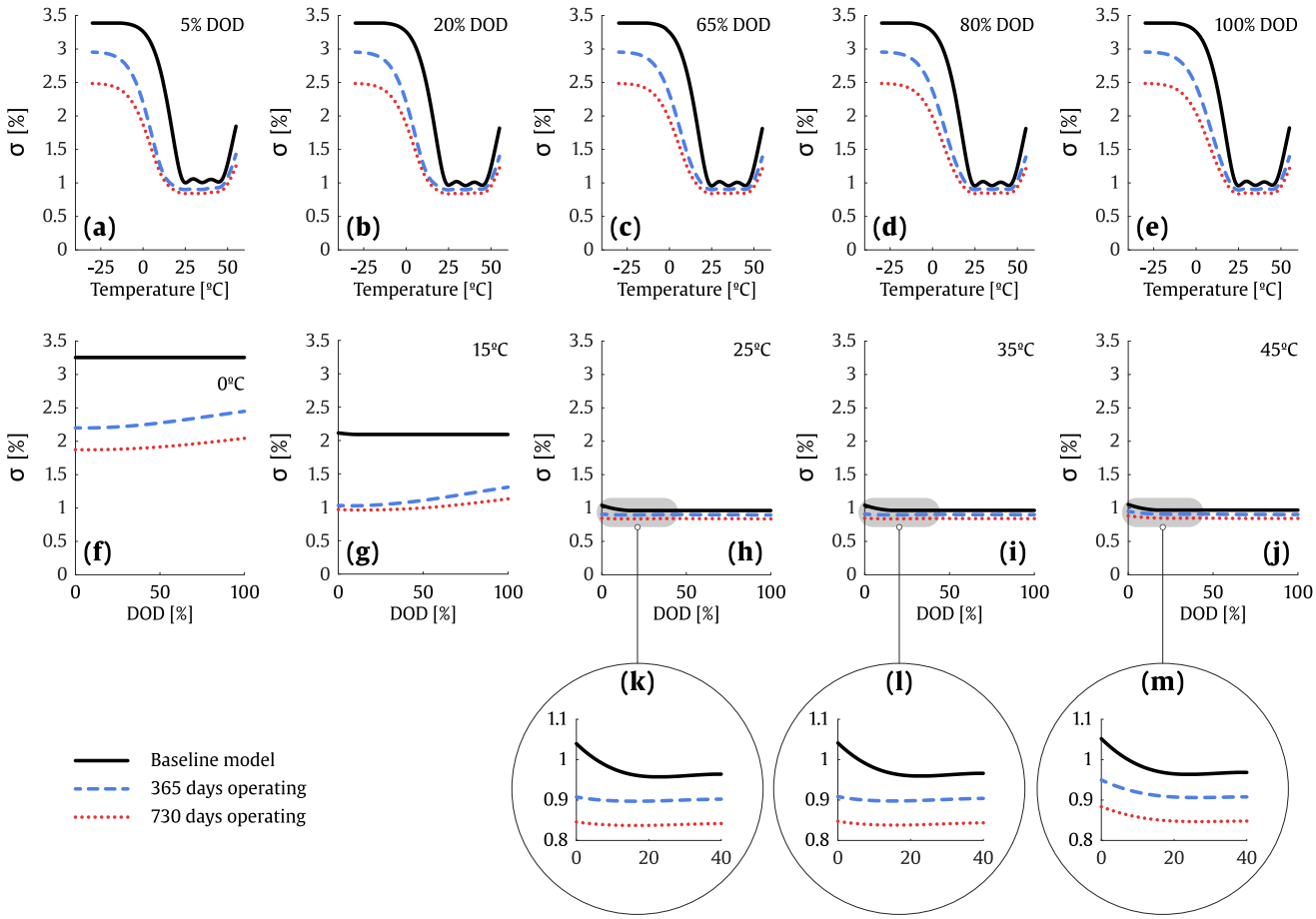

Figure 41. Evolution of the standard deviations of the GP model predictions throughout the DOD and temperature operation window of the Li-ion cell under study, for the cycle components of the baseline model and the updated models after 365 and 730 days operating. (a - e) Evolution throughout the space of the temperature, respectively at constant (a) 5% DOD, (b) 20% DOD, (c) 65% DOD, (d) 80% DOD and (e) 100% DOD. (f - j) Evolution throughout the DOD space, respectively at constant (f) 0°C, (g) 15°C, (h) 25°C, (i) 35°C and (j) 45°C. (k - m) Zoom of the evolution throughout the DOD space, respectively at constant (k) 25°C, (l) 35°C and (m) 45°C.

Uncertain predictions in winter

In Figure 41. (a - e), the standard deviation of the baseline model predictions also showed lowest values at 25°C, 35°C and 45°C cycling temperatures, which corresponded to the training data obtained from laboratory cycling ageing tests. Furthermore, as the training data involved 20%, 65% and 100% DOD cycling conditions, the confidence of the model remained relatively similar throughout a broad segment of the DOD input space (Figure 41. (h - j)). However, slight increases of the standard deviation could be observed focusing on the lowest values of the input space below 15% DOD, as well as around 40% DOD (Figure 41. (k - m)). Figure 41. (f) and (g) revealed a large uncertainty throughout the whole DOD ranges, induced by unobserved cold temperatures.

Learning the effect of low DOD and cold temperatures

After the observation of the operating conditions corresponding to the urban ("Driver 1") and suburban ("Driver 2") real EV profiles, the confidence pattern of the updated models was modified throughout the input space. The models updated after 365 and 730 operation days gained confidence to perform predictions at low DOD values, especially observable in Figure 41. (a), (b), (f) and (g) for winter temperatures, and in Figure 41. (k) and (l) for moderate temperatures. This is due to the relatively low DOD ranges implied by both "Driver 1" and "Driver 2" driving profiles.

Sensitivity

As explained in Chapter 3 and Chapter 4, the sensitivity of the capacity loss to the different stress-factors could be analysed by observing the inverse of their respective hyperparameters. Figure 42 depicts the relative relevance of the different stress-factors with respect to the capacity loss, for the baseline model and the models updated after 365 and 730 days operating. For the calendar ageing models, it could be observed in Figure 42. (a) that the perception of the relative impact of temperature and SOC with respect to the capacity loss was not substantially modified by the observation of the real EV operation profiles. Regarding the cycle ageing models, Figure 42. (b) suggests that the GP model assigned slightly more relevance to the DOD stress-factor after the observation of the real operation data. This is in contradiction with the remark done above about the lower ageing rates induced by dynamical DOD profiles, compared to the static DOD conditions applied in laboratory testing profiles. In fact, the models trained with real operation data should conclude a reduced impact of the DOD on the capacity loss, compared to the baseline model. However, it is noteworthy that, for the models updated after the real profiles' observation, the data corresponding to the static 20%, 65% and 100% DOD profiles collected from the laboratory was not removed from the training dataset. This data hinders the hyperparameter of the DOD to converge towards higher values during the optimisation of the model. Finally, Figure 42. (c) provides a zoom on the participation of the relative relevance of Middle-SOC, charging and

discharging C-rates stress-factors with respect to the capacity loss, which was insignificant compared to the temperature and DOD. It appeared that the model did not need higher implication of such stress-factors to explain the real driving ageing data. It is noteworthy that the optimisation method for the determination of the hyperparameters adopted during the whole thesis was a gradient-based maximum likelihood method. Other optimisation methods e.g. the Bayesian optimisation method could possibly lead to different interpretations of the data.

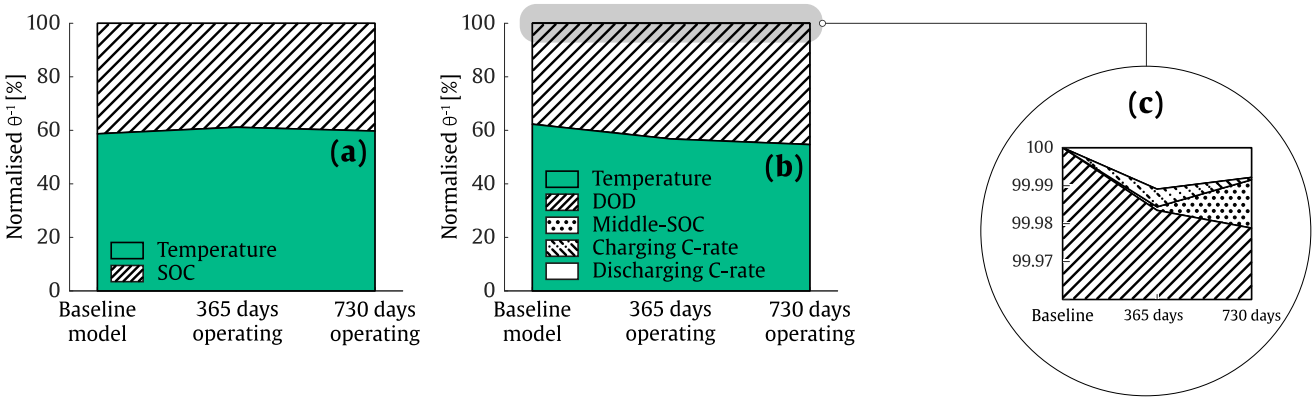

Figure 42. Evolution of the relative relevance of the different stress-factors, from the baseline model to the updated model after 730 days operating, for the (a) calendar ageing models, (b) cycle ageing models. (c) Zoom on the relative relevance of the Middle-SOC, charging and discharging C-rate stress-factors, for the cycle ageing models.

5.4. Use-case 2: power smoothing profiles

This section aims at extending the analysis carried out in the previous section to the power smoothing for renewable energy integration application profiles, which were applied to second life cells and described in Section 5.1.2.

Figure 43. (a), (b) and (c) depict predictions performed with the baseline model and the updated models, for the overall capacity loss, and the calendar and cycle capacity loss components extracted from the target processing algorithm, respectively.

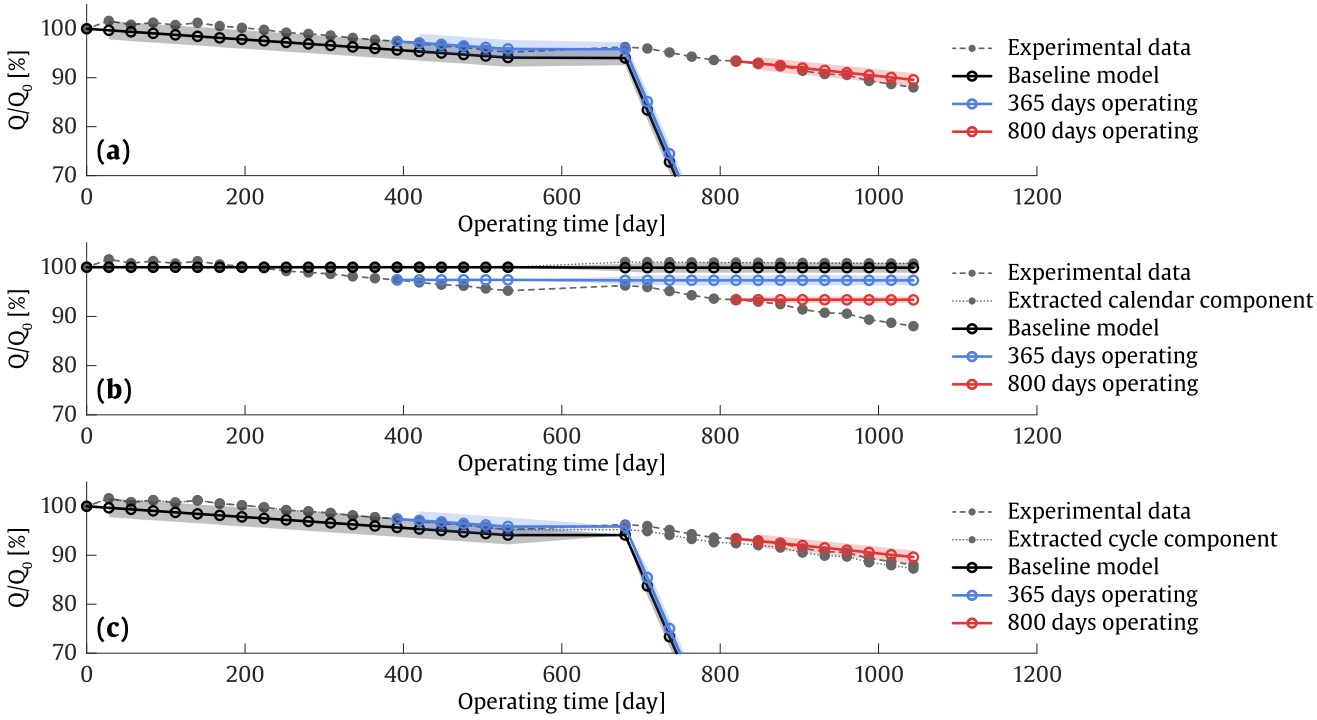

Figure 43. (a) Overall capacity experimental data for the power smoothing profile, capacity loss prediction of the baseline model (black line and grey area), the model updated after 365 days operating (blue line and area) and the model updated after 800 days operating (red line and area). (b) Overall capacity experimental data, calendar capacity curve component extracted from the target processing algorithm, calendar predictions of the baseline model (black line and grey area), the model updated after 365 days operating (blue line and area) and the model updated after 800 days operating (red line and area). (c) Overall capacity experimental data, cycle capacity curve component extracted from the target processing algorithm, cycle predictions of the baseline model (black line and grey area), the model updated after 365 days operating (blue line and area) and the model updated after 800 days operating (red line and area).

As explained in Section 5.1.2, the first life of the cell was simulated by accelerated cycling conditions applied during ca. 532 days, corresponding to a 35°C, 80% DOD, 50% Middle-SOC and C/3 and 1C charging and discharging C-rate operation. The total duration of the first life was ca. 532 days. During this period, in Figure 43. (b) the calendar component of the experimental capacity curve, as well as the prediction of the calendar ageing model were null, due to the purely cycling character of the first life profile. After the first life operation, the cells were submitted to a storage period of 120 days at 20°C and 50% SOC, representing the idle transition period of the cell after the first life operation and before the implementation of the cells in second life operation. Finally, it could be observed in Figure 43. (a) and (b) that the target processing algorithm assigned most of the capacity loss to the cycle ageing component, leaving reduced participation to the calendar component (0.3% capacity loss during the whole second life).

Reduced participation of the calendar ageing

The prediction of the baseline model during the whole first life resulted in a 0.28% $MAE_{\Delta Q}$ and 0.36% MAE_{Q} accuracy. In fact, the model already observed similar cycling conditions during the training phase, namely static 65% and 100% DOD profiles, and the accurate generalisation performances of the cycle ageing model under static cycling conditions were already demonstrated in Chapter 4. After the first life of the battery, a calendar component of the ageing appeared. However, the prediction of the model was insignificant, due to the reduced storage time processed by the input processing algorithm, and relatively suitable storage conditions experienced during this time.

Strong overestimation of the cycle ageing

During the second life of the battery, the prediction of the baseline model was clearly overestimated, which is in accordance with the observations made in Section 5.3 for the real driving profiles predictions. The DOD and Middle-SOC ranges processed from the second-life time series by the input processing algorithm were respectively between ca. 0.5% - 40% DOD and 37% - 80% Middle-SOC, with ca. 7700 Ah-throughput per month. The strong overestimation of the model may be caused again by the lower ageing rates induced by dynamical DOD profiles, compared to the static DOD conditions applied in laboratory testing profiles. The effect of such deviation is here amplified by the high cycling character of the power smoothing profiles (ca. 7700 Ah-throughput per month, compared to ca. 4000 Ah-throughput for the accelerated cycling ageing tests).

After 365 days operating, the cell was still operating within a first life, and therefore, the model updated at this stage did not show any significant improvement regarding the prediction of the second life capacity loss. However, after 800 days operating, the effect of the second life profiles on ageing could be observed for 120 days, and the overestimation of the cycle

Corrected predictions

ageing model could be corrected in the updated models' predictions. In fact, the predictions of the updated model seem to follow correctly the capacity curve corresponding to the cycle ageing component, Figure 38. (c), achieving a 0.40% $MAE_{\Delta Q}$ and 1.48% MAE_{Q} accuracy for the overall second life capacity curve.

Figure 44 depicts the evolution of the standard deviation of the cycle ageing models components, for the baseline model and the models updated after 365 and 800 operation days. As expected, it could be observed from Figure 44. (f - j) that the baseline ageing model performed confident predictions between a 25°C - 45°C temperature range, while the uncertainty increased for colder and warmer temperatures. The observation of the 80% DOD and 25°C cycling condition during the first life of the cell endorsed the confidence peak around the 25°C temperature, which was the global minimum of the standard deviation throughout the whole temperature input space (the global minima were highlighted in Figure 44. (a - e)). During the second life, the effect of the whole range between 0.5% - 40% DOD was explored at a constant temperature of 35°C. Accordingly, the global minimum of the standard deviation shifted from 25°C to 35°C for the predictions performed at reduced DOD ranges, as illustrated in Figure 44. (a - c). Furthermore, Figure 44. (k - o) illustrates the standard deviation throughout the DOD input space. It could be observed that the model gained confidence to perform prediction at low DOD ranges, particularly when cycling at 35°C, Figure 44. (q).

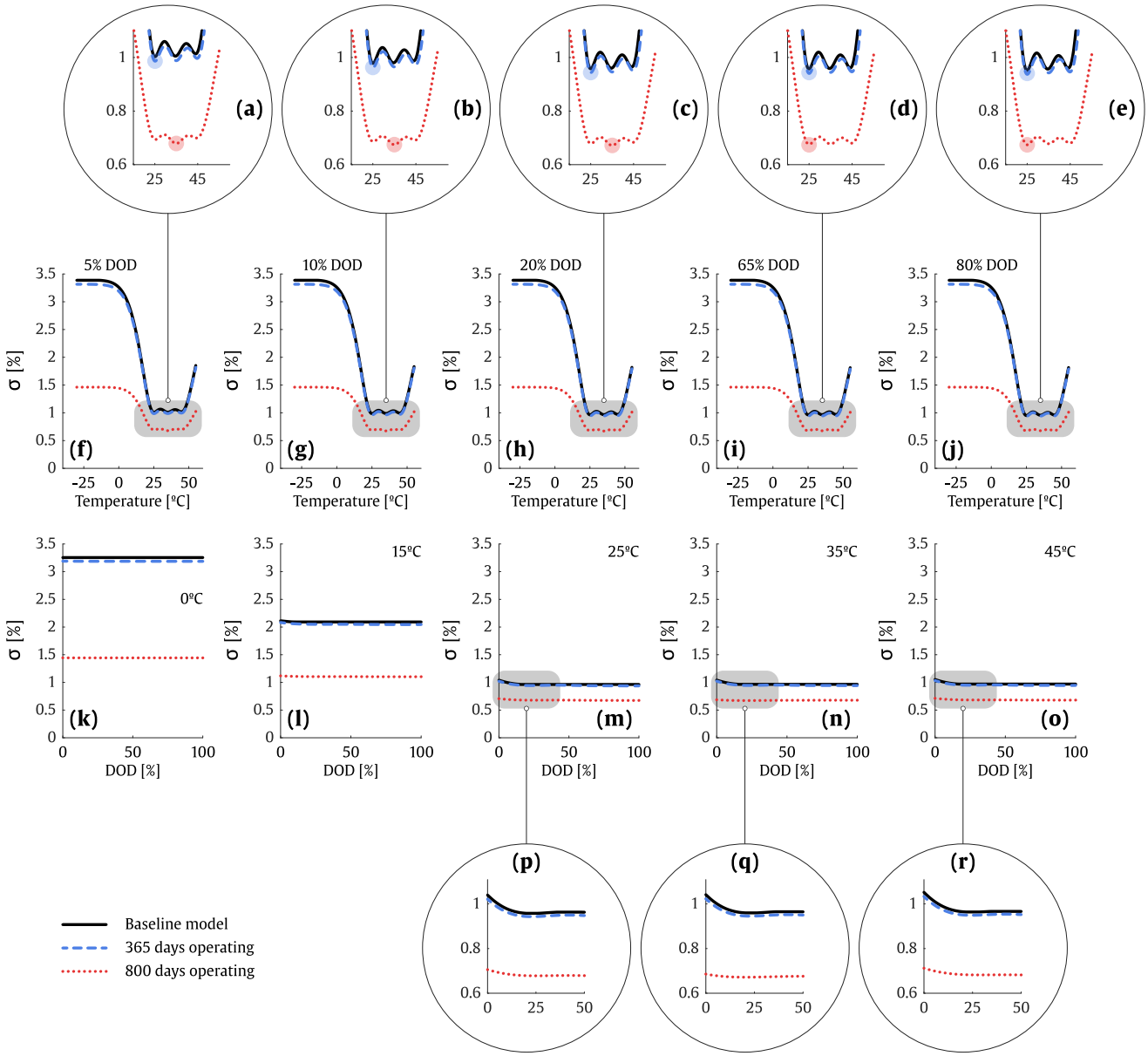

Figure 44. Evolution of the standard deviations of the GP model predictions throughout the temperature and DOD operation window of the Li-ion cell under study, for the cycle components of the baseline model and the updated models after 365 and 800 days operating. (f - j) Evolution throughout the space of the temperature, and (a - e) zoom of the evolution throughout the space of temperature, respectively at constant (a, f) 5% DOD, (b, g) 10% DOD, (c, h) 20% DOD, (d, i) 65% DOD and (e, j) 80% DOD. (k - o) Evolution throughout the DOD space, and (p - r) zoom of the evolution throughout the DOD space, respectively at constant (k) 0°C, (l) 15°C, (h, p) 25°C, (i, q) 35°C and (j, r) 45°C.

Sensitivity

Figure 45 depicts the relative relevance of the different stress-factors with respect to the capacity loss, for the baseline model and the models updated after 365 and 800 days operating. For the calendar ageing models, **Figure 45**. (a), it appeared that the relative impact of the temperature increased for the model updated after 800 operating days. As the second life operating profiles implied relatively reduced calendar ageing implication, such variation could be induced by the observation of the capacity recovery corresponding to the storage transition phase between the first and second life. According to [103], the capacity recovery could be provoked by the effect of the anode overhang, which acts here as a sink or a source of lithium depending on the SOC before and during the characterisation tests. As the cells were stored at 20°C and 50% SOC during such transition period and the resulting capacity loss was substantially different from those observed in 25°C and 50% SOC laboratory storage tests, the model interpreted higher covariance between the temperature and the capacity loss, and reduced the hyperparameter corresponding to the temperature.

Regarding the cycle ageing models, **Figure 45**. (b) suggests that the GP model assigned slightly more relevance to the DOD stress-factor after the observation of the real operation data. Again, and due to the reasons already enlightened in Section 5.3, this was in contradiction with the remark done above about the lower ageing rates induced by dynamical DOD profiles, compared to the static DOD conditions applied in laboratory testing profiles. Finally, **Figure 45**. (c) provides a zoom on the participation of the relative relevance of Middle-SOC, charging and discharging C-rates stress-factors with respect to the capacity loss, which was insignificant compared to the temperature and DOD. As for the real driving ageing data, it appeared that the model did not need higher implication of such stress-factors to explain the power smoothing ageing data.

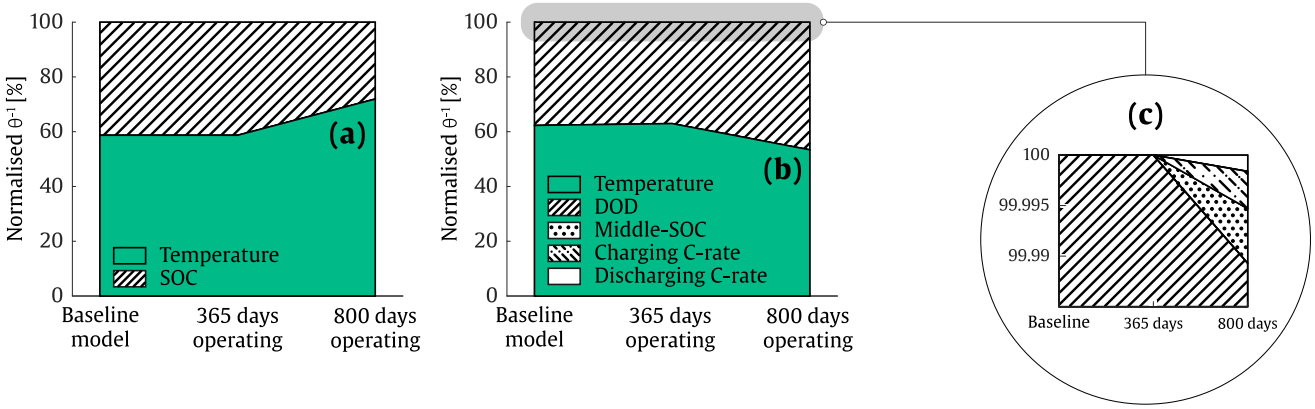

Figure 45. Evolution of the relative relevance of the different stress-factors, from the baseline model to the updated model after 800 days operating, for the (a) calendar ageing models, (b) cycle ageing models. (c) Zoom on the relative relevance of the Middle-SOC, charging and discharging C-rate stress-factors, for the cycle ageing models.

5.5. Conclusions of the chapter

In this chapter, the calendar and cycle ageing models developed and validated respectively in Chapter 3 and Chapter 4 were combined to provide a holistic view of the Li-ion battery ageing and predict the degradation under realistic operating conditions.

The initial holistic GP model was composed of the calendar and cycle ageing models trained with the minimal number of training data determined in Chapter 3 and Chapter 4, respectively. The predictions provided by such models were initially overestimated, for both EV and power smoothing applications, as depicted in Figure 38. (a) and Figure 43. (a). Such an overestimation was associated with the predictions of the cycle ageing model component, corroborating the findings already noticed in Chapter 4.

Nevertheless, the overestimation of the cycle ageing model was corrected in the updated models' predictions. In fact, the predictions of the updated models seem to follow correctly the capacity curve in e.g. Figure 38. (a) and Figure 43. (a). The improvement of the model's prediction accuracy testified about the ability of the model to learn from the real operating profiles. This was also reflected on the evolution of the confidence boundaries throughout the input space of both calendar and cycling model: the reduction of the standard deviation in e.g. Figure 40 and Figure 41, testified about the increment of the model's confidence to perform prediction throughout a broad operating window, as input spaces are progressively explored.

Finally, Figure 42. (c) and **Figure 45**. (c) provides a zoom on the participation of the relative relevance of Middle-SOC, charging and discharging C-rates stress-factors with respect to the capacity loss, which was insignificant compared to the temperature and DOD. It appeared that the model did not need higher implication of such stress-factors to explain the real driving and power smoothing ageing data.

The following and last chapter summarises the different research activities carried out in the thesis. The main conclusions are drawn, the contributions of the thesis are enumerated, and the limitations of developed models are stated, highlighting the identified further works and uncertainty areas in the study. The formulated hypotheses are evaluated, and future research paths are proposed for the development of next generation ageing models for Li-ion batteries

Chapter 6.

General conclusions, discussion & future trends

In order to round off the different research activities carried out in this thesis, the final chapter aims to summarise the main findings, highlight the principal contributions, discuss the different results and identify the limitations and further works of the study.

This chapter is structured as follows, Section 6.1 summarises the different research activities carried out in this thesis. The degree of achievement of the different objectives, as well as the hypotheses formulated in the introduction are evaluated. In Section 6.2, the main contributions of the thesis are highlighted. Section 6.3 discusses the results obtained throughout the different chapters of the thesis. Furthermore, the main limitations of the research are identified, and several further works are highlighted. Finally, Section 6.4 closes the thesis, paving the way to future generations of ageing models for Li-ion batteries.

6.1. Summary and general conclusions

The different research activities carried out in this thesis allow taking one step beyond the state of the art on the development of Li-ion battery ageing models capable of learning continuously from the in-field operation data.

From the study of the literature, the following critical gaps were identified:

i) The limited reliability of the proposed data-driven models in the context of real applications, as the effect of the stress-factors on battery ageing rate was typically not considered.

ii) The insufficient validation of most developed models.

iii) The under-representation of holistic ageing models, including both calendar and cycling use-cases.

iv) The unclear nature of the learning mechanisms of the methods identified in the literature, which hinders the suitable quantification of the required initial laboratory tests and the correct perception of learning capabilities of the models.

Furthermore, the GP framework was identified as the most suitable candidate for the further modelling works, mainly due to its nonparametric and probabilistic character. In fact, these key features provide respectively i) the assurance of a suitable learning capability and ii) a quantification of the reliability of the model predictions in terms of probability densities, necessary in the context of under-trained initial models.

A methodology was designed to develop a model which could comply with the objectives defined in the introduction. The main objective was the development of an ageing model for Li-ion batteries, capable of learning continuously from the operation data collected from the battery systems deployed in real applications. Such capability was validated illustrating the transformation of the corresponding ageing models through i) the improvement of the ageing predictions, ii) the reduction of the confidence intervals and iii) the evolution of the models' sensitivity to the different stress-factors, while new ageing data was progressively explored.

A secondary objective was to ensure the capability of the model to perform accurate predictions for a wide range of applications, implying a suitable behaviour of the model for purely calendar, continuously cycling and mixed operation of Li-ion batteries. This requirement was addressed from the combination of two ageing models, respectively used for prediction in calendar and cycling operation. Their respective accuracy was validated,

achieving overall errors of 0.53% and 1.04% MAE_Q. Furthermore, the accuracy of both models working in tandem was verified in Chapter 5, for an application involving an important calendar component (EV driving), and an application implying a highly cycling use-case (power smoothing renewable energy integration).

Another secondary objective was to quantify the minimum number of laboratory experiments required for the development of a relatively accurate initial ageing model. For the specific case of the dataset under study, it was quantified that 6 storage conditions (i.e. 3 temperatures and 2 SOC levels) were enough to obtain a calendar ageing model able to achieve a 0.53% MAE_Q average prediction errors for 30 cells operating between 25°C-45°C and 20-100% SOC storage conditions. Analogously, 9 cycling conditions (i.e. 3 temperatures and 3 DOD levels) were enough to achieve a cycle ageing model reaching 1.04% MAE_Q average prediction errors for 122 cells operating between 25°C-45°C, 20%-100% DOD, 20%-80% middle-SOC, C/3-2C charging C-rates and C/3-2C discharging C-rates.

Hypotheses re-evaluation

The developed methodology further allowed the evaluation of the formulated hypotheses, reported below for convenience:

> **H0:** the relations between the operation and the underlying ageing of Li-ion batteries could be described based only on in-field measurable variables.

In-field measurable variables

The hypothesis H0 was partially verified: in-field measurable temperature, current and voltage time series were used to extract several stress-factors influencing on the capacity loss rate of Li-ion batteries. The ageing models based on such stress-factors seem to be able to predict the ageing of Li-ion batteries with a significant accuracy while they are working in the Phase 2 of their lifetime (Figure 13 and Figure 21).

> **H1:** The development of separated calendar and cycle ageing models could be a valid approach to predict accurately the overall degradation of Li-ion batteries.

Decoupling calendar and cycling

The hypothesis H1 was verified in Chapter 5, the combination method was successful for a calendar-dominated use-case (EV driving), as well as for a cyclic-dominated use-case (power smoothing renewable energy integration).

> **H2:** Ageing models trained with static ageing laboratory tests may be able to perform accurate predictions at dynamic and realistic operating profiles different from those observed in the laboratory.

About training with static profiles

The hypothesis H2 was partially denied. In fact, the calendar ageing model trained with data collected from static ageing laboratory tests seemed to provide accurate predictions for dynamic operating conditions (Chapter 3). Nevertheless, the cycle ageing model achieved worse accuracy in dynamic operating conditions (Chapter 4). Possible reasons of such discrepancy are discussed in Section 6.3.

> **H3:** Converting the continuous operation data measurable in-field (see Figure 1. (c)) into equivalent dynamic profiles of the different stress-factors (see Figure 1. (b)), could be a valid approach to:
>
> > **H3.1:** perform accurate predictions at real operating conditions.
> >
> > **H3.2:** learn about the influence of new operating conditions on battery degradation and update an ageing model based on laboratory data while still improving its prediction performances.

In-field data processing

Both hypotheses H3.1 and H3.2 were verified. For both EV driving and power smoothing renewable energy integration applications, "equivalent stress-factors profiles" were generated from in-field measurable temperature, current and voltage time series. Such profiles were inputted to the models in order to perform predictions and update the models using at real operating conditions, achieving accurate prediction results. However, it is noteworthy that the in-field time series processing algorithm could have a strong influence on underlying prediction accuracy of the Li-ion ageing model. This is further discussed in Section 6.3.

> **H4:** The development of ageing models able to learn from in-field battery operation data could allow mitigating the needs for exhaustive laboratory testing.

Minimise laboratory tests

In fact, the ability of the developed models to learn progressively from upcoming data was demonstrated. This implies that the learning process could be split into two different phases: a first learning phase from laboratory data before system sizing and deployment, and a second learning phase from data collected in-field. Such splitting of the learning process could allow mitigating the need for exhaustive laboratory testing, by shifting the learning of the influence of some stress-factors combinations to the second learning phase. Accordingly, the main task for the definition of the ageing tests is to estimate which conditions should be learnt before battery system sizing, and which ones could be learnt once the system is deployed.

H5: The nonparametric frameworks are able to learn about the influence of new values of the different stress-factors on battery degradation, including new data in the training set.

Nonparametric frameworks

This capability was reflected by i) the improvement of the predictions accuracy, ii) the reduction of the confidence boundaries and iii) the evolution the models' sensitivity to the different stress-factors. The nature of the nonparametric learning process was especially well visualised by depicting the evolution of the standard deviation of the model's predictions throughout the whole range of the different stress-factors (e.g. Figure 40). The values of the stress-factors which were previously learnt showed a reduced standard deviation. Oppositely, the unexplored areas were characterised by increased values of the standard deviation, traducing a high uncertainty and reduced reliability on the models' predictions for such operating conditions. The progressive observation of the ageing in unexplored stress-factors areas induced the reduction of the standard deviation, testifying about the increase of the reliability on models' predictions. In such a way, the complete picture of the mapping between the different stress-factor combinations and the underlying ageing of Li-ion batteries could be progressively drawn, while new data is integrated in the training dataset.

6.2. Contributions

The main contributions of the research activities carried out throughout the development of this thesis are listed as follows:

- A thorough and critical state of the art was presented on the different methods used in the literature to periodically update Li-ion battery ageing models.
- The ageing of Li-ion batteries was considered from a general prospect, rather than from the scope of a specific application. In fact, the developed models are oriented to broad ranges of operating conditions, and usable for a large diversity of Li-ion battery application.
- A general picture describing the nature of the model updating process was provided, by the detailed illustration of the progressive learning of the developed ageing models, in terms of accuracy improvement, reduction of the confidence boundaries and evolution of the model sensitivity to stress-factors. Such contribution could help to i) optimise the definition of the laboratory ageing test matrix, from the perspective of the test minimisation and ii) perceive the

room for improvement left to the model from the continuous learning of the in-field data.

- New compositional covariance functions were introduced, tailored for use in a Li-ion battery ageing prediction application.
- A sensitivity analysis of the capacity loss with respect to the different stress-factors was studied, from the point of view of the developed model. This could provide some intuitions about e.g. which stress-factors are the most impactful on the capacity loss, producing useful insights for the design of energy management strategies.
- A specific approach was presented to preprocess the real operation data, in order to feed separately the calendar and cycle ageing models and combine their respective predictions.

6.3. General discussion, limitations of the study and further works

Minimal required amount of laboratory tests

One of the objectives of the thesis was the evaluation of the number of experimental laboratory ageing tests necessary for the development of an ageing model able to provide accurate ageing predictions. This issue was addressed in Chapter 3 and Chapter 4 respectively, for the development of a calendar and cycle ageing models. It was quantified that 6 storage conditions and 9 cycling conditions were enough to obtain a calendar and a cycling ageing model able to achieve acceptable prediction accuracy throughout the whole operating range of the battery recommended by the manufacturer.

However, such a quantification could not be generalisable either to the different Li-ion chemistries or to a wide range of applications, and should rather be contemplated as general guideline subject to the following limitations:

i) The cycle ageing model trained with the mentioned ageing conditions would be insensitive to the middle-SOC, charging and discharging C-rate variations, at least before the model could learn the influence of such ageing factors. Although this does not seem to matter regarding the middle-SOC stress-factor (see sensitivity analysis Chapter 4), it could be problematic for the applications involving high charging and discharging C-rates. In such cases, supplementary laboratory tests could be necessary at several C-rate values. This is also the case for the applications involving cell cycling at cold temperatures, as the minimal temperature involved in the dataset under study was 25°C.

ii) Depending on the repeatability of the cells, it could be necessary to carry out more than one experimental test for each ageing condition, to ensure the reproducibility of the generated data. Furthermore, some additional test before deployment would be advisable for model validation purposes but these could be avoided depending on the availability of in-field data, which could be used for such validation purposes.

Summarising, the design of an experimental ageing test matrix is subject to a trade-off between the desired accuracy of the initial ageing model and the corresponding development cost. Further, the key questions to consider during the design phase are i) which operating mode is predominant in the target application (i.e. calendar or cycling), and to which operating conditions the cells will be submitted, and ii) which conditions should be learnt by the model prior to system deployment, and which ones could be learnt a posteriori.

Furthermore, the minimisation of the laboratory testing procedure should also be assessed in terms of testing duration. Nevertheless, such an evaluation would difficultly be categorical, as the required testing duration is strongly constrained by the occurrence of the different ageing phases in the generated capacity curves (see Figure 13 and Figure 21).

Uncertainty propagation: throughout input space

In this thesis, the uncertainty of the GP predictions was studied from the perspective of its evolution throughout a partially explored space of the different stress-factors. The model predictions showed large confidence intervals when the corresponding operating conditions were unknown for the model. Conversantly, the model predicted reduced confidence intervals for operating conditions already observed in the training dataset. The progressive observation of different operating conditions led to the increment of the model's confidence to perform prediction throughout a broad operating window of the battery system. However, both calendar and cycle GP models turned out to be slightly over-confident. The results obtained in Chapter 3 and Chapter 4 suggests that the overconfidence of the model was induced by the error accumulation of the iterative prediction process. Therefore, further investigations would be required in order to study the propagation of model's uncertainty throughout the long-term ageing prediction [161].

Uncertainty propagation: long-term prediction

Uncertainty propagation: inherited from inputs

Furthermore, a more complete view of the model's reliability should also include the analysis of the uncertainty propagated from the inputs of the models, as illustrated in Figure 46.

In order to update periodically the calendar and cycling ageing models, the battery operation data timeseries extracted in-field must be processed to obtain the training data composed of the equivalent input vectors and associated capacity loss. The different algorithms used during this procedure (e.g. SOC and SOH estimators), as well as the battery system sensors they rely on, involve an associated estimation error. Such errors contribute to increase the uncertainty of the system. Therefore, as illustrated in Figure 46, the propagation of the uncertainty from the system measurement sensors to the ageing models' predictions would be required in order to provide a more complete view of predictions' reliability.

Uncertainty propagation

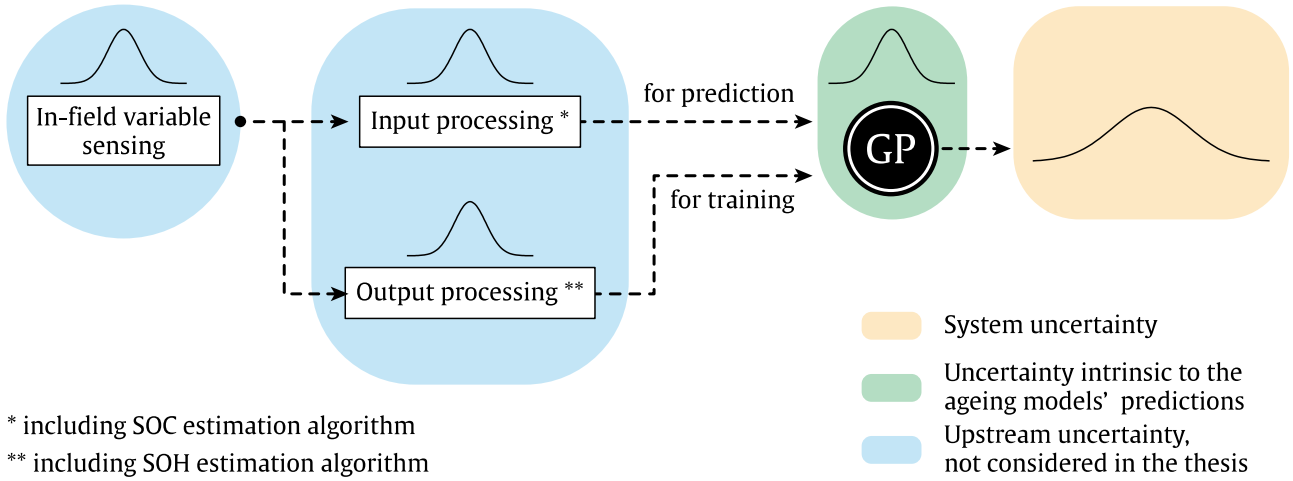

Figure 46. Uncertainty propagated from the inputs of the system, which could reduce the reliability of the ageing models predictions.

Extended sensitivity analysis

In Chapter 3 and Chapter 4, the evolution of the hyperparameters' reciprocal was analysed, in order to illustrate how the model would actually be learning about the sensitivity of the capacity loss to each individual stress-factor. The sensitivity analysis could be extended by involving covariance components corresponding to the interactions between the different stress-factors, in order to have a feedback about which combinations of stress-factors levels are most critical according to the GP model. Such analysis would be difficult to carry out with laboratory data, mainly due to the large amount of ageing data it would require. However, the incorporation of the real-world data collected from the deployed battery-packs could make such analysis possible. This could provide insightful inputs for the development of effective energy management strategies.

Dynamic DOD profiles and overestimation

In Chapter 4 and Chapter 5, it was observed that the cycle ageing models trained with data obtained from static ageing profiles tended to overestimate the degradation at dynamic operating conditions. Such a behaviour was linked in [97] to the dynamic character of the DOD stress-factor's profiles, which may induce lower ageing rates compared to the static DOD ageing profiles. This observation increases the interest of ageing models able to learn from the dynamic profiles observed after deployment, correcting this way the initial model trained with laboratory static ageing experiments. Anyway, this observation should be verified in further work, and the study should be extended involving more cells cycled at dynamic conditions and realistic conditions. The latter point would also allow consolidating the validation of the input and output processing algorithms, described in Chapter 5.

Cycle induced calendar ageing

In the pre-processing stage, it was assumed that the initial capacity rise identified in several cells is not provoked by any ageing mechanism and does not have any influence on the further ageing trend of those cells. These assumptions should be verified in further work. Besides, cycle-induced calendar ageing is another important source of capacity degradation [158]. Once the cells are severely degraded due to cycling, they may suffer a stressed capacity degradation even under moderate storage conditions. In order to undertake such occurrence, the calendar ageing model should be informed about the degradation suffered by the cell because of cycling. Accordingly, the integration of both calendar and cycle ageing models, within the context of defining a holistic view of lithium-ion degradation modelling is a challenging research task, proposed as further research line.

Computational cost

Furthermore, the deployment of the ageing models developed in this study deserves a deeper discussion from the perspective of computational complexity. In fact, the logging of the current, voltage and temperature time series, as well as the extraction of the corresponding inputs variables requires memory and computation considerations. Furthermore, the inherent time and memory complexity of the GP is $\mathcal{O}(n^3)$ and $\mathcal{O}(n^2)$, and the required computations rapidly become prohibitive within the context of increasing training datasets. Within this context, two different approaches could be contemplated for the deployment of ageing models in real applications, considering the implementation of the models i) within the local hardware of each battery system, or ii) in an external data server (cloud server), connected to a fleet of battery systems (Figure 47).

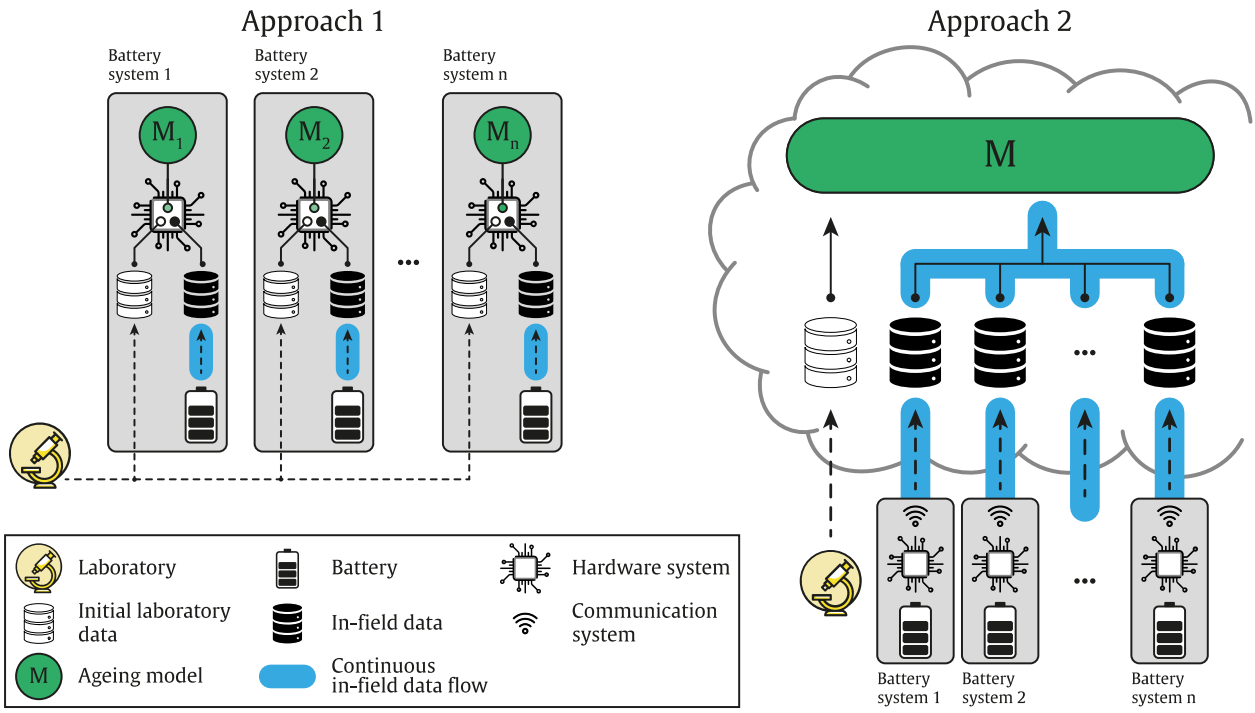

Figure 47. Two different approaches for the deployment of ageing models in real applications. The first approach consists on the implementation of the ageing model in the local hardware device of each battery system. The second approach contemplates the communication and storage of the battery operation data to a data server in the cloud, in which the ageing model is implemented.

Local approach

The first approach presents several issues related to the computational complexity of the ageing model. In fact, the above-mentioned $\mathcal{O}(n^3)$ and $\mathcal{O}(n^2)$ time and memory complexity of the GP questions its ability to be implemented within a device with limited computation resources, in the context of increasing training datasets. This implies that i) approximation methods of the GP algorithm [110] may be required once the training dataset becomes critically large, and ii) the model must be implemented in a hardware system presenting minimal requirements in terms of computation power. In case the model would be implemented in a BMS board, an oversizing of the system could be necessary, as well as an adequate scheduling with the other tasks performed by the BMS (e.g. measurements, safety-related tasks, SOC and SOH estimations, communications, etc.). However, the first approach presents the advantage of avoiding the cost corresponding to the implementation of the data server infrastructure and communication systems with the local devices.

Cloud-based approach

The second approach provides many advantages with respect to the first one. First, it allows a single ageing model to be fed in parallel with the data obtained from several battery systems, empowering it to learn

simultaneously about the effect of a wide range of operating conditions. In this way, the learning process of the GP could be significantly accelerated, and the resulting ageing model could provide reliable predictions on a broader range of the operating conditions, compared to the different models evolving independently in the context of the first approach. Furthermore, the observation of the data collected from several battery systems allows assessing the quality and variability of the obtained data, from a statistical point of view[28]. The main drawback of such an approach is the implementation cost of the data server and the communication systems. Moreover, the issue of the computational complexity of the GP model would be linked to the computation power of the server, which would determine the necessity to use approximation methods oriented to reduce the time and memory complexity of the GP models.

Resistance increase

Finally, although the degradation of Li-ion batteries is mainly expressed in terms of both capacity loss and resistance increase, the research activities in this thesis only focused on the data corresponding to the capacity loss. However, the methodology proposed in this chapter could easily be extended to the development of ageing models oriented to the prediction of resistance increase, as the periodical characterisation tests could also include resistance determination procedures.

6.4. Closure: towards future generations of ageing models

The research activities carried out in this thesis aimed to resolve some of the issues typically encountered during the development of Li-ion ageing models, i.e. i) to reduce the need for exhaustive experimental ageing tests from laboratory, ii) ensure the validity of the model to predict and learn under realistic operating profiles. This was achieved by the development of ageing models capable of evolving and learning progressively from the data collected directly from deployed battery systems.

Nevertheless, the described models are still dependent of some laboratory tests which need to be carried out before system deployment, in order to obtain a relatively accurate ageing model for system sizing. This dependency is partially produced by the early maturity stage of the data collection telemetry technologies applied to the Li-ion battery system deployed in

[28] From a long-term perspective, this second approach would also allow to produce a database traducing the behaviour of the deployed systems in real applications. This information could be exploited for further objectives, e.g. to acquire a better knowledge about the deployed systems, carry out further modelling works, extract new insights for the development of new business models, etc.

Removing the need for laboratory tests?

industry. Consequently, no long-term ageing data is currently available from most battery systems deployed to date. However, the increased interest from industry in the introduction of new data collection systems implies the forthcoming availability of a significant amount of real-world battery operation data, which would be available for use as initial dataset for the development of future Li-ion ageing models. The use of real operation data for initial ageing model development could e.g. reduce the prediction errors induced by the discrepancies observed between the ageing at static operating conditions and dynamic or realistic operation (see Sections 4.5 and 5.4).

A remaining problem would be the sequential timing relation between cell selection, system sizing, system deployment and in-field ageing data gathering, which make impossible the obtention of ageing model before system deployment. This issue could possibly be addressed by the implementation of transfer learning methods [162], which would consist on transferring the patterns between operating conditions and ageing learnt from data collected from previously deployed Li-ion battery system to new battery technologies.

Bridging the gap: physics-based and data-driven ageing models

Further advances in the field of Machine Learning discipline as well as in new technologies of Li-ion cell development could trigger promising synergies, allowing new possibilities in cell diagnosis and ageing prediction. One of them could be the effective prediction of the sudden capacity drop reported in Chapter 3 and Chapter 4. In fact, a recent research trend is to incorporate new sensing technologies directly inside Li-ion cells [163]. These technologies would provide new in-field measurable time series data (internal pressure, voltage at electrode level, electrode concentration, etc), completing the currently available external current, voltage and temperature measurements. Concurrently, recent advances in Machine Learning research could possibly reveal new stress-factors or powerful predictive features.

Reader, if you are still here, rejoice!

Such perspectives promise exciting times for further research!

References

[1] G.A. Jones, K.J. Warner, The 21st century population-energy-climate nexus, Energy Policy. 93 (2016) 206–212. doi:10.1016/j.enpol.2016.02.044.

[2] C. Hickey, T.N. Rieder, J. Earl, Population Engineering and the Fight against Climate Change, Soc. Theory Pract. 42 (2016) 845–870. doi:10.5840/soctheorpract201642430.

[3] F. Creutzig, J. Roy, W.F. Lamb, I.M.L. Azevedo, W. Bruine de Bruin, H. Dalkmann, O.Y. Edelenbosch, F.W. Geels, A. Grubler, C. Hepburn, E.G. Hertwich, R. Khosla, L. Mattauch, J.C. Minx, A. Ramakrishnan, N.D. Rao, J.K. Steinberger, M. Tavoni, D. Ürge-Vorsatz, E.U. Weber, Towards demand-side solutions for mitigating climate change, Nat. Clim. Chang. 8 (2018) 260–263. doi:10.1038/s41558-018-0121-1.

[4] K. McAfee, Green economy and carbon markets for conservation and development: a critical view, Int. Environ. Agreements Polit. Law Econ. 16 (2016) 333–353. doi:10.1007/s10784-015-9295-4.

[5] E. Musk, Making Life Multi-Planetary, New Sp. 6 (2018) 2–11. doi:10.1089/space.2018.29013.emu.

[6] J. Deutch, Decoupling Economic Growth and Carbon Emissions, Joule. 1 (2017) 3–5. doi:10.1016/j.joule.2017.08.011.

[7] C. Shuai, X. Chen, Y. Wu, Y. Zhang, Y. Tan, A three-step strategy for decoupling economic growth from carbon emission: Empirical evidences from 133 countries, Sci. Total Environ. 646 (2019) 524–543. doi:10.1016/j.scitotenv.2018.07.045.

[8] W. Feng, B. Gu, Y. Cai, The End of China's One-Child Policy, Stud. Fam. Plann. 47 (2016) 83–86. doi:10.1111/j.1728-4465.2016.00052.x.

[9] S. Sorrell, Reducing energy demand: A review of issues, challenges and approaches, Renew. Sustain. Energy Rev. 47 (2015) 74–82. doi:10.1016/j.rser.2015.03.002.

[10] I. Levchenko, S. Xu, S. Mazouffre, M. Keidar, K. Bazaka, Mars Colonization: Beyond Getting There, Glob. Challenges. 3 (2019) 1800062. doi:10.1002/gch2.201800062.

[11] H. Ritchie, M. Roser, CO_2 and Greenhouse Gas Emissions, Publ. Online OurWorldInData.Org. (2020). https://ourworldindata.org/co2-and-other-greenhouse-gas-emissions.

[12] J. Rugolo, M.J. Aziz, Electricity storage for intermittent renewable sources, Energy Environ. Sci. 5 (2012) 7151. doi:10.1039/c2ee02542f.

[13] S. Weitemeyer, D. Kleinhans, T. Vogt, C. Agert, Integration of Renewable Energy Sources in future power systems: The role of storage, Renew. Energy. 75 (2015) 14–20. doi:10.1016/j.renene.2014.09.028.

[14] M.A. Hannan, M.M. Hoque, A. Mohamed, A. Ayob, Review of energy storage systems for electric vehicle applications: Issues and challenges, Renew. Sustain. Energy Rev. 69 (2017) 771–789. doi:10.1016/j.rser.2016.11.171.

[15] G. Zubi, R. Dufo-López, M. Carvalho, G. Pasaoglu, The lithium-ion battery: State of the art and future perspectives, Renew. Sustain. Energy Rev. 89 (2018) 292–308. doi:10.1016/j.rser.2018.03.002.

[16] S. Dhundhara, Y.P. Verma, A. Williams, Techno-economic analysis of the lithium-ion and lead-acid battery in microgrid systems, Energy Convers. Manag. 177 (2018) 122–142. doi:10.1016/j.enconman.2018.09.030.

[17] N. Nitta, F. Wu, J.T. Lee, G. Yushin, Li-ion battery materials: present and future, Mater. Today. 18 (2015) 252–264. doi:10.1016/j.mattod.2014.10.040.

[18] R. Schmuch, R. Wagner, G. Hörpel, T. Placke, M. Winter, Performance and cost of materials for lithium-based rechargeable automotive batteries, Nat. Energy. 3 (2018) 267–278. doi:10.1038/s41560-018-0107-2.

[19] S.J.R. Prabakar, K.-S. Sohn, M. Pyo, Enhancement in High-Rate Performance of Graphite Anodes via Interface Modification Utilizing Ca(BF 4) 2 as an Electrolyte Additive in Lithium Ion Batteries, J. Electrochem. Soc. 166 (2019) A591–A597. doi:10.1149/2.0651904jes.

[20] K. Liu, Y. Liu, D. Lin, A. Pei, Y. Cui, Materials for lithium-ion battery safety, Sci. Adv. 4 (2018) eaas9820. doi:10.1126/sciadv.aas9820.

[21] T.-F. Yi, Y.-M. Li, S.-Y. Yang, Y.-R. Zhu, Y. Xie, Improved Cycling Stability and Fast Charge–Discharge Performance of Cobalt-Free Lithium-Rich Oxides by Magnesium-Doping, ACS Appl. Mater. Interfaces. 8 (2016) 32349–32359. doi:10.1021/acsami.6b11724.

[22] A. Saez-De-Ibarra, A. Milo, H. Gaztanaga, V. Debusschere, S. Bacha, Co-Optimization of Storage System Sizing and Control Strategy for Intelligent Photovoltaic Power Plants Market Integration, IEEE Trans. Sustain. Energy. 7 (2016) 1749–1761. doi:10.1109/TSTE.2016.2555704.

[23] E. Martinez-Laserna, E. Sarasketa-Zabala, I. Villarreal Sarria, D.-I. Stroe, M. Swierczynski, A. Warnecke, J.-M. Timmermans, S. Goutam, N. Omar, P. Rodriguez, Technical Viability of Battery Second Life: A Study From the Ageing Perspective, IEEE Trans. Ind. Appl. 54 (2018) 2703–2713. doi:10.1109/TIA.2018.2801262.

[24] V.I. Herrera, A. Milo, H. Gaztanaga, J. Ramos, H. Camblong, Adaptive and Non-Adaptive Strategies for Optimal Energy Management and Sizing of a Dual Storage System in a Hybrid Electric Bus, IEEE Trans. Intell. Transp. Syst. (2018) 1–13. doi:10.1109/TITS.2018.2874092.

[25] J.A. Lopez-Ibarra, M. Lucu, N. Goitia-Zabaleta, H. Gaztanaga, V.I. Herrera, H. Camblong, Battery Aging Conscious Intelligent Energy Management Strategy for Hybrid Electric Buses, in: 2019 Fourteenth Int. Conf. Ecol. Veh. Renew. Energies, IEEE, 2019: pp. 1–7. doi:10.1109/EVER.2019.8813567.

[26] Q. Badey, G. Cherouvrier, Y. Reynier, J. Duffault, S. Franger, Ageing forecast of lithium-ion batteries for electric and hybrid vehicles, Curr. Top. Electrochem. 16 (2011).

[27] J.M. Reniers, G. Mulder, D.A. Howey, Review and Performance Comparison of Mechanical-Chemical Degradation Models for Lithium-Ion Batteries, J. Electrochem. Soc. 166 (2019) A3189–A3200. doi:10.1149/2.0281914jes.

[28] T.R. Ashwin, A. Barai, K. Uddin, L. Somerville, A. McGordon, J. Marco, Prediction of battery storage ageing and solid electrolyte interphase property estimation using an electrochemical model, J. Power Sources. 385 (2018) 141–147. doi:10.1016/j.jpowsour.2018.03.010.

[29] E. Sarasketa-Zabala, E. Martinez-Laserna, M. Berecibar, I. Gandiaga, L.M. Rodriguez-Martinez, I. Villarreal, Realistic lifetime prediction approach for Li-ion batteries, Appl. Energy. 162 (2016) 839–852. doi:10.1016/j.apenergy.2015.10.115.

[30] A. Eddahech, O. Briat, E. Woirgard, J.M. Vinassa, Remaining useful life prediction of lithium batteries

in calendar ageing for automotive applications, Microelectron. Reliab. 52 (2012) 2438–2442. doi:10.1016/j.microrel.2012.06.085.

[31] M. Ecker, J.B. Gerschler, J. Vogel, S. Käbitz, F. Hust, P. Dechent, D.U. Sauer, Development of a lifetime prediction model for lithium-ion batteries based on extended accelerated aging test data, J. Power Sources. 215 (2012) 248–257. doi:10.1016/j.jpowsour.2012.05.012.

[32] M. Ecker, N. Nieto, S. Käbitz, J. Schmalstieg, H. Blanke, A. Warnecke, D.U. Sauer, Calendar and cycle life study of Li(NiMnCo)O2-based 18650 lithium-ion batteries, J. Power Sources. 248 (2014) 839–851. doi:10.1016/j.jpowsour.2013.09.143.

[33] J. Schmalstieg, S. Käbitz, M. Ecker, D.U. Sauer, A holistic aging model for Li(NiMnCo)O2 based 18650 lithium-ion batteries, J. Power Sources. 257 (2014) 325–334. doi:10.1016/j.jpowsour.2014.02.012.

[34] E. Sarasketa-Zabala, I. Gandiaga, E. Martinez-Laserna, L.M. Rodriguez-Martinez, I. Villarreal, Cycle ageing analysis of a LiFePO4/graphite cell with dynamic model validations: Towards realistic lifetime predictions, J. Power Sources. 275 (2015) 573–587. doi:10.1016/j.jpowsour.2014.10.153.

[35] M. Dubarry, G. Baure, A. Devie, Durability and Reliability of EV Batteries under Electric Utility Grid Operations: Path Dependence of Battery Degradation, J. Electrochem. Soc. 165 (2018) A773–A783. doi:10.1149/2.0421805jes.

[36] T. Akyazi, A. Goti, A. Oyarbide, E. Alberdi, F. Bayon, A Guide for the Food Industry to Meet the Future Skills Requirements Emerging with Industry 4.0, Foods. 9 (2020) 492. doi:10.3390/foods9040492.

[37] T.A. Branca, B. Fornai, V. Colla, M.M. Murri, E. Streppa, A.J. Schröder, The Challenge of Digitalization in the Steel Sector, Metals (Basel). 10 (2020) 288. doi:10.3390/met10020288.

[38] A.N. Alekseev, S. V. Lobova, A. V. Bogoviz, Y. V. Ragulina, DIGITALIZATION OF THE RUSSIAN ENERGY SECTOR: STATE-OF-THE-ART AND POTENTIAL FOR FUTURE RESEARCH, Int. J. Energy Econ. Policy. 9 (2019) 274–280. doi:10.32479/ijeep.7673.

[39] P.-L. Sanchez-Gonzalez, D. Díaz-Gutiérrez, T. Leo, L. Núñez-Rivas, Toward Digitalization of Maritime Transport?, Sensors. 19 (2019) 926. doi:10.3390/s19040926.

[40] S. Theodoridis, Machine Learning: a Bayesian and Optimization Perspective, Elsevier Ltd., 2015.

[41] S. Shalev-Shwartz, S. Ben-David, Understanding Machine Learning, Cambridge University Press, Cambridge, 2014. doi:10.1017/CBO9781107298019.

[42] J. Zhou, D. Liu, Y. Peng, X. Peng, Dynamic battery remaining useful life estimation: An on-line data-driven approach, in: IEEE Int. Instrum. Meas. Technol. Conf. Proc., Graz, Austria, 2012: pp. 2196–2199. doi:10.1109/I2MTC.2012.6229280.

[43] A. Nuhic, J. Bergdolt, B. Spier, M. Buchholz, K. Dietmayer, Battery Health Monitoring and Degradation Prognosis in Fleet Management Systems, in: EVS30 Symp., Stuttgart, Germany, 2017.

[44] B. Long, W. Xian, L. Jiang, Z. Liu, An improved autoregressive model by particle swarm optimization for prognostics of lithium-ion batteries, Microelectron. Reliab. 53 (2013) 821–831. doi:10.1016/j.microrel.2013.01.006.

[45] D. Liu, Y. Luo, Y. Peng, X. Peng, M. Pecht, Lithium-ion Battery Remaining Useful Life Estimation Based on Nonlinear AR Model Combined with Degradation Feature, in: Annu. Conf. Progn. Heal. Manag.

Soc., Minneapolis, Minnesota, USA, 2012.

[46] Y. Zhou, M. Huang, Lithium-ion batteries remaining useful life prediction based on a mixture of empirical mode decomposition and ARIMA model, Microelectron. Reliab. 65 (2016) 265–273. doi:10.1016/j.microrel.2016.07.151.

[47] A. Nuhic, T. Terzimehic, T. Soczka-Guth, M. Buchholz, K. Dietmayer, Health diagnosis and remaining useful life prognostics of lithium-ion batteries using data-driven methods, J. Power Sources. 239 (2013) 680–688. doi:10.1016/j.jpowsour.2012.11.146.

[48] M.A. Patil, P. Tagade, K.S. Hariharan, S.M. Kolake, T. Song, T. Yeo, S. Doo, A novel multistage Support Vector Machine based approach for Li-ion battery remaining useful life estimation, Appl. Energy. 159 (2015) 285–297. doi:10.1016/j.apenergy.2015.08.119.

[49] M.A. Patil, US2016259014A1 - METHOD AND APPARATUS FOR AUTOMATICALLY ESTIMATING REMAINING USEFUL LIFE (RUL) OF BATTERY IN REAL TIME, 2016.

[50] D. Liu, J. Pang, J. Zhou, Y. Peng, M. Pecht, Prognostics for state of health estimation of lithium-ion batteries based on combination Gaussian process functional regression, Microelectron. Reliab. 53 (2013) 832–839. doi:10.1016/j.microrel.2013.03.010.

[51] S. Yin, J. Pang, D. Liu, Y. Peng, Remaining Useful Life Prognostics for Lithium-ion Battery Based on Gaussian Processing Regression Combined with the Empirical Model, in: Proc. Annu. Conf. Progn. Heal. Manag. Soc., New Orleans, Louisiana, USA, 2013.

[52] Y. He, J.-N. Shen, J.-F. Shen, Z.-F. Ma, State of health estimation of lithium-ion batteries: A multiscale Gaussian process regression modeling approach, AIChE J. 61 (2015) 1589–1600. doi:10.1002/aic.14760.

[53] R.R. Richardson, M.A. Osborne, D.A. Howey, Gaussian process regression for forecasting battery state of health, J. Power Sources. 357 (2017) 209–219. doi:10.1016/j.jpowsour.2017.05.004.

[54] D. Liu, J. Zhou, D. Pan, Y. Peng, X. Peng, Lithium-ion battery remaining useful life estimation with an optimized Relevance Vector Machine algorithm with incremental learning, Measurement. 63 (2015) 143–151. doi:10.1016/j.measurement.2014.11.031.

[55] Z. Zhang, M. Huang, Y. Chen, S. Zhu, Prediction of Lithium-ion Battery's Remaining Useful Life Based on Relevance Vector Machine, SAE Int. J. Altern. Powertrains. 5 (2016) 2015-01–9147. doi:10.4271/2015-01-9147.

[56] D. Wang, Q. Miao, M. Pecht, Prognostics of lithium-ion batteries based on relevance vectors and a conditional three-parameter capacity degradation model, J. Power Sources. 239 (2013) 253–264. doi:10.1016/j.jpowsour.2013.03.129.

[57] W.-A. Yang, M. Xiao, W. Zhou, Y. Guo, W. Liao, A Hybrid Prognostic Approach for Remaining Useful Life Prediction of Lithium-Ion Batteries, Shock Vib. 2016 (2016) 1–15. doi:10.1155/2016/3838765.

[58] C. Zhang, Y. He, L. Yuan, S. Xiang, J. Wang, Prognostics of Lithium-Ion Batteries Based on Wavelet Denoising and DE-RVM, Comput. Intell. Neurosci. 2015 (2015) 1–8. doi:10.1155/2015/918305.

[59] C. Zhang, Y. He, L. Yuan, S. Xiang, Capacity Prognostics of Lithium-Ion Batteries using EMD Denoising and Multiple Kernel RVM, IEEE Access. 5 (2017) 12061–12070. doi:10.1109/ACCESS.2017.2716353.

[60] Y. Zhou, M. Huang, Y. Chen, Y. Tao, A novel health indicator for on-line lithium-ion batteries remaining useful life prediction, J. Power Sources. 321 (2016) 1–10.

doi:10.1016/j.jpowsour.2016.04.119.

[61] A. Widodo, M.-C. Shim, W. Caesarendra, B.-S. Yang, Intelligent prognostics for battery health monitoring based on sample entropy, Expert Syst. Appl. 38 (2011) 11763–11769. doi:10.1016/j.eswa.2011.03.063.

[62] J. Wu, C. Zhang, Z. Chen, An online method for lithium-ion battery remaining useful life estimation using importance sampling and neural networks, Appl. Energy. 173 (2016) 134–140. doi:10.1016/j.apenergy.2016.04.057.

[63] J. Liu, A. Saxena, K. Goebel, B. Saha, W. Wang, An Adaptive Recurrent Neural Network for Remaining Useful Life Prediction of Lithium-ion Batteries, in: Annu. Conf. Progn. Heal. Manag. Soc., Portland, Oregon, USA, 2010.

[64] Z. Xi, X. Zhao, Data-driven prognostics with lack of training data sets, in: Proc. ASME Des. Eng. Tech. Cenference, Boston, Massachusetts, USA, 2015.

[65] F. Rufus, S. Lee, A. Thakker, Health monitoring algorithms for space application batteries, in: Int. Conf. Progn. Heal. Manag., Denver, Colorado, USA, 2008. doi:10.1109/PHM.2008.4711430.

[66] M. Rezvani, M. AbuAli PhD, S. Lee, J. Lee, J. Ni PhD, A Comparative Analysis of Techniques for Electric Vehicle Battery Prognostics and Health Management (PHM), in: SAE Tech. Pap. 2011-01-2247, 2011: pp. 1–9. doi:10.4271/2011-01-2247.

[67] H. Huang, N. Cui, Y. Shang, C. Zhang, Aging performances and cycle-life predictions of Li-ion battery, in: 2016 35th Chinese Control Conf., IEEE, Chengdu, China, 2016: pp. 8710–8715. doi:10.1109/ChiCC.2016.7554748.

[68] R. Razavi-Far, M. Farajzadeh-Zanjani, S. Chakrabarti, M. Saif, Data-driven prognostic techniques for estimation of the remaining useful life of lithium-ion batteries, in: 2016 IEEE Int. Conf. Progn. Heal. Manag., Ottawa, Ontario, Canada, 2016: pp. 1–8. doi:10.1109/ICPHM.2016.7542870.

[69] R. Razavi-Far, S. Chakrabarti, M. Saif, Multi-step-ahead prediction techniques for Lithium-ion batteries condition prognosis, in: 2016 IEEE Int. Conf. Syst. Man, Cybern., Budapest, Hungary, 2016: pp. 004675–004680. doi:10.1109/SMC.2016.7844969.

[70] Y. Xing, E.W.M. Ma, K.-L. Tsui, M. Pecht, An ensemble model for predicting the remaining useful performance of lithium-ion batteries, Microelectron. Reliab. 53 (2013) 811–820. doi:10.1016/j.microrel.2012.12.003.

[71] D. Wang, F. Yang, K. Tsui, Q. Zhou, S.J. Bae, Remaining Useful Life Prediction of Lithium-Ion Batteries Based on Spherical Cubature Particle Filter, IEEE Trans. Instrum. Meas. 65 (2016) 1282–1291. doi:10.1109/TIM.2016.2534258.

[72] F. Yang, D. Wang, Y. Xing, K.-L. Tsui, Prognostics of Li(NiMnCo)O2-based lithium-ion batteries using a novel battery degradation model, Microelectron. Reliab. 70 (2017) 70–78. doi:10.1016/j.microrel.2017.02.002.

[73] K. Goebel, B. Saha, A. Saxena, J. Celaya, J. Christophersen, Prognostics in Battery Health Management, IEEE Instrum. Meas. Mag. 11 (2008) 33–40. doi:10.1109/MIM.2008.4579269.

[74] B. Saha, K. Goebel, J. Christophersen, Comparison of prognostic algorithms for estimating remaining useful life of batteries, Trans. Inst. Meas. Control. 31 (2009) 293–308.

doi:10.1177/0142331208092030.

[75] B. Saha, K. Goebel, S. Poll, J. Christophersen, Prognostics Methods for Battery Health Monitoring Using a Bayesian Framework, IEEE Trans. Instrum. Meas. 58 (2009) 291–296. doi:10.1109/TIM.2008.2005965.

[76] J. Liu, W. Wang, F. Ma, A regularized auxiliary particle filtering approach for system state estimation and battery life prediction, Smart Mater. Struct. 20 (2011) 075021. doi:10.1088/0964-1726/20/7/075021.

[77] H. Dong, X. Jin, Y. Lou, C. Wang, Lithium-ion battery state of health monitoring and remaining useful life prediction based on support vector regression-particle filter, J. Power Sources. 271 (2014) 114–123. doi:10.1016/j.jpowsour.2014.07.176.

[78] B. Saha, K. Goebel, Modeling Li-ion battery capacity depletion in a particle filtering framework, in: Annu. Conf. Progn. Heal. Manag. Soc., San Diego, California, USA, 2009.

[79] M. Dalal, J. Ma, D. He, Lithium-ion battery life prognostic health management system using particle filtering framework, Proc. Inst. Mech. Eng. Part O J. Risk Reliab. 225 (2011) 81–90. doi:10.1177/1748006XJRR342.

[80] D. Liu, Y. Luo, J. Liu, Y. Peng, L. Guo, M. Pecht, Lithium-ion battery remaining useful life estimation based on fusion nonlinear degradation AR model and RPF algorithm, Neural Comput. Appl. 25 (2014) 557–572. doi:10.1007/s00521-013-1520-x.

[81] Y. Song, D. Liu, C. Yang, Y. Peng, Data-driven hybrid remaining useful life estimation approach for spacecraft lithium-ion battery, Microelectron. Reliab. 75 (2017) 142–153. doi:10.1016/j.microrel.2017.06.045.

[82] W. He, N. Williard, M. Osterman, M. Pecht, Prognostics of lithium-ion batteries based on Dempster–Shafer theory and the Bayesian Monte Carlo method, J. Power Sources. 196 (2011) 10314–10321. doi:10.1016/j.jpowsour.2011.08.040.

[83] D. Liu, L. Guo, J. Pang, Y. Peng, A fusion framework with nonlinear degradation improvement for remaining useful life estimation of lithium-ion batteries, in: Proc. Annu. Conf. Progn. Heal. Manag. Soc., New Orleans, Louisiana, USA, 2013: pp. 598–607.

[84] Y. Jiang, Y. Wang, Y. Wu, Q. Sun, Fault prognostic of electronics based on optimal multi-order particle filter, Microelectron. Reliab. 62 (2016) 167–177. doi:10.1016/j.microrel.2016.03.030.

[85] L. Liao, F. Köttig, A hybrid framework combining data-driven and model-based methods for system remaining useful life prediction, Appl. Soft Comput. 44 (2016) 191–199. doi:10.1016/j.asoc.2016.03.013.

[86] F. Li, J. Xu, A new prognostics method for state of health estimation of lithium-ion batteries based on a mixture of Gaussian process models and particle filter, Microelectron. Reliab. 55 (2015) 1035–1045. doi:10.1016/j.microrel.2015.02.025.

[87] J. Liu, W. Wang, F. Ma, Y.B. Yang, C.S. Yang, A data-model-fusion prognostic framework for dynamic system state forecasting, Eng. Appl. Artif. Intell. 25 (2012) 814–823. doi:10.1016/j.engappai.2012.02.015.

[88] X. Su, S. Wang, M. Pecht, L. Zhao, Z. Ye, Interacting multiple model particle filter for prognostics of lithium-ion batteries, Microelectron. Reliab. 70 (2017) 59–69. doi:10.1016/j.microrel.2017.02.003.

[89] W. Xian, B. Long, M. Li, H. Wang, Prognostics of Lithium-Ion Batteries Based on the Verhulst Model, Particle Swarm Optimization and Particle Filter, IEEE Trans. Instrum. Meas. 63 (2014) 2–17. doi:10.1109/TIM.2013.2276473.

[90] Q. Miao, L. Xie, H. Cui, W. Liang, M. Pecht, Remaining useful life prediction of lithium-ion battery with unscented particle filter technique, Microelectron. Reliab. 53 (2013) 805–810. doi:10.1016/j.microrel.2012.12.004.

[91] E. Walker, S. Rayman, R.E. White, Comparison of a particle filter and other state estimation methods for prognostics of lithium-ion batteries, J. Power Sources. 287 (2015) 1–12. doi:10.1016/j.jpowsour.2015.04.020.

[92] Z. Liu, G. Sun, S. Bu, J. Han, X. Tang, M. Pecht, Particle Learning Framework for Estimating the Remaining Useful Life of Lithium-Ion Batteries, IEEE Trans. Instrum. Meas. 66 (2017) 280–293. doi:10.1109/TIM.2016.2622838.

[93] X. Peng, C. Zhang, Y. Yu, Y. Zhou, Battery remaining useful life prediction algorithm based on support vector regression and unscented particle filter, in: 2016 IEEE Int. Conf. Progn. Heal. Manag., Ottawa, Ontario, Canada, 2016: pp. 1–6. doi:10.1109/ICPHM.2016.7542844.

[94] C. Chen, M. Pecht, Prognostics of lithium-ion batteries using model-based and data-driven methods, in: Proc. IEEE 2012 Progn. Syst. Heal. Manag. Conf., Beijing, China, 2012: pp. 1–6. doi:10.1109/PHM.2012.6228850.

[95] X. Zhang, Q. Miao, Z. Liu, Remaining useful life prediction of lithium-ion battery using an improved UPF method based on MCMC, Microelectron. Reliab. 75 (2017) 288–295. doi:10.1016/j.microrel.2017.02.012.

[96] H. Zhang, Q. Miao, X. Zhang, Z. Liu, An improved unscented particle filter approach for lithium-ion battery remaining useful life prediction, Microelectron. Reliab. 81 (2018) 288–298. doi:10.1016/j.microrel.2017.12.036.

[97] E. Sarasketa-Zabala, I. Gandiaga, E. Martinez-Laserna, L.M. Rodriguez-Martinez, I. Villarreal, Cycle ageing analysis of a LiFePO4/graphite cell with dynamic model validations: Towards realistic lifetime predictions, J. Power Sources. 275 (2015) 573–587. doi:10.1016/j.jpowsour.2014.10.153.

[98] I. Baghdadi, O. Briat, J.-Y. Delétage, P. Gyan, J.-M. Vinassa, Lithium battery aging model based on Dakin's degradation approach, J. Power Sources. 325 (2016) 273–285. doi:10.1016/j.jpowsour.2016.06.036.

[99] M. Tipping, Sparse Bayesian Learning and the Relevance Vector Machine, J. Mach. Learn. Res. 1 (2001) 211–244. doi:10.1162/15324430152748236.

[100] M.J. de Smith, STATSREF: Statistical Analysis Handbook - a comprehensive handbook of statistical concepts, techniques and software tools, Winchelsea Press. (2015).

[101] NIST/SEMATECH, e-Handbook of Statistical Methods, (2012). http://www.itl.nist.gov/div898/handbook/.

[102] J. Wilhelm, S. Seidlmayer, P. Keil, J. Schuster, A. Kriele, R. Gilles, A. Jossen, Cycling capacity recovery effect: A coulombic efficiency and post-mortem study, J. Power Sources. 365 (2017) 327–338. doi:10.1016/j.jpowsour.2017.08.090.

[103] M. Lewerenz, P. Dechent, D.U. Sauer, Investigation of capacity recovery during rest period at different states-of-charge after cycle life test for prismatic Li(Ni1/3Mn1/3Co1/3)O2-graphite cells, J. Energy Storage. 21 (2019) 680–690. doi:10.1016/j.est.2019.01.004.

[104] A.J. Smola, B. Schölkopf, A tutorial on support vector regression, Stat. Comput. 14 (2004) 199–222. doi:10.1023/B:STCO.0000035301.49549.88.

[105] V.N. Vapnik, The Nature of Statistical Learning Theory, Springer New York, New York, NY, 2000. doi:10.1007/978-1-4757-3264-1.

[106] B. Saha, K. Goebel, "Battery Data Set", NASA Ames Prognostics Data Repository, (2007). http://ti.arc.nasa.gov/project/prognostic-data-repository. [dataset].

[107] USABC, Electric Vehicle Battery Test Procedures Manual, Revision 2, 1996.

[108] J. Ma, J. Theiler, S. Perkins, Accurate On-line Support Vector Regression, Neural Comput. 15 (2003) 2683–2703. doi:10.1162/089976603322385117.

[109] Zhi-Qiang Zeng, Hong-Bin Yu, Hua-Rong Xu, Yan-Qi Xie, Ji Gao, Fast training Support Vector Machines using parallel sequential minimal optimization, in: 3rd Int. Conf. Intell. Syst. Knowl. Eng., IEEE, Xiamen, China, 2008: pp. 997–1001. doi:10.1109/ISKE.2008.4731075.

[110] C.E. Rasmussen, C.K.I. Williams, Gaussian Processes for Machine Learning, MIT Press, 2006. http://www.gaussianprocess.org/gpml/chapters/RW.pdf.

[111] N.A. Syed, H. Liu, K.K. Sung, Incremental Learning with Support Vector Machines, in: Proc. Work. Support Vector Mach. Int. Jt. Conf. Artif. Intell., 1999.

[112] Center for Advances Life Cycle Engineering; University of Maryland College Park, CALCE Battery Group data, (n.d.). https://www.calce.umd.edu/batteries/data.htm. [dataset].

[113] M. Tipping, A. Faul, Fast Marginal Likelihood Maximisation for Sparse Bayesian Models, in: 2006.

[114] A. Ranganathan, M.-H. Yang, J. Ho, Online Sparse Gaussian Process Regression and Its Applications, IEEE Trans. Image Process. 20 (2011) 391–404. doi:10.1109/TIP.2010.2066984.

[115] L. Csató, M. Opper, Sparse On-Line Gaussian Processes, Neural Comput. 14 (2002) 641–668. doi:10.1162/089976602317250933.

[116] L.C. Jain, M. Seera, C.P. Lim, P. Balasubramaniam, A review of online learning in supervised neural networks, Neural Comput. Appl. 25 (2014) 491–509. doi:10.1007/s00521-013-1534-4.

[117] Z. Ma, J. Jiang, W. Shi, W. Zhang, C.C. Mi, Investigation of path dependence in commercial lithium-ion cells for pure electric bus applications: Aging mechanism identification, J. Power Sources. 274 (2015) 29–40. doi:10.1016/j.jpowsour.2014.10.006.

[118] G. Cybenko, Approximation by superpositions of a sigmoidal function, Math. Control. Signals, Syst. 2 (1989) 303–314. doi:10.1007/BF02551274.

[119] R.M. Neal, Bayesian Learning for Neural Networks, Springer New York, New York, NY, 1996. doi:10.1007/978-1-4612-0745-0.

[120] C.M. Bishop, Improving the Generalization Properties of Radial Basis Function Neural Networks, Neural Comput. 3 (1991) 579–588. doi:10.1162/neco.1991.3.4.579.

[121] A. González, J.R. Dorronsoro, Natural conjugate gradient training of multilayer perceptrons,

Neurocomputing. 71 (2008) 2499–2506. doi:10.1016/j.neucom.2007.11.035.

[122] O. Giustolisi, Sparse solution in training artificial neural networks, Neurocomputing. 56 (2004) 285–304. doi:10.1016/j.neucom.2003.09.005.

[123] M.S. Arulampalam, S. Maskell, N. Gordon, T. Clapp, A tutorial on particle filters for online nonlinear/non-Gaussian Bayesian tracking, IEEE Trans. Signal Process. 50 (2002) 174–188. doi:10.1109/78.978374.

[124] Z. Chen, Bayesian Filtering: From Kalman Filters to Particle Filters, and Beyond, Statistics (Ber). 182 (2003) 1–69. doi:10.1.1.107.7415.

[125] Z. Zhu, Z. Meng, Z. Zhang, J. Chen, Y. Dai, Robust particle filter for state estimation using measurements with different types of gross errors, ISA Trans. 69 (2017) 281–295. doi:10.1016/j.isatra.2017.03.021.

[126] M. Berecibar, I. Gandiaga, I. Villarreal, N. Omar, J. Van Mierlo, P. Van Den Bossche, Critical review of state of health estimation methods of Li-ion batteries for real applications, Renew. Sustain. Energy Rev. 56 (2016) 572–587. doi:10.1016/j.rser.2015.11.042.

[127] J. Taylor, A. Barai, T.R. Ashwin, Y. Guo, M. Amor-Segan, J. Marco, An insight into the errors and uncertainty of the lithium-ion battery characterisation experiments, J. Energy Storage. 24 (2019) 100761. doi:10.1016/j.est.2019.100761.

[128] R.R. Richardson, M.A. Osborne, D.A. Howey, Battery health prediction under generalized conditions using a Gaussian process transition model, J. Energy Storage. 23 (2019) 320–328. doi:10.1016/j.est.2019.03.022.

[129] M. Lucu, E. Martinez-Laserna, I. Gandiaga, K. Liu, H. Camblong, W.D. Widanage, J. Marco, Data-driven nonparametric Li-ion battery ageing model aiming at learning from real operation data - Part B: Cycling operation, J. Energy Storage. 30 (2020) 101410. doi:10.1016/j.est.2020.101410.

[130] M. Dubarry, N. Qin, P. Brooker, Calendar aging of commercial Li-ion cells of different chemistries – A review, Curr. Opin. Electrochem. 9 (2018) 106–113. doi:10.1016/j.coelec.2018.05.023.

[131] L. Zhou, S. Pan, J. Wang, A. V. Vasilakos, Machine learning on big data: Opportunities and challenges, Neurocomputing. 237 (2017) 350–361. doi:10.1016/j.neucom.2017.01.026.

[132] A.J. Warnecke, Degradation Mechanisms in NMC-Based Lithium-Ion Batteries, RWTH Aachen University, 2017.

[133] M. Lewerenz, J. Münnix, J. Schmalstieg, S. Käbitz, M. Knips, D.U. Sauer, Systematic aging of commercial LiFePO 4 |Graphite cylindrical cells including a theory explaining rise of capacity during aging, J. Power Sources. 345 (2017) 254–263. doi:10.1016/j.jpowsour.2017.01.133.

[134] M. Lewerenz, G. Fuchs, L. Becker, D.U. Sauer, Irreversible calendar aging and quantification of the reversible capacity loss caused by anode overhang, J. Energy Storage. 18 (2018) 149–159. doi:10.1016/j.est.2018.04.029.

[135] M. Dubarry, N. Qin, P. Brooker, Calendar aging of commercial Li-ion cells of different chemistries – A review, Curr. Opin. Electrochem. 9 (2018) 106–113. doi:10.1016/j.coelec.2018.05.023.

[136] M. Dubarry, A. Devie, K. McKenzie, Durability and reliability of electric vehicle batteries under

electric utility grid operations: Bidirectional charging impact analysis, J. Power Sources. 358 (2017) 39–49. doi:10.1016/j.jpowsour.2017.05.015.

[137] T. Waldmann, B.-I. Hogg, M. Wohlfahrt-Mehrens, Li plating as unwanted side reaction in commercial Li-ion cells – A review, J. Power Sources. 384 (2018) 107–124. doi:10.1016/j.jpowsour.2018.02.063.

[138] M. Petzl, M. Kasper, M.A. Danzer, Lithium plating in a commercial lithium-ion battery – A low-temperature aging study, J. Power Sources. 275 (2015) 799–807. doi:10.1016/j.jpowsour.2014.11.065.

[139] K.A. Severson, P.M. Attia, N. Jin, N. Perkins, B. Jiang, Z. Yang, M.H. Chen, M. Aykol, P.K. Herring, D. Fraggedakis, M.Z. Bazant, S.J. Harris, W.C. Chueh, R.D. Braatz, Data-driven prediction of battery cycle life before capacity degradation, Nat. Energy. 4 (2019) 383–391. doi:10.1038/s41560-019-0356-8.

[140] M. Lucu, E. Martinez-Laserna, I. Gandiaga, H. Camblong, A critical review on self-adaptive Li-ion battery ageing models, J. Power Sources. 401 (2018) 85–101. doi:10.1016/j.jpowsour.2018.08.064.

[141] K. Liu, Y. Li, X. Hu, M. Lucu, D. Widanalage, Gaussian Process Regression with Automatic Relevance Determination Kernel for Calendar Aging Prediction of Lithium-ion Batteries, IEEE Trans. Ind. Informatics. (2019) 1–1. doi:10.1109/TII.2019.2941747.

[142] A. Nuhic, J. Bergdolt, B. Spier, M. Buchholz, K. Dietmayer, Battery Health Monitoring and Degradation Prognosis in Fleet Management Systems, World Electr. Veh. J. 9 (2018) 39. doi:10.3390/wevj9030039.

[143] D. Duvenaud, J.R. Lloyd, R. Grosse, J.B. Tenenbaum, Z. Ghahramani, Structure Discovery in Nonparametric Regression through Compositional Kernel Search, Proc. 30th Int. Conf. Mach. Learn. PMLR. 28 (3) (2013) 1166–1174. http://arxiv.org/abs/1302.4922.

[144] X. Yang, C. Wang, Understanding the trilemma of fast charging, energy density and cycle life of lithium-ion batteries, J. Power Sources. 402 (2018) 489–498. doi:10.1016/j.jpowsour.2018.09.069.

[145] D. Li, H. Li, D. Danilov, L. Gao, J. Zhou, R.A. Eichel, Y. Yang, P.H.L. Notten, Temperature-dependent cycling performance and ageing mechanisms of C6/LiNi1/3Mn1/3Co1/3O2batteries, J. Power Sources. 396 (2018) 444–452. doi:10.1016/j.jpowsour.2018.06.035.

[146] R.D. Deshpande, D.M. Bernardi, Modeling Solid-Electrolyte Interphase (SEI) Fracture: Coupled Mechanical/Chemical Degradation of the Lithium Ion Battery, J. Electrochem. Soc. 164 (2017) A461–A474. doi:10.1149/2.0841702jes.

[147] A. Marongiu, M. Roscher, D.U. Sauer, Influence of the vehicle-to-grid strategy on the aging behavior of lithium battery electric vehicles, Appl. Energy. 137 (2015) 899–912. doi:10.1016/j.apenergy.2014.06.063.

[148] I. Laresgoiti, S. Käbitz, M. Ecker, D.U. Sauer, Modeling mechanical degradation in lithium ion batteries during cycling: Solid electrolyte interphase fracture, J. Power Sources. 300 (2015) 112–122. doi:10.1016/j.jpowsour.2015.09.033.

[149] A. Mukhopadhyay, B.W. Sheldon, Deformation and stress in electrode materials for Li-ion batteries, Prog. Mater. Sci. 63 (2014) 58–116. doi:10.1016/j.pmatsci.2014.02.001.

[150] R. Deshpande, M. Verbrugge, Y.-T. Cheng, J. Wang, P. Liu, Battery Cycle Life Prediction with Coupled Chemical Degradation and Fatigue Mechanics, J. Electrochem. Soc. 159 (2012) A1730–A1738. doi:10.1149/2.049210jes.

[151] S. Ahmed, I. Bloom, A.N. Jansen, T. Tanim, E.J. Dufek, A. Pesaran, A. Burnham, R.B. Carlson, F. Dias, K. Hardy, M. Keyser, C. Kreuzer, A. Markel, A. Meintz, C. Michelbacher, M. Mohanpurkar, P.A. Nelson, D.C. Robertson, D. Scoffield, M. Shirk, T. Stephens, R. Vijayagopal, J. Zhang, Enabling fast charging – A battery technology gap assessment, J. Power Sources. 367 (2017) 250–262. doi:10.1016/j.jpowsour.2017.06.055.

[152] M. Tutuianu, P. Bonnel, B. Ciuffo, T. Haniu, N. Ichikawa, A. Marotta, J. Pavlovic, H. Steven, Development of the World-wide harmonized Light duty Test Cycle (WLTC) and a possible pathway for its introduction in the European legislation, Transp. Res. Part D Transp. Environ. 40 (2015) 61–75. doi:10.1016/j.trd.2015.07.011.

[153] J. de Hoog, J.-M. Timmermans, D. Ioan-Stroe, M. Swierczynski, J. Jaguemont, S. Goutam, N. Omar, J. Van Mierlo, P. Van Den Bossche, Combined cycling and calendar capacity fade modeling of a Nickel-Manganese-Cobalt Oxide Cell with real-life profile validation, Appl. Energy. 200 (2017) 47–61. doi:10.1016/j.apenergy.2017.05.018.

[154] E. Martinez-laserna, Methodology for the Techno-Economic Assessment of Second Life Lithium-Ion Batteries, (2017).

[155] Z. Li, J. Huang, B.Y. Liaw, J. Zhang, On state-of-charge determination for lithium-ion batteries, J. Power Sources. 348 (2017) 281–301. doi:10.1016/j.jpowsour.2017.03.001.

[156] A. Damianou, N.D. Lawrence, Semi-described and semi-supervised learning with Gaussian processes, Uncertain. Artif. Intell. - Proc. 31st Conf. UAI 2015. (2015) 228–237. http://arxiv.org/abs/1509.01168.

[157] A.G. Wilson, R.P. Adams, Gaussian Process Kernels for Pattern Discovery and Extrapolation, 28 (2013). http://arxiv.org/abs/1302.4245.

[158] E. Redondo-iglesias, Calendar and cycling ageing combination of batteries in electric vehicles, Microelectron. Reliab. 88–90 (2018) 1212–1215. doi:10.1016/j.microrel.2018.06.113.

[159] E. Redondo-iglesias, Étude Du Vieillissement Des Batteries Lithium-Ion Dans Les Applications " Véhicule Électrique " : Combinaison Des Effets De Vieillissement Calendaire Et De Cyclage, Université de Lyon, 2017. https://tel.archives-ouvertes.fr/tel-01668529/document.

[160] J.A. Lopez, V.I. Herrera, H. Camblong, A. Milo, H. Gaztanaga, Energy Management Improvement Based on Fleet Learning for Hybrid Electric Buses, in: 2018 IEEE Veh. Power Propuls. Conf., IEEE, 2018: pp. 1–6. doi:10.1109/VPPC.2018.8605025.

[161] J.Q. Candela, A. Girard, J. Larsen, C.E. Rasmussen, Propagation of uncertainty in Bayesian kernel models - application to multiple-step ahead forecasting, in: 2003 IEEE Int. Conf. Acoust. Speech, Signal Process. 2003. Proceedings. (ICASSP '03)., IEEE, 2003: pp. II-701–4. doi:10.1109/ICASSP.2003.1202463.

[162] G. Skolidis, Transfer learning with Gaussian Processes, University of Edinburgh, 2012.

[163] European Comission, SENSIBAT European Project, grant agreement H2020-LC-BAT-2020-3 / GA #957273, (2020).

Appendices

Appendix A. Calendar ageing

Raw data, variance, and prediction results

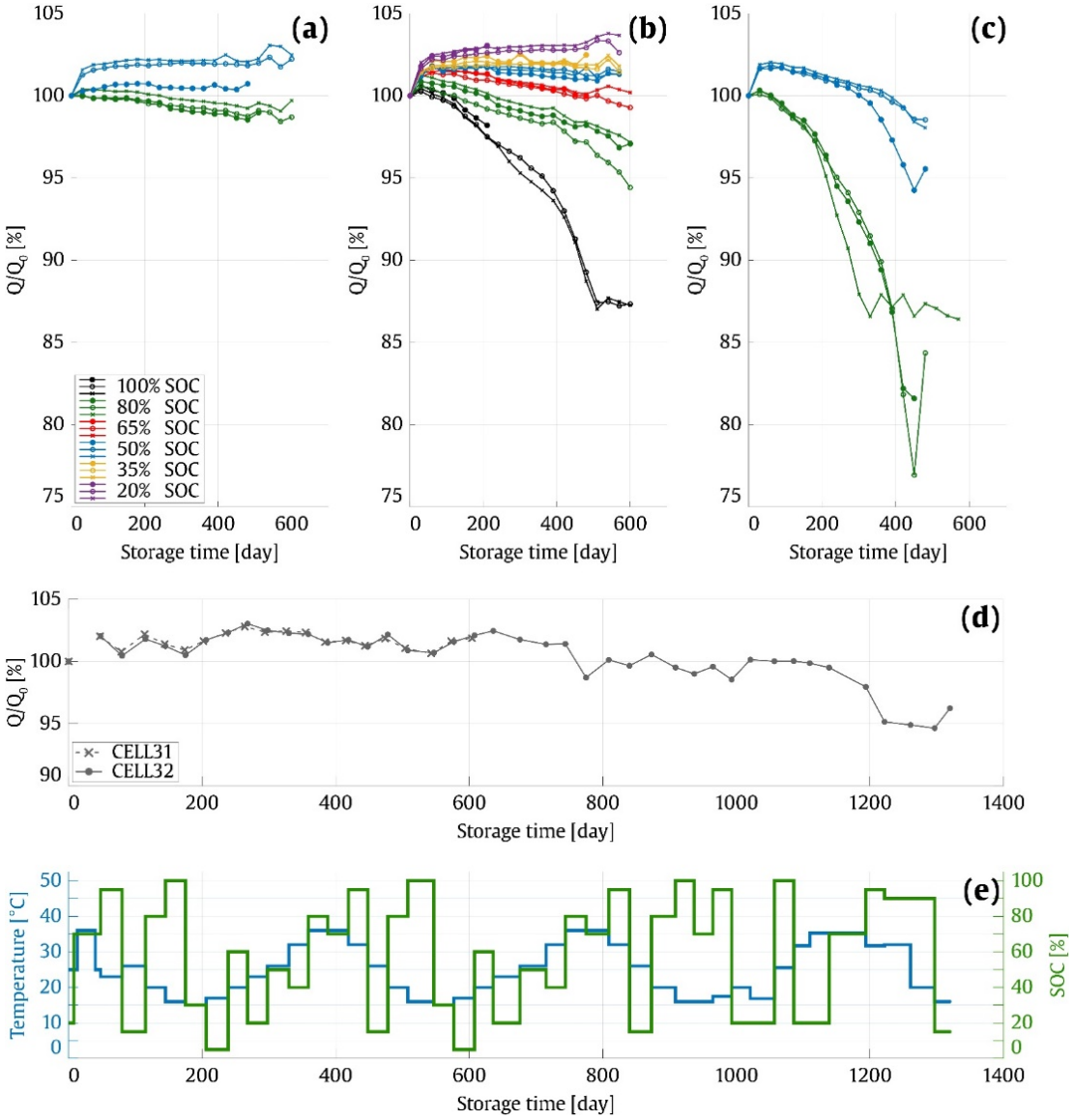

Figure A. 1. Normalised (with initial value Q_0) capacity, obtained from the experimental static ageing tests at (a) 25°C, (b) 35°C and (c) 45°C. (d) Normalised capacity, and (f) corresponding temperature and SOC storage conditions, obtained from the experimental dynamic ageing tests for CELL31. (e) Normalised capacity, and (g) corresponding temperature and SOC storage conditions, obtained from the experimental dynamic ageing tests for CELL32.

Table A. 1. Mean variance of the capacity curves, for the three cells tested at identical storage conditions (in [%²]).

Temperature [°C]	SOC [%]					
	100	80	65	50	35	20
25		0.09		0.67		
35	0.05	0.42	0.02	0.03	0.04	0.03
45		3.51		0.95		

Table A. 2. Results obtained with the models resulting from the different training cases, for the training, validation, and all the cells, in terms of ΔQ and Q.

	Capacity loss (ΔQ)									Capacity (Q)								
	Training			Validation			All			Training			Validation			All		
	MAE	RMSE	CS	MAE	RMSE	CS	MAE	RMSE	CS	MAE	RMSE	CS	MAE	RMSE	CS	MAE	RMSE	CS
CASE 1	0.37	0.45	85.27	0.66	0.75	90.74	0.60	0.69	89.61	0.72	0.78	61.54	2.02	2.30	59.75	1.75	1.98	60.12
CASE 2	0.31	0.39	89.93	0.53	0.61	84.08	0.46	0.54	85.90	0.639	0.703	69.66	1.33	1.54	58.87	1.11	1.28	62.22
CASE 3	0.26	0.33	94.51	0.37	0.44	99.49	0.30	0.37	96.42	0.47	0.53	83.03	0.64	0.76	89.04	0.53	0.62	85.31
CASE 4	0.27	0.34	94.87	0.28	0.33	100	0.27	0.33	96.28	0.50	0.55	81.99	0.37	0.41	100	0.46	0.51	86.95
CASE 5	0.28	0.34	95.31	0.26	0.30	100	0.27	0.33	96.28	0.49	0.54	83.55	0.44	0.53	94.44	0.48	0.54	85.80
CASE 6	0.25	0.32	95.75	0.38	0.43	100	0.27	0.33	96.19	0.44	0.49	84.99	0.41	0.42	100	0.43	0.48	86.54
CASE 7	0.26	0.33	96.19	-	-	-	0.26	0.33	96.19	0.45	0.50	86.54	-	-	-	0.45	0.50	86.54

Appendix B. Cycle ageing

Ageing test matrix, raw data, variance, and prediction results

Table B. 1. Cycle ageing tests matrix, for the tests at static ageing conditions. Numbers indicate the number of cells tested at each cycling condition.

Temperature [°C]		25		35							45
C-Rate [C] (charge - discharge)		C/3-1C	1C-1C	C/3-C/3	C/3-1C	C/3-2C	C/2-1C	1C-1C	2C-1C	2C-2C	C/3-1C
DoD [%]	MidSOC [%]										
100	50	3			3						3
80	50	8	3	3	8	3	3	3	3	3	8
65	50	3			3						3
50	65				3						
	50	3			8						3
	35				3						
35	50	3			3						3
20	80				3						
	65				3						
	50	3			3						3
	35				3						
	20				3						
10	80				3						
	65				3						
	20				3						

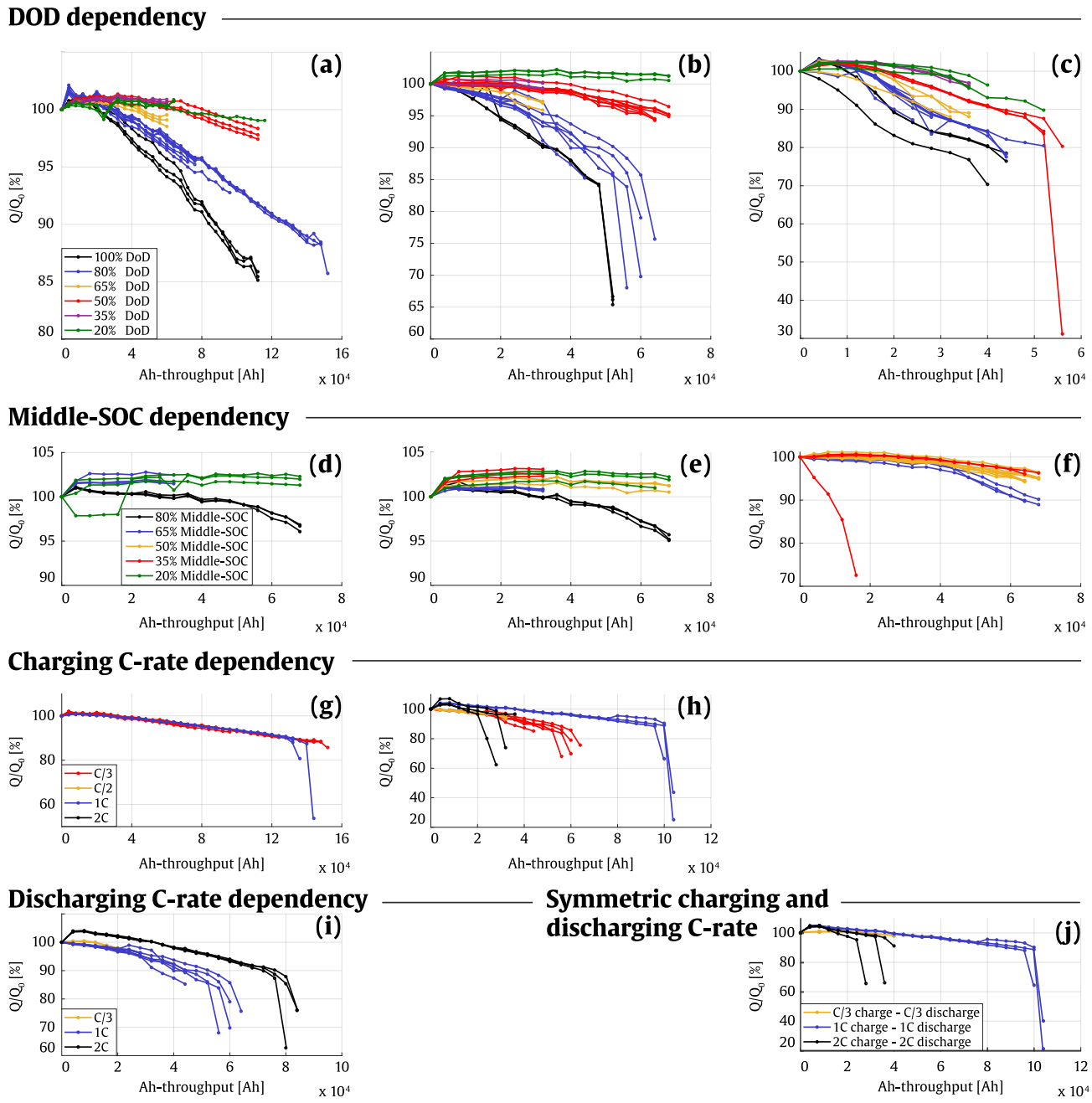

Figure B.1. Normalised capacity (with initial value Q_0), obtained from the experimental static ageing tests at (a) 25°C, 50% middle-SOC, C/3 – 1C, and several DOD values, (b) 35°C, 50% middle-SOC, C/3 – 1C, and several DOD values, (c) 45°C, 50% middle-SOC, C/3 – 1C, and several DOD values, (d) 35°C, 10% DOD, C/3 – 1C, and several middle-SOC values, (e) 35°C, 20% DOD, C/3 – 1C, and several middle-SOC values, (f) 35°C, 50% DOD, C/3 – 1C, and several middle-SOC values, (g) 25°C, 80% DOD, 50% middle-SOC, 1C discharging rate, and several charging rate values, (h) 35°C, 80% DOD, 50% middle-SOC, 1C discharging rate, and several charging rate values, (i) 35°C, 80% DOD, 50% middle-SOC, C/3 charging rate, and several discharging rate values, and (j) 35°C, 80% DOD, 50% middle-SOC and several symmetric charging and discharging rate values.

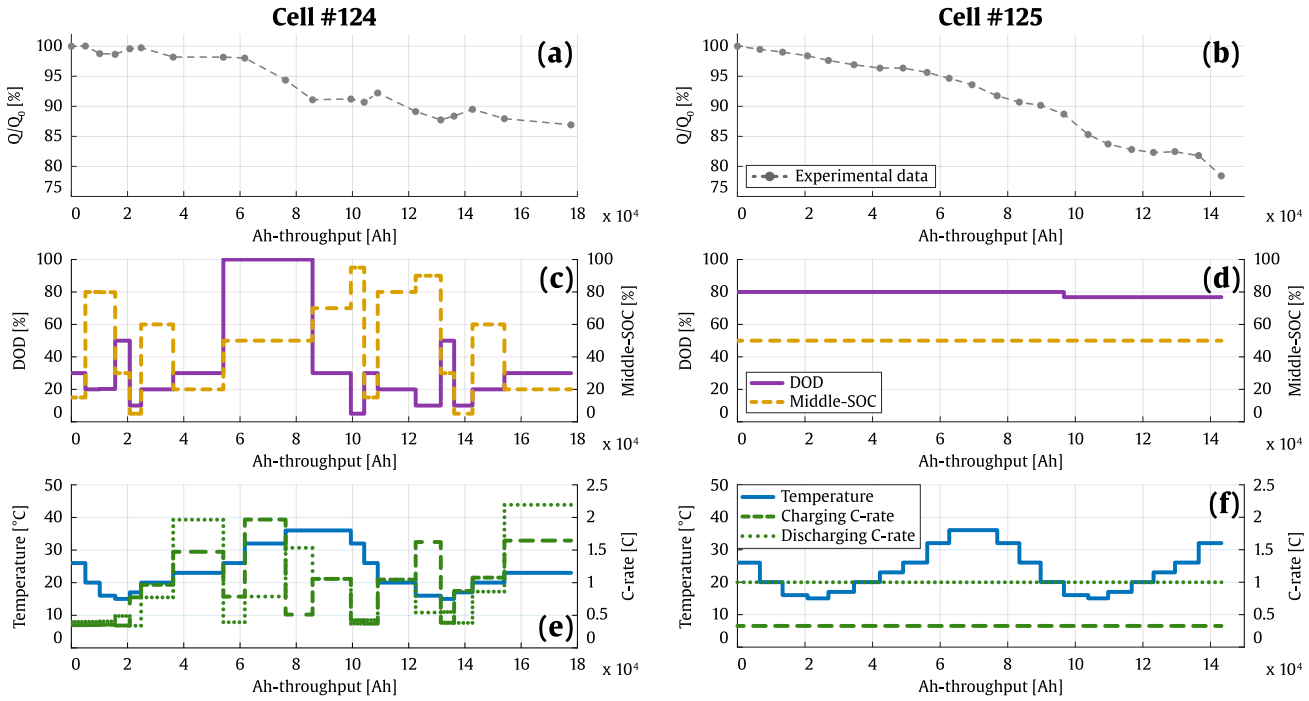

Figure B.2. (a) Normalised capacity (with initial value Q_0), and the corresponding (c) DOD and middle-SOC, and (e) temperature and charging and discharging C-rate profiles, for the cell #124. (b) Normalised capacity (with initial value Q_0), and the corresponding (d) DOD and middle-SOC, and (f) temperature and charging and discharging C-rate profiles, for the cell #125.

Table B. 2. Mean variance of the raw capacity curves, for all the cells tested at identical storage conditions (in [%²]).

Temperature [°C]		25		35							45
C-Rate [C] (charge - discharge)		C/3-1C	1C-1C	C/3-C/3	C/3-1C	C/3-2C	C/2-1C	1C-1C	2C-1C	2C-2C	C/3-1C
DoD [%]	MidSOC [%]										
100	50	0.26			0.41						12.82[1]
80	50	0.11	0.03	0.01	0.27	9.29[2]	0.13	7.94[3]	69.89[4]	40.88[5]	1.93
65	50	0.04			0.21						3.26
50	65				0.41						
	50	0.12			0.29						0.40
	35				74.06[6]						
35	50	0.01			0.16						0.06
20	80				0.05						
	65				0.01						
	50	0.03			0.14						1.04
	35				0.15						
	20				0.37						
10	80				0.03						
	65				0.23						
	20				1.18						

[1] This high variance is induced by a shift between the different curves obtained at this testing conditions, Figure B.1. (c), Appendix B.
[2] This high variance is induced by the sudden capacity drops observable in the black curves, Figure B.1. (i), Appendix B.
[3] These high variances are induced by the sudden capacity drops observable in the blue curves respectively, Figure B.1 (j), Appendix B.
[4] This high variance is induced by the sudden capacity drops observable in the black curves, Figure B.1. (h), Appendix B.
[5] These high variances are induced by the sudden capacity drops observable in the black curves respectively, Figure B.1 (j), Appendix B.
[6] This high variance value is induced by the cell #56, which depicts a clearly defective behaviour (isolated red curve in Figure B.1. (f), Appendix B.

Table B. 3. Results obtained with the models resulting from the different training cases, for the training, validation, targeted validation and all the cells, in terms of ΔQ and Q.

	Capacity loss (ΔQ)												Capacity (Q)											
	Training			Validation			Targeted validation			All			Training			Validation			Targeted validation			All		
	MAE	RMSE	CS	MAE	RMSE	CS	MAE	RMSE	CS	MAE	RMSE	CS	MAE	RMSE	CS	MAE	RMSE	CS	MAE	RMSE	CS	MAE	RMSE	CS
CASE 1	1.13	1.36	84.72	2.09	2.36	84.35	1.01	1.22	100.00	2.04	2.31	84.37	1.43	1.67	80.36	5.97	6.63	36.57	4.02	4.25	43.32	5.74	6.38	38.76
CASE 2	0.94	1.16	87.60	1.72	1.97	70.26	1.72	1.98	71.54	1.66	1.91	71.56	1.56	1.74	80.71	4.91	5.44	26.89	4.89	5.40	23.10	4.66	5.16	30.93
CASE 3	0.70	0.85	90.87	0.68	0.84	95.22	0.77	0.96	94.26	0.69	0.84	94.57	1.06	1.19	81.61	1.92	2.11	56.84	2.18	2.36	47.30	1.79	1.97	60.55
CASE 4	0.68	0.84	90.65	0.55	0.70	94.02	0.61	0.77	93.12	0.58	0.73	93.26	1.12	1.23	77.75	1.02	1.16	82.01	1.06	1.19	80.81	1.04	1.17	81.05
CASE 5	0.57	0.71	90.03	0.58	0.73	90.48	0.71	0.89	87.12	0.58	0.72	90.33	1.06	1.17	72.31	1.04	1.18	75.18	1.12	1.25	69.62	1.05	1.17	74.20
CASE 6	0.66	0.82	88.14	0.53	0.66	93.56	0.66	0.79	100.00	0.60	0.75	90.62	1.21	1.32	68.96	1.09	1.26	78.77	0.74	1.00	99.31	1.16	1.29	73.45
CASE 7	0.62	0.77	88.79	0.50	0.63	92.20	0.32	0.43	96.26	0.58	0.72	90.10	1.14	1.24	68.74	1.11	1.25	75.05	0.50	0.62	93.75	1.13	1.25	71.16
CASE 8	0.61	0.75	88.84	0.50	0.62	91.93	0.28	0.34	96.96	0.57	0.71	89.87	1.11	1.22	70.09	1.14	1.26	70.76	0.37	0.44	92.58	1.12	1.23	70.32
CASE 9	0.57	0.71	89.28	0.55	0.68	89.81	0.30	0.38	95.17	0.57	0.70	89.43	1.04	1.14	71.53	1.28	1.40	65.63	0.40	0.46	91.88	1.11	1.22	69.86
CASE 10	0.56	0.69	90.37	0.64	0.77	89.39	0.24	0.29	100.00	0.57	0.71	90.16	1.04	1.14	71.51	1.60	1.76	58.47	0.40	0.54	93.24	1.16	1.27	68.80
CASE 11	0.54	0.67	90.59	0.71	0.86	87.37	0.78	0.94	85.31	0.57	0.70	90.03	1.01	1.11	71.77	1.83	1.99	51.02	2.15	2.36	44.32	1.15	1.26	68.13
CASE 12	0.56	0.69	90.11	0.65	0.77	91.00	0.67	0.79	90.63	0.57	0.70	90.24	1.03	1.13	71.12	2.03	2.25	44.80	2.74	3.07	25.58	1.18	1.30	67.18
CASE 13	0.54	0.67	89.79	0.64	0.77	89.85	0.71	0.84	90.48	0.55	0.68	89.80	1.01	1.11	71.35	1.29	1.42	59.88	1.32	1.47	61.40	1.04	1.14	70.21
CASE 14	0.54	0.67	89.94	0.61	0.75	89.65	0.61	0.75	89.65	0.54	0.67	89.92	1.00	1.10	71.97	1.29	1.40	59.37	1.29	1.40	59.37	1.02	1.12	71.02
CASE 15	0.54	0.67	89.89	0.63	0.80	85.19	0.63	0.80	85.19	0.54	0.67	89.77	1.00	1.09	72.28	1.08	1.12	61.90	1.08	1.12	61.90	1.00	1.10	72.02
CASE 16	0.54	0.67	89.74	-	-	-	-	-	-	0.54	0.67	89.74	1.00	1.09	71.97	-	-	-	-	-	-	1.00	1.09	71.97

Appendix C. Processing algorithms

input: profiles of time, temperature, current and SOC

2: **for** j := 1 …number of half-cycles

3: $Ah_{half\text{-}cycle\text{-}j} := \int I_{profile\text{-}j}\, dt$

4: $T_{half\text{-}cycle\text{-}j} := mean(T_{profile\text{-}j})$

5: $DOD_{half\text{-}cycle\text{-}j} := \left| max(SOC_{profile\text{-}j}) - min(SOC_{profile\text{-}j}) \right|$

6: $Middle\text{-}SOC_{half\text{-}cycle\text{-}j} := mean(SOC_{profile\text{-}j})$

7: **if** $I_{profile\text{-}j} > 0$

8: $charging\ C\text{-}rate_{half\text{-}cycle\text{-}j} := mean(I_{profile\text{-}j}) / Ah_{nominal}$

9: $discharging\ C\text{-}rate_{half\text{-}cycle\text{-}j} := NaN$

10: **else**

11: $charging\ C\text{-}rate_{half\text{-}cycle\text{-}j} := NaN$

12: $discharging\ C\text{-}rate_{half\text{-}cycle\text{-}j} := mean(I_{profile\text{-}j}) / Ah_{nominal}$

13: **end if**

14: $SF_{half\text{-}cycle\text{-}j} = [Ah_{half\text{-}cycle\text{-}j},\ T_{half\text{-}cycle\text{-}j},\ DOD_{half\text{-}cycle\text{-}j},\ Middle\text{-}SOC_{half\text{-}cycle\text{-}j},\ C\text{-}rate_{charging\text{-}j},\ C\text{-}rate_{discharging\text{-}j}]$

15: SF = concatenate $SF_{half\text{-}cycle\text{-}j}$ rows in table

16: **end for**

return: SF (table of stress-factors, for all half-cycles)

Algorithm 1. Generate equivalent stress-factors values in cycling operation, for each half-cycle.

input: profiles of time, temperature and SOC

2: $\Delta time := sum(time_{profile})$

3: $T := mean(T_{profile})$

4: $SOC := mean(SOC_{profile})$

5: $SF := [\Delta time, T, SOC]$

return: SF (table of stress-factors of the storage time)

Algorithm 2. Generate equivalent stress-factors values in calendar operation.

input: table of stress-factors of all half-cycles, equivalence ranges assumptions

2: **for** j := 1 …number of equivalence ranges

3: Cluster j := regroup half-cycle rows which belong within the equivalence range #j

4: $Ah_{group\text{-}j} := \sum Ah_{half\text{-}cycles}$

5: $T_{group\text{-}j} := mean(T_{half\text{-}cycles})$

6: $DOD_{group\text{-}j} := mean(DOD_{half\text{-}cycles})$

7: $Middle\text{-}SOC_{group\text{-}j} := mean(Middle\text{-}SOC_{half\text{-}cycles})$

8: $Charging\ C\text{-}rate_{group\text{-}j} := mean(Charging\ C\text{-}rate_{half\text{-}cycles})$

9: $Discharging\ C\text{-}rate_{group\text{-}j} := mean(Discharging\ C\text{-}rate_{half\text{-}cycles})$

10: $SF_{group\text{-}j} = [Ah_{group\text{-}j}, T_{group\text{-}j}, DOD_{group\text{-}j}, Middle\text{-}SOC_{group\text{-}j}, Charging\ C\text{-}rate_{group\text{-}j}, Charging\ C\text{-}rate_{group\text{-}j}]$

11: HC_{table} := concatenate $SF_{group\text{-}j}$ rows in table

12: **end for**

return: HC_{table} (table of stress-factors, for all clusters of equivalence ranges)

Algorithm 3. Accumulate the Ah-throughput of the half-cycles (charge and discharge separately) belonging within the same "equivalence ranges", for which the corresponding influence on cell ageing is assumed to be equivalent.

input: table of half-cycles (HC_{table})

for j := 1 … # equivalence ranges clusters

  while isempty(cluster #j) == 0

    $hc_{CHA-largest}$:= find the charging half-cycle with largest ΔAh

    $hc_{DCH-largest}$:= find the discharging half-cycle with largest ΔAh

    Synthesize full-cycle (fc):

      $\Delta Ah_{fc} := 2 \cdot \min(\Delta Ah\text{-}hc_{CHA-largest}, \Delta Ah\text{-}hc_{DCH-largest})$

      $\Delta Ah_{hc\text{-}residual} := \left| \Delta Ah\text{-}hc_{CHA-largest} - \Delta Ah\text{-}hc_{DCH-largest} \right|$

      $FC := [\Delta Ah_{fc}, T_{cluster-j}, DOD_{cluster-j}, Middle\text{-}SOC_{cluster-j}, \ldots$

        $charging\ C\text{-}rate_{cluster-j}, discharging\ C\text{-}rate_{cluster-j}]$

      $HC_{residual} := [\Delta Ah_{hc\text{-}residual}, T_{cluster-j}, DOD_{cluster-j}, Middle\text{-}SOC_{cluster-j}, \ldots$

        $charging\ C\text{-}rate_{cluster-j}, discharging\ C\text{-}rate_{cluster-j}]$

    FC_{table} := concatenate FC rows in table

    Re-incorporate $HC_{residual}$ in HC_{table}

    if $HC_{residual}$ is the last row in the cluster #j

      break

    end if

  end while

  $HC_{residuals\text{-}table}$:= concatenate $HC_{residual}$ rows in table

end for

$HC_{last\ residual}$:= hc with lowest $\Delta Ah_{hc\text{-}residual}$ within $HC_{residuals-table}$.

Remove $HC_{last\ residual}$ from $HC_{residuals-table}$.

Synthesize a single full-cycle from $HC_{residuals-table}$:

  T_{fc} := average of hc temperatures, weighted by $\Delta Ah_{hc\text{-}residual}$

  DOD_{fc} := maximum of hc DOD

  $Middle\text{-}SOC_{fc}$:= average of hc temperatures, weighted by $\Delta Ah_{hc\text{-}residual}$

  $Charging\ C\text{-}rate_{fc}$:= average of charging hc C-rates, weighted by $\Delta Ah_{hc\text{-}residual}$

  $Discharging\ C\text{-}rate_{fc}$:= average of discharging hc C-rates, weighted by $\Delta Ah_{hc\text{-}residual}$

  $FC := [T_{fc}, DOD_{fc}, Middle\text{-}SOC_{fc}, Charging\ C\text{-}rate_{fc}, Discharging\ C\text{-}rate_{fc}]$

  FC_{table} := concatenate FC in FC_{table} table

return: FC_{table} (table integrating the obtained full-cycles)

Algorithm 4. Synthesis of full-cycles, from each cluster involving charging and discharging half-cycles corresponding to identical stress-factors ranges.

ΔQ := Capacity data $_i$ – Capacity data $_{i-1}$.

$\Delta t_{total-profile}$:= duration of the total operating profile.

$\Delta t_{calendar\ component}$:= duration of the extracted calendar component profile.

$\Delta t_{cycle\ component}$:= duration of the extracted cycle component.

input: ΔQ, $\Delta t_{total-profile}$, $\Delta t_{calendar\ component}$, $\Delta t_{cycle\ component}$

2:

3: $\Delta Q_{calendar\ component} := \Delta Q \,.\, \Delta t_{calendar\ component} / \Delta t_{total-profile}$

4: $\Delta Q_{cycle\ component} := \Delta Q \,.\, \Delta t_{cycle\ component} / \Delta t_{total-profile}$

5 :

6 : **for** i … dim(calendar input training data)

7: $\Delta Q_i := \Delta Q_{calendar\ component} \,.\, \Delta t_i / \Delta t_{calendar\ component}$

8: $\Delta Q_{calendar\ output\ training\ vector}$:= concatenate (ΔQ_i) in vector

9: **end for**

10:

11: **for** j … dim(cycle input training data)

12: $\Delta Q_j := \Delta Q_{cycle\ component} \,.\, \Delta Ah_j / \Delta Ah_{cycle\ total}$

13: $\Delta Q_{cycle\ output\ training\ vector}$:= concatenate (ΔQ_i) in vector

14: **end for**

return: $\Delta Q_{calendar\ output\ training\ vector}$, $\Delta Q_{cycle\ output\ training\ vector}$

Algorithm 5. Target processing algorithm: the overall capacity loss measured between two characterisation tests is split into several components, further assigned to the different rows of the input data obtained from the input processing algorithm